IOWA STATE UNIVERSITY
Digital Repository

Retrospective Theses and Dissertations

Iowa State University Capstones, Theses and Dissertations

1988

Synthesis and characterization of ternary Zintl phases

Weir-Mirn Hurng
Iowa State University

Follow this and additional works at: https://lib.dr.iastate.edu/rtd

 Part of the Inorganic Chemistry Commons

Recommended Citation
Hurng, Weir-Mirn, "Synthesis and characterization of ternary Zintl phases " (1988). *Retrospective Theses and Dissertations*. 8775.
https://lib.dr.iastate.edu/rtd/8775

This Dissertation is brought to you for free and open access by the Iowa State University Capstones, Theses and Dissertations at Iowa State University Digital Repository. It has been accepted for inclusion in Retrospective Theses and Dissertations by an authorized administrator of Iowa State University Digital Repository. For more information, please contact digirep@iastate.edu.

www.manaraa.com

INFORMATION TO USERS

The most advanced technology has been used to photograph and reproduce this manuscript from the microfilm master. UMI films the original text directly from the copy submitted. Thus, some dissertation copies are in typewriter face, while others may be from a computer printer.

In the unlikely event that the author did not send UMI a complete manuscript and there are missing pages, these will be noted. Also, if unauthorized copyrighted material had to be removed, a note will indicate the deletion.

Oversize materials (e.g., maps, drawings, charts) are reproduced by sectioning the original, beginning at the upper left-hand corner and continuing from left to right in equal sections with small overlaps. Each oversize page is available as one exposure on a standard 35 mm slide or as a 17″ × 23″ black and white photographic print for an additional charge.

Photographs included in the original manuscript have been reproduced xerographically in this copy. 35 mm slides or 6″ × 9″ black and white photographic prints are available for any photographs or illustrations appearing in this copy for an additional charge. Contact UMI directly to order.

Accessing the World's Information since 1938

300 North Zeeb Road, Ann Arbor, MI 48106-1346 USA

Order Number 8825926

Synthesis and characterization of ternary Zintl phases

Hurng, Weir-Mirn, Ph.D.

Iowa State University, 1988

U·M·I
300 N. Zeeb Rd.
Ann Arbor, MI 48106

PLEASE NOTE:

In all cases this material has been filmed in the best possible way from the available copy. Problems encountered with this document have been identified here with a check mark ✓.

1. Glossy photographs or pages _____
2. Colored illustrations, paper or print _____
3. Photographs with dark background _____
4. Illustrations are poor copy _____
5. Pages with black marks, not original copy _____
6. Print shows through as there is text on both sides of page _____
7. Indistinct, broken or small print on several pages ✓
8. Print exceeds margin requirements _____
9. Tightly bound copy with print lost in spine _____
10. Computer printout pages with indistinct print _____
11. Page(s) _____ lacking when material received, and not available from school or author.
12. Page(s) _____ seem to be missing in numbering only as text follows.
13. Two pages numbered _____. Text follows.
14. Curling and wrinkled pages _____
15. Dissertation contains pages with print at a slant, filmed as received ✓
16. Other _____

_____

_____

U·M·I

Synthesis and characterization of ternary Zintl phases

by

Weir-Mirn Hurng

A Dissertation Submitted to the

Graduate Faculty in Partial Fulfillment of the

Requirements for the Degree of

DOCTOR OF PHILOSOPHY

Department: Chemistry
Major: Inorganic Chemistry

Approved:

Signature was redacted for privacy.

In Charge of Major Work

Signature was redacted for privacy.

For the Major Department

Signature was redacted for privacy.

For the Graduate College

Iowa State University
Ames, Iowa

1988

TABLE OF CONTENTS

INTRODUCTION

The name "Zintl phase" was proposed by Laves[1] to recognize the contributions of Eduard Zintl in this field. The original definition of Zintl phase was limited to those compounds composed of alkali or alkaline earth elements with other main-group elements from IIIA to VIA groups. There are two common characters for the Zintl phases: a) they crystallize in "nonmetallic" and typically salt-like structures (antifluorite, anti-Mn_2O_3, anti-La_2O_3, anti-tysonite and Li_3Bi), b) they are always that phase of a binary system which contains the greatest amount of the active element. According to this definition, the upper limit of the alkali or alkaline earth metal in such a compound is determined by the maximum negative valence of the more electronegative element. However, this has proved to be inapplicable in such as NaTl or most ternary Zintl phases.

Later, Klemm and Busmann[2] expanded this concept to those compounds in which the active metal transfers electrons to the more noble component of the alloy, the "anion former" forming atomic arrangements that correspond to that of the element having the same number of valence electrons. The Zintl-Klemm-Busmann concept is the same as the general valence rule proposed by Pearson.[3] According to this rule, phases made up of elements on opposite sides of the Zintl line comply with the condition: $(n_e+b_a-b_c)/n_a = 8$ (n_e = total number of valence electrons; n_a of anions; b_a = number of electrons required for formation of anion bonds; b_c = number of electrons required for formation of cation-

cation bonds including all valence electrons of the cations not participating in a bond). For example, in KSi ($n_e = 5$; $n_a = 1$; $b_c = 0$), a value of 3 for b_a bonding electrons is obtained, i.e., a coordination number of 3 for the anion partial lattice. Generally, the role of the (8-N) rule for a Zintl phase is equivalent to the 18-electron rule in transition metal chemistry. The source of both rules is the same and from simple valence bond concepts.

In our laboratory, the bonding and structures of Zintl anions,[4] which are always incorporated with organic ligated cations, have been studied for several years. Recently, we started to study the solid Zintl phases due to the attractiveness of the amassing data on structure variations and less known physical properties of these compounds.[5,6] During the research, a couple of systems of ternary Zintl phases have also been examined and promising results found.

There were not any ternary compounds reported in K-Si-As system before we started to study it. Two compounds in the system were found and structurally characterized during the research. K_2SiAs_2 is isostructural with K_2SiP_2[7] with infinite $[SiAs_2]^{2-}$ chains parallel to the c-axis, while puckered layers of $[Si_3As_3]^-$ was observed in KSi_3As_3. Both fulfill the Zintl-Klemm-Busmann concept.

Work on interstitial elements of Zr_5Sb_3 (Mn_5Si_3 structure) was initiated in our laboratory[8] and showed that the properties of Zr_5Sb_3X (X = interstitial elements including transition metal and main-group elemets) were quite dependent on interstitial elements.[9] Thus, the study of interstitial elements in M_5X_3 (M = Ca, Sr, Ba, Ce, Yb; X = Sb, Bi)

which also have Mn_5Si_3 structure (except Ca_5Bi_3) was stimulated. From the result of studies, it is concluded that the pure binary M_5X_3 with Mn_5Si_3 structure can exist, although they violate the simple Zintl valence rule. Also, they have been speculated to contain impurity oxygen.[10] When interstitial elements were introduced, they followed the valence rule strictly and only halogen can be put in successfully. Moreover, three different structures, filled-Mn_5Si_3, filled-β-Yb_5Sb_3[11] and anti-Th_3P_4,[12] have been observed on changing interstitial elements from Cl or Br to F or I. It is believed that an anion size effect causes this.

During the study of Ca_5Sb_3X, a new compound was observed with stoichiometry of Ca/Sb close to 3/2. Since the stoichiometry of it was close to Ca_5Sb_3 and it sometimes was even observed in attempts to synthesize the high temperature phase of Ca_5Sb_3, we studied th structure of it to broaden the basis of pure binary phases in the Ca-Sb system. The structure was solved by a model based on W_5Si_3 structure. The real structure was confirmed by single crystal study and the stoichiometry turned out to be $Ca_{16}Sb_{11}$. The structure of $Ca_{16}Sb_{11}$ was a new member of $R_{5n+6}T_{3n+5}$ (R = rare earth metal; T = transition metal).[13,14] To rationalize this series, the relationship between r_R/r_T and ΔV within the series was studied too. Based on this relationship, the $Sr_{16}Bi_{11}$ analogue was also synthesized.

Finally, the mixed cation effects in Zintl phases also attracted our attention, because it has been shown that mixed cations can yield unique and unusual structures such as Li_3NaSi_6,[15] Li_8MgSi_6,[16] LiK_3Si_4,[17]

$Cs_2Na_2Ge_4$,[18] $Na_{6.25}Rb_{0.6}Ga_{20.02}$,[19] $Na_{13}K_4Ga_{49.57}$,[20] $Li_3Na_5Ga_{19.56}$,[21] $Li_9K_3Ga_{28.83}$,[22] Li_5NaSn_4,[23] and $Li_5Na_2Sn_4$.[24] None of these phases is observed in a pure binary compound. Thus, we started the study of mixed cation in Sr-Mg-Ge system where there was only one compound reported — SrMgGe. In the research, we found two nonstoichiometric compounds — $Sr_{2+x}Mg_{12-x}Ge_7$ and $Sr_{5+y}Mg_{19-y}Ge_{12}$ which are isostructural with $Zr_2Fe_{12}P_7$[25] and $Ho_5Ni_{19}P_{12}$.[26] Also, $SrMg_3Ge_3$ and $SrMg_2Ge_2$ were discovered to be new compounds with new structure types. Based on powder patterns and reasonable postulates, the structure of $SrMg_3Ge_3$ might be related to that of Rh_4P_3.[27]

EXPERIMENTAL

Materials

Most of the starting elements and reagents were from commercial sources. In some cases, they are pretreated to satisfy the experimental requirements. The sources and purities of these elements and reagents that did not need further treatments are summarized in Table 1.

Reagent-grade alkaline-earth-metal halides from commercial sources ($CaCl_2$ (Fisher Co.), $SrCl_2$ (Baker Co.), $BaCl_2$ (Baker Co.) and $BaBr_2$ (ROC/RIC Co. 99% purity)) were dried from room temperature to 200°C — 400°C under high vacuum to eliminate the absorbed moisture. The halides were stored in sealed glass ampoules outside the dry box or in glass vials with tightly fitting plastic stoppers inside the argon-filled dry box where reaction vessels were usually loaded.

Some of the halides such as $CeCl_3$, SbI_3 and $BiBr_3$ were selected from the previous products synthesized in this laboratory and kept well protected since in sealed glass ampoules.

BiI_3 and Sb_2S_3 were prepared by loading stoichiometric amounts of elements in glass ampoules, which were then sealed under vacuum and heated at 750° or 850°C for a couple of days. The high purities of them were confirmed by the Guinier powder patterns.

BaF_2 was formed by adding $BaCO_3$ powder to the HF aqueous solution (35%), then drying the white precipitate. The precipitate was further heated under vacuum at ~400°C in a glass ampoule for a couple of hours to remove the moisture. The glass tube was sealed and transferred to the dry box.

Table 1. Source, purity of starting materials

Starting Materials	Source	Appearance	Purity
Li	Alpha Products	rod	purified
Na	J. T. Baker Chem.	lump	purified
K	J. T. Baker Chem.	lump	purified
Mg	Fisher	chip	reagent grade
Ca	Ames Lab	gem	distilled
Sr	Ames Lab	gem	distilled
Ba	Ames Lab	gem	distilled
Ga	Alpha Products	chunk	99.999%
In	Ames Lab	chunk	distilled
C	Union Carbide	powder	spect. grade
Si	Ames Lab	chunk	zone refined
Ge	Ames Lab	chunk	zone refined
Sn	Ames Lab	granular	distilled
Pb	Ames Lab	granular	distilled
P	J. T. Baker Chem.	powder	technical grade
As	Alpha Products	chunk	99.999%
Sb	Ames Lab	chunk	zone refined
Bi	Oak Ridge Lab	chunk	reactor grade
S	Alpha Products	powder	99.5%
Ce	Ames Lab	chip	99.999%
Yb	Ames Lab	rod	99.999%
LiI	Alpha Products	powder	99.9%
NaI	Alpha Productsts	powder	99.9%
RbI	Alpha Products	powder	99.8%
CsI	Alpha Products	powder	99.9%
CaF_2	Fisher	powder	reagent grade
CaO	Dr. McCarley's group	powder	ACS grade
BaO	Dr. McCarley's group	powder	reagent grade

The synthesis of BaS was made by flowing a mixture of H_2S and H_2 gas into a fused silica jacket which contained $BaCO_3$ (~2g) powder in a fused silica boat. The whole jacket was kept in a furnace at ~930°C for a couple of hours. During the cooling process, only H_2 gas flow was introduced to remove excess H_2S. The whole procedure was modified from the reaction described in Brauer's handbook.[28]

For alkali metals, the dirty oxides on the surface were removed with a scalpel to ensure the cleanness of the alkali metals.

General Synthetic Methods

Due to the hydroscopic and air sensitive characteristics of the reactants and products, all the transfers and manipulations were made in the dry box or on a vacuum line. The dry box was constantly purged with dry nitrogen or argon which was circulated through separate vertical columns of Molecular Sieves and the oxygen scavenger Redox. This and a tray of P_4O_{10} in the dry box typically reduced the moisture content to 1 — 5 ppm. The amount of oxygen was not quantitatively determined, but as a regular check-up, a 60-watt light bulb without glass burned for 30 — 50 minutes. A Pyrex vacuum line with a mercury diffusion pump was used for evacuation of sample tubes, sublimation, etc.

The syntheses of the Zintl phases needs to overcome a high energy barrier, thus a high temperature reaction condition is required. The container should be inert during the reactions. Generally, Ta tubing was a good container. Sometimes, fused silica ampoules were used as the containers, when it was observed that Ta tubing was not inert to some of

the nonmetal elements, especially for As. However, the weak point of fused silica ampoules is their poor resistance to alkali and alkaline earth elements at high temperature. To compensate this, slow heating can reduce the attack of alkali and alkaline earth metals to the fused silica ampoules, because the heat released can be slowed down and the binary compounds formed instead. A better way to solve the above problem is to use a two step reaction. First, alkali or alkaline earth element was prereacted with a nonmetal which does not react with Ta tubing, then the products transferred into a fused silica ampoules for further reactions with other components.

The cleanness of the container is an important requirement, because "everything reacts with everything at high temperature". Ta tubing (5-cm x 0.95-cm o.d.) was placed in cleaning solution (55% concentrated H_2SO_4, 25% concentrated HNO_3, and 20% concentrated HF, by volume) for a few minutes until the tubing was judged to be sufficiently clean. The tubing was then rinsed with distilled water several times and was dried in an oven at 100°C. A quartz ampoule connected to a ball joint at one end first was filled with 10% HF aqueous solution (by volume) for one hour. Then, it was emptied and rinsed with distilled water a couple of times and dried in an oven.

After drying, one end of Ta tubing was crimped in a vise and was then welded under helium atmosphere. The reactants were weighed in the dry box on an electronic balance (±1 mg) and loaded into the tube; then the open end of the tubing was crimped closed with a pair of Vice-Grip pliers. The tube was then placed into a sample bottle, which was tightly

closed and rapidly transferred to the arc-welder. After welding, the tube was subsequently sealed into the silica jacket, and the latter attached to the vacuum line, strongly flamed with a gas-oxygen torch to remove traces of water absorbed on the surface of the fused silica and was then sealed.

As mentioned, a high temperature is required for the synthesis of most Zintl phases. Five different types of furnaces were used during the research. Tube and Marshall furnaces were used for most reactions. They functioned similarly; the only difference is that the insulation of the latter is better than the former so that the temperature gradient was quite small in the latter. A Lindberg furnace was used when a temperature gradient was required such as for chemical transport reactions. An induction furnace was adopted when fast heating and quenching were needed, for such as the syntheses of Ca_5X_3F (X = Sb, Bi). Also, a high temperature furnace connected with programmable temperature controller was used in attempts to grow single crystals. The temperature of reactions was monitored by attaching a chromel-alumel thermocouples on the outside of the fused silica jackets. The temperature of the reactions was regulated by a temperature controller. Both on-off and proportional controllers were used. The reaction time varied depending on demands for different reactions. Usually, two weeks was enough for most reactions.

After the reactions were completed, all the containers were opened in a dry box equipped with a nearly horizontal window that allowed for careful microscopic examination of reaction products. If appropriate size crystals (<0.3-mm) were observed, they were mounted in 0.2-mm or

0.3-mm o.d. capillaries with the aid of glass or fused silica pickers. The open end of the capillary was temporarily sealed by Vaseline or silicon grease. Once outside the dry box, the capillaries were sealed with an oxygen-gas microtorch, and both ends were covered with black wax. Samples of products were ground in a mortar and mounted between layers of Scotch brand tape for Guinier powder diffraction. The rest of the products were stored under vacuum in sealed glass ampoules.

Characterization

Powder X-ray diffraction

Powder X-ray diffraction is the main tool to characterize reaction products so that information on the identity, relative yield, and the precise lattice constants could be obtained. Two different Guinier cameras were used during the research. Although a Hagg-Guinier camera could cover wider range of $2\theta(\sim 90°)$ than Enraf-Nonius (Delft) Guinier camera ($<85°$), the latter proved to give sharper lines in the patterns than the former. Thus, most of the patterns were collected by the latter. Both cameras have silicon monochromaters to give Cu $K\alpha_1$ radiation free of Cu $K\alpha_2$. National Bureau of Standards silicon was added to samples as an internal standard.

Patterns were read using an Enraf-Nonius film reader. The readings from the film were converted to 2θ values by applying a quadratic equation obtained from the least square fit of the five silicon lines to known diffraction angles using the program GUIN.[29] The accurate lattice constants of the products could be further derived from LATT[30] program

after assigning the proper structure type and indices to the reflections.

PWDR[31] is a very useful program for calculating the powder patterns of known or postulated structures. It is followed by PPPLOT[32] program to generate the powder patterns with the same scale as the experimental ones. Therefore, comparison of the intensities as well as positions in the calculated with those in the experimental powder patterns allowed many products be identified. However, it should be noted that the intensities sometimes depend on either grinding damage or preferred orientation which are commonly encountered in layered compounds with weak interactions between layers. Also, the intensities of the reflections at high angles always were weaker than calculated ones. Moreover, whether a single powder pattern can represent the whole product is the important questions that needs to be considered before reaching any conclusion.

If the known compounds already have been collected on ASTM file, the calculated powder pattern can be generated by PLOT[32] program directly by imputing d spacings and relative intensities of the reflections without PWDR.

The output of GUIN may also be indexed by TREOR[33] program to obtain the cell constants of an unknown, single phase. For a mixture, the real cell constants sometimes could be found after carefully excluding those reflections of known phases. The reliability of the result from TREOR program are determined by how many lines are input, the accuracy of those lines, and how many lines can be indexed. The more lines input and indexed, the more the result is trustable. An accurate reading is

important since the tolerance of the program in 2θ is around 0.03°. Generally, ten lines is the minimum required, and the figure of merit should be larger than 6 if the result is to be considered a reliable one.

Single crystal X-ray diffraction

The powder X-ray diffraction only serves as a preliminary identification of the products. If accurate distances and the atom positions of products are desired or if a new structure is formed, then single crystal X-ray diffraction is an invaluable tool to study the structures of the products. Especially, it is the only way to determine the compositions of compounds if they are minor products and their powder patterns can not be obtained due to the low yield.

Since all the Zintl phases are air and moisture sensitive, crystals loaded in 0.2-mm or 0.3-mm capillaries for study for single crystal X-ray diffraction. Before putting the crystals on the diffractometers, preliminary film work should be done to confirm the quality of the crystals and to provide important information on cell constants. Usually oscillation photographs were used to identify the singularity of the crystals and to derive one axis. The zeroeth and first level Weissenberg photographs can give the systematic absences and the lengths of the other two axes. Also, they can provide information on the cell such as superstructure or disordering.

In this research, the three diffractometers used were SYNTEX $P2_1$, DATEX, and CAD-4. For SYNTEX $P2_1$, the software for indexing and data

collection are available from the company, but that of DATEX is provided by Dr. Jacobson's group and is called ALICE.[34] The software for structure determination with data collected by the SYNTEX $P2_1$ and by DATEX are provided by Dr. Jacobson's group too, namely CHESCAT. For CAD-4, it has its own software called SDP (Structure Determination Package)[35] to execute the jobs.

Although three different diffractometers were used, the procedures for the data collection and structure determination are all similar. First, 15 to 25 reflections from Polaroid oscillations photographs are input to determine a cell. There is another option called SEARCH for CAD-4 which scans the reciprocal space randomly for up to 25 strong reflections.

After a cell is obtained and confirmed by axial photographs, the data collection was always of the ω-scan type, because it was much faster than other modes such as θ-2θ scan and less critical of the quality of crystals, i.e., ω-scan should be adopted if the crystals do not look very good. Usually, the 2θ(max) collected was set at $50° - 55°$.

To correct for absorption, ϕ-scan method was used by which diffractometers scanned a peak every $10°$ in ϕ to collect the intensities. The typical 2θ value for the ϕ-scan was $20° - 30°$ and at least three ϕ-scans were carried out (one of them in the high angle range $>30°$). Before data reduction and averaging, an absorption correction program such as ABSN[36] or EMP[37] was applied.

After finishing data reduction, the Lorentz and polarization effects were corrected by REDDAT[38] or DATA[37] program, and redundant data averaged

according to the proper space groups by FDATA[39] or PAINT[37] program so that the data were ready for refinement.

Before proceeding with a refinement, a couple of programs can be run to derive the atom positions such as PATTERSON, SUPERPOSITION, ALCAM, MULTAN and SHELEX. The first three programs were well developed by Dr. Jacobson's group based on the Patterson method, while the last two based on direct method can give solutions after the right space groups and compositions were input. However, they always created some ghost solutions too. Therefore, the user should have some ideas about the bonding and the real components in the structure before using them, or he might be mislead by the results.

Block matrix and full matrix least-squares were both used to refine the data. Usually, a block matrix was used in the initial steps and the full matrix was executed for the final cycles, because refinement by a block matrix was less time consuming. ALLS[40] or LSFM[37] were the programs used to refine the structural data. The typical refinement procedures started from atom positions, then thermal parameters were varied. In some case, a secondary extinction correction was necessary if the size of crystals was very big and quite isotropic. Also, the occupancies of atom positions were sometimes varied to determine the compositions or to examine unusually high thermal parameters.

The structures were illustrated by ORTEP[41] program. Most of atoms were represented as 90% thermal ellipsoids.

Emission spectroscopy

These spectra were measured by E. L. DeKalb in Ames Lab to qualitatively determine the compositions of samples. It was especially helpful when the components of one particular product were completely unknown. The amount of samples needed was about 100 mg. However, the result could not tell whether the appearance of oxygen was from the products or was a limitation of the instrument.

REFERENCES

1. Laves, F. Naturwissenschaften 1941, 29, 244.
2. Klemm, W.; Busmann, E. Z. Anorg. Allg. Chem. 1963, 319, 297.
3. Pearson, W. B. Acta Crystallogr. 1964, 17, 1.
4. Corbett, J. D. Chem. Rev. 1985, 85, 383.
5. Schäfer, H.; Eisenmann, B.; Müller, W.. Angew. Chem., Int. E. Engl. 1973, 12, 694.
6. Schäfer, H. J. Solid State Chem. 1985, 57, 97.
7. Eisenmann, B.; Somer, M. Z. Naturforsch. 1984, 39b, 736.
8. Garcia, E., Ph.D. Dissertation, Iowa State University, Ames, IA, 1987.
9. Garcia, E.; Ku, H. C.; Shelton, R. N.; Corbett, J. D. Solid State Commun., accepted, 1988.
10. Schäfer, H.; Ann. Rev. Mater. Sci. 1985, 15, 1.
11. Bruton, G. D.; Steinfink, H. Inorg. Chem. 1971, 10, 2301.
12. Kripyakevich, P. I. Kristallografiya 1963, 7, 556.
13. Leroy, J.; Moreau, J. M.; Paccard, D.; Parthe, E. J. Less-Common Met. 1980, 76, 131.
14. Villaro, P.; Calvert, L. D. "Pearson's Handbook of Crystallographic Data for Intermetallic Phases"; Vol. 1-3; Am. Soc. Met: Metals Park, OH, 1985.
15. von Schnering, H.-G.; Schwarz, M.; Nesper, R. J. Less-Common Met. 1988, 137, 297.
16. Nesper, R.; Curda, J.; von Schnering, H.-G. J. Solid State Chem. 1986, 62, 199.
17. von Schnering, H.-G.; Schwarz, M.; Nesper, R. Angew. Chem. Int. Ed. Engl. 1986, 25, 566.
18. Llanos, J.; Nesper, R.; von Schnering, H.-G. Acta Crystallogr. 1984, A40, Suppl. C-228, Abstr. 08.2-40.

19. Charbonnel, M.; Belin, C. J. Solid State Chem. 1987, 67, 210.

20. Belin, C.; Charbonnel, M. J. Solid State Chem. 1986, 64, 57.

21. Charbonnel, M.; Belin, C. Nouv. J. Chim. 1984, 8, 595.

22. Belin, C. J. Solid State Chem. 1983, 50, 225.

23. Volk, K.; Müller, W. Z. Naturforsch. 1978, 33b, 593.

24. Volk, K.; Müller, W. Z. Naturforsch. 1978, 33b, 823.

25. Ganglberger, E. Monatsh. Chem. 1968, 99, 557.

26. Pivon, J. Y.; Guerin, R.; Sergent, M. Inorg. Chem. Acta 1985, 109, 3.

27. Runqvist, S.; Hede, A. Acta Chem. Scand. 1960, 14, 893.

28. Brauer, G. "Handbook of Preparative Inorganic Chemistry", 2nd ed.; Vol. 1; Academic Press: New York, 1960; p. 938.

29. Imoto, H., Ames Laboratory, Iowa State University, Ames, IA, unpublished research, 1978.

30. Takusagowa, F., Ames Laboratory, Iowa State University, Ames, IA, unpublished research, 1981.

31. Clark, C. M.; Smith, D. K.; Johnson, G. J. "A Fortran IV Program for Calculation X-Ray Diffraction Pattern — Version 5", Department of Geosciences, Pennsylvania State University, University Park, PA, 1973.

32. Ziebarth, R. P., Ames Laboratory, Iowa State University, Ames, IA, unpublished research, 1984.

33. Werner, P. E. "TREOR-4 Trial and Error Program for Indexing Unknown Powder Patterns", Department of Structural Chemistry, Arrhnius Laboratory, University of Stockholm; S-106 91 Stockholm, Sweden, 1984.

34. Jacobson, R. A., United States AEC Report IS-3469, Iowa State University, Ames, IA, 1974.

35. Frenz, B. "Enraf-Nonius Structure Determination Package"; Delft University Press: Delft, The Netherlands, 1982.

36. Karcher, B. A., Ph.D. Dissertation, Iowa State University, Ames, IA, 1981.

37. A subprogram in SDP (ref. 35).

38. Roger, J.; Jacobson, R. A., United States AEC Report IS-2155, Iowa State University, Ames, IA, 1967.

39. Helland, B., Ames Laboratory, Iowa State University, Ames, IA, unpublished research, 1981.

40. Lapp, R. L.; Jacobson, R. A., United States DOE Report IS-4708, Iowa State University, Ames, IA, 1979.

41. Johnson, C. K. "ORTEP: A Fortran Thermal-Ellipsoid Plot Program for Crystal Structure Illustrations", ORNL Report 3794, Oak Ridge National Laboratory, Oak Ridge, TN, 1970.

PART I. K–Si–As TERNARY SYSTEM

Introduction

Binary compounds between silicon, germanium, etc. (A) and phosphorus, arsenic, etc., (B) have been known for a long time.[1-3] The most common stoichiometries are AB and AB_2 which at ambient temperature and pressure often exhibit layered structures. In the former GaTe type, A is bonded to three B and one A atoms in a structure of condensed tetrahedra, while in the latter, typified by $GeAs_2$, A is bound to four B atoms which share edges to form layers that bear some resemblance to those in the former. These are all valence or Zintl[4,5] phases and semiconductors at room temperature.[6]

There are only a few known ternary phases $M_xA_yB_z$ for these A and B elements in which M is an alkali metal.[7-9] The structure of the $A_yB_z^{x-}$ anion in such ternary phases is expected to be different from that of the neutral analog A_yB_z. For instance, the layer structure of SiP_2 ($GeAs_2$ type) is broken down to chains in the formation of K_2SiP_2.[8] It is easy to rationalize this in terms of the reduction that accompanies the formation of SiP_2^{2-}. The latter is isoelectronic with SiS_2, and thus K_2SiP_2 has a structure similar to that of SiS_2. Likewise, the layered anions in the isostructural KSnAs and KSnSb phases are isoelectronic with and have a structure like that of $CaSi_2$ but with ordered tin and arsenic or antimony atoms.[9] The anion layers in the $CaSi_2$[10] structure can in turn be related to the puckered neutral layers found in the isoelectronic element arsenic, etc.

Recently a new composition and structure type has been discovered in our laboratory for MSi_3As_3 (M = K, Na). The relatively low proportion of the alkali metal also allows a clear relationship to be discerned between the $Si_3As_3^-$ structure and that of the binary phase SiAs (GaTe type).[2]

MSi_3As_3 (M = Na, K)

Synthesis

Materials utilized were purified potassium (J. T. Baker Chem. Co.) which was first trimmed of oxidation products in the dry box, arsenic lumps (99.99% total, Alpha Products) and zone-refined, electronic grade silicon.

The new KSi_3As_3 was first encountered after a reaction of the three elements in a 1:1:1 ratio. This was carried out in a fused silica ampoule that had been sealed under vacuum and further jacketed in a second evacuated silica jacket in order to protect the products if container attack led to cracking when the reaction was cooled. The loading of the reactants and the examination of the products were carried out in a glove box flushed with nitrogen and kept at a moisture level below 5 ppm. Purple, needle-shaped crystals were found on the inner surface of the container after the reaction had been run in a vertical tube furnace at around 800°C for 5 days. X-ray emission spectroscopy confirmed the presence of all three elements in the product.

Since potassium attacks a silica container and arsenic attacks the alternative container tantalum, a two-step synthetic process was developed to avoid such side reactions. After the correct stoichiometry

of the needles had been determined from a solution of the crystal structure, KSi[11] or "KSi_3", an intimate fused mixture of Si and KSi, were first prepared in high purity by reaction of elemental potassium and silicon in a sealed tantalum container at 800°C. Stoichiometric amounts of As were then reacted with KSi plus Si or "KSi_3 " in sealed fused silica ampoules at 910 – 950°C for 4 – 5 days according to the equation:

$$KSi + 2Si + 3As \longrightarrow KSi_3As_3 \qquad (1)$$

This approach greatly reduced the attack of potassium and provided a high yield of the evidently single-phase product, >95% judging from Guinier powder diffraction. Large needle crystals about 8 mm long were found at the top of the ampoules where the temperature had been lower. It is presumed that a chemical transport reaction was responsible for this crystal growth, but the process has not been studied further. Iodine does not effect transport in this system, evidently because the stability of the alternate KI is too high.

Attempts at the synthesis of KGe_3As_3 and $NaSi_3As_3$ by the above method in silica and of KGe_3As_3 and KSi_3P_3 by the two-step process were without success although a few small needle crystals were seen in the first of these. However, the phase $NaSi_3As_3$ could be obtained by a cation exchange method. Equimolar amounts of KSi_3As_3 and NaI were ground together, pressed into a pellet, sealed in a silica tube under vacuum, and heated in a horizontal tube furnace at ~500°C for one week. The end of the tube not containing the pellet was slightly exposed at the end of the furnace, either from the beginning or after several days. Crystals of KI were found at the cold end of the tube (as identified by X-ray

lattice constant and qual tests), while pure $NaSi_3As_3$ was left in the hot end. Cell constants for $NaSi_3As_3$, a = 10.002(4), b = 18.54(3) and c = 3.648(1) A, were determined by least-squares refinement of 2θ values for the clearest 10 of the 17 rather broad lines observed in the Guinier powder pattern.

Similar exchange reactions with RbI, CsI were also tried but without success. Exchange reactions at 500°C employing equimolar amounts of LiI and KSi_3As_3 either as a pressed pellet in SiO_2 under a temperature gradient or as the mixed powders in sealed Ta isothermally likewise produced pure KI judging from the lattice constant. However, the presumed $LiSi_3As_3$ product has a different and unknown crystal structure; the pattern could also result from a mixture.

The potassium phase is not oxidized by benzophenone in THF at ~86°C, contrary to the observations for Li_7Ge_{12},[11] presumably because of either a low potassium mobility or an insufficient reducing power. The lithium product gives only a faint yellow color under the same conditions so the latter explanation is more likely. KSi_3As_3 is not very sensitive to moist air but reacts with water or dilute HCl with vigorous evolution of hydrogen and the formation of a black amorphous product. The lithium product is quite air-sensitive.

Structural studies

A suitable needle crystal (about 0.02 x 0.02 x 0.8 mm) of what turned out to be KSi_3As_3 was mounted and sealed in a 0.2-mm diameter, thin-walled capillary. Oscillation and zero- and first-level Weissenberg

photographs showed that the cell was orthorhombic with a ≅ 10.1, b ≅ 19.1, c ≅ 3.65 Å and that the diffraction data exhibited the nonextinction conditions: $h0\ell$, h = 2n; $0k\ell$, k = 2n; h00, h = 2n; 0k0, k = 2n. Only two space groups, Pbam and Pba2, satisfy these, and the structural refinement proved that the centric Pbam was correct.

Diffraction data were collected from the same crystal at room temperature and to $2\theta = 55°$ with the aid of graphite-monochromated Mo $K\alpha$ radiation (λ = 0.71069 Å) and a DATEX four-circle diffractometer. No decay of the standard reflections was observed.

The positions of the three heavier arsenic atoms were first determined with the aid of a Patterson map, and those of the other atoms were then deduced from Fourier F-synthesis maps. It turned out that all atoms occupy the 4(g) (x,y,0) or 4(h) (x,y,1/2) positions of m symmetry. The data were corrected for absorption by the psi-scan method together with the program ABSN. This program as well as ALLS for structure factor calculations and least-squares refinement, FOUR for Fourier syntheses, and ORTEP for drawings have been referenced before.[12] Scattering factors included the real and imaginary part of anomalous dispersion.[13] A difference map computed after the final cycle showed maximum residual densities between +1.9 and +1.5 e/Å^3. These were all located 0.8 — 1.4 Å from the As(1), As(2), As(3) or Si(1) positions, generally in outward directions from the layers as might be produced by a small amount of cation defects. Details of crystal data collection and refinement parameters are given in Table 1. Lattice parameters calculated from Guinier powder

Table 1. Diffraction and refinement data of KSi_3As_3

Space group	Pbam (No. 55)
Z	4
Cell param. (Å)[a]	
a	10.010(4)
b	19.139(8)
c	3.664(1)
Size of crystal (mm)	0.05 x 0.05 x 0.8
Octants collected	h,k,ℓ; -h,-k,ℓ
Scan type	ω
2θ-max, deg. (Mo Kα)	55
μ(Mo Kα), cm^{-1}	112.9
Transm. coeff. range	0.87 – 1.00
Number of reflections	
meas.	2405
obs. (>3σ(I))	1551
indep.	674
R(ave)	0.038
R[b]	0.044
R_w	0.050

[a]The cell dimensions calculated from 21 lines of the Guinier powder pattern, Cu $K\alpha_1$, λ = 1.54056 Å.

[b]$R = \sum||F_o| - |F_c||/\sum|F_o|$, $R_w = [\sum w(|F_o| - |F_c|)^2/\sum w|F_o|^2]^{1/2}$.

pattern data with Si as an internal standard[13] were used for distance calculations.

Results and Discussion

The positional parameters for KSi_3As_3 are listed in Table 2 and some important distances and angles are given in Table 3.

Structure description

The unit cell of KSi_3As_3 is depicted in Figure 1 while a portion of the anion layer therein along with some bond distances is shown in Figure 2, both in perspective views down the short c axis. The layers can be seen to consist of puckered rings of the metalloid element condensed into chains and then into sheets, or vice versa. Thus, nonplanar five-membered rings consisting of —Si(1,2)As(2)Si(3)As(3)— are condensed into columns or tubes through sharing the last four atoms while the remaining Si(1) atoms are bridged by the exocyclic As(1) atoms. These groups are then joined head-to-head and tail-to-tail into sheets via Si(3)—Si(3) and Si(2)—Si(2) bridges. The last are easiest to see in the Figures as the centers of these bonds lie at points of 2/m symmetry with the rotation axis normal to the figure. If the construction is instead centered on these Si—Si bonds, $Si(3)_{4/2}As(2)_{4/2}As(3)_2$ and $Si(2)_2As(2)_{4/2}Si(1)_2[As(1)_{4/2}]As(3)_2$ units of C_{2h} symmetry are joined into strings parallel to [100] via their common As(2) and As(3) atoms, and then condensed into sheets along $\vec{c}$. The structural arrangement is very reasonable as it makes all silicon atoms four-bonded and two of the arsenic atoms three-bonded, while the terminal As(1) atoms are only

Table 2. Positional and isotropic thermal parameters for KSi_3As_3[a]

Atom	x	y	z	B[b]
As(1)	0.4000(1)	0.19698(6)	0.0	1.38(3)
As(2)	0.7191(1)	0.04102(5)	0.0	1.17(3)
As(3)	0.5861(1)	0.38496(6)	0.5	1.23(3)
K[c]	0.1962(3)	0.3048(2)	0.5	2.63(8)
Si(1)	0.3251(3)	0.1320(1)	0.5	1.24(7)
Si(2)	0.1126(3)	0.5147(1)	0.5	1.00(7)
Si(3)	0.4072(3)	0.5365(1)	0.0	1.02(7)

[a]Space group Pbam, Z = 4, all atoms in 4h or 4g positions.

[b]Average of anisotropic values, A^2.

[c]Refined occupancy = 0.98(1).

Table 3. Distances (Å) and angles (deg) in KSi_3As_3

Atom 1	Atom 2	Distance	Atom 1	Atom 2	Atom 3	Angles
As(1)	– 2 Si(1)	2.337(2)	Si(1)	– As(1)	– Si(1)	103.2(1)
As(1)	– 2 K	3.431(3)				
As(1)	– 2 K	3.486(3)				
As(2)	– 2 Si(2)	2.372(2)	Si(2)	– As(2)	– Si(2)	101.2(1)
As(2)	– Si(3)	2.399(3)	Si(2)	– As(2)	– Si(3)	94.31(9)
As(2)	– 2 K	3.482(3)				
As(3)	– 2 Si(3)	2.370(2)	Si(1)	– As(3)	– Si(3)	93.28(9)
As(3)	– Si(1)	2.416(3)	Si(3)	– As(3)	– Si(3)	101.3(1)
K	– 2 As(2)	3.482(3)	As(2)	– K[a]	– As(1)	77.71(5)
K	– 2 As(1)[a]	3.431(3)	As(2)	– K[a]	– As(1)[a]	100.95(5)
K	– 2 As(1)	3.486(3)	As(1)	– K[a]	– As(1)[a]	102.67(5)
Si(1)	– Si(2)	2,331(4)	As(1)	– Si(1)	– As(1)	103.2(1)
Si(1)	– 2 As(1)	2.337(2)	As(1)	– Si(1)	– As(3)	112.86(9)
Si(1)	– As(3)	2.416(3)	As(1)	– Si(1)	– Si(2)	115.3(1)
Si(1)	– 2 Si(3)	3.480(4)	As(3)	– Si(1)	– Si(2)	97.8(1)
Si(2)	– Si(2)	2.322(6)	As(2)	– Si(2)	– As(2)	101.2(1)
Si(2)	– Si(1)	2.331(4)	As(2)	– Si(2)	– Si(1)	108.2(1)
Si(2)	– 2 As(2)	2.372(2)	As(2)	– Si(2)	– Si(2)	109.1(1)
Si(2)	– 2 Si(3)	3.497(4)	Si(1)	– Si(2)	– Si(2)	119.4(2)
Si(3)	– Si(3)	2.325(6)	As(2)	– Si(3)	– As(3)	114.47(9)
Si(3)	– 2 As(3)	2.370(2)	As(2)	– Si(3)	– Si(3)	104.8(2)
Si(3)	– As(2)	2.399(3)	As(2)	– Si(3)	– As(3)	101.3(1)
Si(3)	– 2 Si(1)	3.480(4)	As(3)	– Si(3)	– Si(3)	111.0(1)
Si(3)	– 2 Si(2)	3.497(4)				

[a] x+1/2, 1/2-y, z.

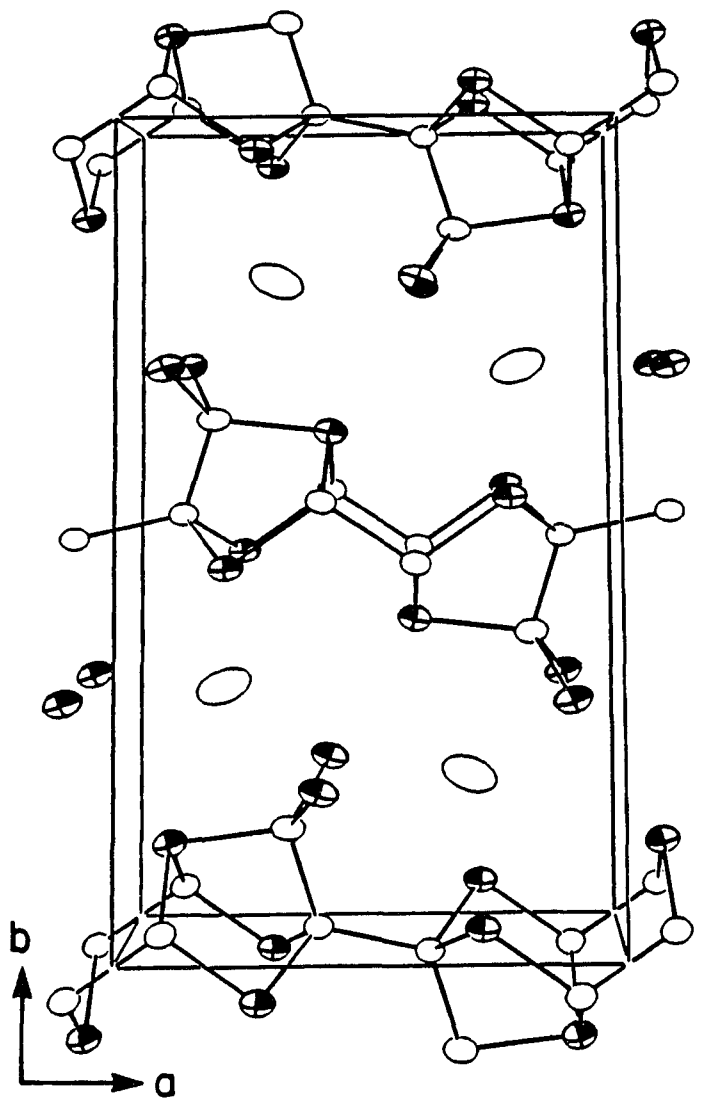

Figure 1. A [001] perspective of the unit cell of KSi_3As_3 (space group Pbam) with all atoms at z = 0 or 1/2. Open atoms: Si (in chain) and K; shaded atoms: As. (90% probability thermal ellipsoids.)

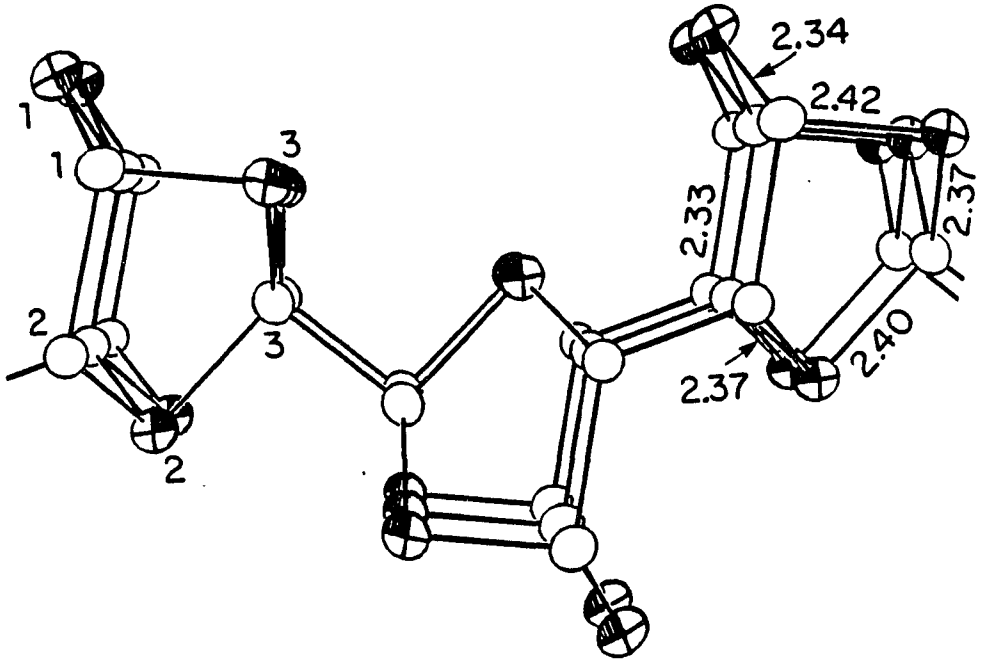

Figure 2. A perspective view of a portion of the $^{2}_{\infty}[Si_3As_3]$ layers in KSi_3As_3. Arsenic atoms are shaded

two-bonded. The last are then formally As^{1-}, isoelectronic with selenium. Formulation of the dark-purple compound as $K^+Si_3As_3^-$ gives the anion the electron count of a valence (Zintl[6]) compound, and conventional two-center bonding should apply.

Bond distances

Important distances and angles are listed in Table 3, and some distances are marked on Figure 2. Several general points are observed. First, all Si—Si distances are almost the same, the average 2.326 Å being close to those in many silanes, ~2.34 Å[14] consistent with the simple bonding expected. All bonds formed by three-bonded arsenic atoms (2) and (3) connect to one end of an Si_2 group, and for most of these the bonds lengths cluster around 2.38 Å. Different values occur around the silicon (1). The latter atoms are bridged by the unique, two-bonded As(1) at a shorter 2.337 Å, a normal contraction, while the neighboring Si(1)— As(3) bonds are a somewhat longer 2.416 Å. We suspect that the latter may be induced by strain as the interior angle at Si(1) is only 97.8°. Effects of the polar $(K^+)_{4/4}(As(1)^-)_{4/4}$ interactions (below) may also be important.

Two-bonded arsenic also occurs in the Zintl phases $(M^{II})_3Si_2As_4$, M^{II} = Sr, Ba, where the anion chains contain $Si(As)As_2Si(As)$ units, four-membered rings condensed at silicon with a terminal arsenic on each.[15,16] Bond distances therein vary in a consistent manner but are uniformly larger than reported here, perhaps because of strain or the larger polarity. The bonds between silicon and the terminal (one-bonded)

As^{2-} are now 0.06 – 0.08 Å less than to bridging As^{-1} but the latter average 2.40 Å vs 2.33 Å in KSi_3As_3. The Si–Si bonds at 2.36 and 2.39 Å ($\sigma \sim 0.01$ Å) likewise average 0.05 Å greater than those in KSi_3As_3. Similarly, $SiAs_4^{8-}$ tetrahedra with only terminal arsenic atoms that occur in Ba_4SiAs_4[17] have the Si–As distances increased to 2.40 Å,[17] perhaps because of the high charge on the anion groups. These data on Si–As distances are summarized in Table 4.

The potassium atoms in KSi_3As_3 are coordinated by two pair of the unique As(1) atoms as well as two As(2) atoms from two different layers to give a rather distorted trigonal prismatic environment but one with fairly uniform K–As distances of 3.43 – 3.49 Å. This unit, as shown in Figure 3, shares both As(1)–As(1) vertical edges and the top and bottom faces with other like prisms so each As(1) has four potassium neighbors and As(2), two. The next nearest neighbors, As(3) atoms in the plane of the potassium at 4.22 and 4.37 Å, are disposed on the more open faces of the prism, and their secondary interactions with the cation may be the source of the shortening of two of four of the K–As(1) distances to 3.43 Å.

Cation exchange

The potassium ions may be readily exchanged by sodium or lithium on reaction with the stoichiometric amount of MI at 500°C. The crystal ionic radius of sodium is 0.34 Å less than that of potassium,[18] and the decreases observed in a, b and c on the formation of the sodium derivative, ~0.008 (4), 0.60 (3) and 0.016 (1) Å, respectively, are consistent

Table 4. Silicon — arsenic bond lengths (Å) in different ternary compounds

Compounds	Si—As(3b[a])	Si—As^{-}(2b)	Si—As^{2-}(1b)	Ref.
KSi_3As_3	2.372(2),2.370(2) 2.399(3),2.416(3)	2.337(2)		this work
$Sr_3Si_2As_4$		2.40_2,2.39_2	2.32_0	16[b]
$Ba_3Si_2As_4$		2.396(8),2.416(8)	2.350(8)	17
Ba_4SiAs_4			2.407(5),2.393(5)	18[b]

[a]Three-bonded, etc.

[b]Refined with isotropic thermal parameters and a limited absorption correction.

with the layered nature of the structure, Figure 1. The lithium product has a different, unknown structure. The exchange behavior with NaI and LiI, and the absence of reaction with RbI and CsI, are unusual with regard to the usual course of such reactions which form the small cation — small anion and large cation — large anion pairs. The problem here is somewhat different, however, in that the arsenic "anion" separations within the layers are fixed in position. Improved nesting of the sheets and polarization of the arsenic atoms may be involved.

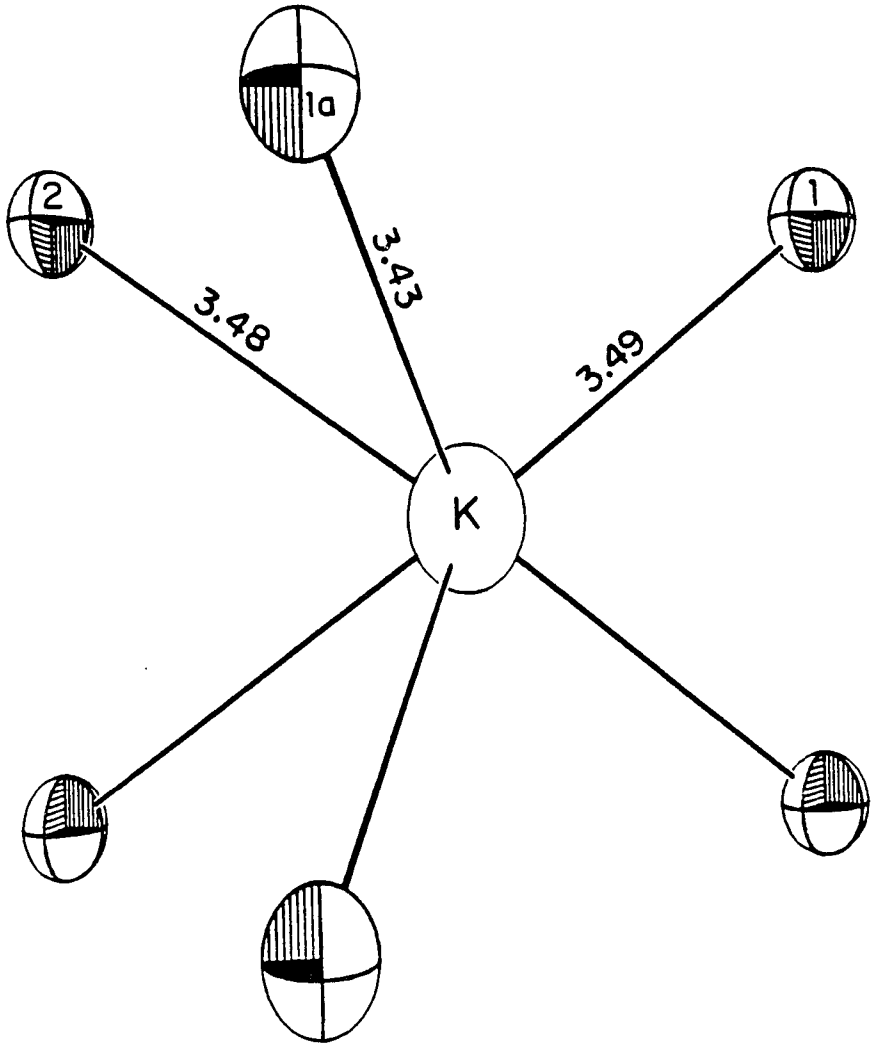

Figure 3. The arsenic environment about potassium in KSi_3As_3. The cation lies on a horizontal mirror plane normal to the figure

Relationship with Li_3NaSi_6

We have very recently become aware of the existence of a remarkably similar layered anion structure in Li_3NaSi_6.[19] The isoelectronic layers there contain the same columns or tubes of shared, five-membered rings, but their interconnection is slightly different. The relative positions of one half of the exocylic bridges are altered in Li_3NaSi_6 as would be accomplished by inverting alternate columns (Figure 4). Thus, the central ring system seen in Figure 2 becomes related to those on both sides by a horizontal screw axis or glide plane centered on the Si(3) — Si(3) connection rather than by the normal two-fold axis found at that point with KSi_3As_3. The altered arrangement appears to generate much better cavities along the chain for lithium.

Relationship with SiAs

The structure determined by Wadsten[3] for SiAs in space group C2/m is closely and logically related to that of KSi_3As_3. The former is shown in Figure 5 in the [010] projection. The tricyclic units can be derived from Si_3As_2As rings in KSi_3As_3 by joining these in pairs at the exocyclic As(1) atoms. This generates a pair of puckered five-member rings condensed onto a central six-membered ring at the disilicon edges in the latter. Such a member is centered about a screw axis at 1/4,y,0 in Figure 5. These ring systems are then linked into strings in the plane of the Figure through Si(3)—Si(3) bonds and condensed along $\vec{b}$ to form layers as before. Two-fold axes are again found normal to the centers of the Si(3)—Si(3) bonds.

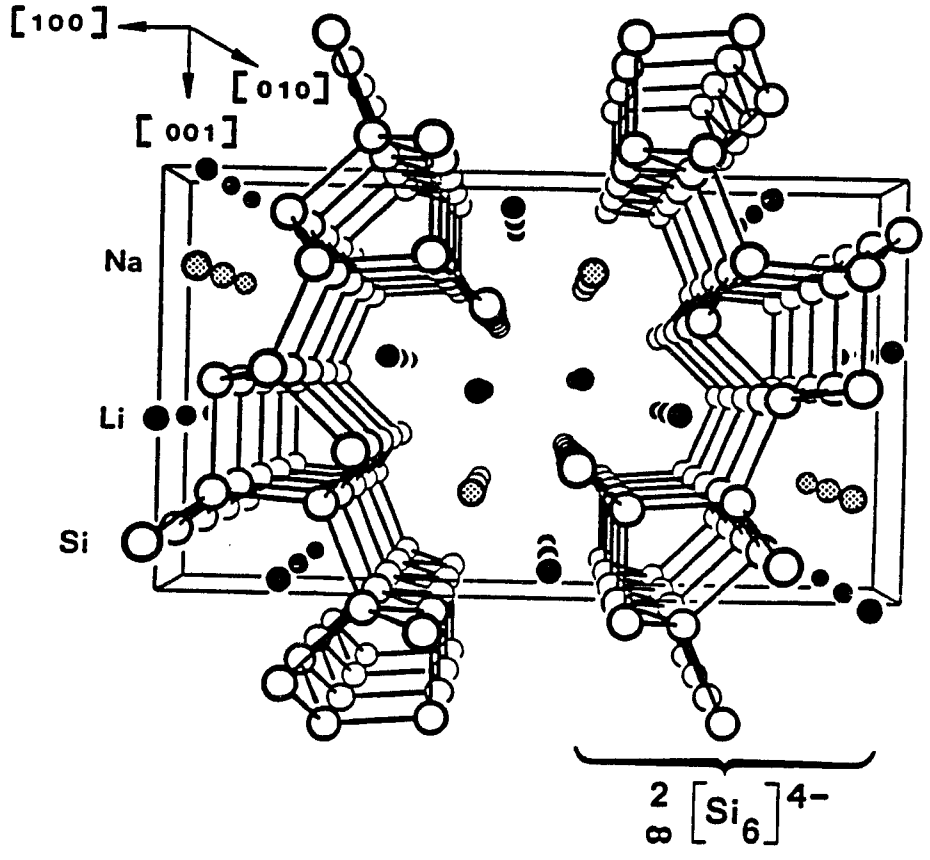

Figure 4. The structure of Li_3NaSi_6 projected along [010] (quoted from ref. 19)

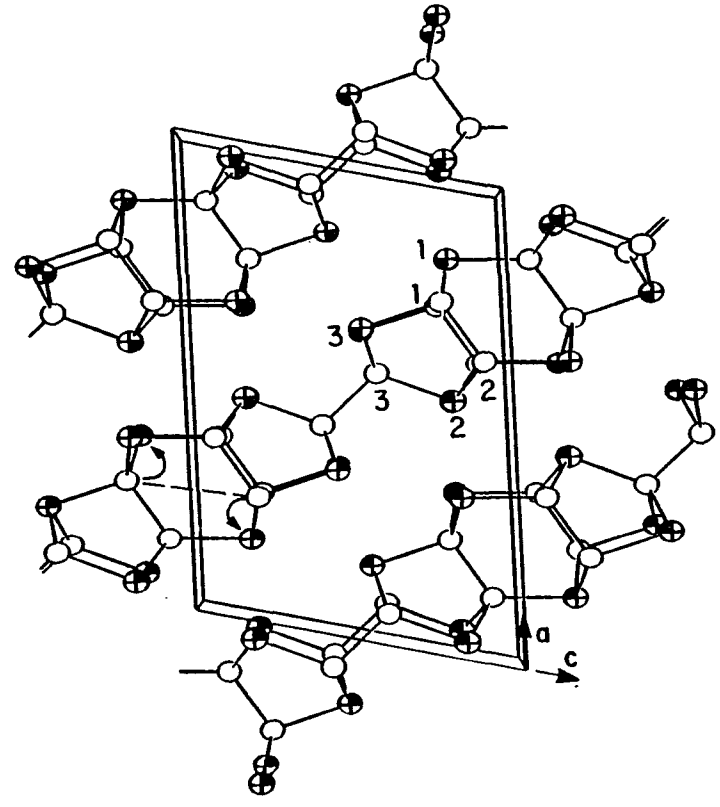

Figure 5. A [010] view of the structure of SiAs, space group C2/m (ref. 3). Arsenic atoms are shaded. The changes necessary to convert these layers to those in KSi_3As_3 on reduction are depicted in the unit centered around 1/4,1/2,0

The chemical and structural conversion

$$6SiAs + 2K \longrightarrow 2KSi_3As_3 \qquad (2)$$

within one layer of SiAs can be achieved by (1) cleavage of opposite As(1)—Si(2) edges of the six-membered rings to form chains of dibonded As(1) atoms, Figure 1 and 2, and (2), displacement of one-half of the result by b/2 with respect to the other and rotation to allow formation of the Si(2)—Si(2) bonds in KSi_3As_3. The change is depicted symbolically on the same tricyclic unit around 1/4,1/2,0 in Figure 5. The direction of opening of these six-membered rings in the conversion to KSi_3As_3 alternates between layers in order to provide good interlayer bonding sites for potassium. It is not obvious, however, that such a reduction (or oxidation) process could actually be achieved in a truly concerted manner. Not surprisingly, KSi_3As_3 and SiAs exhibit very comparable distances as well as similar distributions of angles about equivalent atoms, the latter suggesting somewhat similar strain problems in both structures. The same may pertain to the closely related $GeAs_2$[4] as well.

Further reduction of the anion layers in KSi_3As_3 leads to the chain structure noted before in $Sr_3Si_2As_4$ where the connectivity is $^1_\infty[Si_2(As_2)As_{4/2}]$ via four-membered Si_2As_2 rings. It is interesting that in the related $Sr_3Ge_2As_4$, five-membered $Ge_{1/2}$—Ge—(As_2)—As—$Ge_{1/2}$—As— rings analogous to those found condensed in KSi_3As_3 occur in chains, but with one germanium now common to two rings. The anion structure of KSi_3As_3 was presumably not found during earlier studies with alkaline earth metal cations because half as many cations of higher field would not support a stable layered structure.

K_2SiAs_2

In the study of K–Si–As system, some needle crystals were found with a needle axis ~6.3 Å, based on oscillation photographs, much longer than that of KSi_3As_3 which is only 3.664 (1) Å. In reviewing literature, K_2SiP_2[9] was found to have a needle-like habit with an axis of 6.107 (4) Å. Therefore, it was quite possible that the needle crystals were K_2SiAs_2. To confirm that, rxn. Q137 was run by loading stoichiometric amounts of elementary starting materials into a fused silica ampoule which was sealed under Ar and then loaded into another larger fused silica jacket. To prevent the attack by moisture and oxygen, the whole loading process was carried out in a dry box flushed with nitrogen gas. After slowly heating the contents from room temperature to 750°C in 8 hrs. and maintaining the temperature there for 6 hrs., then furnace cooling, some light brown needle crystals were found at the top of the residue. The residue also contained unreacted silicon and arsenic elements as confirmed by the Guinier powder pattern. Since the yield of the needle crystals was not very high, the attempt to take a powder pattern of the crystals was not very successful, as all the lines of the powder pattern were very weak and diffuse. However, several crystals were mounted into 0.2-mm capillaries. From the oscillation and Weissenberg photographs, the lattice constants were derived: a = 13.22(2), b = 7.02(2) and c = 6.33(2) Å, $\alpha = \beta = \gamma = 90°$. Compared with lattice constants of K_2SiP_2: a = 12.926(6), b = 6.687(4) and c = 6.107(4) Å, $\alpha = \beta = \gamma = 90.0°$, the needle crystals could be K_2SiAs_2 and isostructural

with K_2SiP_2. Moreover, the systematic absences for the needle crystals derived from the zeroth and first level Weissenberg photographs are: $hk\ell$:$h+k+\ell = 2n$; $0k\ell$:$k,\ell = 2n$; $h0\ell$:$h,\ell = 2n$; all consistent with the space group of K_2SiP_2:Ibam.

Structure solution

One of the needle crystals with suitable size (0.04 x 0.04 x 0.75 mm) was indexed and data collected by the four-circle DATEX diffractometer. A total of 1361 reflections data were collected from two octants ($\pm h,\pm k,\ell$) with 2θ(max) equal to 50°. The details of data collection and structure solution was summarized in Table 5. After finishing data collection, the lattice constants were accurately derived from 30 reflections of the single crystal: a = 6.336(6), b = 13.219(3) and c = 6.977(2) Å . After finishing absorption correction, data reduction and averaging, the coordinates of K_2SiP_2 were used as a starting point in refinement of the data since the preliminary examinations already confirmed it to be isostructural with K_2SiP_2. After a couple of cycles including anisotropic temperature factors refinements, the R and R_w dropped to 0.022 and 0.026, respectively. The final difference map did not show any residual peaks greater than 1.0 e/Å^3. The positional and thermal parameters are listed in Table 6.

Description of the structure

The K_2SiAs_2 has the infinite $[SiAs_2]^{-2}$ chains parallel to the c-axis and perpendicular to [001] plane (Figure 6) with potassium cations packed between those chains. The chemical environment of potassium

Table 5. Diffraction and refinement data of K_2SiAs_2

Space group	Ibam (No. 72)
Z	4
Cell param (Å)[a]	
a	6.336(6)
b	13.219(3)
c	6.977(2)
Size of crystal (mm)	0.04 x 0.04 x 0.75
Octants collected	h,k,ℓ; -h,-k,ℓ
Scan type	ω
2θ-max, deg. (Mo Kα)	50
μ(Mo Kα), cm^{-1}	128.8
Range of transm. coeff.	0.065 — 0.083
Number of refl.	
meas.	1361
obs. (>3σ(I))	511
indep.	254
R(ave)	0.011
Structure solution	
R^b	0.022
R_w	0.026

[a] The cell dimensions calculated from 30 reflections of single crystal Mo K_{α_1}, λ = 0.71034 Å.

[b] $R = \sum||F_o| - |F_c||/\sum|F_o|$, $R_w = [\sum w(|F_o| - |F_c|)^2/\sum w|F_o|^2]^{1/2}$, $w = 1/\sigma_F^2$.

Table 6. Positional and thermal parameters of K_2SiAs_2[a,b]

Si	As	K
x = 0	x = -0.09880(4)	x = 0.1445(1)
y = 1/2	y = 0.33229(9)	y = 0.1617(2)
z = 1/4	z = 0	z = 0
B_{11} = 1.27(4)	B_{11} = 1.50(3)	B_{11} = 1.99(6)
B_{22} = 1.39(7)	B_{22} = 1.94(3)	B_{22} = 2.27(6)
B_{33} = 1.26(8)	B_{33} = 1.43(3)	B_{33} = 2.68(6)
$B_{12} = B_{13} = B_{23} = 0$	B_{12} = -0.54(2)	B_{12} = 0.31(5)
	$B_{13} = B_{23} = 0$	$B_{13} = B_{23} = 0$

[a]Space group Ibam (No. 72).

[b]The needle axis is consistent with the c=axis.

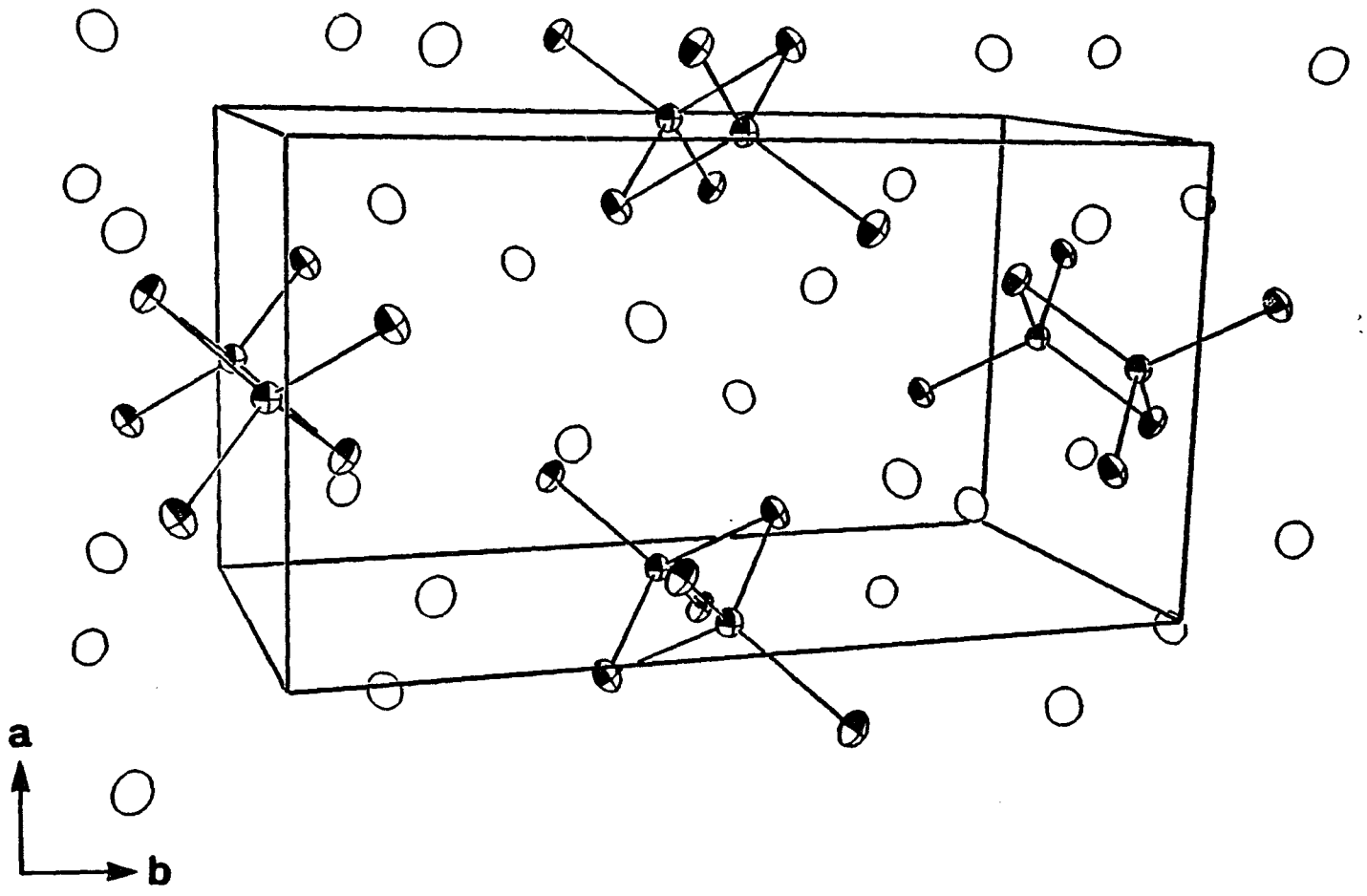

Figure 6. The unit cell of K_2SiAs_2 viewed along [001]. Open atoms: K; shaded atoms: Si (4 bonded) and As (2 bonded). 90% probability thermal ellipsoids

cations is quite different from that in KSi_3As_3. The potassium cations are in the rather distorted octahedral sites (Figure 7) while those in KSi_3As_3 are located in trigonal prism sites. All the arsenic atoms are bridging between two adjacent silicon atoms similar to the selenium atoms in $SiSe_2$ which is isoelectronic with $[SiAs_2]^{-2}$ (Figure 8). The bonding distances between Si and As is 2.370 (1) Å, but the angles of As—Si—As are in the range from 96.14 (3)° to 120.84 (4)°. The details of the distances and angles in K_2SiAs_2 are listed in Table 7.

Comparisons of Si—As⁻(2b) distances in different ternary compounds

The distances of Si—As⁻(2b) in K_2SiAs_2 (2.370 (1) Å) is longer than that of KSi_3As_3 which is only 2.337 (2) Å. This might be caused by the high strain in KSi_3As_3, because the As(2b) atoms are bridging between Si(1) atoms to form sheets in KSi_3As_3. However, compared with $(M^{III})_3Si_2As_4$, M^{III} = Sr, Ba, the Si—As⁻(2b) of K_2SiAs_2 is shorter (see Table 4). Again, the strain or the polarity might play an important role. Also, the chain in $(M^{II})_3Si_2As_4$ is puckered while that of K_2SiAs_2 is linear. That might cause different strain for them.

Conclusion

In the study of K—Si—As system, two structure type compounds were found. One of the KSi_3As_3 — is a new structure type with puckered layer. For them, the ratios of Si/As are equal to those of molecular compounds. In KSi_3As_3, due to the low proportion of cation, the structure can be related to SiAs, while K_2SiAs_2 is completely different from $SiAs_2$,

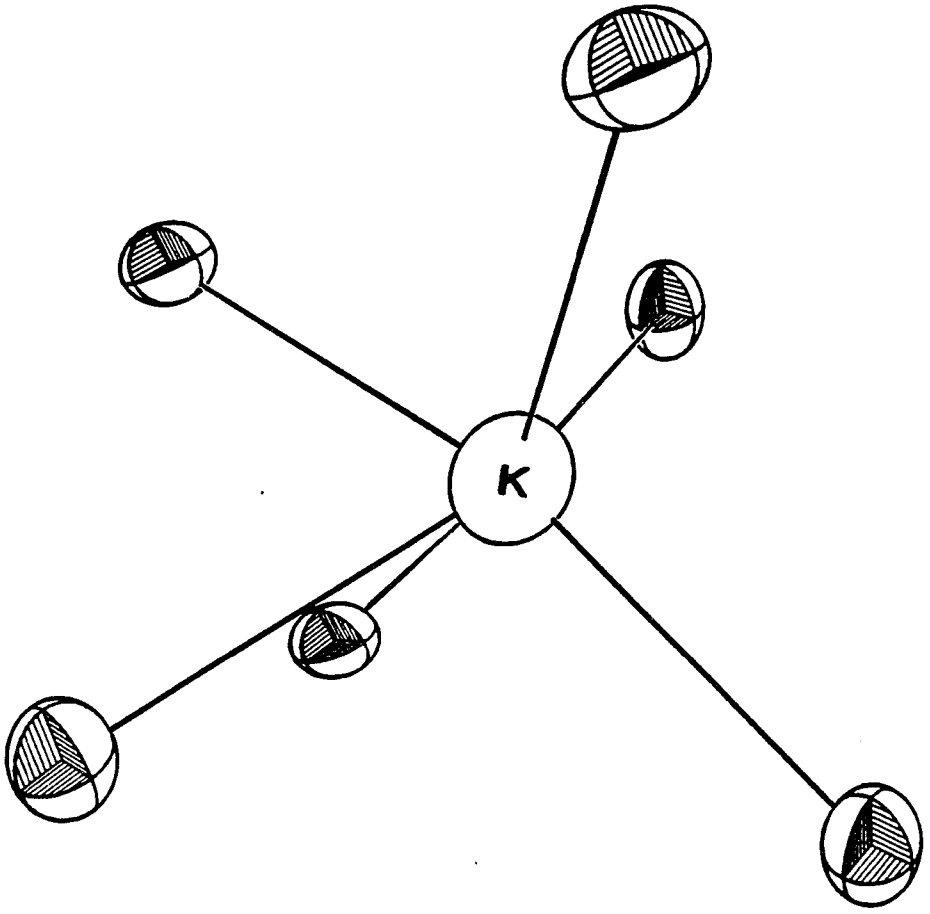

Figure 7. The arsenic environment about potassium in K_2SiAs_2

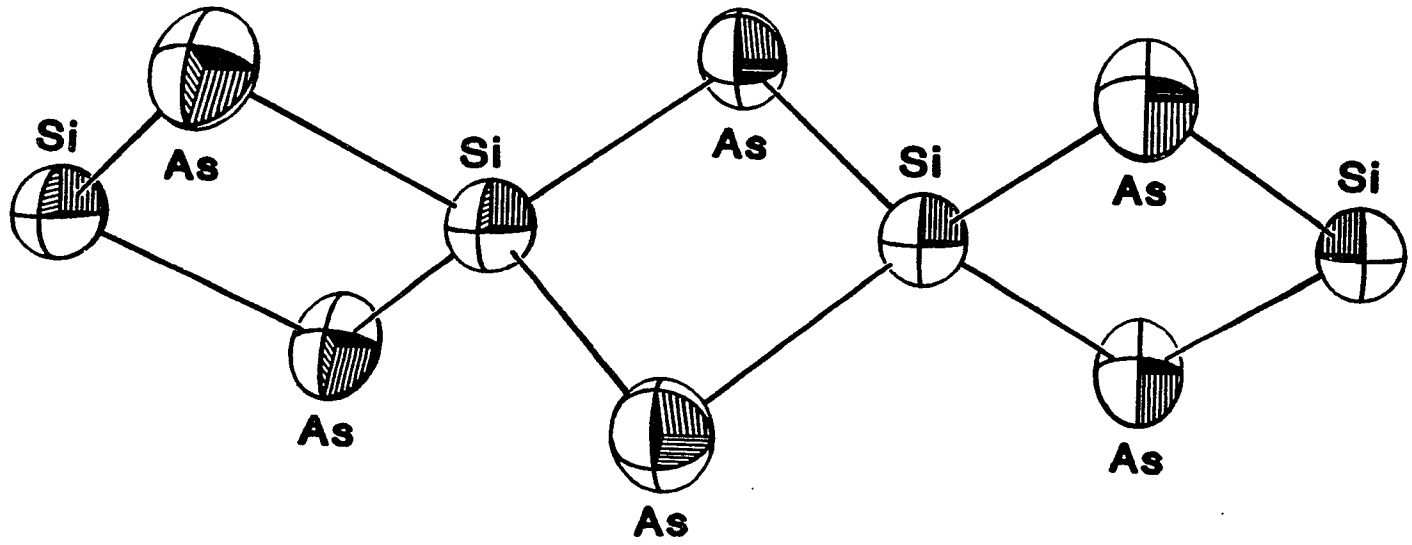

Figure 8. A perspective view of a portion of the $^1_\infty[SiAs_2]$ chains in K_2SiAs_2

Table 7. Bonding distances (Å) and angles (deg) in K_2SiAs_2

Atom 1	Atom 2	Distance	Atom 1	Atom 2	Atom 3	Angle
Si —	4 As	2.370(1)	As —	Si —	As	96.14(3)
Si —	2 Si	3.168(1)	As —	Si —	As	120.84(4)
Si —	4 K	3.425(1)	As —	Si —	As	112.36(4)
As —	2 Si	2.370(1)				
As —	K	3.380(2)	Si —	As —	Si	83.86(3)
As —	2 K	3.435(1)				
As —	K	3.442(2)				
As —	K	3.497(2)				
As —	As	3.527(2)				
As —	K	3.579(2)				
K —	As	3.380(2)				
K —	2 Si	3.425(1)				
K —	2 As	3.435(1)				
K —	As	3.442(2)				
K —	As	3.497(2)				
K —	As	3.579(2)				

because all the arsenic atoms accepted one charge from potassium atoms to form arsenic anions. Therefore, the structure of K_2SiAs_2 is more like $SiSe_2$ which is isoelectronic with $[SiAs_2]^{-2}$. The sodium analogue of KSi_3As_3 can be generated through cation exchange reaction.

References

1. Wadsten, T. Acta Chem., Scand. 1965, 19, 1232.
2. Wadsten, T. Acta Chem., Scand. 1967, 21, 593.
3. Bryden, J. H. Acta Crystallogr. 1962, 15, 167.
4. Schäfer, H.; Eisenmann, B.; Müller, W. Angew. Chem., Int. Ed. Engl. 1973, 12, 694.
5. Schäfer, H. Ann. Rev. Mater. Sci. 1985, 15, 1.
6. Hulliger, F.; Mooser, E. J. Phys. Chem. Solids 1963, 24, 283.
7. Schuster, H.-U. Z. Anorg. Allg. Chem. 1954, 65, 275.
8. Eisenmann, B.; Somer, M. Z. Naturforsch. 1984, 39b, 736.
9. Lii, K.-H.; Haushalter, R. J. Solid-State Chem., submitted.
10. Schäfer, R.; Klemm, W. Z. Anorg. Allg. Chem. 1961, 312, 214.
11. Grüttner, A.; Nesper, R., v. Schnering, H.-G. Angew. Chem., Int. Ed. Engl. 1981, 20, 594.
12. Hwu, S.-J.; Corbett, J. D. Poeppelmeier, K. R. J. Solid State Chem. 1985, 37, 43.
13. "International Tables for X-Ray Crystallography"; Volume IV; Kynoch Press; Birmingham, England, 1974, pp. 72-146, 149-150.
14. Wells, A. F. "Structural Inorganic Chemistry"; 5th ed., Clarendon Press: Oxford, 1984, p. 992.
15. Eisenmann, B.; Schäfer, H. Angew. Chem., Int. Ed., Engl. 1980, 19, 490.
16. Eisenmann, B.; Jordon, H.; Schäfer, H. Z. Naturforsch. B 1982, 37, 1564.
17. Eisenmann, B.; Jordon, H.; Schäfer, H. Z. Anorg. Allg. Chem. 1981, 475, 74.
18. Shannon, R. D. Acta Cryst. Sec. A 1976, 32, 751.
19. Schwartz, M., Dissertation, Universität Stuttgart (FRG), 1987.

PART II. M_5X_3 BINARY SYSTEM

Introduction

There are two structure types reported for M_5X_3 (M = Ca, Sr, Ba; X = Sb, Bi).[1] One is Mn_5Si_3 type (hexagonal cell),[2] the other is β-Yb_5Sb_3[3] (orthorhombic cell) (see Table 1). For Ca_5Sb_3 and Sr_5Bi_3, these two types were reported[1] to both exist with Mn_5Si_3 as the high temperature form. The original motive to study these M_5X_3 systems was based on a curiosity about the nature of these two phases, whether they are really binary phases or one of them belongs to the class of interstitially stabilized phases.

This kind of phenomenon was already observed in a couple of cases. For example, M_2X (M = alkaline earth metal; X = group VA nonmetal)[4] and M_3Y (M = alkaline earth metal; Y = group IVA nonmetal)[5] have all been proven to be oxygen-stabilized compounds, and the right stoichiometries for them are M_4X_2O and M_3YO, respectively. They all satisfy the simple valence rule. Apparently, the above M_5X_3 phases all have one extra electron available according to the simple valence counting rule. This further supports the suspicion about M_5X_3 perhaps being halides. Also, it was speculated that the might be oxygen-stabilized $M_{10}X_6O$.[6,7] In the research, not only Ca_5Sb_3 and Sr_5Bi_3 but also Yb_5Sb_3 were studied (Table 2).

Ca_5Sb_3

It was reported that Ca_5Sb_3 with β-Yb_5Sb_3 structure forms by a peritectic reaction at 825°C.[8] Thus, rxn. 5 — 3 and rxn 243 were started at

Table 1. Reported structure types of M_5X_3[1] (M = Ca, Sr, Ba; X = Sb, Bi)

	Ca_5Sb_3		Sr_5Sb_3		Ba_5Sb_3	
Structure Type	(Mn_5Si_3) (β-Yb_5Sb_3)	ref. 9 ref. 10	(Mn_5Si_3)	ref. 12	(Mn_5Si_3)	ref. 13
r_M/r_X	1.257		1.369		1.423	
	Ca_5Bi_3		Sr_5Bi_3		Ba_5Bi_3	
Structure type	(β-Yb_5Sb_3)	ref. 11	(Mn_5Si_3) (β-Yb_5Sb_3)	ref. 13 ref. 9	(Mn_5Si_3)	ref. 13
r_M/r_X	1.169		1.274		1.324	

Table 2. Reaction conditions and products of stoichiometric M_5X_3 reactions

rxn. #	reaction conditions[a]	products[b]
	Ca_5Sb_3	
5 — 3	850°C — 2.5 wks, 600°C — 3 days	hex. 40%; ortho. 60%
243	850°C — 4 days, water quenching	hex. 40%; ortho. 60%
292	1100°C — 2 days, 850°C — 5 days	hex. 60%; ortho. 40%
293[c]	same as 292	same as 292
373	950°C — 1 day, 810°C — 1 day, 760°C —2 days, 700°C — 8 hrs., 650°C — 1 day	hex. 70%; ortho. 30%
376	950°C — 12 hrs., air quenching 820°C — 4 weeks	hex. 70%; ortho. 30%
454	induction heating (~1200°C) air quenching	$Ca_{16}Sb_{11}$, 90%; unidentified ?
459	970°C — 4 days, water quenching	hex. 80%; ortho. 20%
	Sr_5Bi_3	
480	970°C — 3 days, 730°C — 5 days, 650°C —5 days, 450°C — 1 day	hex. 30%; ortho. 40% $Sr_{16}Bi_{11}$, 20%; ?
	Yb_5Sb_3	
515	Induction heating — 4 hrs. (~1300°C) air quenching	hex. 99%
509	900°C — 22 days	Yb_4Sb_3 65%; ortho. 35%
511	800°C — 22 days	Yb_4Sb_3 40%; ortho. 60%
512	700°C — 3 months	?

[a]All reactions were furnace cooled unless specified.

[b]The relative yields were estimated from the powder patterns; hex. and ortho. represented Mn_5Si_3 type and β-Yb_5Sb_3 type, respectively.

[c]The Ca was exposed in the air for 4 hours before loading in Ta tubing.

~850°C then annealed and water quenched, respectively. Both contained about 40% Mn_5Si_3 type and 60% β-Yb_5Sb_3. To ensure the cleanness of Ca metal, distilled Ca metal from Dr. Peterson's group was used in the reactions thereafter. Rxn. 292 and rxn. 293 were used to test a possible source of impurity; the Ca used in rxn. 293 was exposed to the air for 4 hours before it was loaded in Ta tubing. Both reactions were heated at 1100°C to get better homogeneity then annealed at 850°C. However, both reactions gave the similar relative yields of Mn_5Si_3/β-Yb_5Sb_3 of 60:40. Apparently, if there is an impurity to stabilize the hexagonal phase, it was not from the air.

Rxn. 373 and rxn. 376 were designed to synthesize single phase of Ca_5Sb_3 (β-Yb_5Sb_3) and Ca_5Sb_3 (Mn_5Si_3), respectively, by carefully controlling the reaction conditions. In principle, rxn. 373 should give high yield of β-Yb_5Sb_3 type while the rxn. 376 should produce high yield of Mn_5Si_3 type product because the former adopted annealing while the latter adopted quenching from 950°C. However, the relative yields of the two phases was the same with Ca_5Sb_3 (Mn_5Si_3)/Ca_5Sb_3 (β-Yb_5Sb_3) close to 70:30. That strongly suggested that the transition temperature between these two phases was above 820°C, also the annealing time should be longer than 4 weeks to complete the phase transition.

Rxn. 454 was carried out using induction furnace; the temperature was set ~1300°C. The cooling rate should have been fast, the identified product was $Ca_{16}Sb_{11}$ plus a couple of unidentified lines. Apparently, $Ca_{16}Sb_{11}$ is the high temperature peritectic product and with a

stoichiometry close to 5/3; thus, as the reaction cooled from 1300°C, the product formed mainly was $Ca_{16}Sb_{11}$ not Ca_5Sb_3.

When the reaction temperature set at 970°C in rxn. 459, 80% Ca_5Sb_3 (Mn_5Si_3) and 20% Ca_5Sb_3 (β-Yb_5Sb_3) were found. Although water quenching was adopted, the single phase of Ca_5Sb_3 (Mn_5Si_3) still could not be reached. That suggested the transition was very fast, because the only time to form Ca_5Sb_3 (β-Yb_5Sb_3) was a couple of seconds when the container was first exposed to the air.

It was also tried to add CaO as the impurity source. The product indicated that the Ca_4Sb_2O and $Ca_{11}Sb_{10}$ were the major products. That excluded the possibility of a CaO impurity.

From this study, a couple of points could be made. When reaction temperature at ~970°C, the yield of Ca_5Sb_3 (Mn_5Si_3) can be as high as ~80%, while for a temperature set at ~850°C the yield would drop to 40%. Thus, it was clear that the Ca_5Sb_3 (Mn_5Si_3) was the high temperature phase. However, the transition temperature could not have been told because the reactions probably have not reached equilibria.

Sr_5Bi_3

Sr_5Bi_3 is the only other compound reported with two structures of Mn_5Si_3 and β-Yb_5Sb_3. Therefore, rxn. 480 was run to explore the relationship between these two phases. It was reported Sr_5Bi_3[14] was a congruently melting compound with melting point at 945°C. Thus, rxn. 480 started with temperature at 970°C, then annealed at 730°C, 650°C and 450°C, successively. The products contained: 40% Sr_5Bi_3 (β-Yb_5Sb_3), 30%

Sr_5Bi_3 (Mn_5Si_3) and 20% $Sr_{16}Bi_{11}$ (isostructural with $Ca_{16}Sb_{11}$) judging by the powder pattern only. From this it was proven that Sr_5Bi_3 could exist with Mn_5Si_3 and β-Yb_5Sb_3 structure types. However, some of the lines (mostly are from β-Yb_5Sb_3 structure) in the powder pattern were broad and blurred, indicating equilibrium was not reached or some kind of solid solution occurred during the annealing, i.e., the annealing temperature chosen might not have been proper to observe the phase transition.

Other M_5X_3 Phases

The structures of other M_5X_3 also have been tested by following proper reaction conditions.[11-13] It turned out that Ca_5Bi_3 only has β-Yb_5Sb_3 type structure, while Sr_5Sb_3, Ba_5Sb_3 and Ba_5Bi_3 only adopt Mn_5Si_3 type. The lattice constants of these compounds and those of Ca_5Sb_3 are summarized in Table 3.

Also, single crystal study of Sr_5Sb_3 was carried out. The results confirm the literature about the structure of Sr_5Sb_3[12] and clearly indicate the Sr_5Sb_3 is an interstitial free pure binary compound without anything in the octahedral sites (see report 10/1/86 – 12/31/86).

Yb_5Sb_3

It was reported that Yb_5Sb_3 with the Mn_5Si_3 structure was the high temperature phase.[15] To check that, rxn. 515 was run in the induction furnace at ~1400°C. The product was a single hexagonal phase with a = b = 9.0344(2) and c = 6.9112(4) Å (from 35 lines). That proved the hexagonal phase of Yb_5Sb_3 is the pure binary phase and the high temperature phase.

Table 3. Lattice constants[a] of M_5X_3 binary compounds

Compounds	a (Å)	b (Å)	c (Å)	c/a	b/a	source
Ca_5Sb_3	9.0321(3)		7.0280(8)	0.778		rxn. 231
Ca_5Sb_3	9.02_4		7.05_7	0.782		ref. 9
Ca_5Sb_3Cl	9.0805(3)		7.0898(6)	0.781		rxn. 296
Sr_5Sb_3	9.5037(5)		7.4095(8)	0.780		rxn. 368
Sr_5Sb_3	9.496(5)		7.422(5)	0.782		ref. 12
Sr_5Sb_3Cl	9.5541(4)		7.4328(7)	0.778		rxn. 398
Sr_5Bi_3	9.63(1)		7.63(2)	0.792		ref. 13
Ba_5Sb_3	9.964(3)		7.694(4)	0.772		rxn. 305
Ba_5Sb_3	9.97(1)		7.73(2)	0.775		ref. 13
Ba_5Bi_3	10.098(2)		7.768(3)	0.769		rxn. 308
Ba_5Bi_3	10.13(1)		7.79(2)	0.769		ref. 13
Ba_5Bi_3Cl	10.188(3)		7.837(4)	0.769		rxn. 307
Ca_5Sb_3	12.537(4)	9.555(2)	8.296(2)	0.662	0.762	rxn. 231
Ca_5Sb_3	12.502(8)	9.512(7)	8.287(7)	0.663	0.761	ref. 10
Ca_5Sb_3F	12.442(2)	9.653(2)	8.381(2)	0.674	0.776	rxn. 364
Ca_5Bi_3	12.766(1)	9.706(2)	8.437(2)	0.661	0.760	rxn. 408
Ca_5Bi_3	12.722(8)	9.666(6)	8.432(6)	0.663	0.760	ref. 11
Ca_5Bi_3F	12.602(2)	9.771(2)	8.501(2)	0.675	0.775	rxn. 407
Sr_5Bi_3	12.37_0	10.23_3	8.89_0	0.665	0.765	ref. 9

[a]The lattice constants calculated from Guinier powder patterns, Cu $K\alpha_1$ (λ = 1.540562 Å).

The product of rxn. 515 was further divided into three parts for further studies and loaded as rxn. 509, 511 and 512. These three reactions were annealed at 900 °C. 800°C and 700°C, respectively (see Table 2). The products of rxn. 509 and 511 were the same and contained Yb_4Sb_3 (anti-Th_3P_4)[15] and β-Yb_5Sb_3, but the relative yields were different. The relative yield of Yb_4Sb_3/β-Yb_5Sb_3 in rxn. 509 was around 2/1, while that in rxn. 511 was 2/3. In other words, the low temperature annealing favors the formation of β-Yb_5Sb_3. It was suspected that these two reactions have not reached equilibria even after 22 days annealing. Also the composition is not balanced, and there may be some Yb rich phases such as Yb_2Sb not detected on the powder pattern. Another possibility is that the Yb_4Sb_3 might be a nonstoichiometric phase such as $Yb_4Sb_{2.4}$ = Yb_5Sb_3, then the $Yb_4Sb_{2.4}$ would be an intermediate phase between the hexagonal and the orthorhombic phase.

The reaction time for rxn. 512 was 3 months. The product did not contain any known binary Yb—Sb or Ta—Sb phases. Also, the lines of the powder pattern were broad and could not be indexed by the TREOR program. That suggested they might be a mixture of the decomposition products. From this study, the existence of the pure binary hexagonal and orthorhombic phase was confirmed. However, $Yb_4Sb_{2.4}$ might exist as the intermediate phases and the product decomposed to unidentified mixture after a long time of annealing at 700°C.

Discussion

Structure relationship between β-Yb_5Sb_3 and Mn_5Si_3

Since β-Yb_5Sb_3 type and Mn_5Si_3 type coexist in some M_5X_3 compounds, close relationship between these two structures is expected. Wang et al.[16] has already discussed the relationship by using different arrangements of the M-centered (M = transition metal) trigonal prisms. Here, we provide another way, which seems much easier to recognize, to rationalize the relationship.

Figure 1 shows the unit cell of Ca_5Sb_3 (β-Yb_5Sb_3) projected on [010] plane. There are two differently oriented hexagonal nets composed of Ca trigonal prisms sharing corners and filled by Sb atoms. Inside the hexagonal nets, two Sb and two Ca atoms form zig-zag, ribbon-like parallelograms along b-axis (Figure 2). One of the nets is along the c-axis while the other one is almost perpendicular to the a-axis. The angle between the orientations of these two nets is almost 37°.

The structure of Ca_5Sb_3 (Mn_5Si_3) can be represented as the same way. There are three differently oriented hexagonal nets on the unit cell. To illustrate the orientation of nets, Figure 3(a), 3(b) and 3(c) only show each of them, respectively. In the figures, the dotted lines connect Ca atoms at z = 1/4; solid lines connect Ca atoms at z = 3/4; double lines connect Ca atoms from z = 1/4 or z = 3/4 to z = 0 or z = 1/2. Clearly, Figure 3(a), 3(b) and 3(c) show the orientation of the nets along a-axis, b-axis and (110), respectively. Therefore, the angle between the last two nets is 30° smaller than that of Ca_5Sb_3 (β-Yb_5Sb_3).

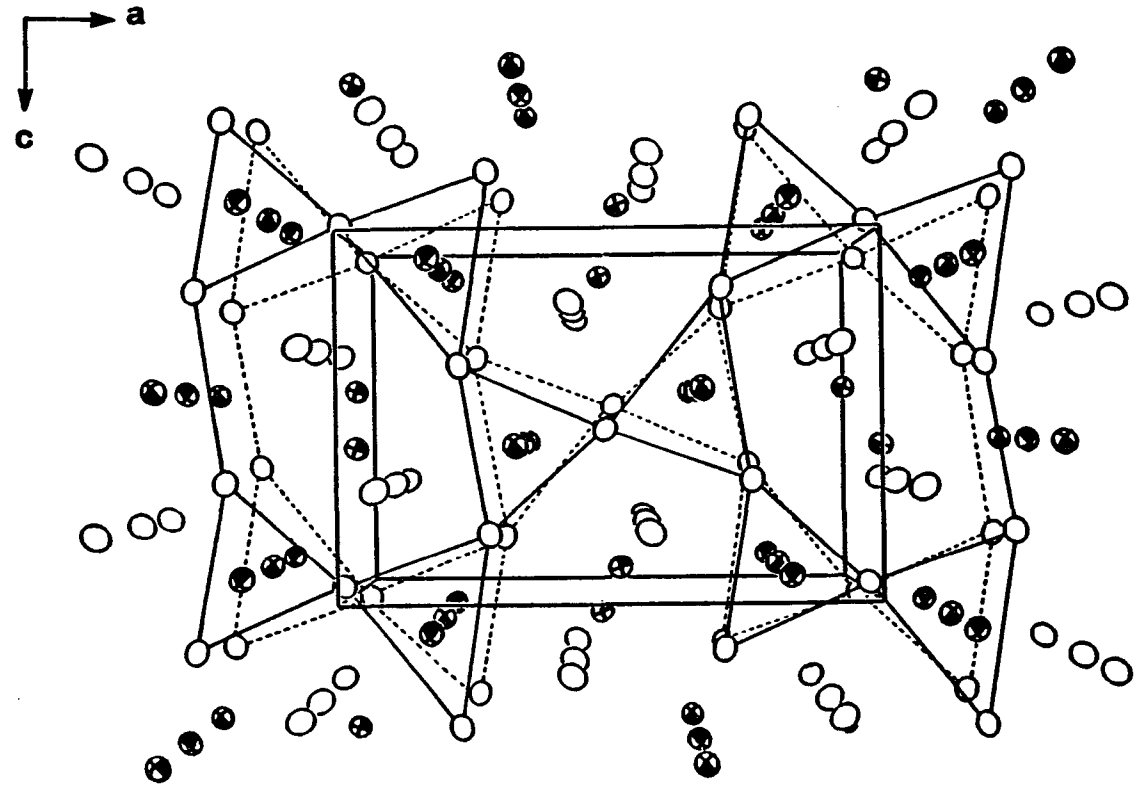

Figure 1. The unit cell of Ca_5Sb_3 (β-Yb_5Sb_3) projected on [010] plane. Open ellipsoids: Ca atoms; shaded ellipsoids: Sb atoms. The dotted lines connect Ca atoms at y = 1/4; the solid lines connect Ca atoms at y = 3/4

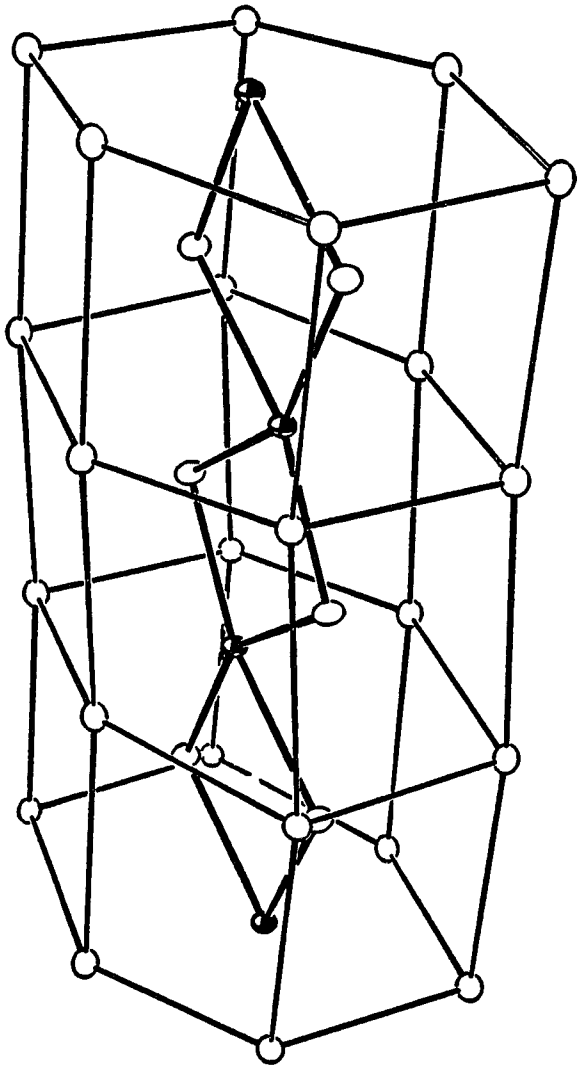

Figure 2. The hexagonal net in β-Yb_5Sb_3 structure extended along the b-axis. The ribbons form a zig-zag chain inside the net

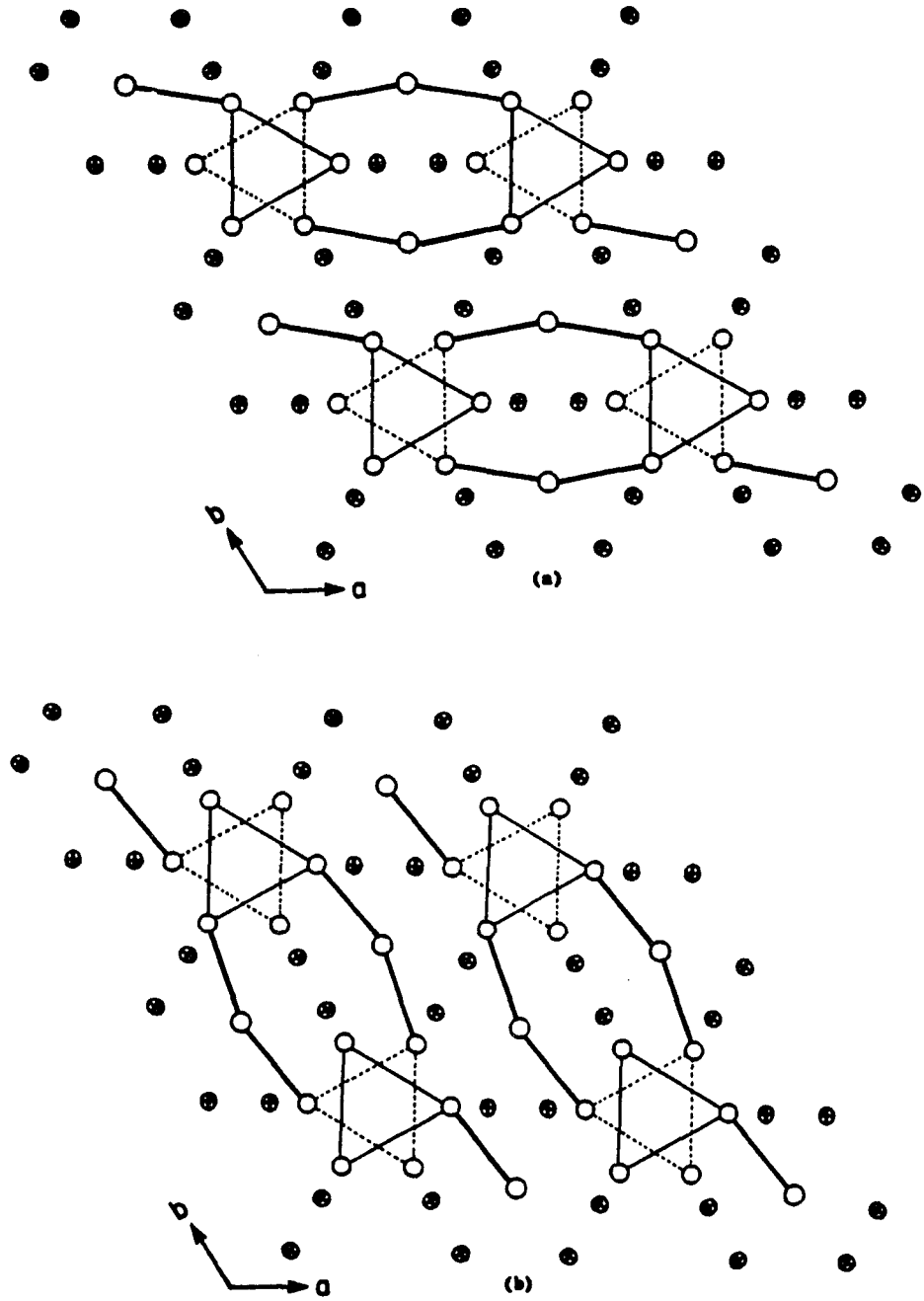

Figure 3. The unit cell of Ca_5Sb_3 (Mn_5Si_3) projected on [001] plane (a), (b) show different hexagonal nets along a- and b-axis

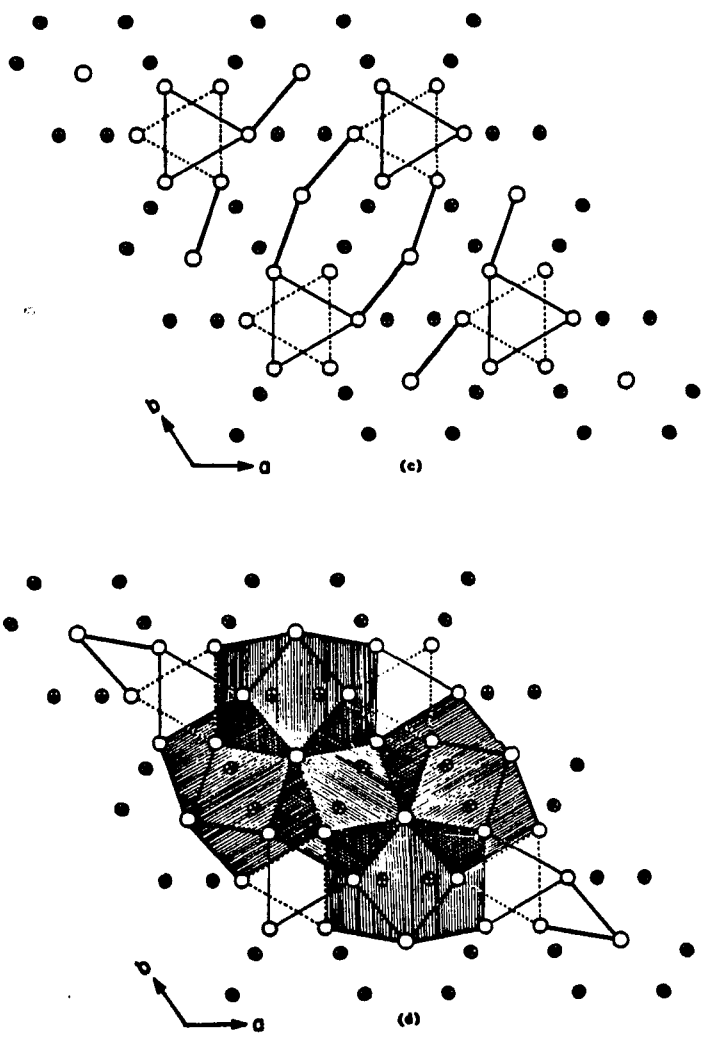

Figure 3. (continued)
(c) The hexagonal net extends along (110) direction. Dotted lines connect Ca atoms at z = 1/4; solid lines connect Ca atoms at z = 3/4; double lines connect Ca atoms from z = 1/4 or 3/4 to z = 0, or z = 1/2. (d) Shows the hexagonal nets penetrating together. To clarify the overlapping, the areas of the hexagonal nets are shaded

These three hexagonal nets are not shared by corners at those of β-Yb_5Sb_3 type but are penetrated and overlapped together such as Figure 3(d). In the figure, the overlapping areas are easily distinguished by shading the original hexagonal nets.

Another main difference between these two types is that the hexagonal nets in Mn_5Si_3 type are puckered ones while those in β-Yb_5Sb_3 type are almost flat. To illustrate this point, Figure 4(a) and 4(b) are drawn for the cross sections of the hexagonal nets in these two types parallel to the (402) and (010) directions. From these figures, it becomes clear that the hexagonal nets for Mn_5Si_3 are puckered and centered with a Ca atom in the ribbon due to the puckering, while the nets in β-Yb_5Sb_3 are much flatter without anything in the center of the ribbon. Three pairs of different hexagonal nets are fused together to form the octahedral sites on the origin in Mn_5Si_3 structure.

Using the resemblance and the difference between these two structures, we can explain the sizes of the lattice constants of these two types for Ca_5Sb_3. Since the hexagonal nets is the same size as c-axis in β-Yb_5Sb_3 type but smaller than the b-axis in Mn_5Si_3 type, the size of c-axis in β-Yb_5Sb_3 type (8.296(2) Å) is smaller than that of b-axis in Mn_5Si_3 type (9.0321(3) Å). On the other hand, the size of a-axis in β-Yb_5Sb_3 type (12.537(4) Å) across two different hexagonal nets by sharing corners is expected to be larger than that of a-axis in Mn_5Si_3 type (9.0321(3) Å) which is composed by two penetrated nets. Finally, half the size of the b-axis (4.7775(1) Å) is smaller than that of the c-axis in Mn_5Si_3 type (7.0280(8) Å), because the hexagonal nets are not

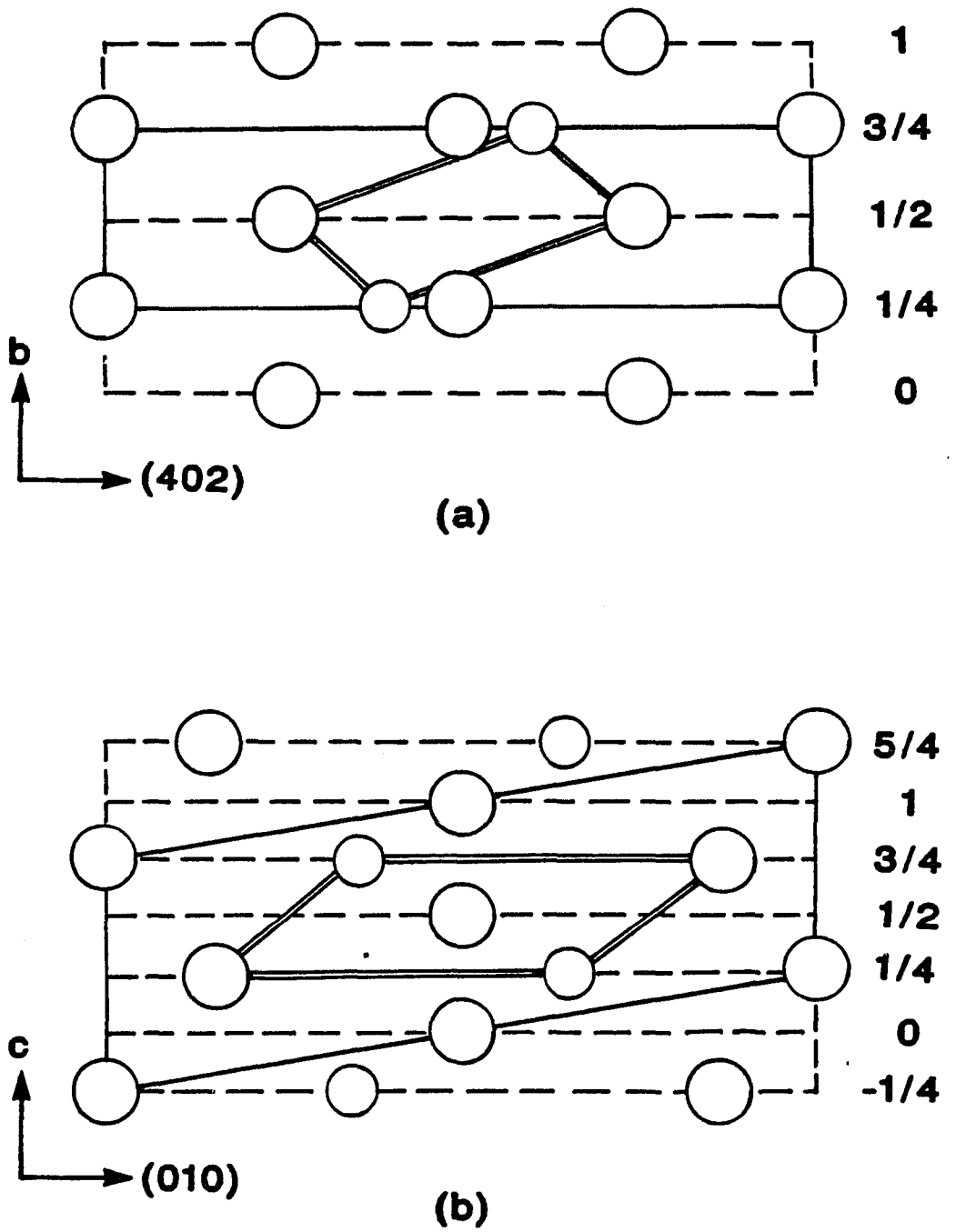

Figure 4. The cross sections of the hexagonal nets in the two structures are drawn (a) parallel to (402) direction for β-Yb_5Sb_3 type; (b) parallel to (010) direction for Mn_5Si_3 type. The solid lines outline the hexagonal nets. The ribbons are outlined by the double lines.

only puckered but also centered by a Ca atom in Mn_5Si_3 type to cause the expansion along the c-axis.

Also, using the resemblance a phase transition between these two types can be imagined. As temperature is raised, the corner-shared hexagonal nets in β-Yb_5Sb_3 type become mobile to interpenetrate to form Mn_5Si_3 type. Of course, the centered Ca in the ribbon in Mn_5Si_3 type is generated during the penetration process.

Comparisons between our M_5X_3 and reported M_5X_3 phases

The possibility of M_5X_3 filled with Y (Y = halogen) to form M_5X_3Y with the same structures as those of M_5X_3 will be demonstrated in part III. Some structures of M_5X_3 such as Ca_5Sb_3 (β-Yb_5Sb_3),[9] Ca_5Bi_3[10] and Sr_5Sb_3[12] have been well investigated by single crystals studies. In these studies, the intensities of reflections were corrected for Lorenz and polarization effects.[12] Sr_5Bi_3 (β-Yb_5Sb_3) and Ca_5Sb_3 (Mn_5Si_3)[9] were investigated by powder patterns only. For Sr_5Bi_3 (Mn_5Si_3), Ba_5Sb_3 and Ba_5Bi_3,[13] authors did not report the refined isotropic temperature parameters, although they did single crystal studies. Since these works were done in the '70s, the possibility of interstitials might have been neglected. Therefore, we compare their data with ours which are listed in Table 3. For easy comparison, the lattice constants of M_5X_3Y from part III are listed together too.

From the table, it is clear that all the lattice constants of M_5X_3 with the Mn_5Si_3 structure are different from ours. Some of them such as Ba_5Sb_3 and Ba_5Bi_3[13] have larger lattice constants while Ca_5Sb_3 (Mn_5Si_3)[9]

and Sr_5Sb_3[12] have smaller a-axes but larger c-axes than ours. Presumably, that is caused by different methods used to derive the lattice constants. Also, the ratios of the lattice constants (c/a) are not comparable (Table 3). Thus, telling whether the reported M_5X_3 are interstitial free can not be made by comparison of the lattice constants or c/a ratio directly.

However, as discussed in Part III, the introduction of interstitials effects the local bonding significantly. For instance, the distances between intratrigonal M(2) atoms in M_3X_3Y with the filled-Mn_5Si_3 type become longer while the interactions between intertrigonal M(2) atoms are about the same compared to those of the M_5X_3. So the ratio between the distances of intertrigonal M(2) atoms and that of intratrigonal M(2) atoms can be used to distinguish whether they are interstitial-free. For example, from our single crystal study the ratio of Sr_5Sb_3 is 1.063 very close to the data (1.061) reported in literature.[12] Thus, the reported Sr_5Sb_3 is confirmed to be a pure binary phase. Using the same way, the ratio reported for Ba_5Sb_3[13] is 1.065 larger than that (1.040) derived from Ba_5Sb_3Cl and 1.050 for Ca_5Sb_3Cl (see Part III). Again, that appears to have been a pure binary phase too. The ratios of Sr_5Bi_3 (Mn_5Si_3)[13] and Ba_5Bi_3[13] are 1.081 and 1.064 indicate that they could be pure binary phases, because they are larger or close to that of Ba_5Sb_3[13] (1.065).

For M_5X_3 with the β-Yb_5Sb_3 type, the reported lattice constants[10,11] all smaller than ours (Table 3), but the c/a or b/a ratios are very close to each other and quite different from those of M_5X_3Y. Therefore, the c/a or b/a ratio alreay indicates that Ca_5Sb_3[10] and

Ca_5Bi_3[11] were truly binary phases. The c/a or b/a of Sr_5Bi_3[9] is close to that of Ca_5X_3 (X = Sb, Bi). Thus, it might be also a pure binary phase.

Using our data, we confirm that the reported Sr_5Sb_3,[12] Ba_5Sb_3,[13] Ca_5Sb_3 (β-Yb_5Sb_3)[10] and Ca_5Bi_3[11] were probably all binary phases without any interstitials inside of them. Also, the reported Sr_5Bi_3 (Mn_5Si_3), Ba_5Bi_3[13] and Sr_5Bi_3 (β-Yb_5Sb_3)[9] could be pure binary phases too. The only unconfirmed compound is Ca_5Sb_3 (Mn_5Si_3); because no single crystal study has been done on it.

Relationship between r_M/r_X and structure type

In Table 1, it seems that there is a clear boundary that separates these two structure types. Furthermore, Ca_5Sb_3 and Sr_5Bi_3 are located on the boundary line. Therefore, the r_M/r_X (using metallic radii for coordination number 12[17]) were calculated and listed in Table 1. Comparing the values of r_M/r_X, it becomes clear that those with $r_M/r_X > 1.3$ form Mn_5Si_3 structure, and with $r_M/r_X < 1.2$, β-Yb_5Sb_3 structure is adopted. When r_M/r_X at ~1.25 both structures can exist. So the structure types might be dependent on the relative size of the M and X atoms.

Conclusion

From the study, the coexistences of hexagonal and orthorhombic phases of Ca_5Sb_3, Sr_5Bi_3 and Yb_5Sb_3 were confirmed, although the transition temperature and the nature of the phase transitions were still not clear. Furthermore, the hexagonal phase is the high temperature phase. From the results, it seems that the time needed to reach equilibria could be longer than 1 month.

The relationship between these two types are discussed using hexagonal nets to reveal the resemblance and differences. Also, the structure type might be determined by the ratio of r_M/r_X.

Reference

1. Franceschi, E. A.; Ricaldone, F. Revue de Chimie Minirale, 1984, 21, 202

2. Hohnke, D.; Parthe, E. J. Less-Common Met. 1969, 17, 291.

3. Bruton, G. D.; Steinfink, H. Inorg. Chem. 1971, 10, 2301.

4. Widera, A.; Schäfer, H. Mater. Res. Bull. 1980, 15, 1805.

5. Eisenmann, B.; Limartha, H.; Schäfer, H. Z. Naturforsch. 1980, 35b, 1518.

6. Schäfer, H.; Eisenmann, B. Rev. Inorg. Chem. 1981, 3, 29.

7. Schäfer, H. Ann. Rev. Mater. Sci. 1985, 15, 1.

8. Niyazova, Z. V.; Vakhobov, A. V.; Dzhuraev, T. D. Inorg. Mat. 1976, 12, 1074.

9. Bruzzone, G.; Franceschi, E.; Merlo, F. J. Less-Common Met. 1978, 60, 59.

10. Martinez-Ripoll, M.; Haase, A. Brauer, G. Acta Crystallogr. 1974, B30, 1083.

11. Martinez-Ripoll, M; Brauer, G. Acta Crystallogr. 1974, B30, 2004.

12. Martinez-Ripoll, M.; Haase, A.; Brauer, G. Acta Crystallogr. 1973, B29, 2717.

13. Eisenmann, B.; Deller, K. Z. Naturforsch. 1975, 30b, 66.

14. Schukarev, S. A.; Morozova, M. P.; Kan, K.-Y.; Kokosh, G. V. J. Gen. Chem. 1956, 26, 1705.

15. Bodnar, R. E.; Steinfink, H. Inorg. Chem. 1967, 6, 327.

16. Wang, Y.; Gabe, E. J.; Calvert, L. D.; Taylor, J. B. Acta Crystallogr. 1976, B32, 1440.

17. Teatum, E. T.; Gschneidner, J., K. A.; Waber, J. T., Rep. LA-4003, 1968, (U. S. Department of Commerce, Springfield VA).

PART III. M_5X_3Y TERNARY SYSTEM

Introduction

Recently, it was found in our laboratory that Zr_5Sb_3[1] with the Mn_5Si_3 structure, which has octahedral holes surrounded by zirconium atoms, could take up to fourteen different elements in this position including transition metal and main group elements. The physical properties of Zr_5Sb_3X (X = interstitial element) also varied dramatically on changing different interstitial elements. For instance, Zr_5Sb_3Fe[2] showed strong ferromagnetism.

The M_5X_3 (M = Ca, Sr, Ba; X = Sb, Bi) phases all have the Mn_5Si_3 structure except Ca_5Bi_3 which belongs to β-Yb_5Sb_3 structure (see Part II). Therefore, a couple of interstitial elements were tried to expand knowledge from Zr_5Sb_3X to the M_5X_3Y (Y = interstitial element) systems.

M_5X_3 with C, O

The studies of M_5X_3Y were started by adding C and O as the interstitial sources, because these are the most common source for the interstitials. Instead of the desired products, M_5X_3Y, the reactions seemed to proceed as follows:

$$5\ Ca + 3\ Sb + C \xrightarrow[1\ week]{870^\circ C} 1/2\ CaC_2 + 3/2\ "Ca_3Sb_2"$$

$$4\ Ca + 3\ Sb + CaO \xrightarrow[1\ week]{900^\circ C} Ca_4Sb_2O + 1/11\ Ca_{11}Sb_{10}[3] + \ldots$$

In the carbon reaction, the product "Ca_3Sb_2" turned out to be a new phase and will be discussed in Part IV. Although these two reactions did

not give the positive results, they all strongly suggested that the products followed simple valence rules. There are five M atoms to furnish ten electrons, while the three Sb or Bi atoms, will each accept three electrons. The total amounts of electrons accepted is nine. There should be one electron available for the interstitial elements. Therefore, halogen was tried as the interstitial elements.

M_5X_3 with Cl

MCl_2 (M = Ca, Sr, Ba) and $CeCl_3$ were used as the source for M_5X_3Y reactions. They were all loaded with the right stoichiometries into tantalum containers, sealed and reacted at 850°C — 950°C, which is above the melting points of all of the chlorides, for 1 — 2 weeks in tube or Marshall furnaces to give M_5X_3Y products with the filled-Mn_5Si_3 structure. The reactions can be represented by the following equations:

$$9/2\ M + 1/2\ MCl_2 + 3\ X \xrightarrow[1 - 2\ \text{weeks}]{850°C - 950°C} M_5X_3Cl,\ M = Ca,\ Sr \text{ and } Ba$$

$$14/3\ Ce + 1/3\ CeCl_3 + 3\ X \xrightarrow[1 - 2\ \text{weeks}]{850°C - 950°C} Ce_5X_3Cl,\ X = Sb \text{ and } Bi$$

The products of the listed reactions were all obtained in quantitative yield (Table 1) and also with good crystallinity judging by the powder patterns of the products. They were chunk-like mixed with a few spherical crystals together and all showed dark gray or black luster. The lattice constants of these compounds were refined by the LATT[4] program and listed in Table 1. Two of them, Ca_5Sb_3Cl and Ba_5Sb_3Cl, were further studied by single crystal diffraction.

Table 1. Lattice constants[a] (Å) of M_5X_3[b] (Mn_5Si_3) and M_5X_3Y[b]

Compounds	a	b	c/a	source
Ca_5Sb_3	9.0321(3)	7.0280(8)	0.778	rxn. 231
Ca_5Sb_3Cl	9.0805(3)	7.0898(6)	0.781	rxn. 296
Ca_5Bi_3Cl	9.220(1)	7.166(1)	0.777	rxn. 300
Ca_5Bi_3Br	9.2743(5)	7.2832(8)	0.785	rxn. 331
Sr_5Sb_3	9.5037(5)	7.4095(8)	0.780	rxn. 368
Sr_5Sb_3Cl	9.5541(4)	7.4328(7)	0.778	rxn. 398
Ba_5Sb_3	9.964(3)	7.694(4)	0.772	rxn. 305
Ba_5Sb_3Cl	10.062(4)	7.770(6)	0.772	rxn. 306
Ba_5Sb_3Br	10.1213(9)	7.852(2)	0.776	rxn. 525
Ba_5Bi_3	10.098(2)	7.768(3)	0.769	rxn. 308
Ba_5Bi_3Cl	10.188(3)	7.837(4)	0.769	rxn. 307
Ba_5Bi_3Br	10.251(2)	7.918(2)	0.772	rxn. 531
Ce_5Sb_3	9.30_2	6.51_4	0.700	ref. 5
Ce_5Sb_3Cl	9.4416(9)	6.568(4)	0.696	rxn. 333
Ce_5Bi_3	9.53_1	6.58_7	0.691	ref. 5
Ce_5Bi_3Cl	9.5812(5)	6.6334(6)	0.692	rxn. 334
Ce_5Bi_3Br	9.6252(5)	6.6974(6)	0.696	rxn. 340

[a]The lattice constants were calculated from as many sharp lines as possible in the powder patterns. Usually, 10 — 20 lines were used for M_5X_3 while 20 — 30 lines were used for M_5X_3Y during the calculations.

[b]All the M_5X_3 and M_5X_3Y are single products from the reactions except Ca_5Sb_3 (see Part II).

The structures of Ca_5Sb_3Cl and Ba_5Sb_3Cl

Suitable spherical crystals of Ca_5Sb_3Cl (0.10 x 0.10 x 0.10 mm) from rxn. 296 and Ba_5Sb_3Cl (0.08 x 0.08 x 0.08 mm) from rxn. 306 were mounted into 0.2-mm capillaries. The singularities and qualities of the crystals were investigated by unaligned oscillation photographs only. No Weissenberg photographs were taken owing to the difficulties of the alignment of crystals without regular shapes. Before collecting the reflection data of the crystals, their singularities were further checked by taking axial photographs on the diffractometer where the lattice constants of Ca_5Sb_3Cl and Ba_5Sb_3Cl were: a = 9.114(2), b = 9.108(2), c = 7.113(4) Å; α = 90.02(4)°, β = 90.08(4)°, γ = 120.05(2)° and a = 10.096(6), b = 10.072(7), c = 7.762(1) Å, α = 90.01(6)°, β = 90.01(6)°, γ = 120.06(5)°, respectively, after indexing 12 and 9 reflections for each crystal from a SYNTEX $P2_1$ diffractometer. Those lattice constants are fairly consistent with the constants indexed from Guinier powder patterns (see Table 2).

All single crystals data sets were collected with monochromatic Kα radiation (λ = 0.71034 Å) on the SYNTEX $P2_1$ four-circle diffractometer. No evidence of decay was noted after checking standard reflections every 75 reflections. Details regarding the data collections and structure solution are summarized in Table 2. Both data sets were corrected for absorption using a psi-scan method with the reflections turned every 10° in ϕ and the program ABSN[6] (2θ = 23.07° and 47.16° for Ba_5Sb_3Cl; 2θ = 18.84° and 23.36° for Ca_5Sb_3Cl). Two octants of data collected with no restrictions yielded an independent data set with no reflections eliminated by a cutoff of 6σ from the average. Structure factors calculations

Table 2. Diffraction and refinement data of M_5Sb_3Cl (M = Ca, Ba)

	Ba_5Sb_3Cl	Ca_5Sb_3Cl
Space group	$P6_3/mcm$ (No. 193)	$P6_3/mcm$ (No. 193)
Z	2	2
Cell dimensions,[a] Å		
a	10.062(4)	9.0805(3)
c	7.770(6)	7.0898(6)
Size of crystal (mm)	0.10 x 0.10 x 0.10	0.08 x 0.08 x 0.08
Octants measured	$h,k,\pm\ell$	$h,k,\pm\ell$
Scan type	ω	ω
2Θ-max, deg. (Mo Kα)	50	50
μ(Mo Kα), cm^{-1}	206.6	105.8
Transm. coeff. range	0.52 — 1.00	0.32 — 1.00
Number of reflections		
meas.	945	737
obs. (>3σ(I))	756	571
indep.	248	190
R(ave)	0.028	0.035
Structure solution		
R^b	0.051	0.038
R_w	0.089	0.059

[a]The cell dimensions calculated from 9 and 15 lines of the Guinier powder pattern of Ba_5Sb_3Cl and Ca_5Sb_3Cl, respectively, Cu $K\alpha_1$, λ = 1.54056 Å.

[b]$R = \sum||F_o| - |F_c||/\sum|F_o|$, $R_w = [\sum w(|F_o| - |F_c|)^2/\sum w|F_o|^2]^{1/2}$.

and full-matrix least-square refinements were carried out with the program ALLS[7] while Fourier series calculations were done with FOUR.[8]

The refinement of the structures of Ca_5Sb_3Cl and Ba_5Sb_3Cl were carried out on the space group $P6_3/mcm$. The initial step used the parameters of Ba_5Sb_3,[9] then added the Cl positions at (0,0,0) and 0,0,1/2). Before doing anisotropic temperature factor refinements, the R values were 0.058 anbd 0.062 for Ca_5Sb_3Cl and Ba_5Sb_3Cl, respectively. The R's and R_w's for Ca_5Sb_3Cl and Ba_5Sb_3Cl ended with 0.038, 0.059 and 0.051, 0.089, respectively, after refining the anisotropic temperature factors. The occupancies of the chlorine atom positions were refined to be fully occupied. The stoichiometries turned out to be $Ca_5Sb_3Cl_{1.00(4)}$ and $Ba_5Sb_3Cl_{1.10(6)}$. The final atom positions and temperature factors are listed in Table 3.

The most significant features are the anisotropic "motion" of the Ca(2), Ba(2) and Cl atoms parallel to the c-axis with $B_{33}/B_{11} \leq 2.2$. Similar phenomena have also been noted in Eu_5As_3.[10] It has the same Mn_5Si_3 structure, the B_{33} of Eu(2) is much larger (about 10 times) compared with B_{11} and B_{22}. To overcome this problem, lower symmetry space groups ($P\bar{6}2c$, $P\bar{6}c2$, $P6_3cm$ and $P\bar{3}c_1$) were tried for averaging and refinements. The R_{ave}'s and R's were all about the same for those space groups. Since the Cl atom is located in the octahedral site composed by Ca(2) or Ba(2) atoms, these phenomena might be caused by the correlation effect between Cl and Ca(2) or Ba(2).

The final difference map of Ca_5Sb_3Cl showed two independent residual densities smaller than 1.2 e/Å^3. The first (~1.0 eÅ^3) was located not

Table 3. The atomic and thermal[a] parameters of M_5Sb_3Cl (M = Ca,Ba)

Atom	x	y	z	B_{11}	B_{22}	B_{33}
Sb	0.3909(1)	0	1/4	0.70(6)	0.81(7)	0.97(8)
Ca(1)	1/3	2/3	0	1.2(1)	B_{11}	0.6(2)
Ca(2)	0.2568(4)	0	3/4	1.0(1)	1.0(2)	2.2(2)
Cl	0	0	0	0.9(2)	B_{11}	1.9(4)
Sb	0.3912(2)	0	1/4	1.5(1)	1.3(1)	1.6(1)
Ba(1)	1/3	2/3	0	2.0(1)	B_{11}	1.1(1)
Ba(2)	0.2578(2)	0	3/4	1.5(1)	1.4(1)	2.6(1)
Cl	0	0	0	1.8(4)	B_{11}	2.4(6)

[a] $B_{12} = 1/2B_{11}$ and $B_{13} = B_{23} = 0$ for all atoms.

only close to Sb (~1.3 A) but also close to Ca(2) (~1.9 A). The second (~0.9 e/A^3) was close to Sb atoms (~2.1 A). For Ba_5Sb_3Cl, there were three independent residual densities in the final difference map with values smaller than 1.2 e/A^3. The first (~1.1 e/A^3) was very close to Ba(2) (~0.1 A). The second one (~0.8 e/A^3) was also close to Ba(2) (~2.0 A), while third one (~0.9 e/A^3) was close to Sb (~0.8 A).

Description of the structure

Figure 1 shows a projection of the structure of M_5Sb_3Cl (M = Ca and Ba) on the [001] plane. The alkaline earth metals occupy two different crystallographic sites corresponding to the point symmetries mm for M(1) forming infinite linear chains parallel to the c-axis and 32 for M(2) which forms trigonal antiprismatic infinite chains also parallel to the c-axis. There is one crystallographic type of Sb atom at the point symmetry mm which is located between those infinite trigonal prisms. Finally, the Cl atom at a point of symmetry of 3m occupies the trigonal antiprism sites generated in the trigonal antiprism chains.

To illustrate the trigonal antiprism chains further, Figure 2 shows the chain extended along the c-axis. The Cl atoms are centered at the octahedral sites formed by six alkaline earth metals. The Sb atoms are outside the chain with the same z coordinates as those of alkaline earth metals M(2).

The crystal structure of M_5Sb_3Cl can also be described in terms of SbM_9 units.[9,11] Each one of these units contains four M(1) and five

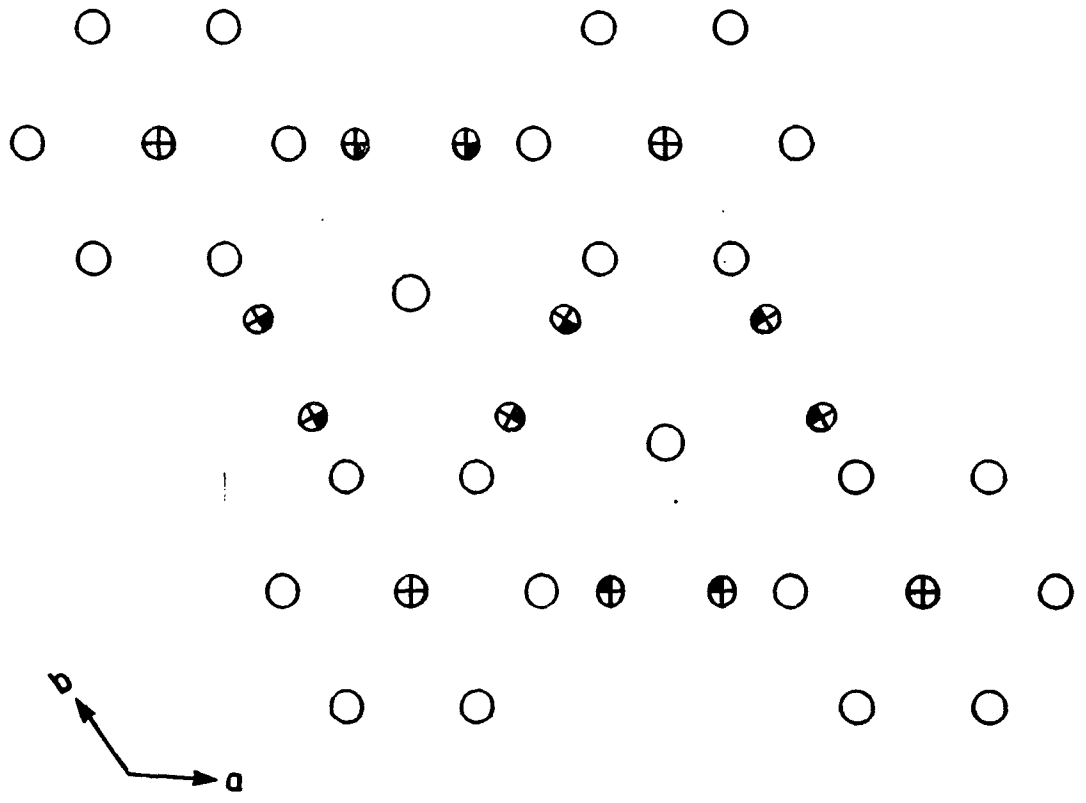

Figure 1. The projection of [001] plane of M_5Sb_3Cl (M = Ca, Ba). Open ellipsoids = Ca or Ba atoms; shaded ellipsoids = Sb atoms; crossed ellipsoids = Cl atoms

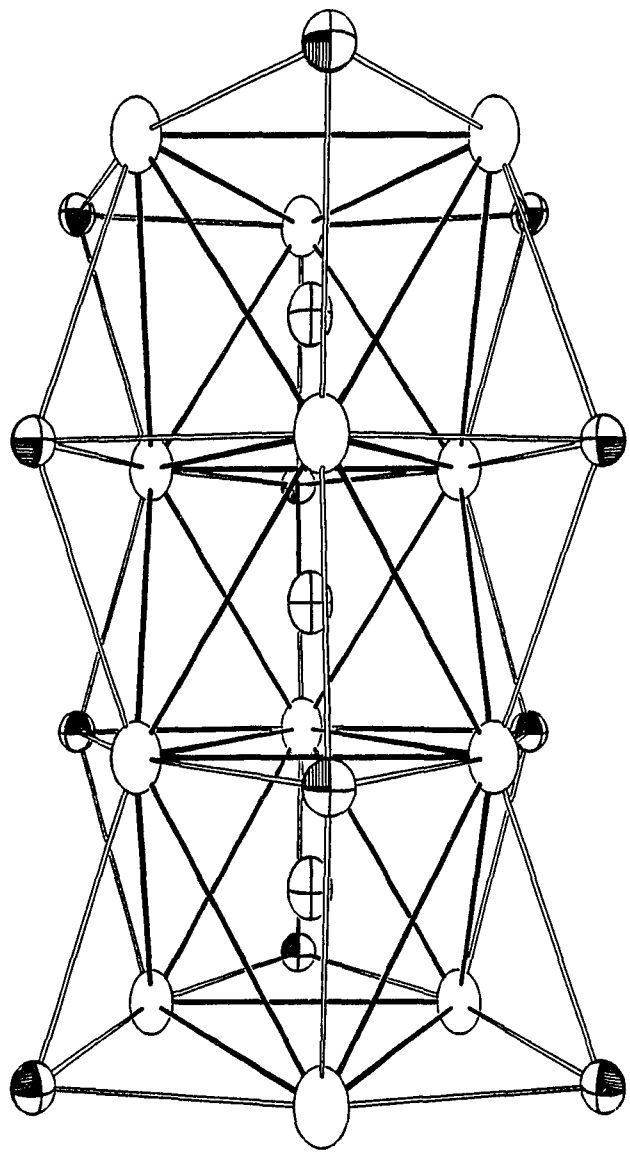

Figure 2. The antiprismatic chain extending along the c-axis in M_5Sb_3Cl. The representations of the ellipsoids are the same as Figure 1

M(2) (antiprism) atoms. These nine M atoms are arranged at the corners of a very distorted tetrakaidecahedron centered by a Sb atom. Such a unit is shown in Figure 3. Each SbM_9 group shares its nine M atoms with other groups but not all the M atoms are equally shared. The M(1) atoms are common to six groups. The M(2) atoms, on the other hand, are shared among five SbM_9 groups only. So the stoichiometry of the combined tetrakaidecahedral is $M(1)_{4/6}M(2)_{5/5}Sb = M(1)_2Ma(2)_3Sb_3 = M_5Sb_3$. Figure 4(a), (b) show the structure of M_5Sb_3 around Sb at z = 0.25 and z = 0.75, respectively, while (c) is composed by superimposing (a) and (b). The octahedral sites of Cl atoms are located at the center of (c).

Comparisons of the bond distances

The main difference of bond distances between Ba_5Sb_3[9] and Ba_5Sb_3Cl is the distances between trigonally related Ba(2) atoms. It expands from 4.32 Å in Ba_5Sb_3 to 4.493(5) Å in Ba_5Sb_3Cl. This is due to the insertion of Cl in the latter causing such expansion. However, the distances between intertrigonal Ba(2) atoms did not change very much from 4.60 Å in Ba_5Sb_3 to 4.672(3) Å in Ba_5Sb_3Cl. These indicate that the interaction between intratrigonal Ba(2) atoms becomes weaker as Cl is added into the octahedral sites while the interactions between intertrigonal Ba(2) is the same or even less than that of Ba_5Sb_3. All the distances (<4.8 Å) are listed in Table 4. The distances in Ca_5Sb_3Cl are also summarized in Table 4. Since no single crystal study of Ca_5Sb_3 (Mn_5Si_3) has been reported, no further comparison between Ca_5Sb_3 and Ca_5Sb_3Cl can be made.

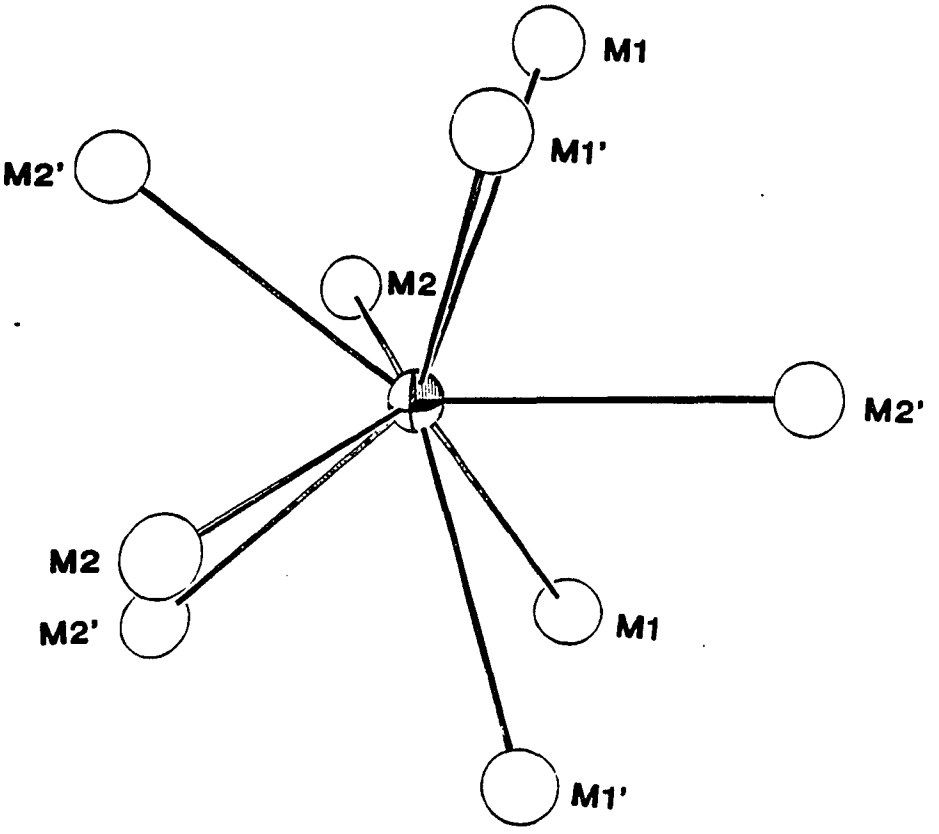

Figure 3. Arrangements of [SbMg] in M_5Sb_3Cl. Two minor planes pass through Sb, containing the two M_2 and two M_2' atoms, respectively

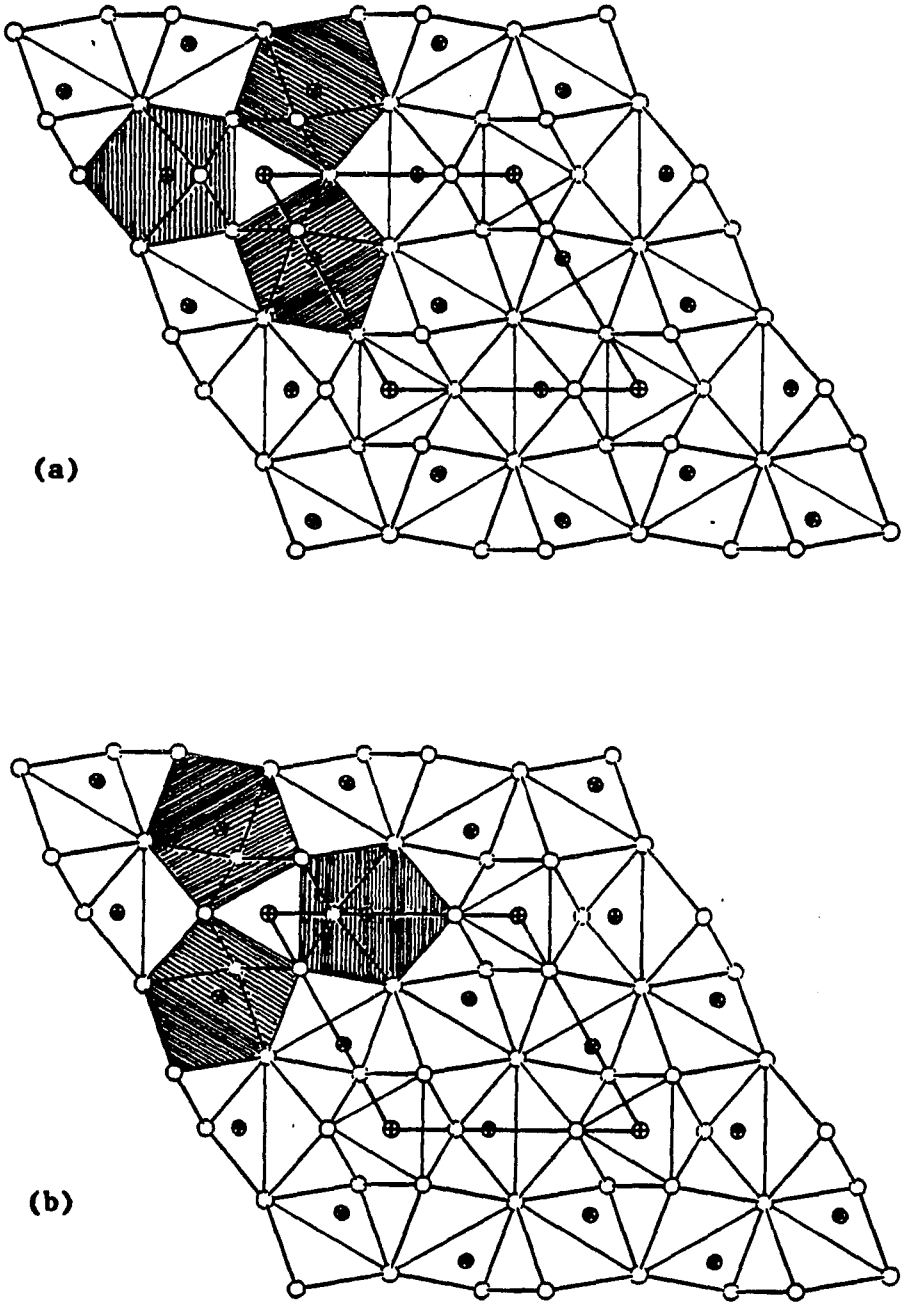

Figure 4. The linkage of [SbMg] in M_5Sb_3Cl (a) projection on [001] plane at z = 0.25 for Sb atoms (b) at z = 0.75 for Sb atoms. To illustrate the units of [SbMg], some of them are shaded

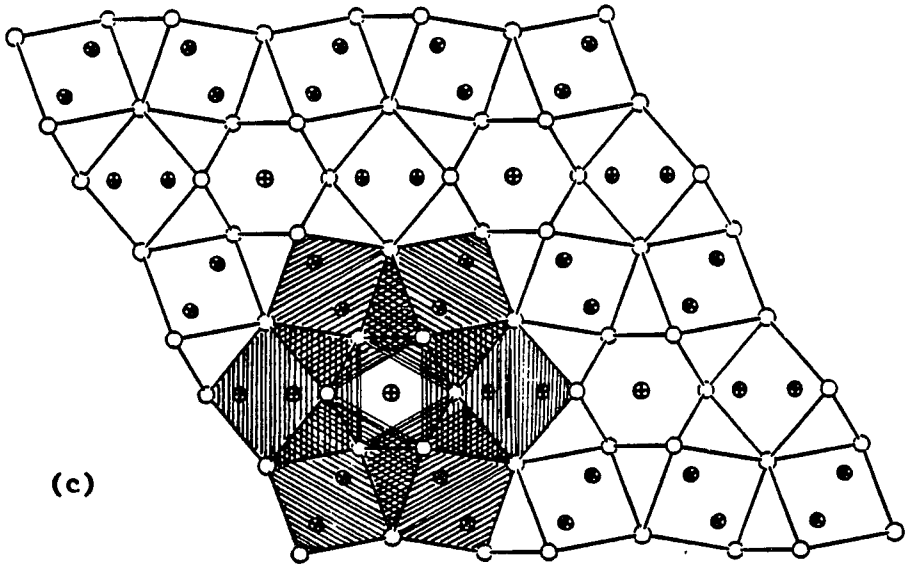

Figure 4. (continued)
(c) The operlapping of (a) and (b) around Cl atoms

Table 4. Distances (Å) of Ba_5Sb_3, Ba_5Sb_3Cl and Ca_5Sb_3Cl

Atom 1 —	Atom 2	Ba_5Sb_3[a]	Ba_5Sb_3Cl	Ca_5Sb_3Cl
Sb —	M(2) (2x)	3.43	3.466(3)	3.135(1)
Sb —	M(2) (1x)	3.57	3.532(4)	3.209(4)
Sb —	M(2) (2x)	4.11	4.110(3)	3.761(1)
Sb —	M(1) (4x)	3.63	3.662(2)	3.327(1)
M(1) —	M(1) (2x)	3.87	3.885(4)	3.556(2)
M(1) —	M(2) (6x)	4.27	4.260(3)	3.871(2)
M(1) —	Sb (6x)	3.63	3.662(2)	3.327(1)
M(2) —	M(1) (4x)	4.27	4.260(3)	3.871(2)
M(2) —	M(2) (2x)	4.32	4.493(5)	4.053(7)
M(2) —	M(2) (4x)	4.60	4.672(3)	4.257(3)
M(2) —	Sb (2x)	3.43	3.466(3)	3.135(1)
M(2) —	Sb (1x)	3.57	3.532(4)	3.209(4)
M(2) —	Sb (2x)	4.11	4.110(3)	3.761(2)
Cl —	M(2) (6x)		3.241(2)	2.939(3)
Cl —	Cl (2x)		3.885(4)	3.556(2)
Cl —	Sb (6x)		4.389(3)	3.981(1)

[a]These values adopted from ref. 9.

Bonding distances between M and Cl in M_5Sb_3Cl

The distances between M and Cl are around the order of the sum of the ionic radii,[12] e.g., the sum of the ionic radius of Ca^{+2} and Cl^- is 2.81 Å, while the distance between Ca and Cl in Ca_5Sb_3Cl is 2.939(2) Å. The same thing is observed in Ba_5Sb_3Cl. The sum of ionic radii[12] of Ba^{2+} and Cl^- is 3.16 Å is a little bit shorter than the distance (3.241(2) Å) between Ba and Cl in Ba_5Sb_3Cl too. Probably, the same conclusion can be applied to other M_5X_3Cl and M_5X_3Br phases.

M_5X_3 With Br

The syntheses of Ca_5Bi_3Br, Ce_5Bi_3Br, Ba_5Sb_3Br and Ba_5Bi_3Br were all from the elementary starting materials of Ca, Ce, Ba and Bi or Sb plus the appropriate amount of $BiBr_3$ or $BaBr_2$. The reactions were run at ~890°C for a couple days. The reactions can be represented as the following equation:

$$5\ Ca + 8/3\ Bi + 1/3\ BiBr_3 \longrightarrow Ca_5Bi_3Br$$

$$5\ Ce + 8/3\ Bi + 1/3\ BiBr_3 \longrightarrow Ce_5Bi_3Br$$

$$9/2\ Ba + 1/2\ BaBr_2 + 3\ Bi \longrightarrow Ba_5Bi_3Br$$

$$9/2\ Ba + 1/2\ BaBr_2 + 3\ Sb \longrightarrow Ba_5Sb_3Br.$$

The structures of M_5X_3Br are the same with M_5X_3Cl. Most of the products are dark gray with metallic luster. The lattice constants of them are also listed in Table 1. Compared with M_5X_3Cl, the lattice constants of M_5X_3Br are much larger.

M_5X_3 With F

Syntheses of Ca_5Sb_3F and Ca_5Bi_3F

The first attempt to make Ca_5Sb_3F at 900°C by loading stoichiometric amounts of elementary calcium, antimony and calcium fluoride (Fisher Co.) did not work. Since the melting point of CaF_2 (1403°C) is very high compared to the reaction temperature tried, the reaction was repeated by induction heating (~1250°C) for a couple of hours. The powder pattern of the product did not show the presence of CaF_2. It also showed the expansion of the lattice constants of the β-Yb_5Sb_3 structure along b and c axes and shrinkage at a direction (see Table 5). Using the similar condition, the analogue Ca_5Bi_3F also was synthesized. The lattice constants of Ca_5Bi_3F calculated by LATT program also showed the same trends as Ca_5Sb_3F (Table 5). Also, the powder patterns indicated that the yields were very high (>95%) in both reactions. Both products also show gray metallic luster. However, it was observed that the annealing of the product at 850°C after quenching from the high temperature in induction furnace did help the growth of the single crystals and improve the crystallinity of the products.

Structure determinations

A suitable size crystal of Ca_5Sb_3F (0.225 x 0.175 x 0.10 mm) was mounted into 0.2-mm capillary and used for X-ray measurement. The cell indexing and data collection were done on an automatic four-circle diffractometer DATEX. A total of 2386 intensity data were collected with $2\theta(max) = 55°$ (Mo Kα radiation, ω-scan mode). After correction for

Table 5. Orthorhombic lattice constants of Ca_5X_3 (β-Yb_5Sb_3) and Ca_5X_3F

	Ca_5Sb_3[a]	Ca_5Sb_3F	Ca_5Bi_3[a]	Ca_5Bi_3F
a	12.537(4)	12.442(2)	12.766(1)	12.602(2)
b	9.555(2)	9.653(2)	9.706(2)	9.771(2)
c	8.296(2)	8.381(2)	8.437(2)	8.501(2)
No. lines	(14/14)	(38/40)	(20/20)	(18/19)
V	993.9(5)	1006.6(3)	1045.3(3)	1046.8(3)
rxn. #	231	364	408	407

[a]The reaction conditions and yields of Ca_5Sb_3 and Ca_5Bi_3 in this structure have already been discussed in Part II.

Lorentz, polarization and absorption effects 2147 reflections with $I \geq 3\sigma(I)$ were used for the structure determination. The systematic absence led to the space group Pnma (No. 62) which is the same as Ca_5Sb_3 (β-Yb_5Sb_3).[13] Since the lattice constants of Ca_5Sb_3F are close to those of Ca_5Sb_3, the refinement of the structure started with the atom positions of Ca_5Sb_3.[13] After two antimony and four calcium atom positions were refined, R and R_W were 0.108 and 0.143. The isotropic temperature parameter refinement led to R and R_W of 0.089 and 0.122. From the difference map, the fluorine position was derived. After adding the fluorine atom and doing anisotropic temperature parameter refinement, the R and R_W turned out to be 0.050 and 0.064. The occupancy of the fluorine position also refined to be fully occupied. Finally, the secondary extinction correction led to 0.025 and 0.033 for R and R_W, respectively. The final difference map did not show any peak greater than 1.2 e/A^3. The maximum residual density group was located at (0.156, 0.906, 0.0625) which is close to the Sb(1) atoms (0.95 A). The refinement data and atom and temperature parameters are listed in Tables 6 and 7, respectively.

The structure of Ca_5Bi_3F also was solved by using the DATEX diffractometer and following a similar procedure to that described for Ca_5Sb_3F case. The occupancy of the fluorine position refined to be fully occupied too. However, the peak profiles of the reflections collected indicated how the crystal might be out of center or be cracked. Thus, the final R and R_W were only lowered to 0.060 and 0.058. The refinement data and thermal, and positional parameters for Ca_5Bi_3F also listed in

Table 6. Diffraction and refinement data of Ca_5Sb_3F[a] and Ca_5Bi_3F[a]

	Ca_5Sb_3F	Ca_5Bi_3F
Space group	Pnma (No. 62)	Pnma (No. 62)
Z	4	4
Cell dimensions,[b] Å		
a	12.442(2)	12.602(2)
b	9.653(2)	9.771(2)
c	8.381(2)	8.501(2)
Size of crystal (mm)	0.23 x 0.18 x 0.10	0.13 x 0.18 x 0.03
Octants measured	$\pm h, \pm k, \ell$	$\pm h, \pm k, \ell$
Scan type	ω	ω
2θ-max, deg. (Mo Kα)	55	55
μ(Mo Kα), cm^{-1}	105.3	530.13
Transm. coeff. range	0.15 – 0.17	0.05 – 0.40
Number of reflections		
meas.	2386	2072
obs. ($>3\sigma(I)$)	2147	1769
indep.	1127	974
R(ave)	0.019	0.037
Structure solution		
R^c	0.025	0.060
R_w	0.033	0.058

[a]Three ϕ-scans were applied for each.

[b]The celldimensions indexed from 38 and 18 lines of the Guinier powder patterns of Ca_5Sb_3F and Ca_5Bi_3F, respectively, Cu $K\alpha_1$, λ = 1.54056 Å.

[c]$R = \sum||F_o| - |F_c||/\sum|F_o|$, $R_w = [\sum w(|F_o| - |F_c|)^2/\sum w|F_o|^2]^{1/2}$.

Table 7. Positional and thermal parameters of Ca_5Sb_3F and Ca_5Bi_5F

Atom	x	y	z	B_{11}
Sb(1)	0.17037(3)	-0.01878(4)	0.07525(4)	1.34(2)
Sb(2)	-0.01841(4)	1/4	0.41771(5)	1.33(2)
Ca(1)	0.07273(9)	0.0422(1)	0.6933(1)	1.94(4)
Ca(2)	0.2290(1)	1/4	0.3229(2)	1.38(5)
Ca(3)	0.2855(1)	1/4	0.8561(2)	1.24(5)
Ca(4)	0.5074(1)	1/4	0.4556(2)	1.33(5)
F[a]	0.6036(3)	1/4	0.6971(5)	1.7(2)
Bi(1)	0.17092(7)	-0.01882(8)	0.0766(1)	0.93(4)
Bi(2)	-0.0188(1)	1/4	0.4171(2)	0.95(5)
Ca(1)	0.0722(4)	0.0443(4)	0.6939(6)	1.5(2)
Ca(2)	0.2300(6)	1/4	0.3209(8)	1.2(3)
Ca(3)	0.2835(6)	1/4	0.8583(9)	1.0(3)
Ca(4)	0.5077(6)	1/4	0.4683(9)	0.8(3)
F[b]	0.605(2)	1/4	0.697(3)	1.7(3)

[a]Refined occupancy = 1.01(1).

[b]Isotropic temperature factor only and refined occupancy 0.98(5).

B_{22}	B_{33}	B_{12}	B_{13}	B_{23}
1.31(2)	1.31(2)	0.052(9)	-0.109(9)	-0.02(1)
1.04(2)	1.12(2)	0	0.09(1)	0
1.14(4)	1.55(4)	-0.03(3)	-0.27(3)	-0.16(3)
1.82(6)	1.56(8)	0	-0.11(4)	0
1.96(6)	1.57(6)	0	-0.17(4)	0
1.54(6)	1.25(5)	0	-0.17(4)	0
1.0(2)	1.3(2)	0	0.0(0)	0
1.30(3)	1.61(3)	0.06(2)	-0.16(3)	-0.03(3)
1.11(4)	1.41(5)	0	0.12(5)	0
1.2(1)	1.7(2)	-0.0(1)	-0.5(2)	0.0(1)
1.8(2)	1.5(3)	0	-0.0(3)	0
1.9(2)	1.7(3)	0	-0.1(3)	0
1.5(2)	1.8(3)	0	-0.1(3)	0

Tables 6 and 7, respectively. The poorer refinement could be seen in the form of the thermal parameters. For instance, the B_{11} of F atom was 2.7 (12). However, it should be noted the absorption coefficient was unusually high 530.1 cm^{-1} due to the heavy Bi atoms, and the crystal was a good diffractor while the 2θ collected only set at 55°. To further investigate the refinement, the final difference map was carefully checked. The difference map showed no peaks (or positions) with densities greater than 1.5 $e/Å^3$. Most of them were found around Bi(1), Bi(2), Ca(1) and Ca(2) atoms at distances from 0.16 Å to 2.26 Å. The result confirmed that the data collection was not done well, because it always showed the streaking along the b-axis on the map.

Description of the structure[14]

Ca_5Sb_3F or Ca_5Bi_3F has a double layer structure (Figure 5). Layers of Ca atoms in the special positions 4(c) with atoms at y = 1/4 and 3/4 (open ellipsoids) that are almost superimposed form trigonal-hexagonal network (Figure 5), then Sb (or Bi) atoms also at y = 1/4 and y = 3/4 almost center the hexagons but are displaced to opposite ends on alternate layers. These successive layers at Ca atoms thus form slightly skewed hexagonal and trigonal prisms. The Sb or Bi and Ca atoms in the general positions 8(d) with y ≈ 0 or 1/2 (shaded ellipsoids) form a puckered diamond-pentagon network (not shown). These Sb or Bi atoms center the trigonal prisms while pairs of Ca atoms center the hexagonal prism.

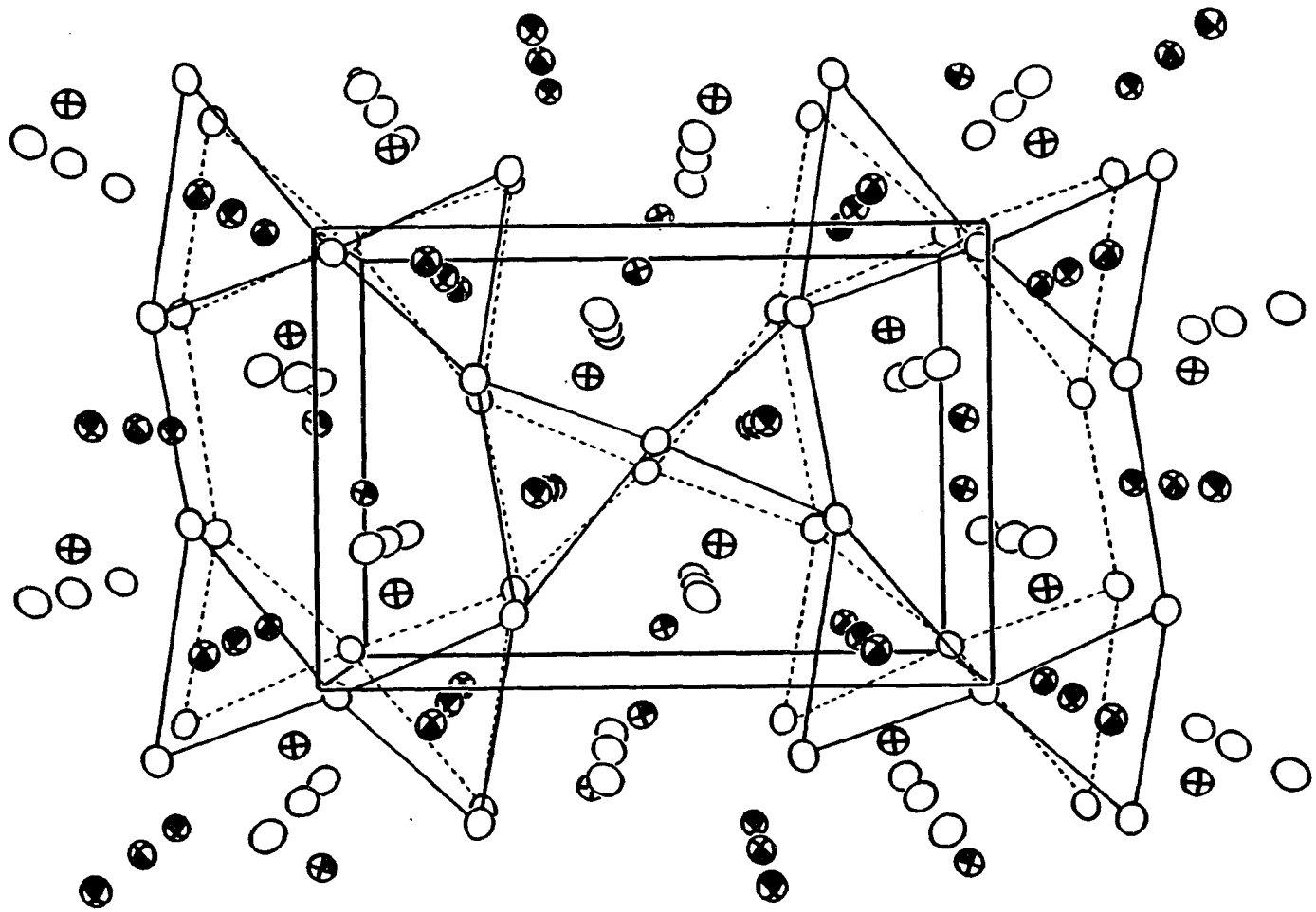

Figure 5. The unit cell of Ca_5Sb_3F projected on [010] plane. Open ellipsoids: Ca atoms; shaded ellipsoids: Sb atoms; cross ellipsoids: F atoms. Dashed lines connect Ca atoms at y = 1/4 while solid lines connect Ca atoms at y = 3/4

The F atoms (crossed ellipsoids) are located at two opposite ends of the hexagon with $y = 1/4$ and $3/4$. Thus, the structure of Ca_5Sb_3F or Ca_5Bi_3F is composed of columns of $[SbCa_6]$ or $[BiCa_6]$ trigonal prisms stacked on their triangular faces parallel to b-axis and sharing edges to form hexagonal channels of Ca atoms (Figure 6) occupied by $[Ca_2Sb_2]$ or $[Ca_2Bi_2]$ parallelograms sharing Sb corners to form a slightly twisted ribbon. The F atoms occupy the rather distorted tetrahedral sites formed by two Ca atoms in the ribbon and two Ca atoms from the hexagonal channels (Figure 7).

Comparisons between Ca_5X_3 and Ca_5X_3F (X = Sb and Bi)

In contrast to M_5X_3 and Ca_5X_3F (X = Sb and Bi), the lattice constants of Ca_5X_3F have not expanded along three axes compared with those of Ca_5X_3 (β-Yb_5Sb_3),[13,15] but only along b and c axes. This reflects to the atom-atom distances (Table 8). Not all the distances became longer after F was inserted. To rationalize this, the environment around F needs to be considered. The F is located at a distorted tetrahedral sites which is composed of two Ca(1), one Ca(3) and one Ca(4) atoms (Figure 7). The distances between F and Ca atoms in Ca_5Sb_5F are not equal ranging from 2.237(2) Å to 2.301(5) Å and one of the angles (127.2(2)°) deviates well from the ideal tetrahedral angle 109.5° (Table 9). Since the distances of F to Ca(4) and Ca(3) are the longer two, the expansion caused by inserting F might not be as significant as the coulomb interaction of the oppositely charged calcium cations and fluoride. Therefore, the a-axis of Ca_5X_3F are smaller than those of Ca_5X_3.

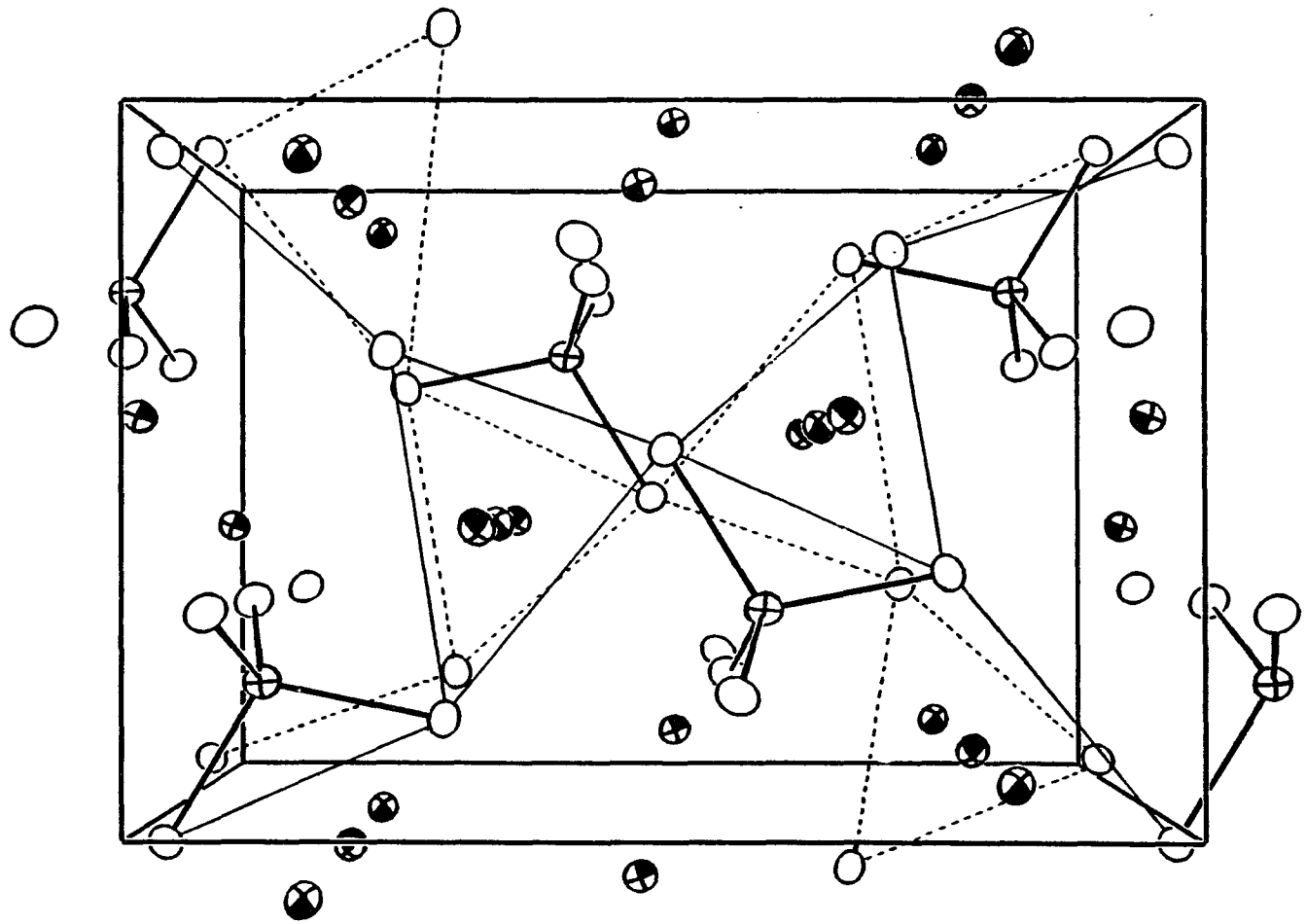

Figure 6. The same projection of Ca_5Sb_3F as in Figure 5 except the shortest distances between F and the four neighboring Ca atoms are drawn in

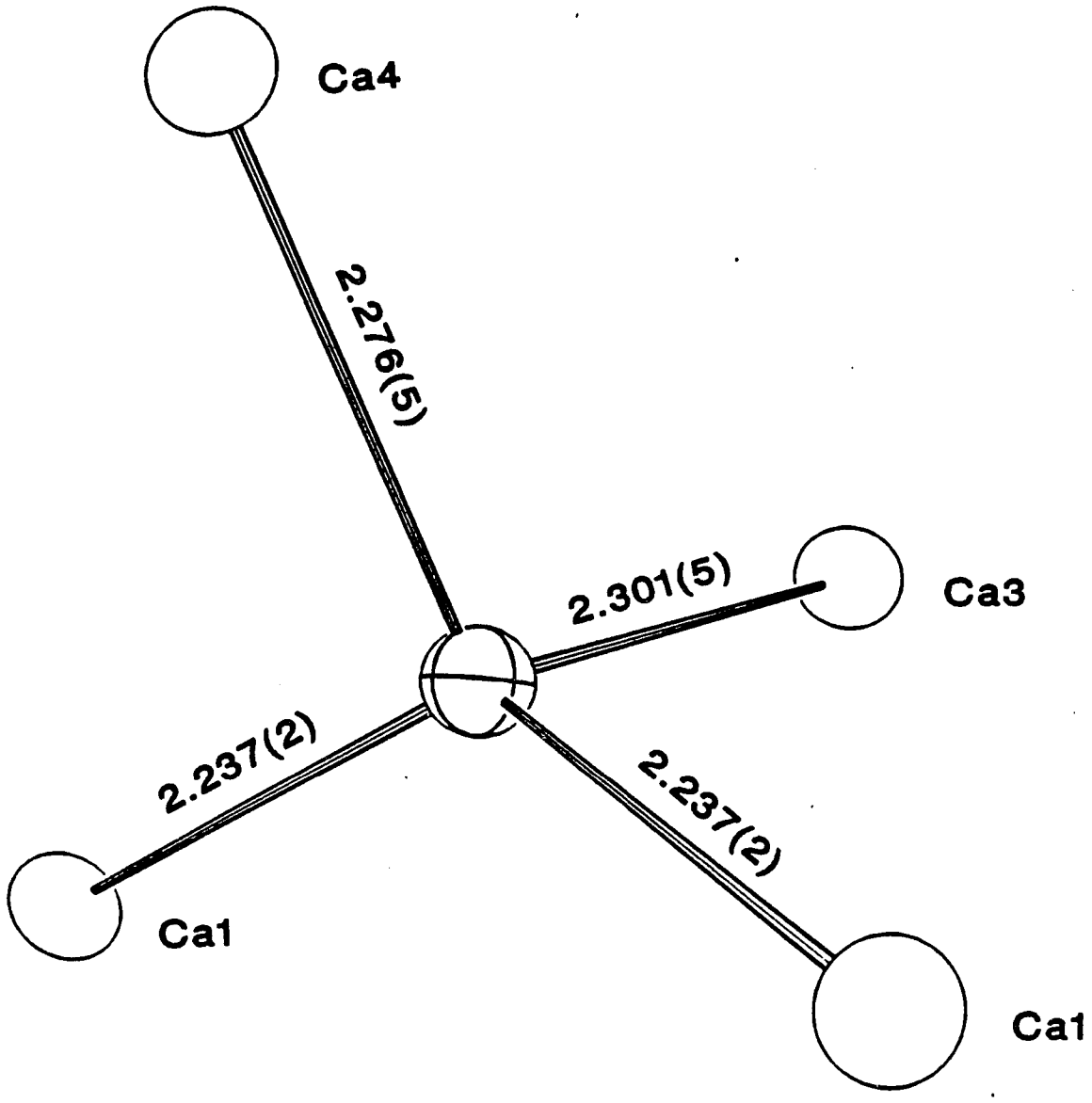

Figure 7. The chemical environment around F in Ca_5Sb_3F

Table 8. Comparisons of bonding distandes between Ca_5X_3[13,15] and Ca_5X_3F (X = Sb, Bi)

Atom 1 —	Atom 2		Ca_5Sb_3	Ca_5Sb_3F	Ca_5Bi_3	Ca_5Bi_3F
Ca(1) —	X(2)	(x1)	3.029(2)	3.042(1)	3.093(8)	3.100(4)
Ca(1) —	X(2)	(x1)	3.207(2)	3.259(1)	3.244(8)	3.300(5)
Ca(1) —	X(1)	(x1)	3.357(2)	3.345(1)	3.409(8)	3.396(6)
Ca(1) —	X(1)	(x1)	3.362(2)	3.471(1)	3.427(8)	3.537(5)
Ca(1) —	X(1)	(x1)	3.670(2)	3.593(1)	3.757(8)	3.641(5)
Ca(1) —	Ca(4)	(x1)	3.564(2)	3.582(2)	3.631(8)	3.599(8)
Ca(1) —	Ca(3)	(x1)	3.576(2)	3.584(2)	3.641(8)	3.617(8)
Ca(1) —	Ca(4)	(x1)	3.721(2)	3.759(2)	3.804(8)	3.837(7)
Ca(1) —	Ca(1)	(x1)	3.798(2)	3.795(2)	3.854(8)	3.864(10)
Ca(1) —	Ca(2)	(x1)	3.866(2)	3.895(2)	3.944(8)	3.955(7)
Ca(1) —	Ca(1)	(x1)	3.948(2)	4.007(2)	3.972(8)	4.021(8)
Ca(1) —	Ca(3)	(x1)	4.100(2)	4.109(2)	4.143(8)	4.181(8)
Ca(1) —	Ca(2)	(x1)	4.123(2)	4.171(2)	4.177(8)	4.248(8)
Ca(1) —	Ca(3)	(x1)	4.314(2)	4.360(2)		
Ca(2) —	X(2)	(x1)	3.164(2)	3.171(2)	3.218(8)	3.240(8)
Ca(2) —	X(1)	(x2)	3.283(2)	3.316(1)	3.340(8)	3.374(5)
Ca(2) —	X(1)	(x2)	3.360(2)	3.398(1)	3.412(8)	3.430(5)
Ca(2) —	X(2)	(x1)	3.778(2)	3.727(2)	3.840(8)	3.758(8)
Ca(2) —	Ca(4)	(x1)	3.641(2)	3.656(2)	3.697(8)	3.718(11)
Ca(2) —	Ca(4)	(x1)	3.682(2)	3.661(2)	3.746(8)	3.727(10)
Ca(2) —	Ca(1)	(x2)	3.866(2)	3.895(2)	3.944(8)	3.955(7)
Ca(2) —	Ca(3)	(x1)	3.969(2)	3.973(2)	4.049(8)	3.990(10)
Ca(2) —	Ca(1)	(x2)	4.123(2)	4.171(2)	4.177(8)	4.248(8)
Ca(2) —	Ca(3)	(x1)	4.462(2)	>4.5		
Ca(3) —	X(2)	(x1)	3.068(2)	3.084(2)	3.118(8)	3.140(8)
Ca(3) —	X(2)	(x2)	3.291(2)	3.286(1)	3.349(8)	3.342(6)
Ca(3) —	X(1)	(x2)	3.425(2)	3.483(1)	3.484(8)	3.515(5)
Ca(3) —	Ca(1)	(x2)	3.576(2)	3.584(2)	3.641(8)	3.617(8)
Ca(3) —	Ca(4)	(x1)	3.854(2)	3.761(2)	3.947(8)	3.775(10)
Ca(3) —	Ca(2)	(x1)	3.969(2)	3.973(2)	4.049(8)	3.990(10)
Ca(3) —	Ca(1)	(x2)	4.100(2)	4.109(2)	4.143(8)	4.181(8)
Ca(3) —	Ca(4)	(x1)	4.200(2)	4.274(2)	4.258(8)	4.356(11)
Ca(3) —	Ca(1)	(x2)	4.314(2)	4.360(2)		
Ca(3) —	Ca(2)	(x1)	4.462(2)	>4.5		

Table 8. (continued)

Atom 1 —	Atom 2		Ca_5Sb_3	Ca_5Sb_3F	Ca_5Bi_3	Ca_5Bi_3F
Ca(4) —	X(2)	(x1)	3.212(2)	3.226(2)	3.255(8)	3.293(8)
Ca(4) —	X(1)	(x2)	3.258(2)	3.268(1)	3.304(8)	3.320(5)
Ca(4) —	X(1)	(x2)	3.258(2)	3.305(1)	3.324(8)	3.358(4)
Ca(4) —	Ca(1)	(x2)	3.564(2)	3.582(2)	3.631(8)	3.599(8)
Ca(4) —	Ca(2)	(x1)	3.641(2)	3.656(2)	3.697(8)	3.718(11)
Ca(4) —	Ca(2)	(x1)	3.682(2)	3.661(2)	3.746(8)	3.727(10)
Ca(4) —	Ca(1)	(x2)	3.721(2)	3.759(2)	3.804(8)	3.837(7)
Ca(4) —	Ca(3)	(x1)	3.854(2)	3.761(2)	3.947(8)	3.775(10)
Ca(4) —	Ca(3)	(x1)	4.200(2)	4.274(2)	>4.5	4.356(11)
X(1) —	Ca(4)	(x1)	3.258(2)	3.268(1)	3.304(8)	3.320(5)
X(1) —	Ca(4)	(x1)	3.258(2)	3.286(1)	3.324(8)	3.358(6)
X(1) —	Ca(2)	(x1)	3.283(2)	3.305(1)	3.340(8)	3.379(4)
X(1) —	Ca(3)	(x1)	3.291(2)	3.316(1)	3.349(8)	3.342(6)
X(1) —	Ca(1)	(x1)	3.357(2)	3.345(1)	3.409(8)	3.396(6)
X(1) —	Ca(2)	(x1)	3.360(2)	3.398(1)	3.412(8)	3.430(5)
X(1) —	Ca(1)	(x1)	3.362(2)	3.471(1)	3.427(8)	3.537(5)
X(1) —	Ca(3)	(x1)	3.425(2)	3.483(1)	3.484(8)	3.515(5)
X(1) —	Ca(1)	(x1)	3.670(2)	3.593(1)	3.757(8)	3.641(5)
X(1) —	X(1)	(x1)	4.412(2)	4.427(1)	4.492(8)	>4.5
X(1) —	X(1)	(x1)	4.478(2)	4.459(1)	>4.5	>4.5
X(2) —	Ca(1)	(x2)	3.029(2)	3.042(1)	3.093(8)	3.100(4)
X(2) —	Ca(3)	(x1)	3.068(2)	3.084(2)	3.118(8)	3.140(8)
X(2) —	Ca(2)	(x1)	3.164(2)	3.171(2)	3.218(8)	3.240(8)
X(2) —	Ca(1)	(x2)	3.206(2)	3.226(2)	3.244(8)	3.300(5)
X(2) —	Ca(4)	(x1)	3.212(2)	3.259(1)	3.255(8)	3.293(8)
X(2) —	Ca(2)	(x1)	3.778(2)	3.727(2)	3.840(8)	3.758(8)
F —	Ca(1)	(x2)		2.237(2)		2.25(1)
F —	Ca(4)	(x1)		2.276(5)		2.30(2)
F —	Ca(3)	(x1)		2.301(5)		2.29(3)
F —	X(1)	(x2)		3.550(3)		3.61(1)
F —	X(2)	(x1)		3.564(4)		3.63(2)
F —	X(1)	(x2)		4.059(4)		4.09(2)
F —	Ca(3)	(x1)		4.166(5)		4.28(2)
F —	X(1)	(x2)		4.192(4)		4.28(3)
F —	Ca(2)	(x1)		4.311(5)		4.39(2)

Table 9. Bonding distances (A) and angles (°) of $[FCa_4]$ in Ca_5Sb_3F

Atom 1 —	Atom 2		Atom 1 — Atom 2 — Atom 3				
F	— Ca(1) (x2)	2.237(2)	Ca(1)	— F —	Ca(1)	127.2(2)	
F	— Ca(4) (x1)	2.276(5)	Ca(1)	— F —	Ca(3)	104.3(1)	
F	— Ca(3) (x1)	2.301(5)	Ca(1)	— F —	Ca(4)	105.0(1)	
			Ca(3)	— F —	Ca(4)	110.5(2)	

The distances between Ca and F in Ca_5X_3F are from 2.237 A to 2.301 A, slightly shorter than that in CaF_2[16] which is 2.36573 (1) A while the distances between F and X atoms range from 3.350 A to 4.09 A, quite a bit longer than those of XF_3[17,18] which are from 2.1 A — 2.8 A, and the former apparently belong to nonbonding distances.

In an attempt to synthesize Ba_5X_3F, BaF_2, from drying the precipitate formed between $BaCO_3$ and HF solution, was used as the source of F together with similar reaction conditions as those for Ca_5X_3F. This did not give promising results. The gray BaF_2 powder was the only recognized product in the powder pattern of the product.

M_5X_3 With S

Since the formation of Ca_5Sb_3Cl had been confirmed by powder pattern and the single crystal studies, it was thought that the sites of Cl positions might be occupied by other nonmetal elements. Thus, rxn. 320 was run to make $Ca_5Sb_3S_{1/2}$. The products are chunk-like with dark gray luster. The powder pattern of the products was complicated and completely different from any M_5X_3 phases.[19] The cell constants determined by TREOR[20] program (19 lines used) indicated a cubic cell with a = 9.6508(3) A, meaning it was also a pure single phase. After reviewing the literature, it was concluded the product's composition should be $Ca_4Sb_{2.4}S_{0.4}$ which stoichiometry is exactly equal to that of $Ca_5Sb_3S_{1/2}$. The structure of $Ca_4Sb_{2.4}S_{0.4}$ belongs to the anti- and defect-Th_3P_4[21] type structure. The calculated and observed intensities from the powder pattern are listed in Table 10. In the structure, Sb or S are surrounded by eight Ca atoms forming an octaverticon (Figure 8(b)) while Ca atoms are at distorted octahedral sites composed of six S and/or Sb atoms (Figure 8(a)) if the vacancies are neglected. In $Ca_4Sb_{2.4}S_{0.4}$, one half of the distorted octahedral CaX_6 (X = Sb, S) groups share two faces (and three edges) and the others share three faces (and one edge) with other octahedra meeting at the common (Figure 8(a)).

Since $Ca_4Sb_{2.4}S_{0.4}$ has a defect structure, it was thought a range of $Ca_4Sb_xS_y$ might exist. Playing a simple mathematical game and assuming $3x + 2y = 8$ and $x + y \leq 3$, the possible range of x and y would be $0 \leq y \leq 1$ and $2 \leq y \leq 8/3$. The two extreme cases are Ca_4Sb_2S

Table 10. The calculated[a] and observed powder patterns for $Ca_4Sb_{2.4}S_{0.4}$

h	k	ℓ	d_{calc}	d_{obs}	I_{calc}	I_{obs}
2	1	1	3.9399	3.941(4)	42	50
2	2	0	3.4121	3.413(3)	1	3
3	1	0	3.0519	3.052(3)	100	100
3	2	1	2.5793	2.579(2)	62	60
4	0	0	2.4127	2.413(2)	1	1
4	2	0	2.1580	2.158(1)	29	35
3	3	2	2.0576	2.058(1)	19	25
4	2	2	1.9700	1.970(1)	10	12
4	3	1, 5 1 0	1.8923	1.8930(9)	22	30
5	2	1	1.7620	1.7621(8)	5	10
4	4	0	1.7060	1.7060(7)	2	2
5	3	2, 6 1 1	1.5656	1.5656(6)	36	40
6	2	0	1.5259	1.5259(6)	19	20
5	4	1	1.4892	1.4894(5)	15	20
6	3	1	1.4229	1.4227(5)	4	2
4	4	4	1.3930	1.3927(4)	8	13
5	4	3	1.3648	-	1	-
6	4	0	1.3883	1.3385(4)	8	15
7	2	1, 6 3 3, 5 5 2	1.3133	1.3133(4)	31	40
6	4	2	1.2896	1.2895(4)	6	7
7	3	0	1.2672	1.2668(4)	1	2
6	5	1, 7 3 2	1.2257	1.2257(3)	6	8
8	0	0	1.2064	1.2065(3)	1	2
6	5	3	1.1535	1.1535(3)	7	10
8	2	2	1.1374	1.1370(3)	3	3
7	4	3, 7 5 0, 8 3 1	1.1219	1.1219(3)	16	20
7	5	2	1.0927	1.0930(2)	6	5

[a]The lattice constants used is a = 9.6508(3) Å and x(Ca) = 0.083, Cu Kα, radiation λ = 1.54056 Å.

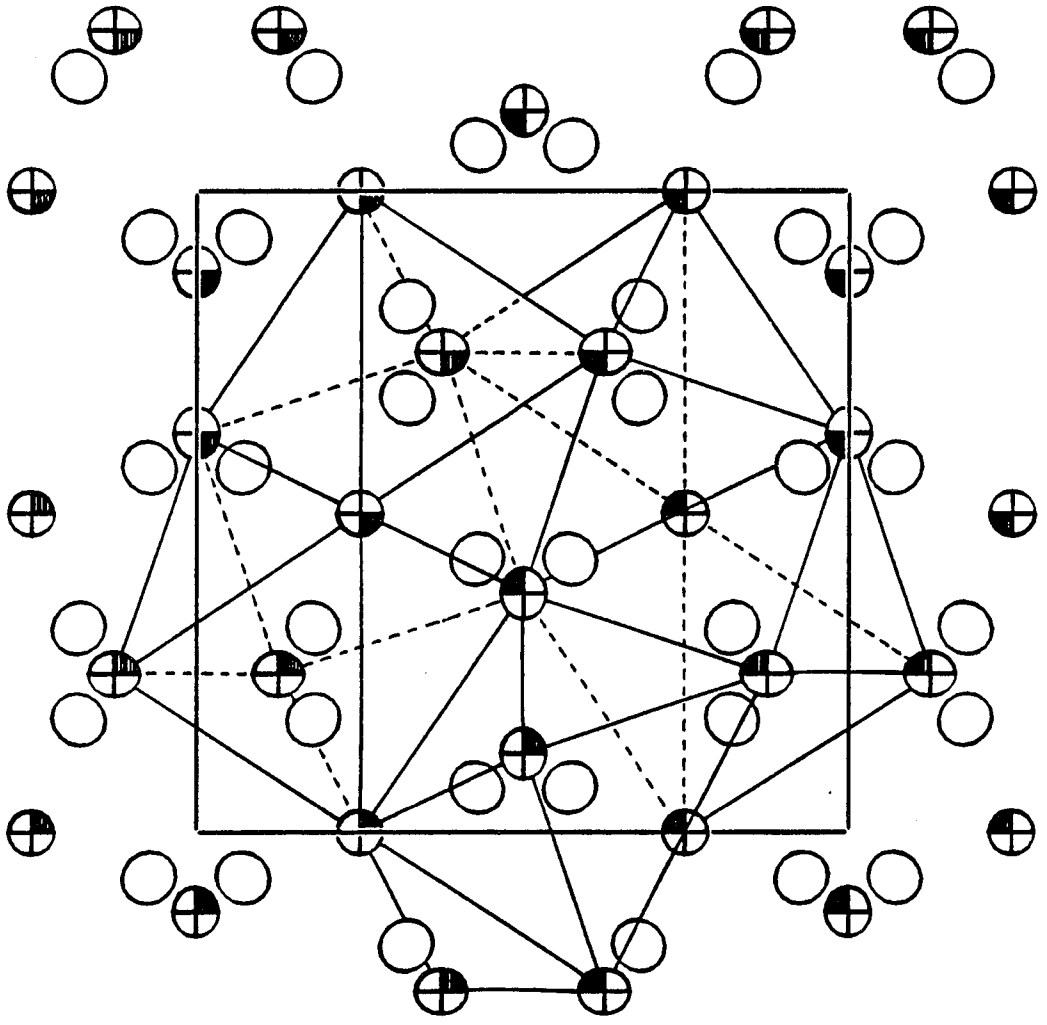

Figure 8. The unit cell of $M_4(Sb_XY_Z)_3$ (M = Ca, Ba,; Y = S, I) projected on [001] plane. Open ellipsoids: Ca or Ba atoms; shaded ellipsoids: Sb/S or Sb/I. (a) shows the arrangement of distorted $[M(Sb/Y)_6]$ octahedra

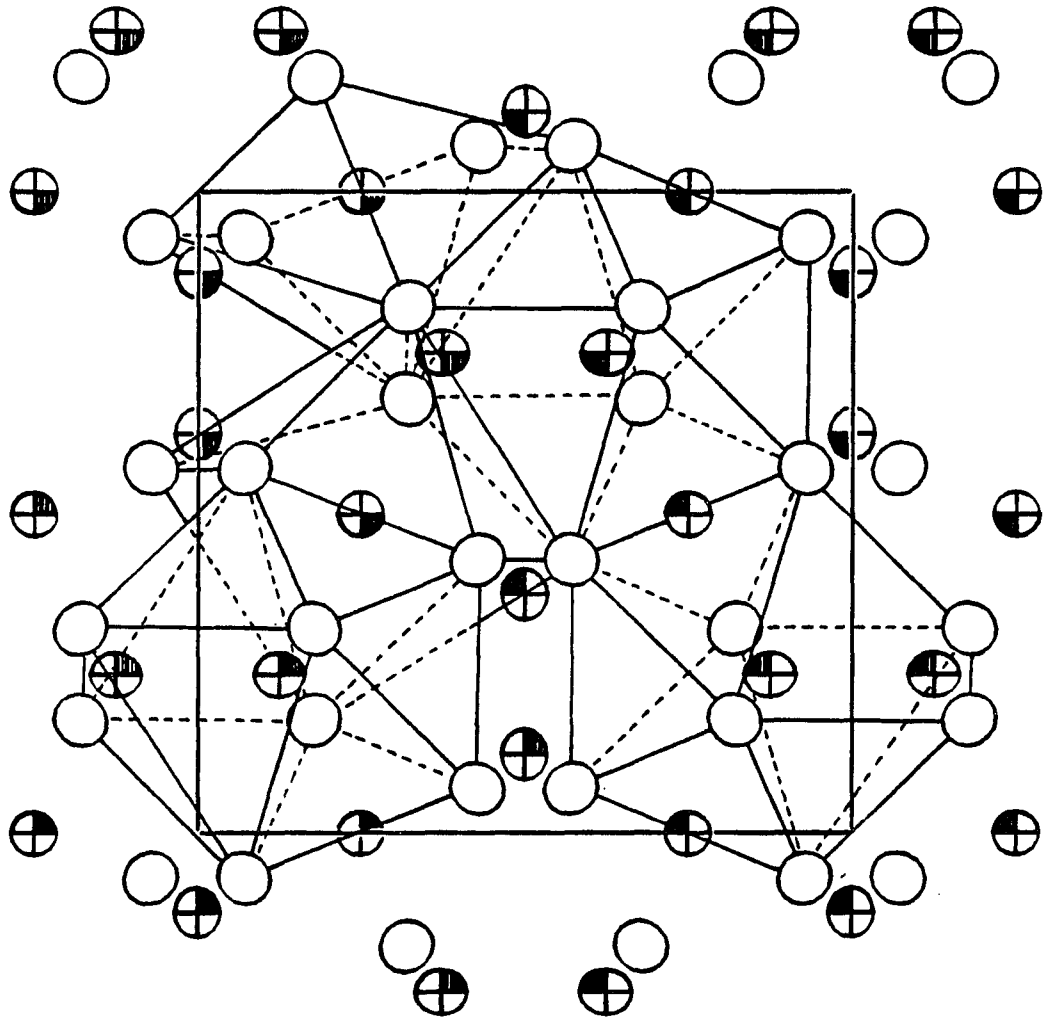

Figure 8. (continued)
(b) Shows the arrangement of $[(Sb/Y)M_8]$ octaverticons

and $Ca_4S_{8/3} = Ca_3Sb_2$; the latter will be proven in Part IV to belong to a different structure, so the range becomes $0 < y \leq 1$ and $2 \leq x < 8/3$.

In an attempt to synthesize Ca_4Sb_2S with an anti-Th_3P_4 structure, the product went the other way. The powder pattern showed not only CaS (NaCl-type) but also a hexagonal phase (indexed from 12 lines) with a = 9.044(1) and c = 7.170(3) Å compared with the lattice constants of Ca_5Sb_3Cl and Ca_5Sb_3 (Mn_5Si_3) which are a = 9.0805(3), c = 7.0898(6) Å and a = 9.0321(3), c = 7.0280 (8) Å, respectively. Apparently, the value of a-axis is between these two limits, but the value of c-axis is larger than either of them. That excludes the possibility of $Ca_5Sb_{3-x}S_y$ (Mn_5Si_3), since the cell of it should be smaller than that of Ca_5Sb_3 (Mn_5Si_3). All the lines in the powder pattern can be assigned to either CaS or the hexagonal phase. The possible product can be derived from the following reaction to gain "$Ca_5Sb_3S_{1/2}$":

$$4\ Ca + 2\ Sb + S \longrightarrow 2/3\ CaS + 2/3\ Ca_5Sb_3S_{1/2}$$

However, a previous rxn. 320 to make $Ca_5Sb_3S_{1/2}$ was without success and formed $Ca_4Sb_{2.4}S_{0.4}$ instead. The comparisons between these two reaction conditions revealed that the reaction temperature for the former was slightly higher than the latter (see Table 11). Even assuming formation of $Ca_5Sb_3S_{1/2}$, the unusual c-axis size still could not be rationalized by a Mn_5Si_3[22] structure. There is another structure type Ca_5Pb_3[23] which is just a distorted Mn_5Si_3 type. The space group of Mn_5Si_3 is $P6_3/mcm$ while that of Ca_5Pb_3 is $P6_3mc$ (acentric). The relationship of lattice constants between Ca_5Pb_3 and Mn_5Si_3 is: $a(Ca_5Pb_3) \simeq \sqrt{3}a(Mn_5Si_3)$ and $c(Ca_5Pb_3) \simeq c(Mn_5Si_3)$. Using the following lattice constants $a = \sqrt{3}$

Table 11. Comparisons of rxn. conditions between rxn. 479 and 320

rxn. #	stoichiometry	rxn. conditions[a]	products
479	Ca_4Sb_2S	900°C — 19 days	CaS, $Ca_5Sb_3S_{1/2}$
		750°C — 2 days	
		550°C — 1 day	
		350°C — 4 hrs	
320	$Ca_5Sb_3S_{1/2}$	870°C — 5 days	$Ca_4Sb_{2.4}S_{0.4}$
		640°C — 4 days	

[a]Furnace cooling.

x 9.044 Å = 15.666(2) and c = 7.170 Å and the atom positions from Ca_5Pb_3, the calculated powder pattern is indistinguishable from not only the experimental one but also the calculated one based on Mn_5Si_3 structure for the same dimensions, even in the low angle lines. Although the structure of Ca_5Pb_3 actually is not a superstructure of Mn_5Si_3, the structure has a very similar arrangement of atoms as that of Mn_5Si_3. If "$Ca_5Sb_3S_{1/2}$" adopted Ca_5Pb_3, then the odd behavior of c-axis was not surprising, because they were not the same structure type any more. It was noted that the c-axis of α-Eu_5As_3 (Ca_5Pb_3) (7.2517(2) Å) is greater

than that of β-Eu_5As_3 (Mn_5Si_3) (7.0811(4) Å).[10] This phenomenon, also observed in La_5Ge_3X (X = Fe, Co)[24] system is consistent with the observation in "$Ca_5Sb_3S_{1/2}$".

M_5X_3 With I

Rxn. 322 was loaded for Ba_5Sb_3I according to the following equation

$$5\ Ba + 8/2\ Sb + 1/3\ SbI_3 \longrightarrow \text{"}Ba_5Sb_3I\text{"}$$

and was heated at 870°C for 6 days then annealed successively at 770°C, 670°C, and 470°C for a couple of days. The powder pattern of the product did not contain the expected hexagonal phase such as Ba_5Sb_3Cl. It was concluded to be a mixture, but not all the lines could be indexed by TREOR program. The products were later proven to be $Ba_4Sb_{2.5}I_{0.5}$ and Ba_2SbI from single crystal studies and subsequent calculations of the powder patterns. So the reaction should be rewritten as the following equation:

$$5\ Ba + 8/3\ Sb + 1/3\ SbI_3 \longrightarrow Ba_4Sb_{2.5}I_{0.5} + 1/2\ Ba_2SbI.$$

Also, these two products were further confirmed in rxn. 477 and rxn. 478 which were loaded with the right stoichiometries of starting materials and followed by similar reaction conditions to that of rxn. 322.

Structure of $Ba_4Sb_{2.5}I_{0.5}$

Suitable crystals of $Ba_4Sb_{2.5}I_{0.5}$ were mounted from rxn. 322 and loaded into 0.2-mm capillaries. After indexing one of them on DATEX diffractometer, ALICE'S PREDICTION[25] gave a rhombohedral cell with a ≈ 9.08 Å and α ≈ 109.3°. At this stage, there were two choices to transform the cell. One was a body centered cubic cell with a ≈ 10.49 Å, the

other was a primitive hexagonal cell with a ≃ 14.84 and c ≃ 9.05 Å. Since Ba_5Sb_3Cl has a hexagonal cell, the hexagonal cell was chosen for the data collection. Lots of effort was used to solve the structure without any success until the structure of $Ca_4Sb_{2.4}S_{0.4}$ was confirmed.

The closeness of the cubic cell size of "Ba_5Sb_3I" to that of $Ca_4Sb_{2.4}S_{0.4}$ raised the thought that the real composition of the crystal might be $Ba_4Sb_xI_y$, isostructural with $Ca_4Sb_{2.4}S_{0.4}$. Before redoing the absorption correction, data reduction and data averaging, the data set was transformed by using the UTILITY[26] program from the hexagonal to the cubic cell. The details of the data collection and structure solution are summarized in Table 12. After anisotropic temperature parameter refinement, the R is 0.088 and R_w is 0.102, assuming the stoichiometry $Ba_4Sb_{2.5}I_{0.5}$. The final atom positions and temperature factors are listed in Table 13. Figure 8(a) and (b) represent the polyhedra around Ba or Sb/I projected on [001] plane.

Determination of the composition of $Ba_4Sb_xI_y$ was tried by refining the relative occupancy of Sb and I. Owing to the close atomic numbers of Sb (51) and I (53), the standard deviation was too large. So the real composition of $Ba_4Sb_xI_y$ was derived by assuming $3x + y = 8$ and $x + y = 3$, i.e., that it was a valence compound with anti-Th_3P_4 structure. However, the composition of $Ba_4Sb_xI_y$ was confirmed in the later rxn. 477 which was loaded as $Ba_4Sb_{2.5}I_{0.5}$ and gave the same powder pattern (80% yield) as that of rxn. 322. Also, $Ba_4P_{2.5}I_{0.5}$[27] has been reported to adopt anti-Th_3P_4 structure.

Table 12. Diffraction and refinement data of $Ba_4Sb_{2.5}I_{0.5}$

Space group	$I\bar{4}3d$ (No. 220)
Z	4
Cell dimensions,[a] Å	
a	10.475(7)
Size of crystal (mm)	0.15 x 0.12 x 0.08
Octants measured	$\pm h, \pm k, \ell$
Scan type	ω
2θ-max, deg. (Mo Kα)	55
μ(Mo Kα), cm^{-1}	205.0
Transm. coeff. range	0.35 — 0.47
Number of reflections	
meas.	722
obs. (>3σ(I))	653
indep.	197
R(ave)	0.030
Structure solution	
R^b	0.088
R_w	0.100

[a]The cell dimensions indexed from 11 lines of the Guinier powder pattern, Cu $K\alpha_1$, λ = 1.54056 Å.

[b]$R = \sum||F_o| - |F_c||/\sum|F_o|$, $R_w = [\sum w(|F_o| - |F_c|)^2/\sum w|F_o|^2]^{1/2}$.

Table 13. Atomic and thermal parameters[a] of $Ba_4Sb_{2.5}I_{0.5}$

Atom		x	y	z	B_{11}	B_{22}	B_{12}
Ba	16(c)	0.0713(2)	x	x	2.2(1)	B_{11}	0.16(8)
Sb, I	12(a)[b]	3/8	0	1/4	2.1(3)	1.6(2)	0

[a] $B_{22} = B_{33}$ and $B_{12} = B_{13} = B_{23}$.

[b] The position assigned as 5/6 Sb and 1/6 I.

After the structure solved, the cell constants of $Ba_4Sb_{2.5}I_{0.5}$ were accurately determined by LATT program to be a = 10.475(7) Å (use 11 of 12 lines). Before leaving this topic, it should be mentioned that there was not any peak greater than 0.57 e/Å^3 on the difference map, although the R value was only 0.088.

Structure of Ba_2SbI

In reviewing the literature, Ca_2PI[28] and Ba_2PI[27] were found to adopt the anti-α-$NaFeO_2$ structure. The structure of Ba_2PI is composed of cubic close packing of Ba with P and I filling alternate octahedral sites. The packing sequence can be expressed as: Ac'BaCb'AcBa'C where a',b' and c' represent P and a,c, represent I layers. However, the powder pattern of rxn. 322 had only four lines left after excluding those lines belonging to $Ba_4Sb_{2.5}I_{0.5}$, and they did not match the calculated powder pattern

based on anti-α-$NaFeO_2$ structure. However, they could be indexed to be a cubic cell with a = 3.5485 (3) A. As mentioned before, the atomic number of Sb is close to I and the size of Sb should be about the same order as that of I. It might be possible that Ba_2SbI adopts a simple cubic structure, but the CsCl structure had been tested and excluded. After doubling a-axis (i.e., a = 7.097 A) and NaCl model was tried, and the calculated powder pattern matched with the experimental one very well (see Table 14), proving that Ba_2SbI adopted NaCl structure. When the size of anions are close to each other, the NaCl structure is formed for M_2XY (M = Ca, Sr, Ba; X = N, P, As; Y = F, Cl, Br, I).[29-33] For instance, M_2NF (M = Ca, Sr and Ba)[29] all adopt the NaCl structure. To illustrate this relationship, Table 15 lists all the structure types of M_2XY.

M_5X_3 With Cu

So far in M_5X_3Y, Y has been restricted in main group elements only. To expand the system further, Cu was tried as the atom in the interstitial sites. Rxn. 449 was run at ~920°C without success. The powder pattern indicated the product was $Ca_{16}Sb_{11}$ and $CaCu_5$ (?). The identification of $CaCu_5$ was not quite sure, because most lines of $CaCu_5$ overlap those of $Ca_{16}Sb_{11}$. However, it is a plausible remainder according to the following equation

$$5\ Ca + 3\ Sb + Cu \longrightarrow 3\ Ca_{1.6}Sb\ (\sim Ca_{16}Sb_{11}) + 1/5\ CaCu_5.$$

Table 14. Comparisons between the calculated and observed powder patterns of Ba_2SbI

h k ℓ	$d_{cal.}$	$d_{obs.}$	$I_{cal.}$[a]	$I_{obs.}$
2 0 0	3.549	3.547(4)	100.0	S
2 2 0	2.509	2.548(4)	79.3	M
2 2 2	2.049	2.042(3)	30.0	W[b]
4 0 0	1.774	1.774(3)	15.0	W
4 2 0	1.587	1.586(3)	43.9	M
4 2 2	1.449	1.449(3)	34.5	W
4 4 0	1.255	1.253(2)	12.5	-

[a]The lines with $I_{cal.}$ <5.0 are not listed.

[b]The line is superimposed by one of the lines from $Ba_4Sb_{2.5}I_{0.5}$.

Table 15. Structure types of M_2XY (M = Ca, Sr, Ba; X = N, P, As; Y = F, Cl, Br, I)

NaCl type	ref.	anti-α-$NaFeO_2$ type	ref.
Ca_2NF	29	Ca_2NCl	30
Sr_2NF	29	Ca_2NBr	30
Ba_2NF	29	Ca_2PI	28
Ca_2PBr	33	Ca_2AsI	28,31
Ca_2PCl	32	Ba_2PI	27
Sr_2PCl	32	Ba_2PCl	27
Sr_2AsCl	31	Ba_2PBr	27
Ca_2AsBr	31	Sr_2PBr	33

Conclusion

From the studies of M_5X_3Y, it seems that they all follow the simple valence rule quite well, but the structures change with different interstitial elements. That is due to the different environments created around interstitial elements in different structures and the fact that only particular sites can be fitted with the particular interstitial elements.

For instance, fluoride favors the tetrahedral sites so they form filled-β-Yb_5Sb_3 structure for Ca_5Sb_3F and Ca_5Bi_3F, while chloride and bromide prefer the octahedral sites to generate filled-Mn_5Si_3 structure. The large iodide can not be put into the six-coordinate octahedral sites so it adopts the anti-Th_3P_4 structure in which the iodide is eight coordinate by calcium cations. Although only one of the rare-earths metals have been tried in M_5X_3Y studies, it is believed that most of them should behave like alkaline earth metals to form ternary but metallic halides. For the sulfur reactions, there are two structures observed. They might be the low and high temperature forms. However, the hexagonal phase of "$Ca_5Sb_3S_{1/2}$" needs further study to confirm whether it is the Mn_5Si_3 or Ca_5Pb_3 structure.

The unsuccessful reactions such as Ba_5Sb_3F might be due to the high r_{Ba}/r_{Sb} ratio. As discussed in Part II, the ratio might be the indication of which structure is stable and possible. However, it can not explain the formations of Ca_5Bi_3Cl and Ca_5Bi_3Br with Mn_5Si_3 structure.

So far, only one transition metal element, Cu, has been tried in the interstitial sites without success. That can be interpreted by the low electronegativity of Cu. Owing to that, Cu can not act as the electron acceptor like the halogen atoms. This might also apply to other transition metal elements.

References

1. Garcia, E., Ph.D. Dissertation, Iowa State University, Ames, IA, 1987.

2. Garcia, E.; Ku, H. C.; Shelton, R. N.; Corbett, J. D. Solid State Commun. 1988.

3. Deller, K.; Eisenmann, B. Z. Naturforsch. 1976, 31b, 29.

4. Takusagawa, F., Ames Laboratory, Iowa State University, Ames, IA, unpublished research, 1981.

5. Iandelli, A. Palenzona, A. in Gschneidner, Jr., K. A.; Eyring, L. (eds.), "Handbook on the Physics and Chemistry of Rare Earth, Vol. 2, North-Holland: Amsterdam, 1977, p. 1.

6. Karcher, B., Ph.D. Dissertation, Iowa State University, Ames, IA, 1981.

7. Lapp, R. L.; Jacobson, R. A., DOE Report IS-4708, Ames Laboratory, Iowa State University, Ames, IA, 1979.

8. Powell, D. R.; Jacobson, R. A., DOE Report IS-4737, Ames Laboratory, Iowa State University, Ames, IA, 1980.

9. Eisenmann, B.; Deller, K. Z. Naturforsch. 1975, 30b, 66.

10. Wang, Y.; Calvert, L. D.; Taylor, J. B. Acta Crystallogr. 1978, B34, 2281.

11. Martinez-Ripoll, M.; Brauer, G. Acta Crystallogr. 1973, B29, 2717.

12. Shannon, R. D. Acta Crystallogr. 1976, A32, 751.

13. Martinez-Ripoll, M.; Brauer, G. Acta Crystallogr. 1974, B30, 1083.

14. Wang, Y.; Gabe, E. J.; Calvert, L. D.; Taylor, J. B. Acta Crystallogr. 1976, B32, 1440.

15. Martinez-Ripoll, M.; Haase, A.; Brauer, G. Acta Crystallogr. 1974, B30, 2004.

16. Smakula, A.; Kalnajs, J. Phys. Rev. 1955, 99, 1737.

17. Edwards, A. J. J. Chem. Soc., A 1970, 2751.

18. Selte, K.; Kjekshus, A.; Andresen, A. F. Acta Chem., Scand. 1974, A28, 55.

19. Franceschi, E. A.; Ricaldone, F. Rev. Chim. Miner. 1984, t21, 202.

20. Werner, P. E. "TREOR-4 Trial and Error Program for Indexing on Unknown Powder Patterns", Department of Structural Chemistry, Arrhenius Laboratory, University of Stockholm: S-106 91 Stockholm, Sweden, 1984.

21. Kripyakevich, P. I. Kristallografiya 1963, 7, 556.

22. Aronsson, B. Acta Chem., Scand. 1960, 14, 1403.

23. Helleis, O.; Kandler, H.; Leicht, E.; Quiring, W.; Wolfel, E. Z. Anorg. Allg. Chem. 1963, 320, 86.

24. Guloy, A.; Corbett, J. D., Iowa State University, Ames, IA, unpublished results, 1987.

25. Jacobson, R. A., DOE Report IS-3469, Ames Laboratory, Iowa State University, Ames, IA, 1974.

26. Miller, L., Ames Laboratory, Iowa State University, Ames, IA, unpublished research, 1987.

27. Hadenfeldt, C. Z. Anorg. Allg. Chem. 1977, 436, 113.

28. Hamon, C.; Marchand, R.; Lang, J. Bull. Soc. Fr. Mineral Crystalloghr. 1974, 97, 6.

29. Ehrlich, P.; Linz, W.; Steifert, H. J. Naturwissenschaften 1971, 58, 219.

30. Hadenfeldt, C.; Herdejurgen, H. Z. Anorg. Allg. Chem. 1987, 545, 177.

31. Hadenfeldt, C. Z. Naturforsch. 1976, 31b, 408.

32. Hadenfeldt, C. Z. Naturforsch. 1975, 30b, 165.

33. Hadenfeldt, C.; Kosiol, W. Z. Naturforsch. 1975, 30b, 378.

PART IV. $Ca_{16}Sb_{11}$ AND $Sr_{16}Bi_{11}$

Introduction

In the studies of Ca_5Sb_3X (X = nonmetal element), it was found that there always were similar patterns in the unsuccessful reactions with the stoichiometry of Ca/Sb close to 3/2. For instance, the pattern occurred for the reaction

$$5\ Ca + 3\ Sb + C \longrightarrow 1/2\ CaC_2 + 3/2\ "Ca_3Sb_2"$$

Since the reproducibility of "Ca_3Sb_2" was quite good, it raised a question about the nature of "Ca_3Sb_2". In reviewing the literature[1-4] and the phase diagram of Ca-Sb,[5] the only phase ever reported as Ca_3Sb_2[5] had the lattice constants of Ca_5Sb_3 with the β-Yb_5Sb_3 structure,[3] suggesting that no Ca_3Sb_2 existed. In this report, we describe the synthesis and identification of a "Ca_3Sb_2" which was later confirmed to be $Ca_{16}Sb_{11}$. The close relationship between $Ca_{16}Sb_{11}$ and $R_{5n+6}T_{3n.5}$ (R = rare earth element; T = transition metal) series compounds will also be discussed.

Experimental Section

Two reactions were loaded with Ca/Sb equal to 3/2. The powder patterns of products indicated the products were the same, although the heat treatments were quite different (see Table 1). The lattice constants of two products were: a = b = 12.237(1) Å, c = 11.325(3) Å, $\alpha = \beta = \gamma = 90°$ for rxn. 337; a = b = 12.2453(5) Å, c = 11.323(1) Å, $\alpha = \beta = \gamma = 90°$ for rxn. 444 from powder data indexed by the TREOR program[6] using the sharpest 20 and 46 lines, respectively. The indices of the lines

Table 1. Different conditions for the syntheses of "Ca_3Sb_2"

Rxn. No.	Ca/Sb	Rxn. Conditions[a] T,°C	Time, (d)	Products[b]
377	3.00 / 2.00	930	4	
444	3.03 / 2.00	920	6	
		850	2.5	
		750	2 hrs	
453	3.03 / 2.00	1200	1	
		(induction heating)		
		700	19	
473	3.00 / 2.00	r.t. —> 1100,	10 hrs[c]	
		1100	3 hrs	
		1100 —> r.t.	3 hrs	
483	16.00 / 11.00	940	6	a few plate
		840	1	crystals
		800	3	
		750	3	
		700	2 weeks	
		650	2	

[a]Furnace cooling.

[b]Polycrystals of $Ca_{16}Sb_{11}$ unless specified.

[c]Program heating and cooling.

also indicated it was a primitive cell. Apparently, the products were the same; the singularity of the phase was also confirmed by finding no line that could not be indexed. Lots of efforts to grow single crystals were not successful (see Table 1) until the ideal model was built up, and the right stoichiometry of "Ca_3Sb_2" was obtained. Then a few plate crystals were found in rxn. 483 after adjusting the stoichiometry and modifying the reaction conditions. They seemed to be formed from a peritectic reaction. Before describing the structure of $Ca_{16}Sb_{11}$, we will describe the building of the ideal model of $Ca_{16}Sb_{11}$ first.

Model of $Ca_{16}Sb_{11}$

The ideal model of $Ca_{16}Sb_{11}$ was derived from the powder pattern and the cell constants. It was observed that doubling the c-axis of a comparable W_5Si_3 structure[7] gave similar lattice constants to those of "Ca_3Sb_2". More importantly, the lines in the calculated powder pattern based on the atom positions of W_5Si_3 with a doubled c-axis and a change of the space group from I4/mcm to its primitive equivalent P4/mbm fit the experimental one. So the basic building blocks of W_5Si_3 might also coexist in "Ca_3Sb_2".

In reviewing the literature, two series of compounds $R_{5n+6}T_{3n+5}$[8] (R = rare earth metal; T = transition metal or $Ca_{31}Sn_{20}$) and $R_{12m+10n+10p}T_{6m+8n+6p}$[9] were found that all had similar building blocks as W_5Si_3. They can be described in terms of the stacking of certain polyhedron units.[8] For instance, W_5Si_3 is composed of Si-centered square antiprisms of W atoms and Si-centered ten-atom W polyhedra (see Figure

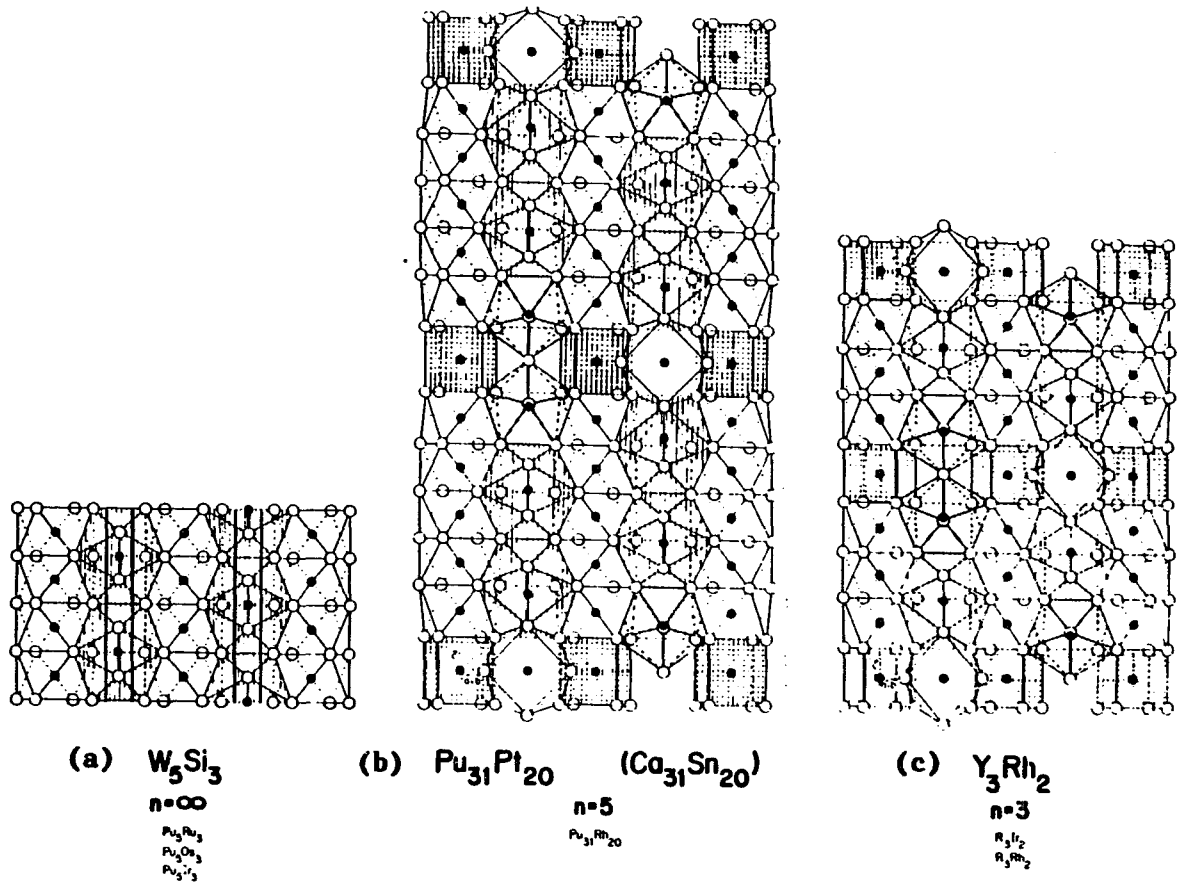

Figure 1. The arrangements of coordination polyhedra in W_5Si_3, $Pu_{31}Pt_{20}$ and Y_3Rh_2 structure types: open circles represent R atoms; closed circles represent T atoms. The plane of projection is [110]. Quoted from ref. 8

1(a)). In both Y_3Rh_2[9] and $Pu_{31}Pt_{20}$[10] (or $Ca_{31}Sn_{20}$[11]) structures, a slab formed from Rh- or Pt- centered Y or Pu cubes and centered square antiprisms is followed by slabs similar to those in W_5Si_3 (five in $Pu_{31}Pt_{20}$ but only three in Y_3Rh_2), and finally a slab similar to the bottom one but displaced sideways (Figure 1(b), 1(c)). A closer study revealed that the W_5Si_3 slabs directly joining a cube slab are distorted. In particular, the coordination polyhedron between the square antiprisms is completed within the cubic slab in a different way, and the resulting eight-atom coordination polyhedron is a new type. The drawings in Figure 1(a)—(c) makes it clear that the W_5Si_3, Y_3Rh_2, and $Pu_{31}Pt_{20}$ structure types belong to a structural series with formula $R_{5n+6}T_{3n+5}$ in which the structures are built up of one slab of R_6T_5 followed by n slabs of R_5T_3 and where n has the values ∞, 3, and 5, respectively.[8-11]

However, this kind of classification already makes an approximation. As pointed out above, not all the W_5Si_3 slabs in the series are the same. The slab next to the bottom slab should be represented as $R_{10}T_8 = R_5T_4$ instead of R_5T_3. Then the bottom slab should be changed to $R_{12}T_6$. So there is another representation for the same series: $R_{12m+10n+10p}T_{6m+8n+6p}$, where m, n, and p are the numbers of $R_{12}T_6$ (bottom slab), $R_{10}T_8$ (the W_5Si_3 slabs next to the bottom slab), and $R_{10}T_6$ fragments in a unit cell, respectively.[9] According to this classification, if $R_{12}T_6$ is called I, $R_{10}T_8$ called II and $R_{10}T_6$ called III, then this series can be represented as as in Figure 2. It should be noted the projection of Figure 2 is along [010] plane, different from Figure 1 which is along [110]. Thus, for W_5Si_3, m = 0, n = 0, p = 2; for Y_3Rh_2,

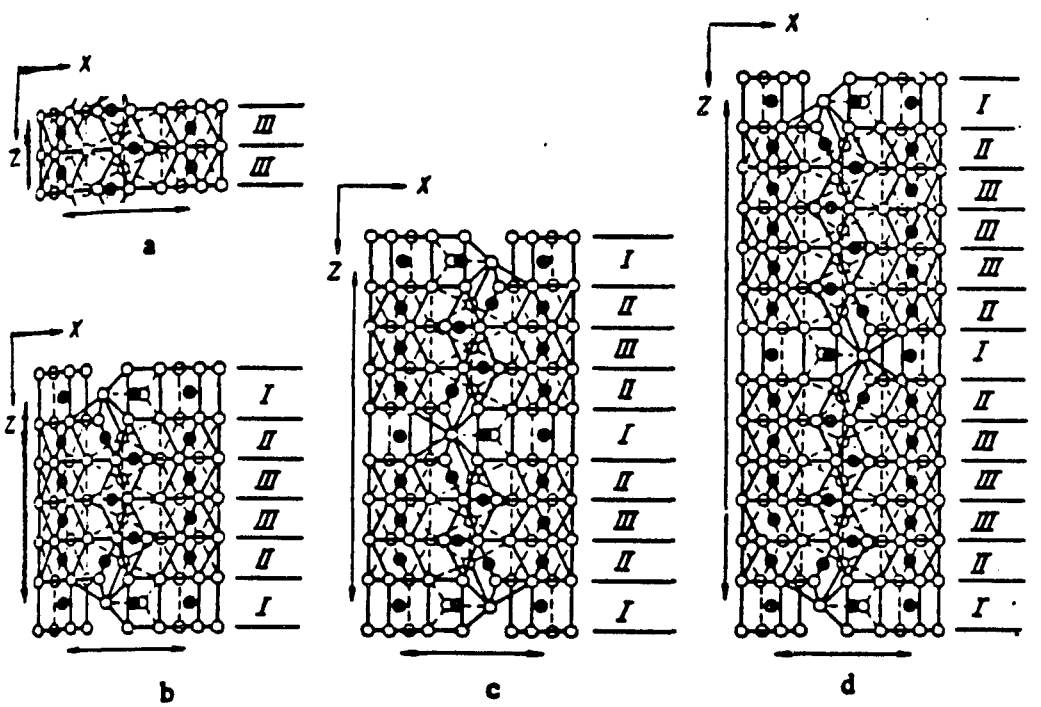

Figure 2. Structures in the series $R_{12m+10n+10p}T_{6m+8n+6p}$:
a) W_5Si_3; b) $Sm_{26}(Ga_{0.35}Co_{0.65})_{17}$; c) Y_3Rh_2; d) $Pu_{31}Pt_{30}$;
I-III, fragments of types of R_2T, R_5T_4, R_5T_3 (W_5Si_3)

$m = 2$, $n = 4$, $p = 2$; for $Sm_{26}(Ga_{0.35}Co_{0.65})_{17}$,[9] $m = 1$, $n = 2$, $p = 2$; for $Pu_{31}Pt_{20}$, $m = 2$, $n = 4$, $p = 6$, where n values are always twice m. It is useful to convert this classification into the former one. Since n is always twice m, $R_{12m+10n+10p}T_{6m+8n+6p} = R_{6m+5n+5p}T_{3m+4n+3p}$ can be further converted to $R_{6m+5n+5p}T_{3m+2m+3n+3p} = R_{6m+5(n+p)}T_{5m+3(n+p)}$. With $n+p = n'$, then $R_{6m+5(n+p)}T_{5m+3(n+p)}$ becomes $R_{6+5n'}T_{5+3n'}$. There are some common features in this series of compounds. $R_{12}T_6$ (I) is built first followed by $R_{10}T_8$ (II) then by $R_{10}T_6$ (III). Also, all the compounds are centrosymmetric.

In the same reference,[9] there is the note that "Structures formed only from two types of fragments are possible only in the series $nR_{10}T_8 \cdot pR_{10}T_6$ and $nR_{10}T_8 \cdot mR_{12}T_6$. Combination of $R_{12}T_6$ and $R_{10}T_6$ fragments is impossible, owing to the absence of planes with the same locations of atoms. Structures of the $nR_{10}T_8 \cdot pR_{10}T_6$ series are represented by the same symmetry as the ternary hybrids (five possible space groups including I4/mcm, P4/mbm, P4/nbm, P4bm and I4cm); structures of $nR_{10}T_8 \cdot mR_{12}T_6$ series belong only to the two space groups P4/mbm and P4bm".

The cell constants of "Ca_3Sb_2" are $a = b = 12.2453(3)$ and $c = 11.323(1)$ Å. The value of the a-axis is very close to the a-axes of this series of compounds, especially close to that of $Ca_{31}Sn_{20}$[12] (Table 2). Considering the c-axis of "Ca_3Sb_2" and assuming the packing of "Ca_3Sb_2" follows the same order as $R_{6+5n'}T_{5+3n'}$, the only possible packing or combination is $n' = 2$ for $R_{6+5n'}T_{5+3n'}$, i.e., $R_{16}T_{11}$. Since the model is only composed by $R_{12}T_6$ and $R_{10}T_8$ fragments, the space group

Table 2. Some examples of $R_{5n+6}T_{3n+5}$ compounds

Compounds	n	space group	a(Å)	c(Å)
Y_3Rh_2	3	I4/mcm	11.232(2)	25.16(1)
Gd_3Rh_2	3	I4/mcm	11.27(1)	25.32(2)
Tb_3Rh_2	3	I4/mcm	11.25(1)	25.20(2)
Dy_3Rh_2	3	I4/mcm	11.16(1)	25.07(2)
Ho_3Rh_2	3	I4/mcm	11.11(1)	24.99(2)
Er_3Rh_2	3	I4/mcm	11.09(1)	24.88(2)
$La_{26}(Ga_{0.40}Co_{0.60})_{17}$	4	P4/mbm	12.28(6)	15.38(9)
$Ce_{26}(Ga_{0.35}Co_{0.65})_{17}$	4	P4/mbm	11.99(6)	14.44(9)
$Pr_{26}(Ga_{0.35}Co_{0.65})_{17}$	4	P4/mbm	11.87(6)	15.22(9)
$Nb_{26}(Ga_{0.40}Co_{0.60})_{17}$	4	P4/mbm	11.88(6)	15.24(9)
$Sm_{26}(Ga_{0.35}Co_{0.35})_{17}$	4	P4/mbm	11.713(4)	15.171(7)
$Pu_{31}Pt_{20}$	5	I4/mcm	11.302(5)	37.388(23)
$Pu_{31}Rh_{20}$	5	I4/mcm	11.076(4)	36.933(12)
$Ca_{31}Sn_{20}$	5	I4/mcm	12.542	40.00
W_5Si_3	∞	I4/mcm	9.605	4.964
Sm_5Tl_3	∞	I4/mcm	12.346	6.140
Pr_5Tl_3	∞	I4/mcm	12.553	6.172
Pu_5Si_3	∞	I4/mcm	11.409	5.448
Pu_5Pb_3	∞	I4/mcm	12.310	6.084
V_5Si_3	∞	I4/mcm	9.429	4.756
Gd_5In_3	∞	I4/mcm	12.340	6.048

should be either P4/mbm or P4bm according to the above note. The indices of the reflections derived from TREOR program are all consistent with the systematic absence 0 k ℓ : k = 2n except for one medium intense reflections. The x,y coordinates of $Ca_{31}Sn_{20}$ were selected for the ideal model owing to the closeness of radii for Sn and Sb atoms and the z coordinates were rescaled. The detail of the atom positions for the model are listed in Table 3. Although the calculated powder pattern based on the model did fit most lines in the experimental ones, still a few lines could not be fitted. This was proven to be caused by the inaccuracy of atom postions and a wrong space group from the predicted model when extended to the Ca–Sb system. However, the model did reveal the real stoichiometry of "Ca_3Sb_2" could be $Ca_{16}Sb_{11}$ and provided the preliminary information on atom positions.

The structure of $Ca_{16}Sb_{11}$

A couple of the plate crystals found in rxn. 483 were mounted in 0.2-mm capillaries and sealed off for further structure determination. One of them of suitable size (0.15 x 0.17 x 0.08 mm) was indexed and diffraction data collected with CAD-4 diffractometer. During the indexing, the right cell could not be found owing to a twinning problem which was later confirmed by taking axial photographs. However, the six strong reflections did give the expected cell. Using these six reflections to get a rough orientation matrix, a couple of hundred reflections were scanned at a high scan rate. This added nineteen more good reflections to the original six, and these gave the following triclinic cell constants a = 12.237(5) A, b = 12.242(3) A, c = 11.305(6) A, α =

Table 3. Comparisons in atom positions between ideal model and real structure of $Ca_{16}Sb_{11}$

Ideal Model[a]				Real Structure			
P4/mbm (S.G. 127)				$P\bar{4}2_1m$ (S.G. 113)			
	x	y	z		x	y	z
Ca(1) 4(g)	0.3405	1/2+x	0	Ca(3) 4(e)	0.3683(5)	1/2+x	-0.0012(7)
Ca(2) 16(1)	0.2103	0.0519	0.1872	Ca(5) 8(f)	0.2032(5)	0.0711(5)	0.1855(6)
				Ca(4) 8(f)	0.2100(5)	0.0752(5)	0.7812(4)
Ca(3) 4(f)	0	1/2	0.2543	Ca(1) 2(c)	0	1/2	0.287(1)
				Ca(6) 2(c)	0	1/2	0.639(1)
Ca(4) 8(j)	0.0808	0.2161	1/2	Ca(2) 8(f)	0.0884(4)	0.2074(4)	0.4994(5)
Sb(1) 2(a)	0	0	0	Sb(6) 2(a)	0	0	0
Sb(2) 4(g)	0.0859	1/2+x	0	Sb(4) 4(e)	0.1267(1)	1/2+x	0.0135(2)
Sb(3) 8(k)	0.3019	1/2+x	0.2649	Sb(2) 4(e)	0.3364(1)	1/2+x	0.2636(2)
				Sb(3) 4(e)	0.3208(1)	1/2+x	0.7382(2)
Sb(4) 40e)	0	0	0.3357	Sb(1) 4(d)	0	0	0.3490(2)
Sb(5) 4(h)	0.1617	1/2+x	1/2	Sb(5) 4(e)	0.1450(1)	1/2+x	0.4618(2)

[a]From $Ca_{16}Sn_{11}$ (ref. 12) x + y coordinates.

89.98(3)°, β = 90.09(4)°, γ = 90.03(3)°. Six φ scans were collected for absorption corrections. The details of data collection are listed in Table 4. The space group was derived to be $P\bar{4}2_1m$ (No. 113) from the systematic absence 0k0, k = 2n. Five Sb and five Ca atom positions derived from the SHELEX program 76 were matched with the model positions. The last Ca position was determined from the model. After refining with isotropic thermal parameters, the R was 0.071 and R_w was 0.092. The final R was 0.032 and R_w 0.034 after finishing the anisotropic thermal parameter refinement. The occupancies of the Sb atoms were refined to be unity (1.008(8) for Sb(6); 0.978(6) for Sb(5); 1.002(6) for Sb(4); 0.998(6) for Sb(3); 0.992(6) for Sb(2); 1.004(4) for Sb(1)). The maximum residual density 1.79 e/Å^3 in the difference map is 0.64 Å away from Sb(6) atom positions.

Results and Discussion

The positional and thermal parameters are summarized and listed in Table 5.

Comparisons between the model and the structure of $Ca_{16}Sb_{11}$

In Table 3, the positions for the model and the structure were listed together. From the Table, it is clear that most of the atom positions in the structure are quite close to the positions in the model. The positions of Ca(2), Ca(3) and Sb(3) in the model are split into two positions Ca(4) and Ca(5); Ca(1) and Ca(6); Sb(2) and Sb(3) in the real structure, respectively. The common difference of the structure is the z-coordinate that deviates from the ideal z = 0 and z = 1/2 positions

Table 4. Diffraction and refinement data of $Ca_{16}Sb_{11}$

Space group	$P\bar{4}2_1m$ (No. 113)
Z	2
Cell dimensions, Å,[a]	
a = b	12.2453(5)
c	11.323(1)
Size of crystal (mm)	0.15 x 0.17 x 0.08
Octants measured	h,k,ℓ; h,k,-ℓ
Scan type	ω
2θ-max, deg. (Mo Kα)	55
μ(Mo Kα), cm^{-1}	221.1
Transm. coeff. range	0.49 – 0.99
Number of reflections	
meas.	3280
obs. (>3σ(I))	1911
indep.	493
R(ave)	0.022
No. of parameters refined	78
Structure solution	
R[b]	0.031
R_w	0.038

[a]The cell dimensions calculated from 46 lines of the Guinier powder pattern, Cu K_{α_1}, λ = 1.54056 Å.

[b]$R = \sum||F_o| - |F_c||/\sum|F_o|$. $R_w = [\sum w(|F_o| - |F_c|)^2/\sum w|F_o|^2]^{1/2}$.

Table 5. Positional and thermal parameters[a] and their estimated standard deviations

Atom	x	y	z	B_{11}
Sb(1)	0.000	0.000	0.3490(2)	1.05(8)
Sb(2)	0.3364(1)	0.8364(1)	0.2636(2)	1.26(5)
Sb(3)	0.3208(1)	0.8208(1)	0.7382(2)	1.21(5)
Sb(4)	0.1267(1)	0.6267(1)	0.0135(2)	1.69(5)
Sb(5)	0.1450(1)	0.6450(1)	0.4681(2)	1.21(5)
Sb(6)	0.000	0.000	0.000	2.4(1)
Ca(1)	0.000	0.500	0.287(1)	1.0(2)
Ca(2)	0.0844(4)	0.2074(4)	0.4994(5)	1.8(2)
Ca(3)	0.3683(5)	0.8683(5)	-0.0012(7)	2.8(2)
Ca(4)	0.2100(5)	0.0752(5)	0.7812(4)	1.9(2)
Ca(5)	0.2032(5)	0.0711(5)	0.1855(6)	3.3(3)
Ca(6)	0.000	0.500	0.639(1)	1.1(2)

[a]Anistropically refined atoms are given in the form of the isotropic equivalent displacement parameter defined as: (4/3) *[a^2*B(1,1) + b^2*B(2,2) + c^2*B(3,3) + ab($\cos\gamma$)*B(1,2) + ac($\cos\beta$)*B(1,3) + bc($\cos\alpha$)*B(2,3)].

B_{22}	B_{33}	B_{12}	B_{13}	B_{23}
0.94(8)	2.9(1)	0.1(1)	0	0
B_{11}	0.55(8)	-0.11(8)	-0.04(7)	B_{13}
B_{11}	0.74(8)	-0.26(8)	-0.03(7)	B_{13}
B_{11}	0.78(8)	0.45(8)	0.00(8)	B_{13}
B_{11}	2.3(1)	-0.07(8)	-0.14(7)	B_{13}
B_{11}	15.0(5)	0	0	0
B_{11}	3.7(6)	0.0(4)	0	0
1.6(2)	0.7(2)	-0.1(2)	-0.5(3)	-0.0(3)
B_{11}	2.0(2)	0.2(3)	0.1(3)	B_{13}
1.9(2)	0.8(2)	-0.4(2)	0.2(2)	-1.1(2)
1.4(2)	2.9(2)	0.3(2)	-1.8(3)	-0.8(2)
B_{11}	2.2(5)	-0.1(4)	0	0

except for Sb(6) which has the same positions as the ideal Sb(1) positions at (0,0,0) and (1/2,1/2,0). The intrinsic reason for lowering space group from centric P4/mbm to acentric $P\bar{4}2_1m$ might be because of the splitting of the positions of Ca(3) in the model. The split positions shift the atoms along z-axis about 0.05 c which is the most significant deviation from the ideal model. The unusual high B_{33} of Sb(6) might be caused by twinning problem or disorder.

Structure of $Ca_{16}Sb_{11}$

The atom positions of $Ca_{16}Sb_{11}$ are close to the model built in the previous section. Thus, the structure of $Ca_{16}Sb_{11}$ can be described as the linkage of different polyhedra. There are four different polyhedra coexisting in the unit cell including Sb(6) centered cubes, Sb(2), Sb(3) and Sb(4) centered trigonal prisms, Sb(1) centered square antiprisms and Sb(5) centered eight-atom polyhedra. The linkage of the polyhedra is exactly the same as the model proposed. Sb(6) centered cubes and Sb(4) trigonal prisms form the bottom slab, then come the Sb(2) centered trigonal prisms, Sb(4) centered square antiprisms and Sb(5) centered eight-atom polyhedra. Finally, stacked are Sb(3) centered trigonal prisms, Sb(4) centered square antiprisms and Sb(5) centered eight-atom polyhedra. The detailed coordination around each Sb atom are represented in Figure 3(a)—(f). The cube around Sb(6) actually is distorted so that Sb(6) lies in the center of two different sized tetrahedra penetrating with two different Ca—Sb distances ($d_{(Sb(6)—Ca(4))}$ = 3.632(5) Å and $d_{(Sb(6)—Ca(5))}$ = 3.367(7)Å). The polyhedron around Sb(5) can be

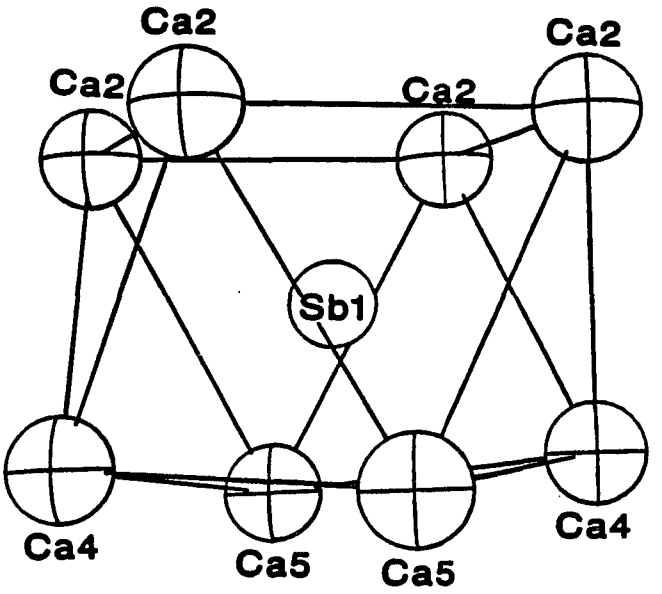

(a)

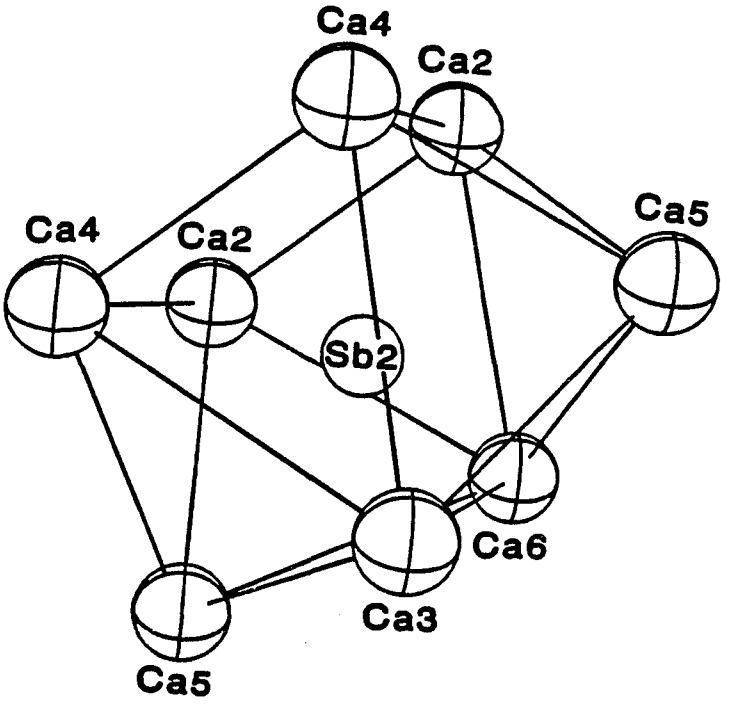

(b)

Figure 3. Different polyhedra around Sb atoms in $Ca_{16}Sb_{11}$.
(a) Square antiprism coordination around Sb(1);
(b) Trigonal prism coordination around Sb(2)

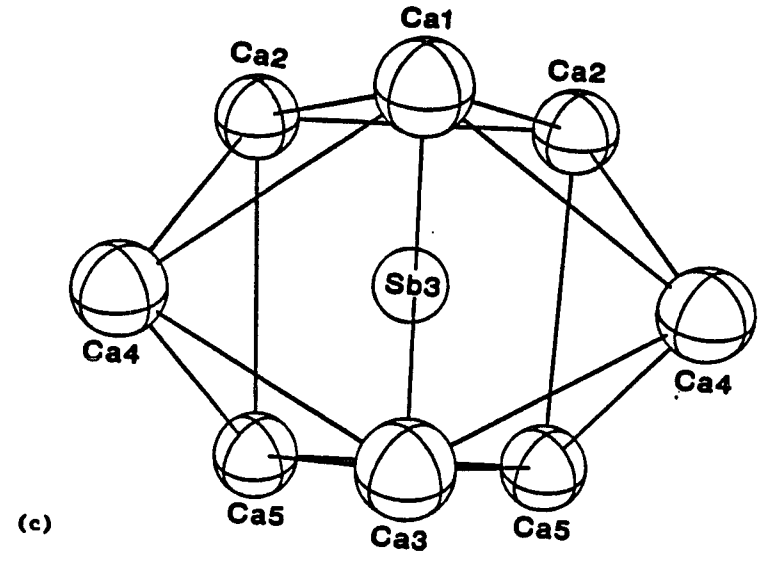

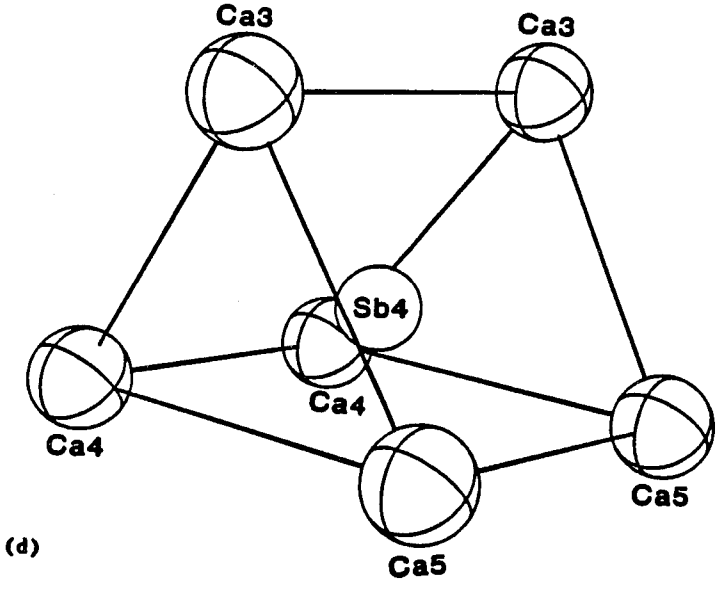

Figure 3. (continued)
(c) Trigonal prism coordination around Sb(3);
(d) Trigonal prism coordination around Sb(4)

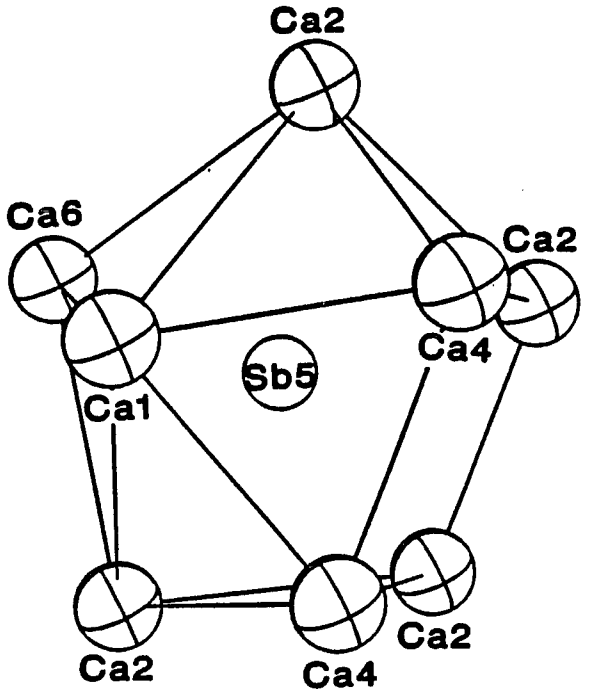

(e)

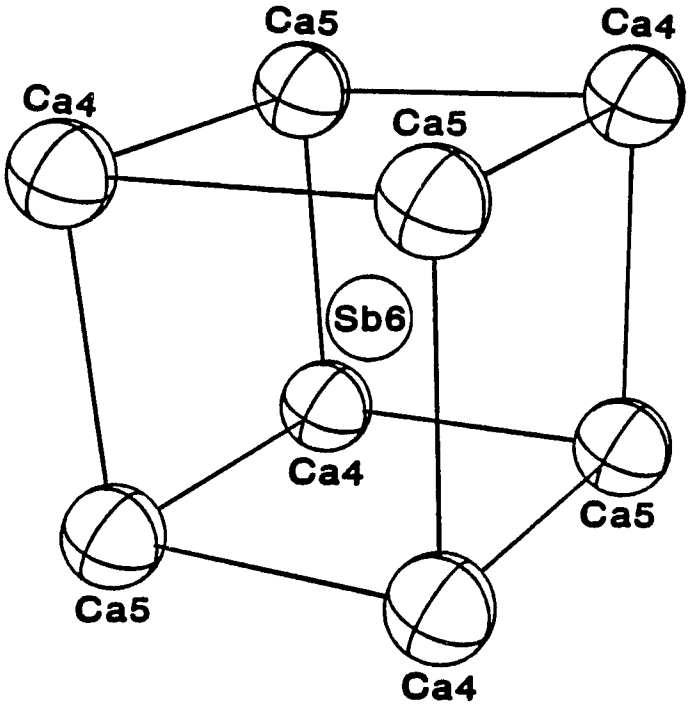

(f)

Figure 3. (continued)
(e) Polyhedra coordination around Sb(5);
(f) Cube coordination around Sb(6)

described as a pentagon with three pairs of Ca atoms on three apex positions perpendicular to the plane of the paper.

A closer look at the cube around Sb(6) reveals that the cube is distorted along the c-axis. The lengths of each edge and diagonal are drawn on Figure 4. In the figure, the faces of the top and the bottom are looked at as pseudo squares. One pair of the edges is equal to 3.801(8) A while the other is equal to 3.829(8) A. The two diagonal lengths are about the same order with one equal to 5.272(7) A and the other equal to 5.463(7) A on the pseudo planes. The other four faces which are around the waist of the cube are all elongated along the c-axis with edges equal to 4.579(8) A and distorted very much so that one of the diagonal lengths is 5.617(7) A shorter than the other one which is 6.283 (7) A.

As mentioned before, the cube might be considered as two penetrated tetrahedra composed of Ca(4) and Ca(5) atoms, respectively. In the tetrahedron composed of Ca(4) atoms, one pair of edges is 5.272(7) A not very deviated from the other pair which is 5.617(7) A. For the other tetrahedron composed of Ca(5) atoms, the long pair of edges is 6.283(7) A longer than the other pair which is 5.463(7) A. This kind of distortion of cube or tetrahedra might be the cause of unusually high B_{33} of Sb(6). To illustrate the linkage between these polyhedra, Figure 5(a), (b) and (c) are plotted as the projection on z = 0 (±0.22z), z = 0.35 (±0.39z) and z = 0.65 (±0.39z), respectively. It is clear that the structure of $Ca_{16}Sb_{11}$ is pseudocentric judged from 5(b) and (c). If the structure of $Ca_{16}Sb_{11}$ is projected as ref. 8 and ref. 9, they are represented as Figure 6 and Figure 7, respectively.

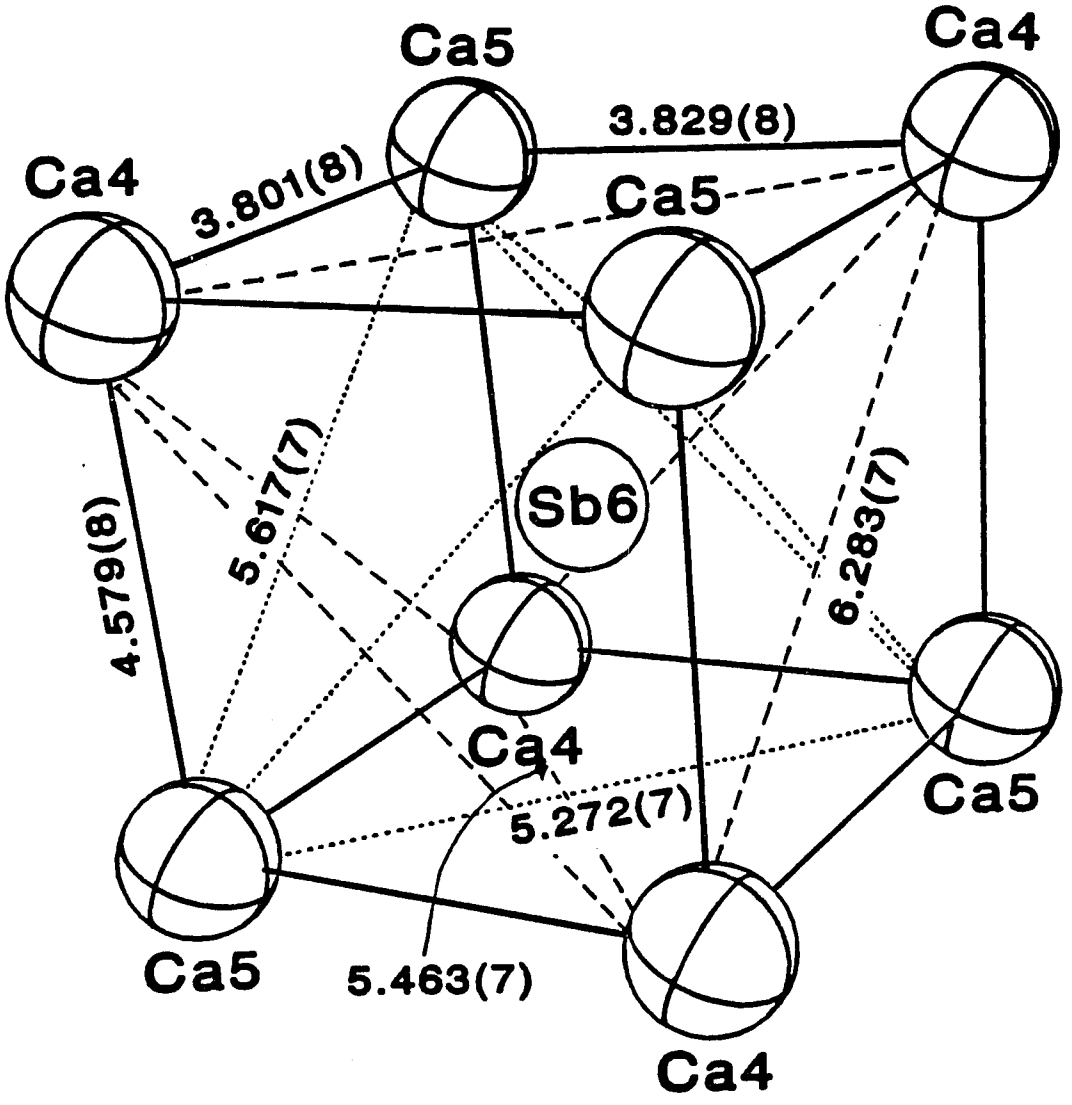

Figure 4. The lengths of the edges and diagonals of the cube around Sb(6) are shown in the figure. Two different dashed lines outline the tetrahedron. The Sb(6) atom is located at $\bar{4}$ position

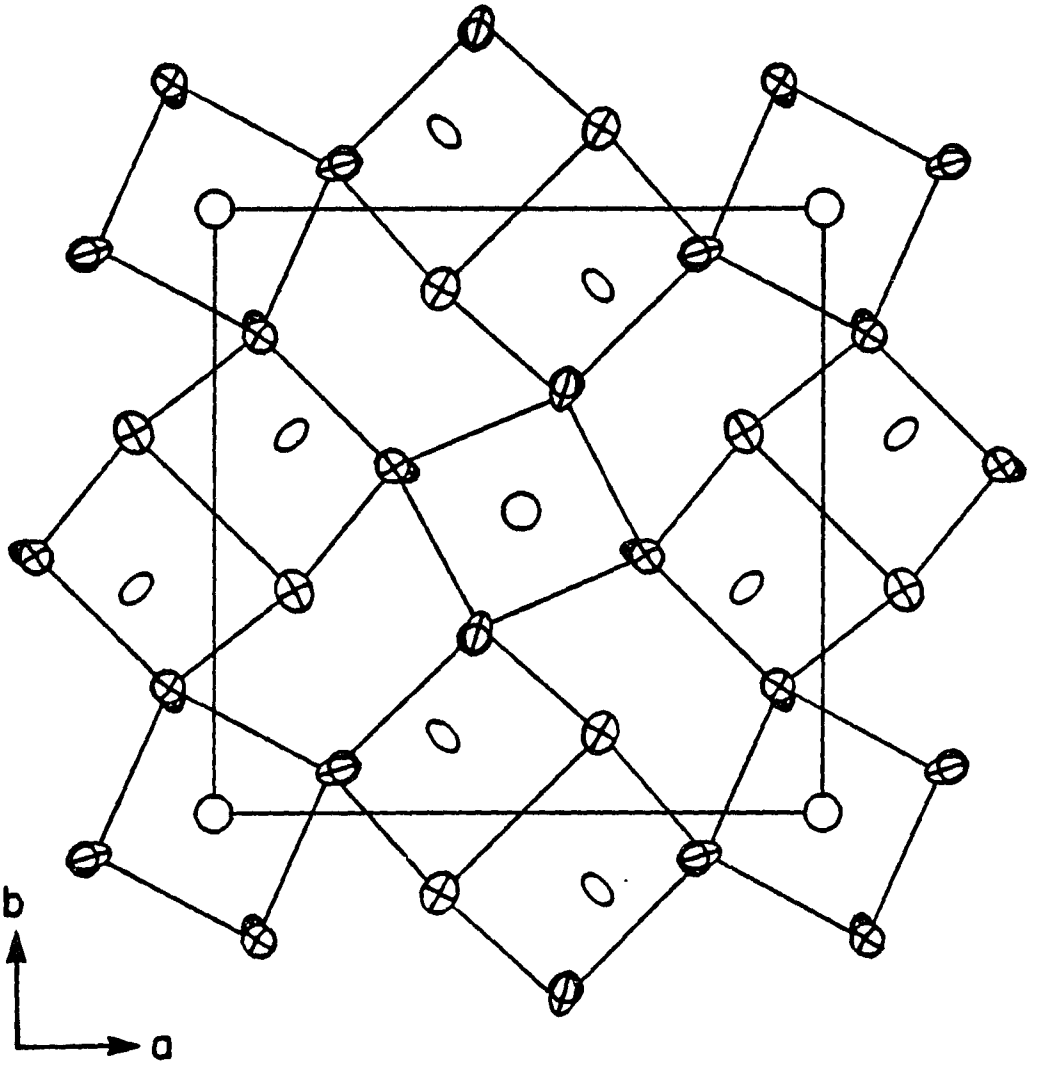

Figure 5. Three different cross sections of $Ca_{16}Sb_{11}$ are drawn. (a) The unit cell of $Ca_{16}Sb_{11}$ on Z = 0 (±0.22 Z). Open figures: Sb atom; crossed ellipsoids: Ca atoms

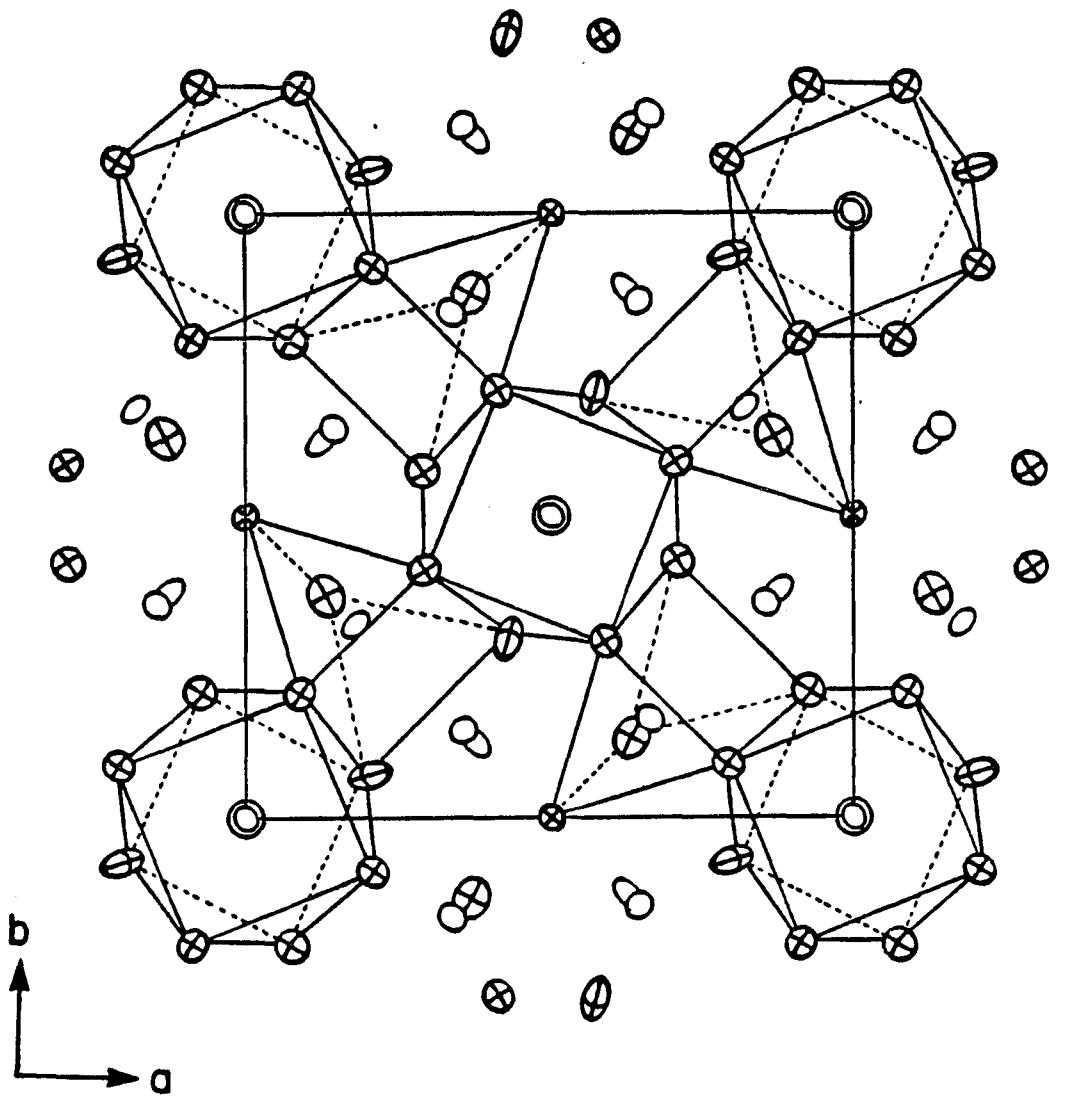

Figure 5. (continued)
(b) The cross section of the unit cell of $Ca_{16}Sb_{11}$ on z = 0.35 (±0.39z). Open figures: Sb atoms; crossed ellipsoids: Ca atoms

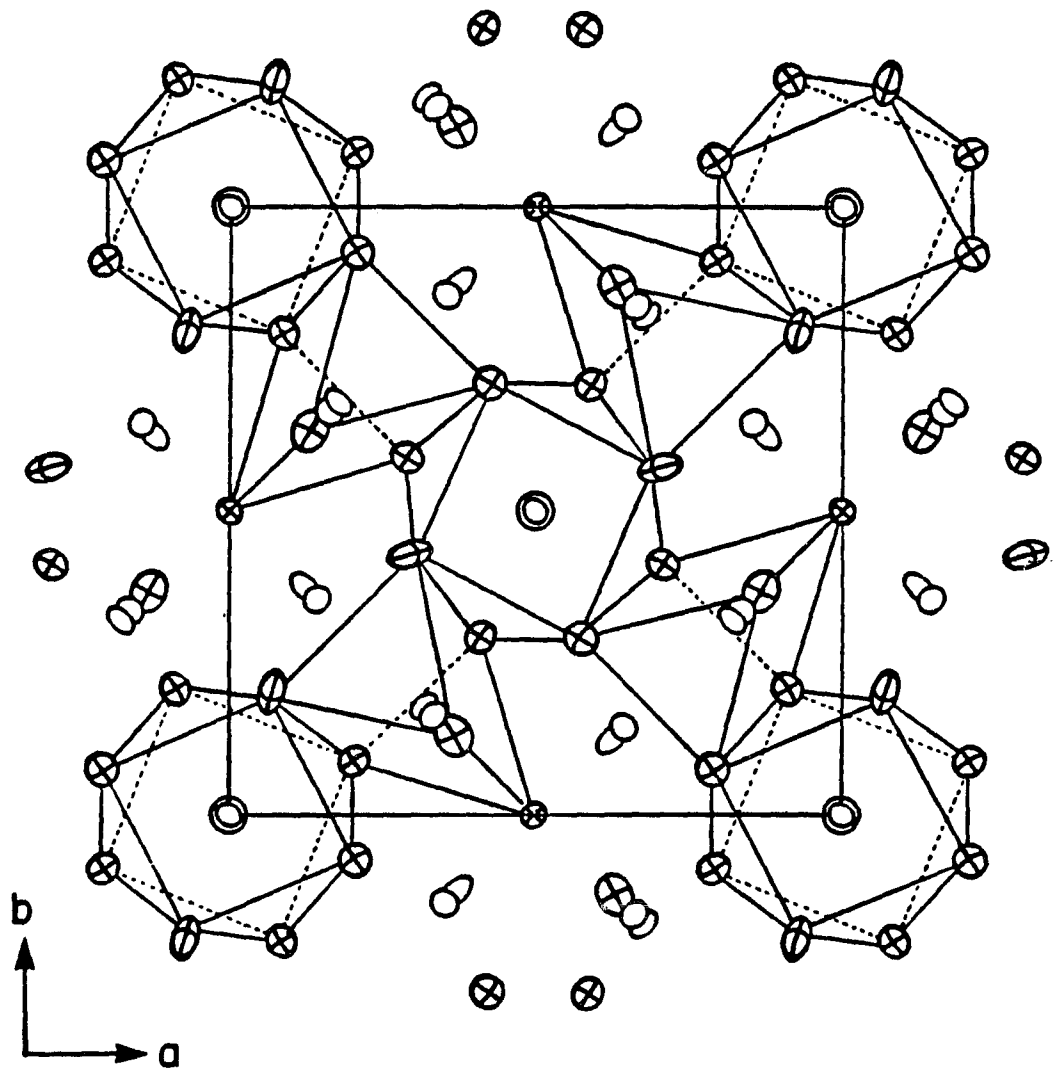

Figure 5. (continued)
(c) The cross section of the unit cell of $Ca_{16}Sb_{11}$ on Z = 0.65(±0.39z). Open figures: Sb atoms; crossed ellipsoids: Ca atoms

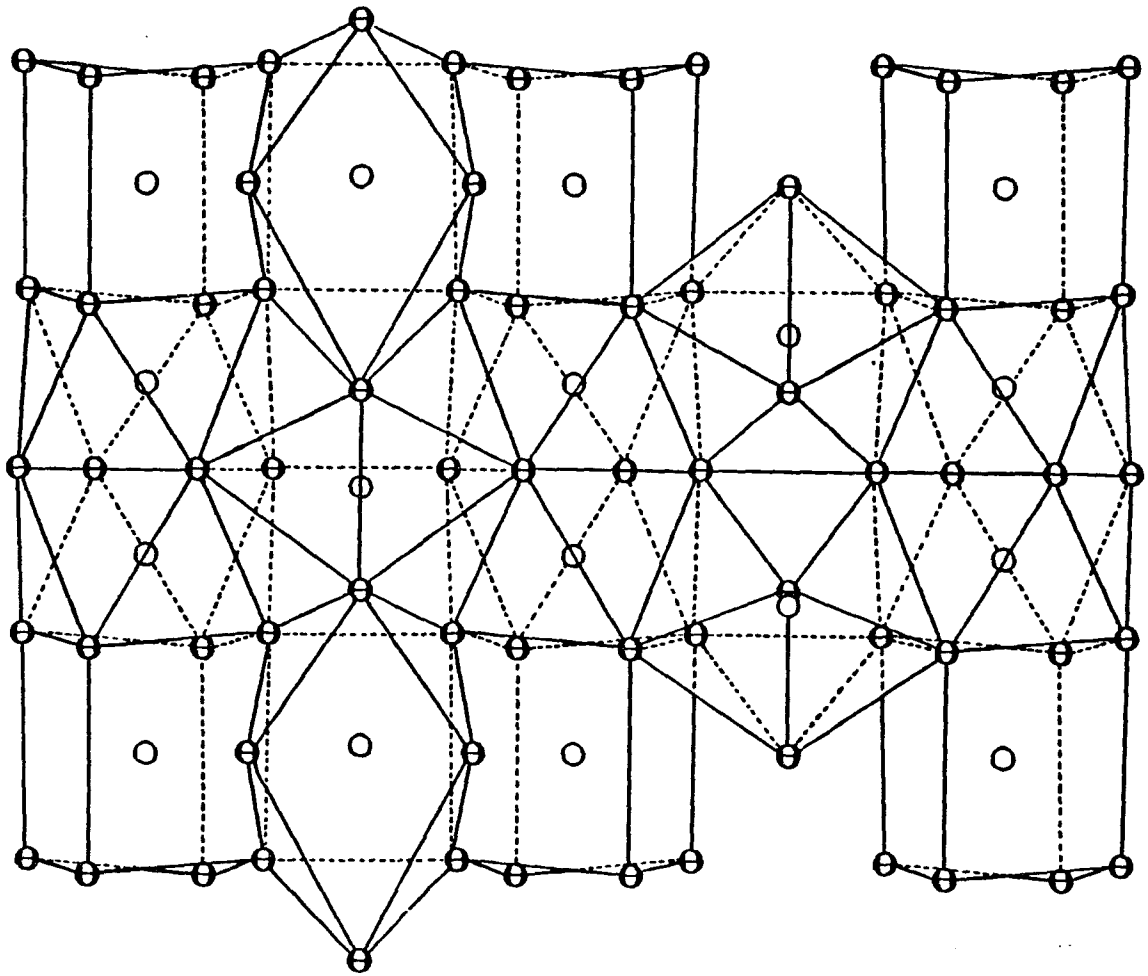

Figure 6. The structure of $Ca_{16}Sb_{11}$ projected on [110] plane and represented as Figure 1. Open ellipsoids = Sb atoms; crossed ellipsoids = Ca atoms

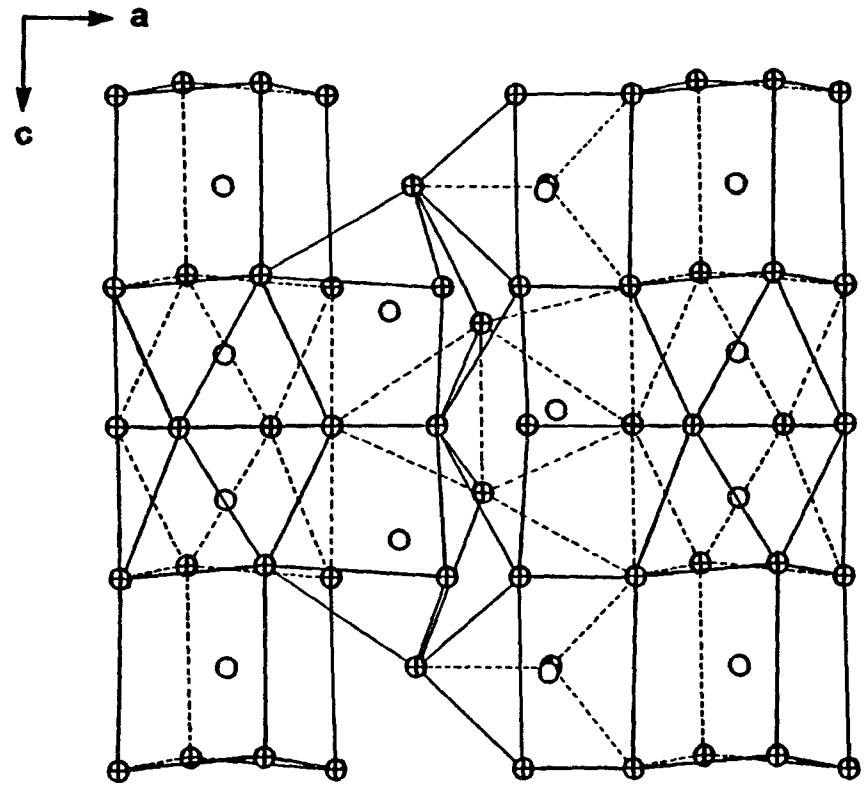

Figure 7. The structure of $Ca_{16}Sb_{11}$ projected on [010] plane as represented as Figure 2. Open ellipsoids = Sb atoms; crossed ellipsoids = Ca atoms

Comparisons between $Ca_{16}Sb_{11}$ and other Ca–Sb binary compounds

In comparing $Ca_{16}Sb_{11}$ with other Ca–Sb binary compounds, it is found there are similar trigonal prisms in Ca_5Sb_3 with the β–Yb_5Sb_3 structure; also square antiprisms and eight-atom polyhedra observed in $Ca_{11}Sb_{10}$. To illustrate the similarity, the distances between Sb and Ca atoms for $Ca_{16}Sb_{11}$, Ca_5Sb_3 and $Ca_{11}Sb_{10}$ are listed together in Table 6. The distances between Ca and Sb in the trigonal prism from 3.283(2) Å to 3.670(2) Å in Ca_5Sb_3 are longer than those of $Ca_{16}Sb_{11}$ which are from 3.041(4) Å to 3.444(6) Å. In general, the distances between Ca and Sb atoms in $Ca_{16}Sb_{11}$ range from 3.041 Å to 3.504 Å which belong to non-bonding distances. Thus, the Sb's in $Ca_{16}Sb_{11}$ seem to be all isolated. According to the simple valence electron counting, there is one negative charge excess from Sb available. Therefore, the electric property of $Ca_{16}Sb_{11}$ should be metallic or paramagnetic.

Existence of $Sr_{16}Bi_{11}$

Recently, a reaction with similar reaction conditions to rxn. 483 for $Sr_{16}Bi_{11}$ was run to synthesize the analogue of $Ca_{16}Sb_{11}$ based on the close metallic radius ratio for Ca/Sb and Sr/Bi. The powder pattern seemed to contain the same phase as $Ca_{16}Sb_{11}$ with a = 13.137(1) Å and c = 11.594(2) Å. However, the calculated powder pattern only matched most of the experimental one in some reflections' intensities. Further single crystal studies might be needed to confirm the structure of $Sr_{16}Bi_{11}$.

Table 6. Comparisons in Ca–Sb distances between $Ca_{16}Sb_{11}$ and other Ca–Sb binary compounds

In square antiprism	Sb(1) – 4Ca(2)	3.249(5)
	Sb(1) – 2Ca(4)	3.140(6)
	Sb(1) – 2Ca(5)	3.218(7)
In trigonal prism	Sb(2) – 2Ca(2)	3.243(6)
	Sb(2) – Ca(3)	3.044(8)
	Sb(2) – 2Ca(4)	3.299(6)
	Sb(2) – 2Ca(5)	3.420(6)
	Sb(2) – Ca(6)	3.041(4)
In trigonal prism	Sb(3) – Ca(1)	3.117(2)
	Sb(3) – 2Ca(2)	3.221(6)
	Sb(3) – Ca(3)	3.058(8)
	Sb(3) – 2Ca(4)	3.444(6)
	Sb(3) – 2Ca(5)	3.189(6)
In trigonal prism	Sb(4) – 2Ca(2)	3.176(6)
	Sb(4) – 2Ca(2)	3.069(6)
	Sb(4) – 2Ca(2)	3.140(7)
In 8-atom polyhedron	Sb(5) – Ca(1)	3.236(8)
	Sb(5) – 2Ca(2)	3.373(5)
	Sb(5) – 2Ca(2)	3.398(5)
	Sb(5) – 2Ca(4)	3.504(6)
	Sb(5) – Ca(6)	3.165(7)
In cube	Sb(6) – 4Ca(4)	3.632(5)
	Sb(6) – 4Ca(5)	3.367(7)

Sb(5) – 2Ca(4)	3.19	
Sb(5) – 2Ca(1)	3.44	in $Ca_{11}Sb_{10}$
Sb(5) – 2Ca(1)	3.55	(ref. 2)
Sb(5) – Ca(3)	3.49	
Sb(5) – Ca(2)	3.75	
Sb(1) – Ca(2)	3.360(2)	
Sb(1) – Ca(2)	3.283(2)	in Ca_5Sb_3
Sb(1) – Ca(3)	3.291(2)	(ref. 3)
Sb(1) – Ca(3)	3.425(2)	
Sb(1) – Ca(1)	3.670(2)	
Sb(1) – Ca(1)	3.362(2)	

Sb(1) – 2Ca(2)	2.93	in $Ca_{11}Sb_{10}$
Sb(1) – 4Ca(4)	3.22	(ref. 2)
Sb(1) – 2Ca(1)	3.47	

Relationships within $R_{5n+6}T_{3n+5}$

It is difficult to give a general interpretation about the occurrence of this series of compounds, since R and T elements vary through a large range of dimension, electronegativity, valence, etc. However, the investigation of radius ratio r_R/r_T (using the metallic radii for coordination number 12)[13] reveals the relationship between r_R/r_T and $R_{5n+6}T_{3n+5}$. Figure 8 shows the distribution of $R_{5n+6}T_{3n+5}$ against r_R/r_T. It is clear that there is a wide range of r_R/r_T for R_5T_3 from ~0.9 — ~1.2 (except for Ca_5Pt_3 which r_R/r_T is ~1.4), while the r_R/r_T's for the rest of $R_{5n+6}T_{3n+5}$ are all limited in narrow ranges: $R_{31}T_{20}$, r_R/r_T ~1.2; $R_{26}T_{17}$, r_R/r_T ~1.4; $R_{21}T_{14}$ (R_3T_2), r_R/r_T ~1.3, and $R_{16}T_{11}$, r_R/r_T ~1.3. From this observation, the r_R/r_T seems to be a good standard classifying the structures within $R_{5n+6}T_{3n+5}$.

The further comparisons in volume percent contraction ΔV (calculated based on the elemental atomic volumes) in $R_{5n+6}T_{3n+5}$ give more understanding about the structures of the compounds. Figure 9 represents the ΔV vs r_R/r_T of $R_{5n+6}T_{3n+5}$. Apparently, $R_{21}T_{14}$ and $R_{26}T_{17}$ which are all composed of rare earth and transition metals show little volume contraction in a narrow range from 9% — 2%, while $R_{16}T_{11}$ which is composed of alkaline earth and main group elements show large volume contraction around 20%. In $R_{31}T_{20}$, both compounds with Pu element have unusual volume expansion around 10%, while $Ca_{31}Sb_{20}$ has the similar volume contraction as $R_{16}T_{11}$.

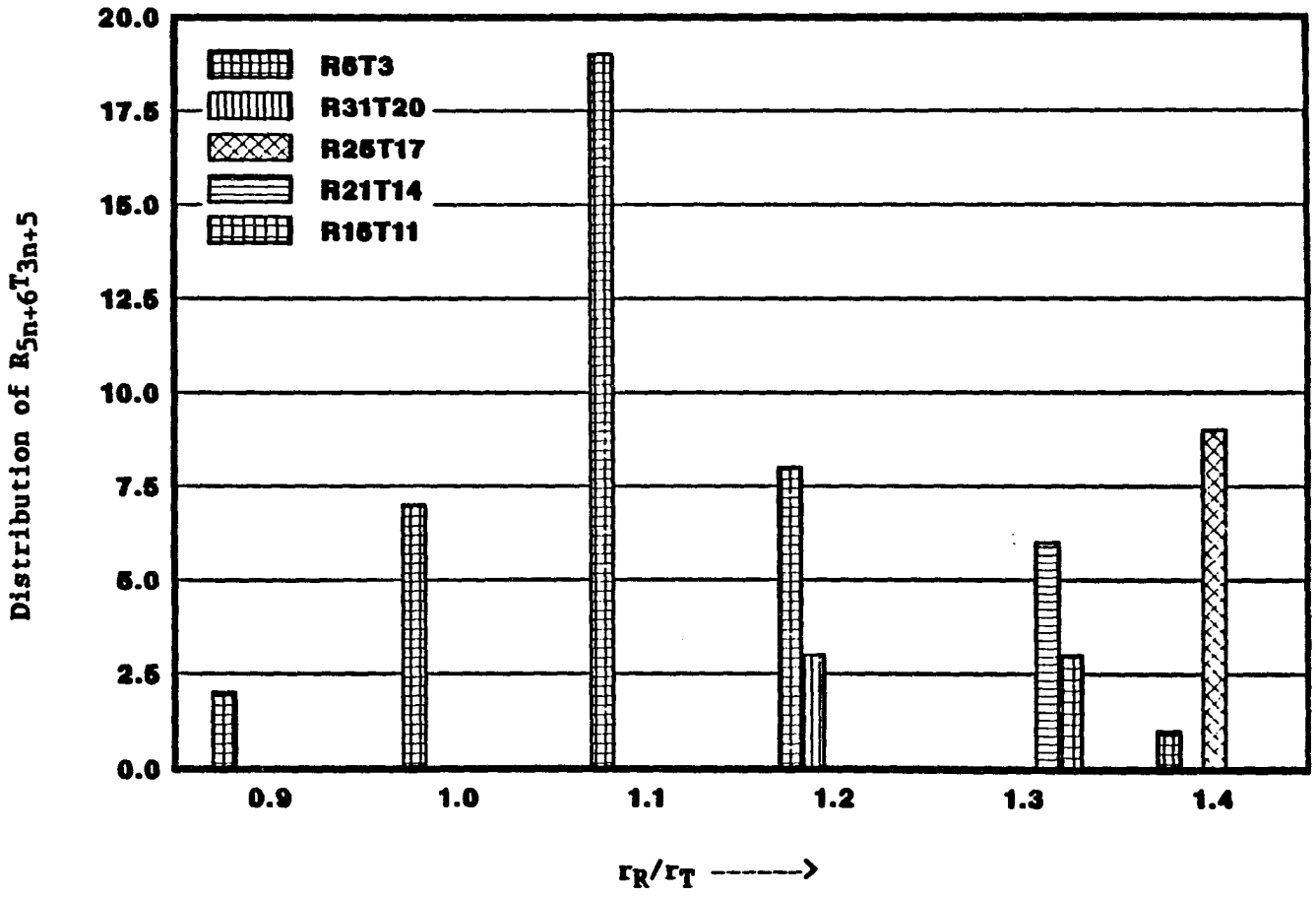

Figure 8. The distribution of $R_{5n+6}T_{3n+5}$ vs the ratios of r_R/r_T

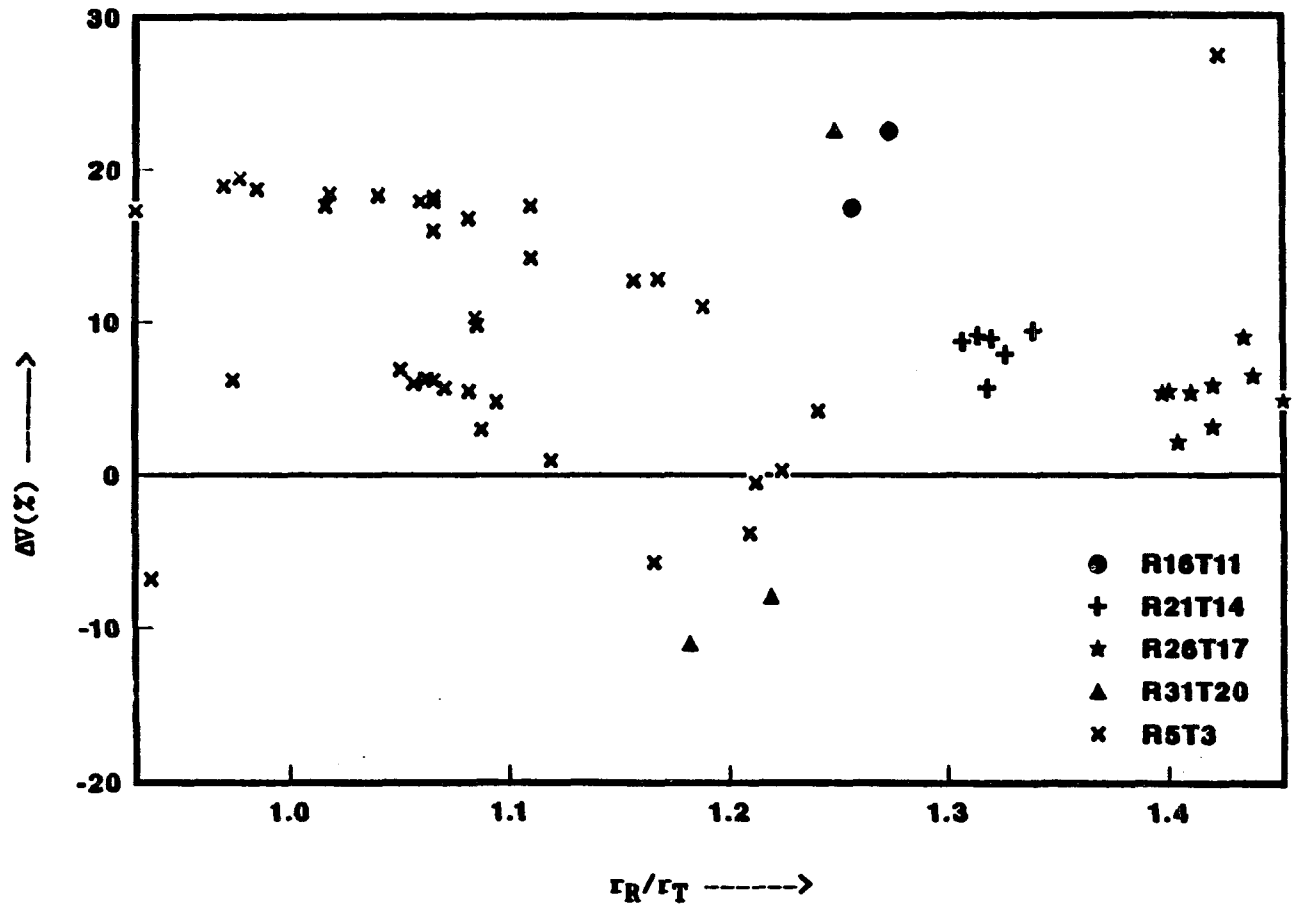

Figure 9. The ΔV (%) of $R_{5n+6}T_{3n+5}$ ($n \neq \infty$) vs the ratios of r_R/r_T

For R_5T_3 with W_5Si_3 structure (R including rare earth, transition metal and alkaline earth; T including transition metal and main group elements), they show a wide range of volume contraction from -10% to 27%. However, a couple of conclusive points can be reached after classifying the R_5T_3 compounds into subgroups. Figure 10 shows the ΔV vs r_R/r_T of R_5T_3 which are divided into eight subgroups: T_5Ga_3, R_5In_3, R_5Tl_3, T_5Si_3, T_5Ge_3, R_5Sn_3, Pu_5T_3 and others. From this Figure, the range of ΔV of R_5Si_3 and R_5Ge_3 are about the same, from 14% — 19%, while T_5Ga_3 had the wide ΔV range from 10% — 17%. Again, R_5In_3 and R_5Tl_3 have very narrow ΔV ranges from 6% — 7%, while the narrow ΔV of R_5Sn_3 is from 11% — 13%. Two of Pu_5T_3 show expansion while the other one almost no contraction at all. In the rest of the R_5T_3 compounds, Pu_5Pb_3 and Eu_5Pb_3 all expand relative to their elemental volumes. The ΔV of γ-V_5As_3 is similar to those of T_5Si_3 and T_5Ge_3. The ΔV's of Zr_5Al_3, Cd_5Au_3 and Pu_5Si_3 are all in the range from 1% — 5% despite that they are quite different in r_R/r_T. Finally, Ca_5Pt_3, which is the only R_5T_3 with r_R/r_T larger than 1.24, shows the highest ΔV (27%).

For R_5T_3, although the wide range of r_R/r_T exists in each subgroup, the ΔV seems to be in a narrow range for a particular subgroup except for T_5Ga_3. Despite the electronic reasons, this might be used to predict the possibility of unknown R_5T_3 phases with the W_5Si_3 structure.

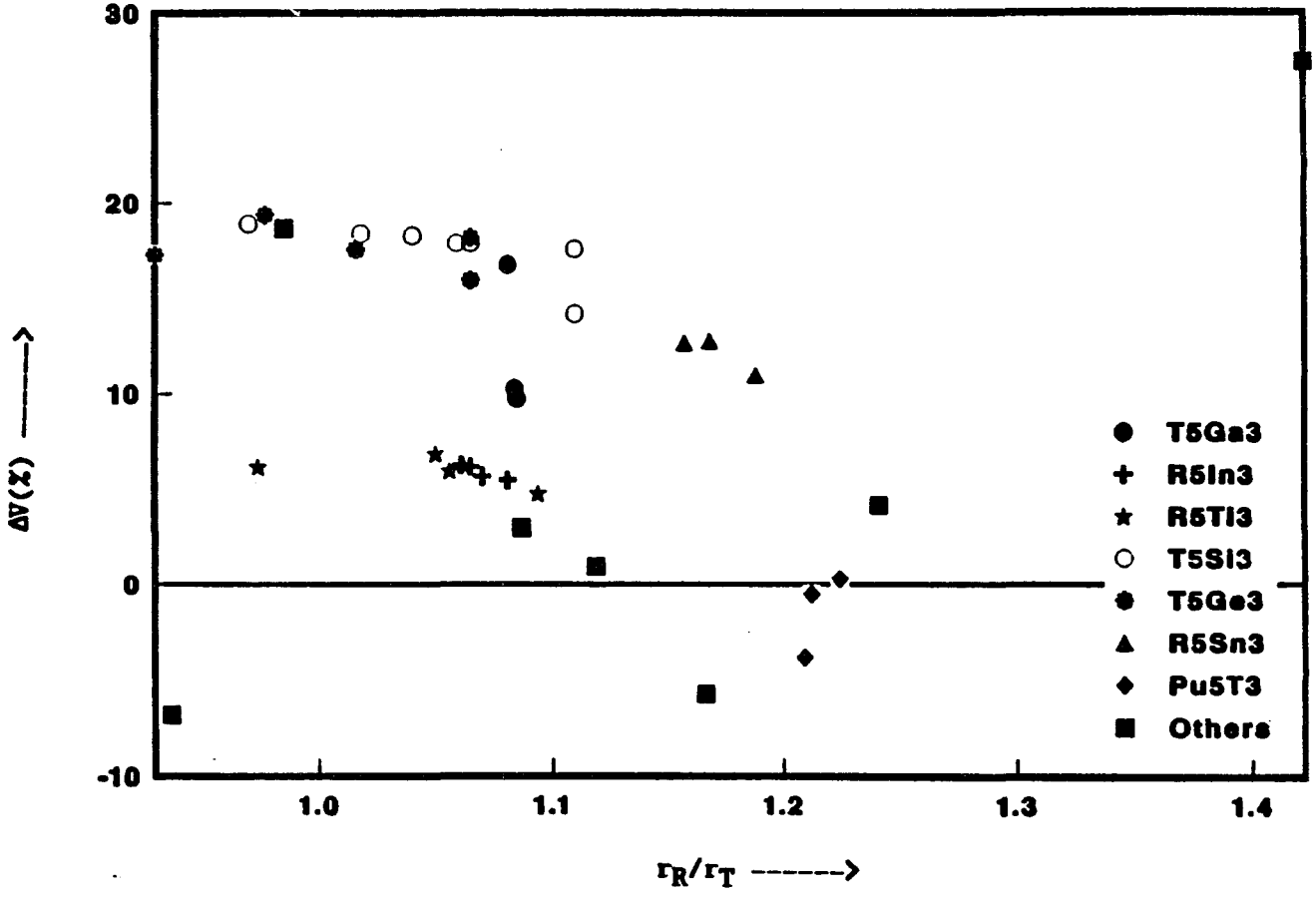

Figure 10. The ΔV (%) of R_5T_3 vs the ratios or r_R/r_T

References

1. Deller, K.; Eisenmann, B. Z. Anorg. Allg. Chem. 1976, 425, 104.

2. Deller, K.; Eisenmann, B. Z. Naturforsch. 1976, 31b, 29.

3. Martinez-Ripoll, M.; Brauer, G. Acta Crystallogr. 1974, B30, 1083.

4. Bruzzone, G.; Franceschi, E.; Merlo, F. J. Less Common Met. 1978, 60, 59.

5. Niyazona, Z. V.; Vakhobov, A. V.; Dzhuraev, T. D. Inorg. Mat. 1976, 12, 1074.

6. Werner, P. E. "TREOR-4 Trial and Error Program for Indexing Unknown Powder Patterns", Department of Structural Chemistry, Arrhnius Laboratory, University of Stockholm: S-106 91 Stockholm, Sweden, 1984.

7. Franceschi, E. A.; Ricaldone, F. Rev. Chim. Miner. 1984, t21, 202.

8. Leroy, J.; Moreau, J. M.; Paccard, D.; Parthe, E. J. Less Common Met. 1980, 76, 131.

9. Yarmolyuk, Y. P.; Grin, Y. N.; Olesh, O. M. Kristallografiya 1980, 25, 248.

10. Moreau, J. M.; Paccard, D.; Parthe, E. Acta Crystallogr. 1976, B32, 1767.

11. Cromer, D. T.; Larson, A. C. Acta Crystallogr. 1977, B33, 2620.

12. Fornasin, M. L.; Franceschi, E. Acta Crystallogr. 1977, B33, 3476.

13. Teatum, E. T.; Gschneidner, Jr., K. A.; Waber, J. T., Rep. LA-4003, 1968 (U. S. Department of Commerce, Springfield, VA).

PART V. $Sr_xMg_yGe_z$ TERNARY SYSTEM

Introduction

The replacement of some cations by different size but the same charge cations often not only changes the structure types, but also creates unique structure types which are not observed in pure binary compounds. In $M_xM'_yX_z$ (M, M' = alkaline earth metals; X = Si, Ge, Sn, Pb), three combinations have been well studied including: $MBe_{0.75}X_{1.25}$, MM'_2X_2, MM'X and $MSrSi_4$.

In $MBe_{0.75}X_{1.25}$,[1] a AlB_2 type structure is found with M from Ca, Sr to Ba and X from Si to Ge. There are two structure types found in MM'_2X_2 which are both derived from $BaAl_4$. For CaM'_2Ge_2 (M' = Be, Mg),[2] they form a $CaBe_2Ge_2$-type structure, while $BaMg_2X_2$ (X = Si, Ge, Pb) form $ThCr_2Si_2$-type.[3] In MM'X, two very similar structures, anti-$PbCl_2$ and anti-PbFCl, are observed. For BaMgX (X = Si, Ge, Sn, Pb),[4,5] they form the anti-PbFCl structure, while BaCaX,[6] CaMgX and SrMgX[7] adopt an anti-$PbCl_2$ structure. In $MSrSi_4$ (M = Ca, Ba), the $BaSi_2$ structure is formed for the Ca analogue,[8] while $SrSi_2$ structure is adopted by the Ba analogue.[9] Apparently, the structures of $M_xM'_yX_z$ are quite dependent on the relative size between M and M'. For example, the combination of Ba and Mg always seems to yield different structures from other combinations of the alkaline earth metals.

In the Sr-Mg-Ge system, SrMgGe is the only known compound and it has the Co_2Si structure, which is the same for the binary compound Sr_2Ge.[10] In this structure, there are Ge-centered trigonal prisms linked by common

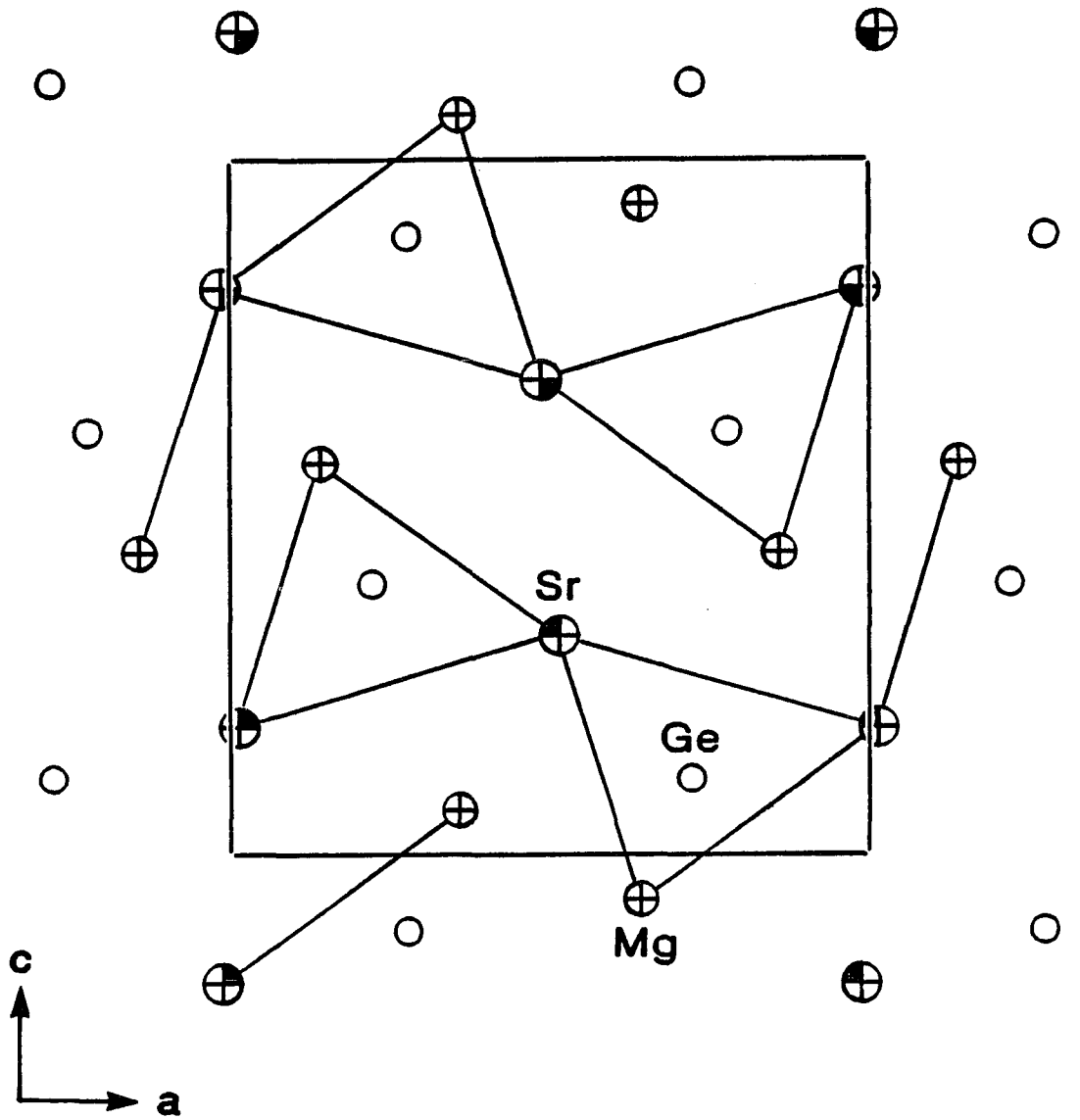

Figure 1. Unit cell of SrMgGe projected on [001] plane. The large shaded circles represent Sr atoms; medium circles represent Mg atoms; small open circles represent Ge atoms. The Sr/Mg atoms are different from the central Ge at z coordinate by 1/2

Sr atoms to form infinite zig-zag chains parallel to the a-axis (Figure 1). In the present study of the Sr-Mg-Ge system, four new compounds were found with similar prisms as that of SrMgGe, but linked and arranged in different ways in $SrMg_3Ge_3$, $SrMg_2Ge_2$, $Sr_{2+x}Mg_{12-x}Ge_7$ and $Sr_{5+y}Mg_{19-y}Ge_{12}$.

$SrMg_3Ge_3$

Due to the similar size of Sr and Eu, synthesis of $SrMg_3Ge_3$ was tried as an analogue of $EuMg_3Ge_3$.[11] Stoichiometric elementary starting materials were loaded into a Ta tubing. These were first heated to 900°C for 2 days, then annealed at 750°C for 2 weeks. The product looked like a homogeneous phase with gray metallic luster. The powder pattern indicated that it is not an analogue of $EuMg_3Ge_3$ (space group Cmcm and a = 4.485, b = 30.60, c = 4.485 Å). Moreover, the cell was determined to be a primitive orthorhombic structure with a = 14.628(2) Å, b = 12.669(2) Å and c = 4.4272 (5) Å, by the TREOR program (31 sharp lines used).

The size of the c-axis of $SrMg_3Ge_3$ is about the same as the b-axis of SrMgGe which is 4.56 Å. That indicated the cell of $SrMg_3Ge_3$ might contain trigonal prisms also with z-coordinates of 1/4, 3/4 or 0, 1/2. In reviewing the literature,[12] Rh_4P_3[13] was found to have a primitive orthorhombic cell with a = 11.662 Å, b = 3.317 Å and c = 9.994 Å which are close to those of $SrMg_3Ge_3$ if the b and c axes are reversed. In Rh_4P_3, all the atoms are on 4(c) positions, i.e., y = 1/4 and 3/4, which is consistent with the expected structure of $SrMg_3Ge_3$. More importantly, the calculated powder pattern based on the atom coordinates of Rh_4P_3 and lattice constants of $SrMg_3Ge_3$ was similar to the experimental one.

A closer look at the structure of Rh_4P_3 revealed further relationship between them, Figure 2(a) show the unit cell of Rh_4P_3 projected on the [010] plane, all the P atoms are in trigonal prisms. Two-thirds of the P atoms are in more regular prisms than the other one-third. If the latter one-third P atoms all are shifted to the neighboring empty regular trigonal prism sites, then the representation of the unit cell become Figure 2(b). In this figure, three trigonal prisms fused together to form corrugated fragments which are connected by common Sr atoms of $SrMg_3Ge_3$. The common Rh atoms are replaced by Sr atoms like the common Sr atoms in SrMgGe. The three Ge atoms in the fragments should form $[Ge–Ge–Ge]^{8-}$ finite fragment. The central Ge atom in the fragment should have 2 e^- and the terminal Ge atoms should have 3 e^-, consistent with the valence rule, because the central Ge atom is two bonded while the terminal Ge atoms are only one bonded.

However, there are still a couple of lines in the calculated powder pattern not matched with the experimental one. This might be caused by inaccuracy of atom coordinates, because the positions of the shifted P atoms were only estimated from the distances; also the fusing of the prisms might effect the geometries of the original prisms. On the other hand, the space group of Rh_4P_3 might be changed because a couple of reflections of $SrMg_3Ge_3$ violate the extinctions of the space group of Rh_4P_3 (Pnma). It is necessary to grow the single crystals before we can further characterize this new compound which is also a new structure type. Although a couple of different reaction conditions have been tried (Table 1), no single crystals have been obtained yet. Most of the

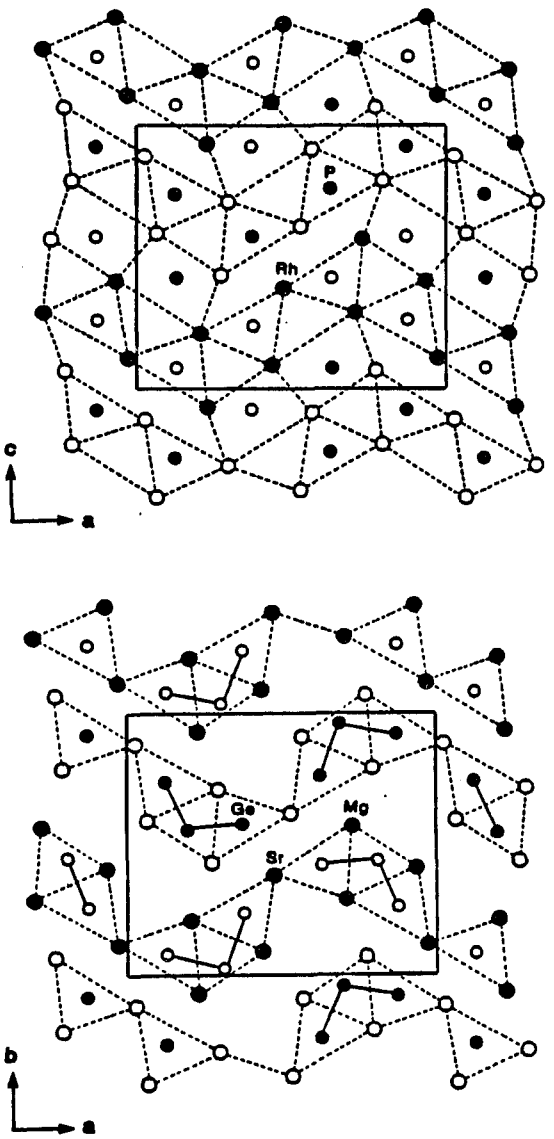

Figure 2. The structure relationship between Rh_4P_3 and $SrMg_3Ge_3$ is shown. (a) Unit cell of Rh_4P_3 projected on [010] plane. Circles represent Rh atoms; small circles represent P atoms; open circles indicate atoms at y = 1/4 and closed circles indicate atoms at y = 3/4. (b) Approximate unit cell of $SrMg_3Ge_3$ derived from Rh_4P_3 and projected on [001] plane. Circles represent Mg atoms except those linked between two fragments are Sr atoms; small circles represents Ge atoms. Open circles indicate the atoms at z = 0 or 1/4 and closed circles indicate the atoms at z = 1/2 or 3/4 coordinate

Table 1. Reaction conditions of Sr–Mg–Ge systems

Rxn no.	Sr/Mg/Ge	Rxn. Conditions	Products[a]
468	1.00/3.00/3.00	900°C 4 days 700°C 2 weeks	"$SrMg_3Ge_3$"
497	2.00/3.00/3.00	800°C 4 days 950°C 2 days 880°C 4 days 820°C 1 day 750°C 1 day 650°C 1 day	"$SrMg_3Ge_3$"
523	1.00/2.99/2.99	1200°C 12 hrs (induction heating) quenching	"$SrMg_3Ge_3$"
514	1.00/5.01/3.00 (2.33/11.69/7.00)	900°C 5 days 700°C 6 days	$Sr_{2+x}Mg_{12-x}Ge_7$
499	1.00/2.00/2.00	the same as rxn. 514	?
538	2.21/11.79/7.00	910°C 2 weeks 840°C 5 days 740°C 28 days	$Sr_{2+x}Mg_{12-x}Ge_7$
537	6.86/17.13/12.00	the same as rxn. 538	$Sr_{5+y}Mg_{19-y}Ge_{12}$
532	5.54/18.37/12.00	the same as rxn. 538	$Sr_{5+y}Mg_{19-y}Ge_{12}$
536	5.58/18.42/12.00	the same as rxn. 538	$Sr_{5+y}Mg_{19-y}Ge_{12}$
535	5.00/19.00/12.00	910°C 2 days 850°C 2 weeks	$Sr_{5+y}Mg_{19-y}Ge_{12}$ (80% yield) $Sr_{2+x}Mg_{12-x}Ge_7$ (20% yield)
548	5.00/19.00/12.00	940°C 10 days, 840°C 2 weeks	$Sr_5Mg_{19}Ge_{12}$

[a]All the products were single phases in each reactions except for 535.

products looked like plates formed by needles and it was very difficult to separate them. However, the morphology of the products also supports the postulation of the expected structure, because low dimension compounds always show plate or needle-like appearances.

$SrMg_2Ge_2$

A stoichiometry of $SrMg_2Ge_2$ was loaded for rxn. 499 (Table 1). The product did not contain any one of the known binary Sr—Ge or Mg—Ge phases judging from the powder pattern. The possibilities of ternary compounds such as SrMgGe, $SrMg_3Ge_3$, $Sr_{2+x}Mg_{12-x}Ge_7$ and $Sr_{5+y}Mg_{19-y}Ge_{12}$ also have been checked and excluded. Surprisingly, it did not form $ThCr_2Si_2$ or $CaBe_2Ge_2$ structures which are very common in MM'_2X_2 (M = Ca or Ba; M' = Be or Mg; X = Si, Ge, Sn, Ph). However, the cell constants of the products could not be derived by using the TREOR program. That indicated that a mixture can not be ignored or that it is a monoclinic or triclinic cell, because sometimes TREOR program can not give a right cell for a monoclinic or a triclinic cell.

$Sr_{2+x}Mg_{12-x}Ge_7$

The title compound was first obtained from rxn. 514 loaded with Sr/Mg/Ge equal to 1.00/5.01/3.00 (Table 1). The structure of the product was confirmed to be isostructural with $Zr_2Fe_{12}P_7$[14] by indexing the powder pattern by TREOR program. Total 23 lines (all the sharp lines) were used to derive the hexagonal cell with a = 11.0728(7) A and c = 4.3626(5) A. Since the loaded stoichiometry was deviated from that of the $Zr_2Fe_{12}P_7$, this phase was represented as $Sr_{2+x}Mg_{12-x}Ge_7$. The atom positions

of ideal $Sr_2Mg_{12}Ge_7$ are close to those of $Zr_2Fe_{12}P_7$ (space group $P\bar{6}$) judging from the comparison between the calculated and experimental powder patterns (Table 2). Both Sr atoms are in the special positions 1(c) and 1(f). In the four Mg atom positions, half of them are in 3(j) positions, while half of them are located in 3(k) positions. One of three Ge atoms is in the origin, while the other two are in 3(j) or 3(k) position. The details of the assumed atom positions of $Sr_2Mg_{12}Ge_7$ are listed in Table 3.

The unit cell of ideal $Sr_2Mg_{12}Ge_7$ is represented in Figure 3. Three Ge-centered trigonal prisms are fused together on the common Sr atoms and one Ge atom is located on the origin position. To illustrate the coordination around the Ge atom on the origin, Figure 4 represents the unit cell expanded on an ab plane. The chemical environment of the Ge atom becomes clear on a triangular plane or tricapped trigonal prisms. This is the first Zintl phase adopted this type structure. The electron counting of the ideal compound indicated it is a valence compound, because two Sr and twelve Mg atoms would provide 28 e^- to the seven Ge atoms to form isolated Ge^{4-} anions.

The same phase also observed in rxn. 538. The stoichiometry of starting material was Sr/Mg/Ge equal to 1.21/11.81/7.00. The lattice constants of the products also different from those of the previous one (see Table 4). Also, as the amount of Sr relative to Mg increased then the lattice constants increased too. This further confirmed it was a nonstoichiometric phase.

Table 2. Observed and calculated[a] powder patterns for $Sr_{2+x}Mg_{12-x}Ge_7$

h k ℓ	d_{cal}, Å	d_{obs}, Å	I_{cal}[b]	I_{obs}[b]
1 0 1	3.966		8	-
1 2 0	3.621	3.619	37	45
1 1 1	3.423	3.423	28	30
2 0 1	3.223	3.226	48	50
3 0 0	3.194	3.194	24	30
2 1 1	2.785	2.786	100	100
2 2 0	2.766	2.763	8	10
3 1 0	2.657	2.658	7	10
3 0 1	2.576	2.577	14	15
4 0 0	2.395	2.396	11	13
2 2 1	2.335	2.336	8	8
3 1 1	2.269	2.269	24	30
0 0 2	2.179	2.179	30	30
4 0 1	2.099	-[c]	9	-
4 1 0	2.091	2.091	41	35
2 3 1	1.962	1.963	33	30
1 4 1	1.885	1.885	5	5
2 1 2	1.867	1.866	11	10
2 4 0	1.811	1.810	5	5
3 0 2	1.800	-	9	-
4 0 2	1.612	1.613	6	5
5 1 1	1.600	1.601	8	10
2 5 0	1.534	-	5	-
4 1 2	1.508	1.510	28	30
4 3 1	1.481	1.482	11	10
1 6 1	1.385	1.385	11	10
3 5 0	1.369	1.370	5	5
1 2 3	1.348	1.348	10	10
3 5 1	1.306	1.306	7	5
7 1 0	1.269	-	7	-
2 5 2	1.254	-	5	-
2 3 3	1.212	-	7	-

[a]The lattice constants adopted from rxn. 538 and assumed 0.21 Sr substituted in 3(j) positions.

[b]Cu $K\alpha_1$ radiation, λ = 1.540562 Å.

[c]These reflections were observed but with low intensities and broad or blurred lines.

Table 3. Atom positions of $Sr_2Mg_{12}Ge_7$[a]

Atom	Position		x	y	z
Sr(1)	1(c)	6	1/3	2/3	0
Sr(2)	1(f)	6	2/3	1/3	1/2
Mg(1)	3(j)	m	0.4309	0.0590	0
Mg(2)	3(j)	m	0.1583	0.2772	0
Mg(3)	3(k)	m	0.3864	0.4359	1/2
Mg(4)	3(k)	m	0.2232	0.0992	1/2
Ge(1)	1(a)	6	0	0	0
Ge(2)	3(j)	m	0.4163	0.2959	0
Ge(3)	3(k)	m	0.1207	0.4096	1/2

[a]Space group $P\bar{6}$ (No. 174); the atom positions are quoted from ref. 14.

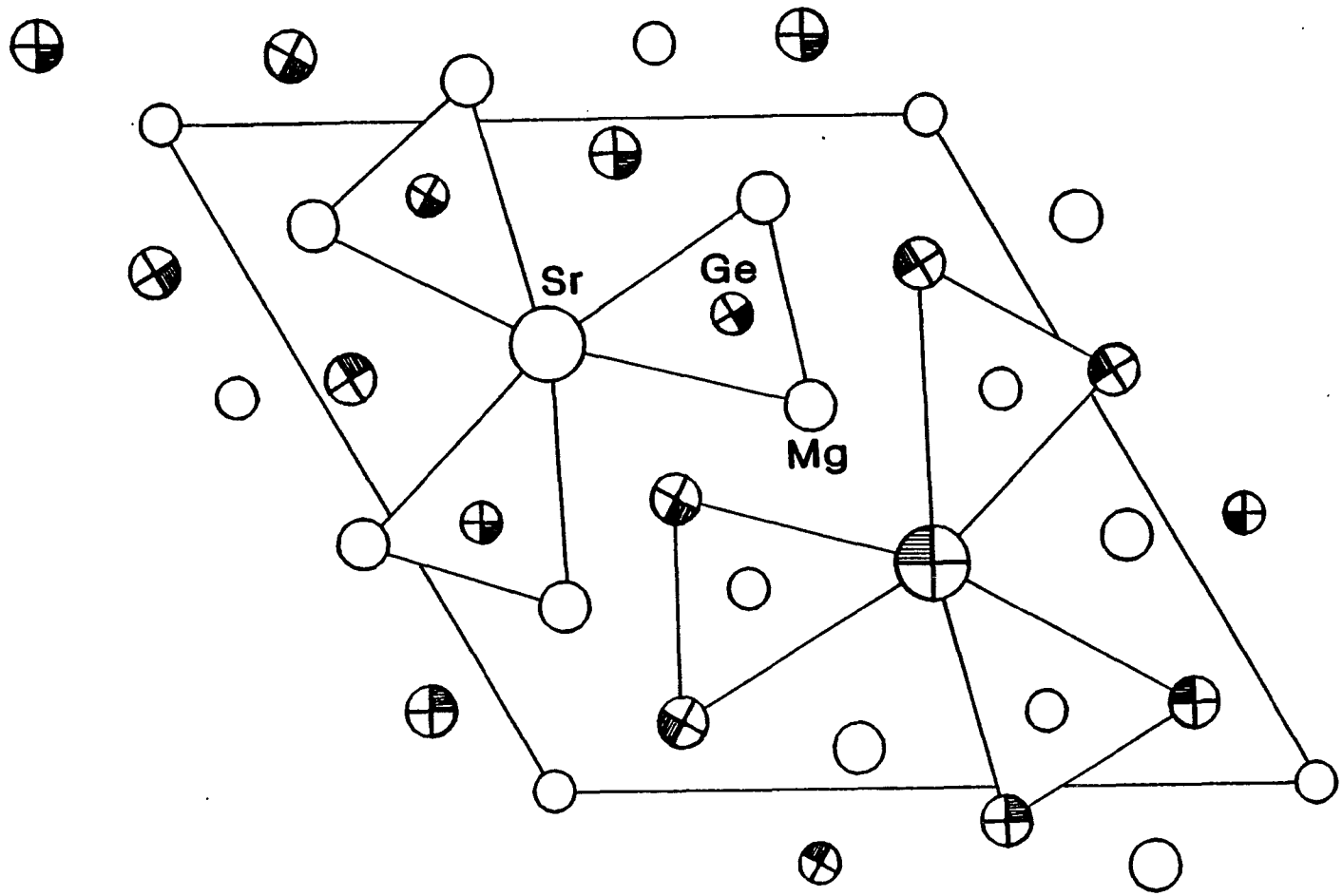

Figure 3. Unit cell of ideal $Sr_2Mg_{12}Ge_7$ based on $Zr_2Fe_{12}P_7$ projected on [001] plane. Circles represent Sr atoms; medium circles represent Mg atoms and small circles represent Ge atoms. Open circles indicate atoms at z = 0; shaded circles indicate atoms at z = 1/2. To illustrate the linkage of trigonal prisms, those cations with same z coordinate are connected together

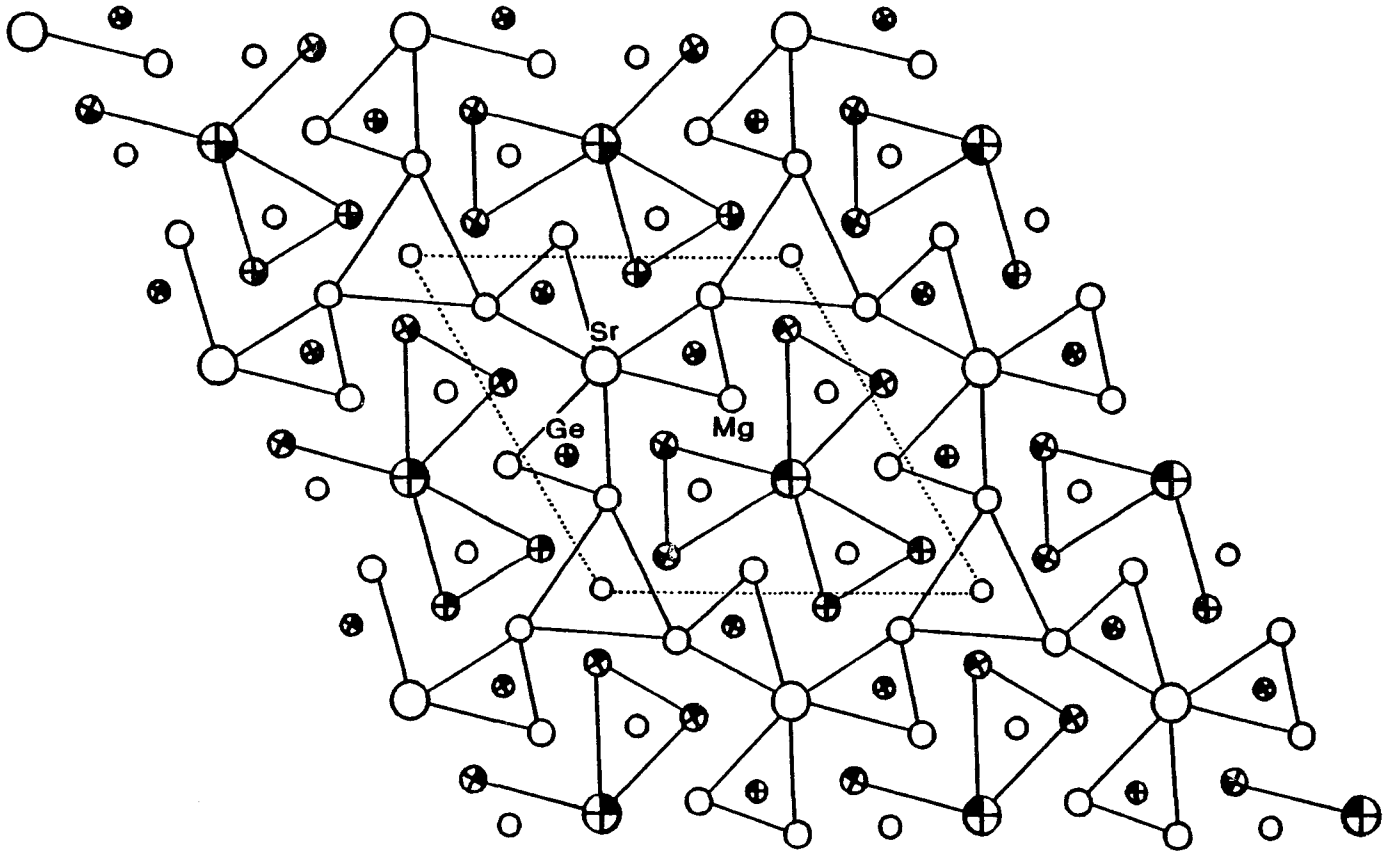

Figure 4. The unit cell of ideal $Sr_2Mg_{12}Ge_7$ expanded along ab plane, so that the relationship between two different fan like fragments become clear. Symbols are the same as Figure 3

Table 4. Lattice constants for $Sr_{2+x}Mg_{12-x}Ge_7$[a] and $Sr_{5+y}Mg_{19-y}Ge_{12}$[a]

Rxn No.	Sr% (mole)	Lattice Constants	# Lines indexed[b]	c/a
538	0.158	a = 11.063(1) c = 4.3572(8)	24	2.539
514	0.166	a = 11.0728(7) c = 4.3626(5)	23	2.538
535	0.208	a = 11.094(1) c = 4.3510(9)	8	2.550
		a = 14.718(2) c = 4.431(2)	26	3.314
548	0.208	a = 14.720(1) c = 4.437(1)		
532	0.231	a = 14.7602(5) c = 4.4539(3)	56	3.314
536	0.232	a = 14.7292(9) c = 4.4435(2)	56	3.314
537	0.286	a = 14.791(2) c = 4.4666(9)	19	3.311

[a]As x = y = 0, the Sr fractions for $Sr_{2+x}Mg_{12-x}Ge_7$ and $Sr_{5+y}Mg_{19-y}Ge_{12}$ are 0.143 and 0.208.

[b]Although not all lines in powder patterns were used for the calculations of lattice constants, they all seemed to belong to a single phase for each reactions except for rxn. 535.

$Sr_{5+y}Mg_{19-y}Ge_{12}$

In rxns. 537, 532 and 536, another hexagonal phase was confirmed as the ratios of Sr:Mg were varied (Table 1) while the ratio of (Sr,Mg)/Ge was kept to 2/1. The powder patterns of the reactions were very similar with high yield (>95%) of the products. The size of c-axis is the same as that of $SrMg_3Ge_3$ or $Sr_{2+x}Mg_{12-x}Ge_7$. This suggests that the structure of this phase should be composed of linked trigonal prisms too.

After carefully comparing different calculated powder patterns which were based on possible compounds, and the dimensions of cell and atom ratio, the structure type of this phase was determined to be that of $Ho_5Ni_{19}P_{12}$[15] (Table 5). The different lattice constant of the products in rxns. 532 or 536 (Table 4) show a nonstoichiometric character. The lattice constants of rxns. 537 and 532 show the tendency of increasing lattice constants as the relative amount of Sr increases but not for lattice constants of rxn. 536. The odd lattice constants of rxn. 536 might be caused from the dirty surface of Sr metal.

The atom positions of ideal $Sr_5Mg_{19}Ge_{12}$ is listed in Table 6. Figure 5 shows the cell projected in a [001] plane. In the unit cell, Sr(2) is located at 2(c) position at z = 0, while Sr(1) sits on 3(g) position to form a triangle centered by Ge(4) atom. There are five Mg positions, Mg(1) and Mg(3) are located at 6(h) and 3(g) positions at z = 1/2 and linked with Sr(1) atom to form a big fragment fused by seven Ge-centered trigonal prism, while Mg(2) and Mg(4) are at 6(j) and 3(f) positions at z = 0 and linked with a Sr(2) atom to form the same fragment as

Table 5. Observed and calculated powder patterns[a] for $Sr_{5+y}Mg_{19-y}Ge_{12}$

h k ℓ	d_{cal}, Å	d_{obs}, Å	I_{cal}[b]	I_{obs}[b]
2 1 0	4.831	4.821	9	5
1 1 1	3.813	3.812	6	3
2 2 0	3.690	3.689	41	40
3 1 0	3.545	3.544	31	35
2 1 1	3.275	3.273	86	90
3 0 1	3.079	3.080	65	70
3 2 0	2.933	2.930	4	3
2 2 1	2.842	2.842	100	100
4 1 0	2.789	2.789	31	30
3 1 1	2.774	2.773	97	90
4 0 1	2.596	2.596	10	10
5 0 0	2.557	2.556	11	13
3 2 1	2.449	2.450	11	15
4 2 0	2.416	2.410	3	5
4 1 1	2.364	2.365	21	25
5 1 0	2.296	2.297	17	20
0 0 2	2.227	2.226	56	50
3 3 1	2.153	2.153	21	25
6 0 0	2.130	2.131	79	80
4 2 1	2.123	2.123	5	5
5 1 1	2.047	2.047	4	5
6 1 0	1.949	1.949	6	5
2 2 2	1.907	1.906	12	10
4 3 1	1.901	1.901	48	50
3 1 2	1.886	1.886	10	10
5 2 1	1.860	1.860	4	5
4 4 0	1.845	1.845	7	5
4 1 2	1.740	1.740	14	20
4 4 1	1.705	1.705	9	8
5 3 1	1.690	1.690	4	5
5 0 2	1.679	1.679	6	5

5 1 2	1.598	1.598	10	15
7 1 1	1.583	1.583	6	10
6 0 2	1.539	1.540	54	65
6 3 1	1.515	1.514	11	13
5 5 0	1.476	1.475	7	30
7 2 1	1.473		19	
6 1 2	1.468	1.467	4	5
7 3 0	1.438	1.438	5	6
4 4 2	1.420		6	
2 1 3	1.419	1.419	7	15
8 1 1	1.418		9	
3 0 3	1.402	1.402	6	10
8 2 0	1.395		4	
6 4 1	1.393	1.393	11	10
2 2 3	1.377	1.377	9	10
3 1 3	1.369		10	
7 3 1	1.369	1.369	12	20
9 0 1	1.353	1.353	4	5
9 1 0	1.340	1.340	5	8
8 2 1	1.331	1.331	4	5
7 4 0	1.326	1.325	4	5
6 5 1	1.283	1.283	7	5
3 3 3	1.271	1.271	4	5
5 5 2	1.230	1.230	8	10
4 3 3	1.212	1.212	12	15
7 3 2	1.208	1.207	6	5
8 2 2	1.182	1.181	4	3

[a]The lattice constants adopted from rxn. 532 and assumed 0.54 Sr substituted in 3(f) positions.

[b]Cu $K\alpha_1$ radiation, λ = 1.540562 Å.

Table 6. Atom positions of $Sr_5Mg_{19}Ge_{12}$[a]

Atom	Position	x	y	z
Sr(1)	3(g)	0.8167(2)	0	1/2
Sr(2)	2(c)	1/3	2/3	0
Mg(1)	6(h)	0.8720(4)	0.5146(4)	1/2
Mg(2)	6(j)	0.8152(4)	0.1899(4)	0
Mg(3)	3(g)	0.2862(6)	0	1/2
Mg(4)	3(f)	0.4397(5)	0	0
Mg(5)	1(a)	0	0	0
Ge(1)	6(k)	0.5174(8)	0.6859(7)	1/2
Ge(2)	3(f)	0.6420(10)	0	0
Ge(3)	3(f)	0.1730(10)	0	0

[a]Space group $P\bar{6}2m$ (No. 189); the atom positions quoted from ref. 15.

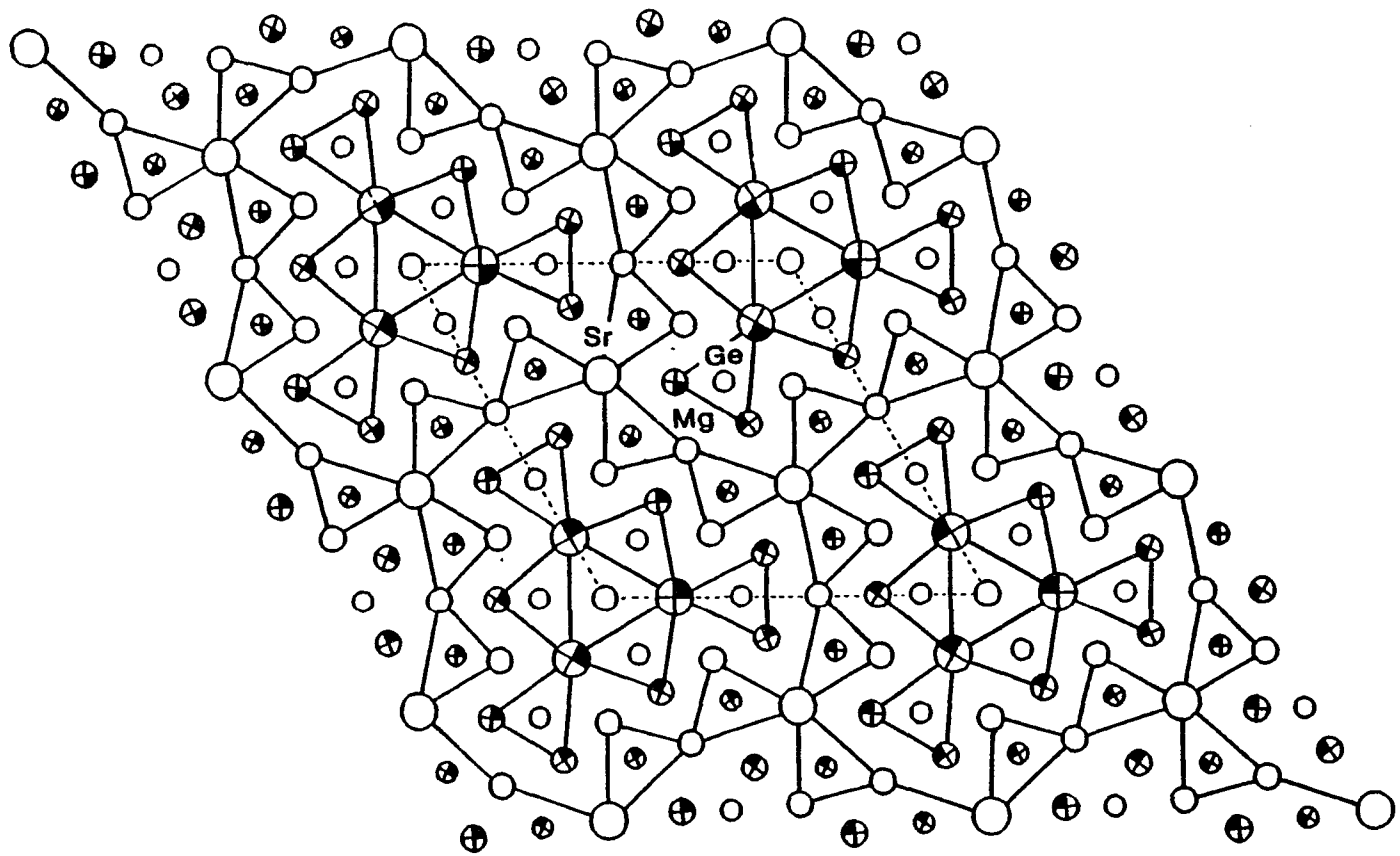

Figure 5. The unit of ideal $Sr_5Mg_{19}Ge_{12}$ based on $Ho_5Ni_{19}R_2$ projected on the [001] plane. Circles represent Sr atoms; medium circles represent Mg atoms and small circles stand for Ge atoms. Open circles indicate atoms at z = 0; shaded circles indicate atoms at z = 1/2 coordinate. To illustrate the linkage of trigonal prisms, those cations with same z coordinate are connected together. Also, the unit cell expanded along ab plane to show the two different fragments

that of $Sr_7Mg_{12}Ge_7$ and shared by Mg(4) atom to surround the big fragment. The charge of this phase also shows that it is a Zintl phase.

Discussion

Since $Sr_{2+x}Mg_{12-x}Ge_7$ and $Sr_{5+y}Mg_{19-y}Ge_{12}$ are all belonging to $Sr_zMg_{2-z}Ge$, the close structure relationship between them is expected.

Relationship between $Sr_{2+x}Mg_{12-x}Ge_7$ and $Sr_{5+y}Mg_{19-y}Ge_{12}$

From a structural point of view, these two ideal structures are built of the similar building blocks of Ge-centered trigonal prism. In $Sr_2Mg_{12}Ge_7$, three of Ge-centered trigonal prisms are linked together to form $[SrMg_6Ge_3]$ fragments. There are two such fragments and one isolated Ge atom in origin in the unit cell. For $Sr_5Mg_{19}Ge_{12}$, there are two similar fragments but shared corners with neighboring fragment and represented as $[SrMg_3Mg_{3/2}Ge_3]$. There is one other type of fragment which is formed by further fusing three fragments of $[SrMg_6Ge_3]$ and centered with one Mg atom, i.e., 3 $[SrMg_2Mg_{2/2}Mg_{1/3}GeGe_{2/2}]$.

It is important to determine the location of the excess Sr and determine the ranges of these nonstoichiometric phases. The structure of SrMgGe provides valuable information that suggests the positions of the extra Sr. In SrMgGe, the Sr atoms are in the common position shared by two trigonal prisms. Also, Sr is in the center of the trigonal prisms composed by 2Sr and 4Mg atoms with coordination number 6. The structures of Sr–Mg binary phases always show the Sr at the octahedral sites with six coordination number too.[16,17] Based on the above facts, the excess Sr probably substitutes at Mg(2) position for $Sr_{2+x}Mg_{12-x}Ge_7$ and Mg(4)

for $Sr_{5+y}Mg_{19-y}Ge_{12}$, respectively. Furthermore, single crystal studies of $Mg_{2.5}Ni_{11.5}P_7$, $Ca_{2.1}Ni_{11.9}P_7$ and $Ca_{2.3}Ni_{11.7}P_7$[18] which all adopt $Zr_2Fe_{12}P_7$ structure provide direct evidence about the above proposal. In these compounds, the occupancy refinements revealed that the excess Mg or Ca was mixed with Ni atoms to filled 3(j) position which is the same as Mg(2) position in $Sr_2Mg_{12}Ge_7$. Therefore, the excess Sr in $Sr_{2+x}Mg_{12-x}Ge_7$ should be mixed with Mg atoms to fill the Mg(2) position, and the excess Sr in $Sr_{5+y}Mg_{19-y}Ge_{12}$ should fill the Mg(4) position and be mixed with Mg atoms too.

In principle, these two positions could be filled up completely, then the range of $Sr_{2+x}Mg_{12-x}Ge_7$ is from $Sr_2Mg_{12}Ge_7$ to $Sr_5Mg_9Ge_7$ (the range of Sr would be from 0.143 to 0.357 atom fraction, if the total Sr and Mg is fixed at 1), while the range of $Sr_{5+y}Mg_{19-y}Ge_{12}$ is from $Sr_5Mg_{19}Ge_{12}$ to $Sr_8Mg_{16}Ge_{12}$ (Sr fraction is ranged from 0.208 to 0.333). Apparently, there would be an overlapping range between these two.

Rxn. 535 was tried to synthesize the ideal $Sr_5Mg_{19}Ge_{12}$. The product did contain 80% desired product and 20% $Sr_{2+x}Mg_{12-x}Ge_7$. The lattice constants of the major product are the smallest ones compared with other products in $Sr_{5+y}Mg_{19-y}Ge_{12}$ while those of the minor product have the largest value of the a-axis for $Sr_{2+x}Mg_{12-x}Ge_7$. Therefore, the two products might be corresponding to the two extreme cases for both phases, i.e., the phase of $Sr_{2+x}Mg_{12-x}Ge_7$ with maximum content of Sr and the phase of $Sr_{5+y}Mg_{19-y}Ge_{12}$ with minimum content of Sr coexisted in the product of rxn. 535. If that is true,

then the boundary for these two phases is at ~0.208 for Sr fraction. The linear relationship between the lattice constants and the Sr fraction could not be derived even when the odd lattice constants of rxn. 536 were excluded. However, the c/a ratio for both phases are very uniform with ~2.539 for $Sr_{2+x}Mg_{12-x}Ge_7$ and with ~3.314 for $Sr_{5+y}Mg_{19-y}Ge_{12}$ except for that of rxn. 535 (Table 4).

To confirm that, rxn. 548 was repeated by using new clean Sr to synthesize $Sr_5Mg_{19}Ge_{12}$. The powder pattern indicated that it was a single phase with lattice constants close to the major phase of rxn. 535 (see Table 4). Therefore, the boundary might be at 0.208 for Sr fraction.

Conclusion

In the study of mixed cation effect in Sr-Mg-Ge system, a couple of promising results have been reached. The existence of $SrMg_3Ge_3$ was confirmed by the powder pattern. It is believed to be related to the structure of Rh_4P_3 after the similarities between the experimental powder patterns and the calculated powder pattern based on the structure of Rh_4P_3 being revealed. In the expected structure of $SrMg_3Ge_3$, Ge_3^{-8} would would be expected and could be rationalized by the valence rule. However, the single crystal study is necessary before making any conclusion.

The existence of $SrMg_2Ge_2$ is still doubtful since the cell constants could not be obtained from TREOR program, although it is clear that the

powder pattern did not contain any known binary on ternary phases of Sr-Mg-Ge. Therefore, more reactions are required to prove that.

Two nonstoichiometric phases were found in $Sr_zMg_{2-z}Ge$, $Sr_{2+x}Mg_{12-x}Ge_7$ and $Sr_{5+y}Mg_{19-y}Ge_{12}$. The structures of both phases contain similar building blocks of Ge-centered trigonal prisms but with different aggregation types or fusing patterns. From the results, it is clear that there are some Sr:Mg ranges for both phases. Generally, the lattice constants increase as the content of Sr increases but not with a linear relationship. The boundary between these two phases might be at 0.208 for Sr fraction assuming the total mole of Sr and Mg equal to 1.

References

1. May, N.; Müller, W.; Schäfer, H. Z. Naturforsch. 1974, 29b, 325.
2. Eisenmann, B.; May, N.; Müller, W.; Schäfer, H. Z. Naturforsch. 1972, 27b, 1155.
3. Eisenmann, B.; Schäfer, H. Z. Anorg. Allg. Chem. 1974, 403, 163.
4. Eisenmann, B.; Schäfer, H.; Weiss, A. Z. Naturforsch. 1970, 25b, 651.
5. Eisenmann, B.; Schäfer, H.; Weiss, A. Z. Anorg. Allg. Chem. 1972, 391, 241.
6. Eisenmann, B.; Schäfer, H.; Turban, K. Z. Naturforsch. 1975, 30b, 677.
7. Axel, H.; Eisenmann, B.; Schäfer, H.; Weiss, A. Z. Naturforsch. 1969, 24b, 815.
8. Eisenmann, B.; Riekel, CH.; Schäfer, H. Weiss, A. Z. Anorg. Allg. Chem. 1970, 372, 325.
9. Evers, J.; Oehlinger, G.; Weiss, A. Z. Naturforsch. 1978, 33b, 456.
10. Bruzzone, G.; Franceschi, E. J. Less-Common Met. 1978, 57, 201.
11. Zmii, O. F.; Gladyshevskii, E. I.; Bul'o, V. S. Kristallografiya 1973, 18, 277.
12. Villar, P.; Calvert, L. D. "Pearson's Handbook of Crystallographic Data for Intermetallic Phases"; Amer. Soc. Met: Metals Park, OH, Vol. 1-3, 1985.
13. Rundqvist, S.; Hede, A. Acta Chem. Scand. 1960, 14, 893.
14. Ganglberger, E. Monatsh. Chem. 1968, 99, 557.
15. Pivan, J. Y.; Gu'erin, R.; Sergent, M. Inorg. Chem. Acta 1985, 109, 221.
16. Wang, F. E.; Kanda, F. A.; Miskell, C. F.; King, J. Acta Crystallogr. 1965, 18, 24.
17. Kanda, F. A.; Carter, W. S. J. Less-Common Met. 1973, 32, 97.
18. Mewis, A. Z. Naturforsch. 1980, 35b, 620.

FUTURE WORK

After the research, there are still some questions that need to be answered. First, the results of "$Ca_5Sb_3S_{1/2}$" are quite ambiguous. The hexagonal phase of "$Ca_5Sb_3S_{1/2}$" might be related to the Ca_5Pb_3 structure. Recently, in the study of La_5Ge_3M (M = transition metal) in our laboratory, $La_5Ge_3Fe_{1/3}$ and $La_5Ge_3Co_{1/3}$ were found to be isostructural with Ca_5Pb_3. Possibly, "$Ca_5Sb_3S_{1/2}$" can exist with similarly half filled octahedral sites. To answer the question the single crystal study is necessary.

Second, the discrepancy between the calculated and observed powder patterns suggests the deviation of atom positions or a different space group between $Sr_{16}Bi_{11}$ and $Ca_{16}Sb_{11}$. The confirmation needs a single crystal study too.

Third, the real structures of $SrMg_3Ge_3$ and $SrMg_2Ge_2$ have not been solved. This must be done so that more bonding information in Sr–Mg–Ge system can be obtained. The positions of excess Sr and accurate distances in $Sr_{2+x}Mg_{12-x}Ge_7$ and $Sr_{5+x}Mg_{19-x}Ge_{12}$ are needed in order to further study the bonding in these compounds.

Two other mixed cation systems, Ca–Mg–Ge and Ba–Mg–Ge, might be worth investigation since they are both isoelectronic with Sr–Mg–Ge. However, the different cation size ratios among these three might lead to unexpected results.

Mixed cation reactions demonstrated in part V here already proven to be a good way to generate new Zintl phases. The reverse direction, mixed anion reactions, might be another way to create unpredictable compounds.

So far no physical properties of any of the synthesized compounds have been measured. Although they all satisfy simple valence rule and are expected to be insulators or semiconductors, they all show dark gray or gray appearance with a metallic luster. Therefore, the electric properties of these compounds are interesting, especially for the comparisons between M_5X_3Y and M_5X_3 which are expected to be metallic.

ACKNOWLEDGEMENTS

The author wished to thank Professor John D. Corbett for the support, patient, and guidance given throughout this research.

Special thanks are due Professor R. A. Jacobson, members of his group and Dr. L. Daniel for assistance with diffractometer and crystallographic programs.

The author is indebted to Professor H. F. Franzen and coworkers for the use of induction furnace, to E. DeKalb for elemental analysis, to A. Guloy for the extended Hückel programs, to S. Slavi for SEM analysis.

The discussions, suggestions, and patience of many friends and coworkers are kindly remembered.

The author wishes to extend special thanks to his parents and relatives, who have provided support during these years. Special thanks to Mrs. Shirley Standley for typing this manuscript and her enthusiasm in doing this.

Finally, the author acknowledges the support, love, patience and sacrifices contributed by his wife Shian-Jy.

This work was performed at Ames Laboratory under contract No. W-7405-eng-82 with the U. S. Department of Energy. The United States government has assigned the DOE Report number IS-T 1361 to this thesis.

APPENDIX A: CALCULATED AND OBSERVED STRUCTURE FACTOR AMPLITUDES FOR KSi_3As_3

OBSERVED AND CALCULATED STRUCTURE FACTORS FOR KSi_3As_3

H = 0

K	L	FO	FC
0	1	19	11
0	2	405	392
0	3	14	17
0	4	191	195
2	0	71	66
2	1	45	41
2	2	48	43
2	4	28	26
4	0	13	13
4	1	211	199
4	3	134	116
6	0	94	89
6	1	24	23
6	2	67	60
6	4	31	30
8	0	42	-41
8	1	237	-230
8	2	26	-26
8	3	163	-147
10	0	91	88
10	1	101	-101
10	2	67	64
10	3	63	-60
10	4	32	31
12	0	257	-253
12	1	68	-68
12	2	210	-199
12	3	48	-46
12	4	117	-107
14	0	128	-125
14	1	52	-51
14	2	102	-100
14	3	34	-34
16	0	54	52
16	1	93	-89
16	2	40	41
16	3	56	-58
18	0	59	-56
18	1	83	-80
18	2	44	-45
18	3	53	-54
20	0	44	47
20	1	84	80
20	2	33	38
22	0	16	-19
22	1	58	59
24	0	38	40
24	1	46	46

H = 1

K	L	FO	FC
1	1	37	-35
1	3	19	-22
2	0	73	-71
2	1	72	66
2	2	51	-48
2	3	42	41
2	4	25	-26
3	0	40	39
3	1	145	136
3	2	24	24
3	3	84	80
4	0	71	68
4	1	209	197
4	2	60	56
4	3	115	108
4	4	33	32
5	0	209	-206
5	1	37	37
5	2	155	-145
5	3	17	19
5	4	81	-73
6	0	146	145
6	1	83	-81
6	2	108	100
6	3	47	-43
6	4	54	49
7	0	67	66
7	1	55	55
7	2	53	48
7	3	37	35
7	4	24	24
8	0	72	73
8	1	101	103
8	2	61	57
8	3	67	61
8	4	33	31
9	0	42	41
9	1	61	-60
9	2	32	31
9	3	39	-37
10	0	48	-49
10	1	129	125
10	2	40	-37
10	3	83	78
10	4	15	-19
11	0	50	-52
11	1	20	-25
11	2	40	-40
11	4	21	-22
12	0	38	-41
12	1	29	-29
12	2	34	-35
12	4	16	-20
13	1	110	103
13	3	70	66
15	0	97	-95
15	1	25	-28
15	2	78	-76
15	3	18	-19
16	0	63	-63
16	1	90	-86
16	2	53	-52
16	3	56	-56
17	0	73	70
17	1	32	-33
17	2	58	57
18	0	81	-78
18	2	63	-64
19	0	22	25
19	1	34	-34
19	2	15	20
19	3	22	-23
20	0	57	-58
20	2	43	-47
21	0	64	-63
21	2	50	-52
22	0	18	-22
22	1	53	-51
23	1	46	45
24	1	21	31

H = 2

K	L	FO	FC
0	0	66	-70
0	1	39	-40
0	2	41	-42
0	3	27	-29
1	0	11	10
1	1	139	142
1	2	10	10
1	3	76	78
2	0	52	-52
2	1	146	-142
2	2	42	-42
2	3	77	-78
2	4	21	-24
3	0	143	-145
3	1	78	-74
3	2	110	-105
3	3	40	-41
3	4	52	-56
4	0	64	-63
4	2	47	-46
4	4	18	-23
5	0	45	-45
5	1	109	-108
5	2	32	-32
5	3	67	-65
5	4	15	-18
6	0	22	-24
6	1	47	48
6	2	13	-15
6	3	26	26
7	0	62	62
7	1	68	-69
7	2	50	49
7	3	47	-45
7	4	26	26
8	0	68	68
8	1	40	-40
8	2	52	48
8	3	19	-21
8	4	28	24
9	0	78	-79
9	1	181	-180
9	2	66	-64
9	3	117	-111
9	4	37	-36
10	0	92	92
10	1	74	73
10	2	79	74
10	3	44	43
10	4	42	41
11	0	17	-16
11	1	95	93
11	3	60	57
12	0	49	51
12	1	43	42
12	2	39	39
12	3	28	28
13	0	15	-15
13	1	28	-30
13	2	12	-13
13	3	16	-19
14	0	12	18
14	1	75	74
14	3	50	48
15	0	96	92
15	1	74	-74
15	2	76	74
15	3	49	-48
16	0	19	28
16	1	38	43
16	2	19	23
16	3	26	27
17	0	128	123
17	1	34	35
17	2	101	101
17	3	16	23
18	0	26	30
18	1	64	-61
18	2	20	24
18	3	38	-40
19	0	21	-23
19	2	19	-19
21	0	36	37
21	1	84	82
21	2	26	31
22	0	66	-63
22	2	48	-52
23	0	52	53
23	1	34	-33
24	0	34	-34

H = 3

K	L	FO	FC
1	0	118	123
1	2	87	85
1	4	39	43
2	0	240	-252
2	2	185	-180
2	4	86	-93
3	0	36	-36
3	1	48	49
3	2	21	-21
3	3	20	24
4	0	21	-21
4	2	15	-18
5	0	85	87
5	2	61	60
5	4	29	29
6	0	148	-150
6	1	228	-229
6	2	117	-112
6	3	149	-144
6	4	57	-59
7	0	16	-17
7	1	45	-47
7	3	30	-32
8	0	24	-27
8	1	84	-85
8	2	21	-22
8	3	54	-53
9	1	43	-43
9	3	26	-27
10	0	118	-119
10	1	28	29
10	2	99	-95
10	3	18	18
10	4	52	-52
11	0	28	-29
11	1	21	-22
11	2	22	-24
12	0	154	-156
12	1	20	20
12	2	128	-124
12	4	71	-67
13	0	71	-72
13	1	32	-32
13	2	58	-57
13	3	20	-22
14	0	128	123
14	1	54	55
14	2	102	98
14	3	36	37
15	0	38	40
15	1	44	-45
15	2	31	32
15	3	25	-29
16	0	34	35
16	1	16	-17
16	2	24	29
17	0	29	-30
17	2	21	-24
18	0	33	35
18	1	117	110
18	2	25	29
18	3	70	74
19	1	28	29
20	1	126	120
21	0	31	33
21	2	19	27
24	0	79	77

H = 4

K	L	FO	FC
0	0	120	-126
0	1	52	53
0	2	94	-94
0	3	30	33
0	4	45	-50
1	0	27	30
1	1	91	94
1	2	16	18
1	3	62	62
2	0	51	53
2	1	130	135
2	2	41	41
2	3	81	82
2	4	18	21
3	0	100	-106
3	1	97	98
3	2	79	-76
3	3	58	58
3	4	34	-39
4	0	30	33
4	1	26	-27
4	2	25	24
5	0	92	94
5	1	23	-25
5	2	76	72
5	4	33	38
6	0	33	-36
6	1	23	-24
6	2	28	-29
6	3	22	24
7	0	183	186
7	1	37	-38
7	2	149	142
7	3	22	-22
7	4	75	74
8	0	42	-44
8	1	108	109
8	2	32	-34
8	3	69	69
8	4	15	-17
9	0	87	-89
9	1	37	38
9	2	70	-68
9	3	20	21
9	4	34	-35
10	0	125	-126
10	1	59	-58
10	2	105	-100
10	3	36	-36
10	4	54	-55
11	1	73	74
11	3	48	49
12	0	26	28
12	1	16	-19
12	2	20	23
13	1	43	-44
13	3	27	-29
14	1	38	-39
14	3	24	-26
15	1	86	-82
15	3	54	-55
16	0	55	-55
16	1	15	-14
16	2	44	-45
18	0	18	18
18	1	64	62
19	0	99	-93
19	2	73	-76
20	1	31	-34
22	0	68	62
23	0	18	22
23	1	17	-25

H = 5

K	L	FO	FC
1	0	126	-133
1	1	11	-15
1	2	102	-101
1	4	48	-53
2	1	29	32
2	3	18	20
3	0	22	-25
3	1	243	-252
3	2	18	-23
3	3	157	-157
4	0	28	31
4	1	35	38
4	2	22	24
4	3	22	24
5	0	115	120
5	1	17	-20
5	2	100	97
5	4	51	53
6	0	51	53
6	1	24	25
6	2	43	42
6	4	20	23
7	0	37	-39
7	1	34	-36
7	2	32	-32
7	3	21	-22
7	4	16	-18
8	0	65	65
8	2	53	51
8	4	26	27
9	1	114	114
9	3	76	74
10	0	16	18
10	1	17	19
10	2	16	15
11	0	129	129
11	1	87	83
11	2	108	105
11	3	52	54
12	0	20	-22

12	1	15	16	11	2	56	-55	13	0	24	-25	13	1	24	23	3	1	47	-45	6	1	22	25
13	0	110	107	12	0	89	85	13	1	80	-79	15	0	83	-77	4	1	39	41	7	0	41	39
13	1	70	-68	12	1	60	57	13	2	18	-20	15	1	27	32	5	0	26	-27	7	1	28	25
13	2	87	86	12	2	71	70	13	3	51	-54	15	2	63	-64	5	1	33	-36	8	0	34	34
13	3	41	-43	12	3	35	38	14	0	38	-40	16	0	18	-17	5	2	21	-22				
14	1	23	-26	13	1	43	47	14	1	38	-41	16	1	15	24	6	0	24	27				
15	0	91	87	13	3	29	31	14	2	31	-33	17	0	86	-80	6	2	19	22				
15	1	130	122	14	0	99	92	15	1	22	-22	17	1	67	-69	7	0	51	-51				
15	2	70	72	14	1	13	-13	16	0	24	27					7	2	43	-42				
15	3	80	81	14	2	77	75	16	1	37	38		H =	9		8	0	21	-24				
16	1	55	-51	15	0	17	20	16	2	21	22	K	L	FO	FC	8	1	68	-66				
16	3	31	-34	15	1	49	48	17	0	47	-45	1	0	60	-59	8	2	15	-19				
17	0	36	-38	15	3	28	33	17	1	17	22	1	1	50	-49	9	0	23	-23				
17	1	32	34	17	1	41	39	17	2	33	-37	1	2	49	-48	9	2	20	-19				
17	2	32	-31	18	1	101	95	18	1	15	-25	1	3	31	-32	10	0	47	45				
18	1	40	-37	19	0	61	57	20	0	25	26	2	0	73	74	10	2	32	36				
20	0	37	-37	19	1	57	53	20	1	49	-54	2	1	27	-28	11	0	33	33				
20	2	26	-30	19	2	45	47					2	2	63	61	11	1	46	-42				
				20	0	20	-20		H =	8		2	3	18	-19	11	2	25	27				
	H =	6		20	1	41	-40	K	L	FO	FC	3	0	34	-33	12	0	74	-67				
K	L	FO	FC	21	1	20	23	0	0	19	-22	3	1	38	39	12	1	28	-30				
0	0	166	-175	22	0	40	38	0	1	55	55	3	2	26	-27	13	0	23	26				
0	1	65	-66					0	2	15	-16	3	3	23	26	14	0	38	-37				
0	2	139	-138		H =	7		0	3	35	35	4	1	45	-46								
0	3	42	-42	K	L	FO	FC	1	0	20	23	4	3	29	-30		H =	11					
0	4	69	-76	1	1	100	99	1	1	80	-82	5	0	87	-86	K	L	FO	FC				
1	0	75	-76	1	3	66	65	1	2	14	18	5	2	71	-70	1	0	60	57				
1	1	39	-41	2	0	73	75	1	3	54	-53	6	0	37	-36	1	1	20	21				
1	2	58	-57	2	2	61	59	2	0	14	16	6	1	99	96	1	2	48	47				
1	3	28	-28	3	0	32	32	2	1	42	-44	6	2	29	-29	2	0	17	19				
1	4	24	-30	3	2	26	26	2	3	29	-28	6	3	64	64	2	1	22	-24				
2	0	38	-40	4	0	49	-49	3	0	139	137	7	0	41	41	3	0	57	53				
2	1	28	30	4	1	58	-60	3	1	37	37	7	1	33	36	3	1	70	68				
2	2	31	-31	4	2	40	-38	3	2	117	111	7	2	34	33	3	2	48	44				
2	3	18	18	4	3	40	-40	3	3	22	25	7	3	20	24	4	0	26	26				
3	1	30	-34	5	0	93	93	4	0	57	58	8	0	19	-18	4	1	48	46				
3	3	16	-20	5	1	24	-27	4	1	43	-45	9	0	22	24	4	2	22	22				
4	1	79	-80	5	2	76	74	4	2	48	47	10	0	46	46	5	0	49	-45				
4	3	50	-51	5	3	14	-16	4	3	25	-30	10	1	42	-43	5	1	18	19				
5	0	71	-73	6	0	76	75	5	0	37	39	10	2	37	38	5	2	41	-37				
5	1	34	-35	6	1	44	46	5	1	126	123	11	1	47	46	6	0	20	-19				
5	2	60	-58	6	2	62	60	5	2	30	32	12	0	40	39	6	1	15	18				
5	3	20	-22	6	3	27	31	5	3	83	82	12	2	30	33	6	2	15	-16				
5	4	26	-32	7	0	60	-61	6	0	16	18	13	0	48	46	7	0	15	16				
6	1	53	-54	7	2	48	-48	7	1	98	94	13	1	72	70	8	1	42	41				
6	3	32	-35	8	0	36	-37	7	3	63	63	13	2	36	38	9	1	58	-54				
7	0	124	-126	8	2	28	-29	8	0	15	-19	14	0	38	-39	11	0	51	-47				
7	1	38	-37	9	0	90	-90	9	0	117	113	14	2	30	-32	11	1	57	-55				
7	2	104	-99	9	1	18	19	9	1	96	96	16	0	20	-20	13	0	45	-42				
7	3	24	-25	9	2	74	-72	9	2	97	92	16	1	44	46								
7	4	55	-54	10	0	21	23	9	3	62	64	17	0	26	26		H =	12					
8	1	117	117	10	1	25	-27	10	1	24	23	17	1	16	19	K	L	FO	FC				
8	3	77	76	10	2	15	19	11	0	26	31					0	0	27	27				
10	0	55	-57	10	3	15	-18	11	1	52	-53		H =	10		0	1	40	-34				
10	1	28	29	11	0	15	-18	11	2	21	25	K	L	FO	FC	1	0	25	28				
10	2	44	-46	11	1	43	-44	11	3	32	-35	0	0	140	135	1	1	36	35				
10	3	18	20	11	3	25	-28	12	0	27	28	0	1	19	21	2	0	18	-20				
11	0	69	-69	12	0	107	101	12	1	48	-49	0	2	117	110	4	0	60	-55				
11	1	16	-19	12	2	84	81	12	2	22	23	1	1	21	-24	4	1	45	43				

APPENDIX B: CALCULATED AND OBSERVED STRUCTURE FACTOR AMPLITUDES FOR K_2SiAs_2

H = 0

K	L	Fo	Fc
0	2	129	130
0	4	121	120
0	6	62	60
2	0	60	60
2	2	84	86
2	4	37	36
2	6	42	42
4	0	45	46
4	2	66	67
4	4	30	30
4	6	35	35
6	0	85	86
6	2	60	60
6	4	63	63
8	0	15	15
8	2	27	27

H = 1

K	L	Fo	Fc
1	0	51	51
1	4	33	34
1	6	5	5
2	1	87	89
2	3	67	68
2	5	45	46
2	7	28	28
3	0	29	29
3	2	57	59
3	4	24	24
3	6	35	35
4	1	60	62
4	3	50	50
4	5	35	36
5	0	35	35
5	2	8	9
5	4	27	26
7	0	16	16
7	4	13	13
8	1	27	27

H = 2

K	L	Fo	Fc
0	0	50	46
0	4	30	30
0	6	6	2
1	1	42	43
1	3	38	39
1	5	31	32
1	7	22	22
2	0	9	9
2	2	27	28
2	4	6	5
2	6	15	15
3	1	4	5
3	5	5	3
4	0	10	10
4	2	19	18
4	4	6	7
4	6	11	11
5	1	26	26
5	3	24	24
5	5	19	19
6	0	22	21
6	2	5	1
6	4	16	16
7	1	22	22
7	3	19	19
8	0	6	2

H = 3

K	L	Fo	Fc
1	0	34	33
1	2	10	10
1	4	17	17
1	6	10	9
2	1	91	95
2	3	74	77
2	5	53	54
2	7	34	35
3	2	25	25
3	4	8	8
3	6	9	9
4	1	69	72
4	3	60	60
4	5	43	44
5	0	14	14
5	2	10	10
5	4	10	10
7	0	12	12
7	2	6	6
8	1	31	30

H = 4

K	L	Fo	Fc
0	0	113	110
0	2	128	127
0	4	71	70
0	6	66	63
1	1	73	73
1	3	56	57
1	5	40	39
1	7	25	25
2	0	72	74
2	2	34	35
2	4	49	49
2	6	15	15
4	0	60	62
4	2	30	30
4	4	43	43
4	6	15	15
5	1	40	40
5	3	33	33
5	5	24	24
6	0	49	48
6	2	63	63
6	4	35	35
7	1	28	28
7	3	24	24
8	0	22	22

H = 5

K	L	Fo	Fc
1	0	26	25
1	2	55	55
1	4	18	18
1	6	30	30
2	1	38	39
2	3	29	29
2	5	18	18
3	0	84	87
3	2	53	54
3	4	63	64
3	6	29	30
4	1	22	22
4	3	17	17
4	5	10	11
5	0	19	19
5	2	39	39
5	4	13	14
6	1	8	8
6	3	8	6
7	0	8	7
7	2	21	21

H = 6

K	L	Fo	Fc
0	0	28	27
0	2	58	57
0	4	24	23
0	6	36	34
1	1	17	17
1	3	17	17
1	5	15	14
2	0	40	40
2	2	7	8
2	4	30	30
2	6	7	6
3	3	5	0
4	0	25	25
4	4	19	19
5	1	12	13
5	3	11	12
5	5	10	10
6	0	15	15
6	2	31	31
6	4	12	12
7	1	10	9

H = 7

K	L	Fo	Fc
1	0	18	17
1	2	44	43
1	4	9	9
1	6	22	22
2	1	61	61
2	3	52	52
2	5	38	38
3	0	67	67
3	2	35	36
3	4	46	46
3	6	17	17
4	1	47	48
4	3	40	41
4	5	30	31
5	0	11	11
5	2	30	29
5	4	7	7
7	0	6	4
7	2	17	17

H = 8

K	L	Fo	Fc
0	0	59	59
0	2	27	26
0	4	42	40
0	6	13	12
1	1	86	86
1	3	73	72
1	5	52	52
2	2	27	27
2	6	15	15
3	3	5	1
4	0	10	11
4	2	31	31
4	4	7	7
5	1	54	54
5	3	45	46
6	0	31	30
6	2	12	12
7	1	37	37

H = 9

K	L	Fo	Fc
1	0	49	47
1	2	19	19
1	4	35	34
1	6	9	10
2	1	7	8
2	3	8	8
2	5	8	8
3	0	47	46
3	2	64	63
3	4	33	33
4	1	13	13
4	3	12	12
4	5	10	10
5	0	29	29
5	2	10	10
5	4	21	22
6	1	9	9

H = 10

K	L	Fo	Fc
0	0	52	51
0	2	26	26
0	4	41	40
1	1	9	9
1	3	7	7
1	5	7	5
2	0	9	9
2	2	30	30
2	4	7	7
3	3	6	3
4	2	20	21
6	0	29	29
6	2	13	14

H = 11

K	L	Fo	Fc
1	0	46	45
1	2	20	21
1	4	33	33
2	1	18	18
2	3	16	16
2	5	13	13
3	0	50	49
3	2	65	64
3	4	35	36
4	1	11	12
4	3	11	10
5	0	32	32
5	2	14	15

H = 12

K	L	Fo	Fc
0	0	26	26
0	2	6	5
0	4	19	20
1	1	60	61
1	3	51	52
2	2	20	19
4	0	9	9
4	2	8	7
5	1	42	42

H = 13

K	L	Fo	Fc
1	0	7	6
1	2	23	23
1	4	6	4
2	1	25	24
2	3	21	22
3	0	34	33
3	2	15	15
4	1	24	24

H = 14

K	L	Fo	Fc
0	0	8	9
0	2	24	24
1	1	19	20
1	3	17	18
2	0	15	16

H = 15

K	L	Fo	Fc
1	0	15	16
1	2	27	28

2 1 10 10

254 REFLECTIONS HAVE BEEN WRITTEN ON 2 PAGES

APPENDIX C: CALCULATED AND OBSERVED STRUCTURE FACTOR AMPLITUDES FOR Ca_5Sb_3Cl

H = 0			
K	L	Fo	Fc
0	2	209	209
0	4	275	272
0	8	162	159

H = 1			
K	L	Fo	Fc
0	0	27	24
0	2	17	14
0	4	26	23
0	6	14	10
0	8	19	18

H = 2			
K	L	Fo	Fc
-1	0	58	61
-1	1	131	123
-1	2	201	196
-1	3	99	109
-1	4	48	46
-1	5	95	91
-1	6	122	120
-1	7	70	71
-1	8	22	22
0	0	91	85
0	2	87	87
0	4	61	62
0	6	56	59
0	8	33	35

H = 3			
K	L	Fo	Fc
-1	0	39	40
-1	1	149	146
-1	2	26	27
-1	3	114	123
-1	4	30	29
-1	5	87	93
-1	6	16	11
-1	7	65	66
-1	8	20	16
0	0	238	235
0	2	100	99
0	4	179	182
0	6	65	60
0	8	105	104

H = 4			
K	L	Fo	Fc
-2	0	11	8
-2	1	103	105
-2	2	124	124
-2	3	92	92
-2	4	14	6
-2	5	79	74
-2	6	76	74
-2	7	54	56
-1	0	66	68
-1	1	138	138
-1	2	55	55
-1	3	117	121
-1	4	51	56
-1	5	93	96
-1	6	44	37
-1	7	78	73
0	0	15	8
0	2	14	13

H = 5			
K	L	Fo	Fc
-2	0	79	81
-2	1	58	59
-2	2	84	85
-2	3	49	49
-2	4	64	65
-2	5	39	35
-2	6	65	60
-2	7	27	24
-1	0	29	30
-1	1	29	30
-1	2	88	87
-1	3	27	27
-1	4	22	20
-1	5	26	22
-1	6	58	59
-1	7	19	17
0	0	179	182
0	2	180	179
0	4	144	147
0	6	112	123

H = 6			
K	L	Fo	Fc
-3	0	65	63
-3	1	88	89
-3	2	43	44
-3	3	75	78
-3	4	49	51
-3	6	33	28
-3	7	45	45
-2	0	101	100
-2	1	134	135
-2	2	88	87
-2	3	119	120
-2	4	77	80
-2	5	96	99
-2	6	69	55
-1	0	50	48
-1	1	69	69
-1	2	40	39
-1	3	60	59
-1	4	35	38
-1	5	44	46
-1	6	19	22
0	0	25	24
0	2	68	68
0	4	24	21
0	6	45	46

H = 7			
K	L	Fo	Fc
-3	0	13	8
-3	1	79	78
-3	2	13	3
-3	3	71	71
-3	4	17	10
-3	5	56	59
-2	0	91	88
-2	1	44	44
-2	3	39	38
-2	4	73	74
-2	5	26	29
-2	6	12	2
-1	0	89	87
-1	1	99	98
-1	2	79	77
-1	3	90	90
-1	4	68	71
-1	5	73	77
-1	6	47	51
0	0	65	61
0	2	65	62
0	4	50	48

H = 8			
K	L	Fo	Fc
-4	0	32	31
-4	1	73	73
-4	2	53	51
-4	3	66	66
-4	4	22	23
-4	5	56	56
-3	0	113	113
-3	1	14	1
-3	2	111	112
-3	3	13	1
-3	4	93	92
-3	5	16	1
-2	1	30	31
-2	3	28	29
-2	5	23	25
-1	0	50	48
-1	1	44	46
-1	2	28	27
-1	3	43	42
-1	4	38	40
-1	5	36	36
0	0	136	136
0	2	133	133
0	4	111	112

H = 9			
K	L	Fo	Fc
-4	0	39	39
-4	1	25	27
-4	2	35	34
-4	3	24	24
-4	4	32	34
-3	0	26	28
-3	1	106	104
-3	2	94	95
-3	3	97	95
-3	4	23	22
-2	0	52	53
-2	1	50	51
-2	2	46	47
-2	3	49	48
-2	4	44	45
-1	0	37	38
-1	1	52	53
-1	2	36	33
-1	3	49	49
0	2	64	64

H = 10			
K	L	Fo	Fc
-5	0	124	123
-5	1	32	28
-5	2	57	58
-5	3	28	25
-4	0	37	36
-4	1	34	34
-4	2	32	31
-4	3	32	32
-3	0	42	40
-3	1	32	33
-3	2	41	41
-2	0	85	83
-2	1	12	4

APPENDIX D: CALCULATED AND OBSERVED STRUCTURE FACTOR AMPLITUDES FOR Ba_5Sb_3Cl

H = 0

K	L	Fo	Fc
0	2	249	230
0	4	424	386
0	6	147	147
0	8	264	260

H = 1

K	L	Fo	Fc
0	0	31	28
0	2	96	95
0	4	31	31
0	6	58	55
0	8	27	27

H = 2

K	L	Fo	Fc
-1	2	291	284
-1	6	217	217
-1	9	24	14
0	0	38	36
0	2	85	86
0	4	28	33
0	6	61	64
0	8	25	16

H = 3

K	L	Fo	Fc
-1	0	130	140
-1	1	216	216
-1	2	22	24
-1	3	193	196
-1	4	107	111
-1	5	153	128
-1	7	107	110
-1	8	59	61
0	0	317	322
0	2	60	61
0	4	287	267
0	6	24	23
0	8	175	175

H = 4

K	L	Fo	Fc
-2	0	58	64
-2	1	78	83
-2	2	238	237
-2	3	67	72
-2	4	49	36
-2	5	54	61
-2	6	165	168
-2	7	42	44
-2	8	44	43
-1	0	61	60
-1	1	138	145
-1	2	47	49
-1	3	123	128
-1	4	51	53
-1	5	95	100
-1	6	32	31
-1	7	73	74
-1	8	40	39
0	0	108	115
0	2	186	197
0	4	72	37
0	6	114	119
0	8	25	22

H = 5

K	L	Fo	Fc
-2	0	24	24
-2	1	142	155
-2	2	73	76
-2	3	126	110
-2	4	22	16
-2	5	97	101
-2	6	57	58
-2	7	70	70
-1	0	145	156
-1	1	21	17
-1	2	134	145
-1	3	19	19
-1	4	120	94
-1	6	97	103
-1	8	72	73
0	0	156	161
0	2	224	213
0	4	120	127
0	6	152	157
0	8	59	64

H = 6

K	L	Fo	Fc
-3	0	113	120
-3	1	147	154
-3	2	142	111
-3	3	137	114
-3	4	97	99
-3	5	110	112
-3	6	103	104
-3	7	81	80
-2	0	164	171
-2	1	139	145
-2	2	84	87
-2	3	126	127
-2	4	140	142
-2	5	104	107
-2	6	48	48
-2	7	77	79
-1	0	136	114
-1	1	155	125
-1	2	51	47
-1	3	136	122
-1	4	108	114
-1	5	107	109
-1	6	25	25
-1	7	78	77
0	0	65	46
0	2	166	141
0	4	55	60
0	6	117	118

H = 7

K	L	Fo	Fc
-3	1	69	73
-3	2	87	71
-3	3	61	63
-3	5	52	51
-3	6	59	60
-3	7	34	39
-2	0	118	110
-2	1	109	94
-2	2	105	95
-2	3	97	102
-2	4	103	107
-2	5	76	80
-2	6	77	77
-2	7	53	56
-1	0	140	133
-1	1	30	40
-1	2	64	66
-1	3	28	29
-1	4	112	118
-1	5	27	27
-1	6	41	38
-1	7	27	25
0	0	90	93
0	2	149	152
0	4	66	70
0	6	98	102

H = 8

K	L	Fo	Fc
-4	0	188	192
-4	1	67	71
-4	2	25	16
-4	3	60	64
-4	4	155	159
-4	5	55	52
-3	0	101	106
-3	2	158	163
-3	4	81	82
-3	6	112	113
-2	0	72	74
-2	4	59	60
-1	0	141	146
-1	1	34	30
-1	2	46	48
-1	3	28	27
-1	4	119	121
-1	5	28	23
-1	6	40	42
0	0	187	188
0	2	228	229
0	4	147	150

H = 9

K	L	Fo	Fc
-4	0	56	55
-4	1	36	36
-4	3	31	32
-4	4	46	48
-4	5	28	26
-3	1	162	168
-3	2	178	176
-3	3	150	151
-3	5	122	123
-2	0	112	110
-2	2	52	48
-2	4	91	90
-1	0	50	50
-1	1	38	35
-1	3	29	32
-1	4	40	44
-1	5	30	28
0	0	50	52
0	2	99	96
0	4	45	45

H = 10

K	L	Fo	Fc
-5	0	128	124
-5	1	99	100
-5	2	36	35
-5	3	87	89
-5	4	106	108
-5	5	67	70
-4	0	86	87
-4	1	24	18
-4	2	32	31
-4	4	67	72
-3	1	73	73
-3	2	52	52
-3	3	65	65
-2	0	97	94
-2	1	25	22
-2	2	50	51
-2	3	24	19
-2	4	84	83
-1	0	101	102
-1	1	52	53
-1	2	53	53
-1	3	45	46
0	0	36	33
0	2	75	73

H = 11

K	L	Fo	Fc
-5	0	45	46
-5	1	68	65
-5	3	61	58
-4	0	91	91
-4	1	74	74
-4	2	45	43
-4	3	71	68
-3	0	60	59
-3	2	94	97
-2	0	81	82
-2	1	111	111

APPENDIX E: CALCULATED AND OBSERVED STRUCTURE FACTOR AMPLITUDES FOR Ca_5Sb_3F

H = 0			
K	L	Fo	Fc
0	2	159	151
0	4	148	149
0	6	196	192
0	8	217	221
0	10	42	42
1	1	29	29
1	3	139	137
1	5	101	100
1	7	15	3
1	9	48	49
2	0	52	52
2	2	40	43
2	6	119	119
2	8	95	96
2	10	19	21
3	1	181	175
3	3	196	193
3	5	145	144
3	7	23	26
3	9	136	135
4	0	346	387
4	2	154	155
4	4	125	127
4	6	175	173
4	8	170	172
4	10	24	24
5	1	88	88
5	3	38	39
5	5	30	30
5	7	19	19
5	9	29	29
6	0	80	77
6	1	15	0
6	2	50	51
6	4	15	14
6	6	80	82
6	8	25	24
7	1	170	175
7	3	201	202
7	5	148	145
7	7	20	17
7	9	146	149
8	0	243	243
8	2	129	124
8	4	81	79
8	6	120	117
8	7	15	0
8	8	77	75
9	1	57	58
9	3	26	26
9	5	19	13
10	0	129	132
10	2	29	27
10	4	19	19
10	5	15	0
10	6	32	28
11	1	95	95
11	3	167	166
11	5	115	115
12	0	88	88
12	2	65	65

H = 1			
K	L	Fo	Fc
0	1	19	18
0	2	161	154
0	3	145	141
0	4	247	236
0	6	90	87
0	7	17	17
0	8	123	122
0	9	26	25
0	10	101	100
1	1	10	0
1	2	118	115
1	4	102	101
1	5	29	30
1	6	22	22
1	7	35	34
1	8	104	101
1	9	15	18
1	10	78	77
2	1	174	169
2	2	257	255
2	3	51	52
2	4	86	88
2	5	238	234
2	6	67	68
2	7	124	124
2	8	48	49
2	9	27	26
2	10	103	105
3	1	126	125
3	2	112	114
3	3	20	20
3	4	33	31
3	5	64	61
3	6	14	13
3	7	51	51
3	8	86	87
3	10	61	62
4	1	12	14
4	2	106	110
4	3	83	83
4	4	211	211
4	5	24	23
4	6	60	60
4	7	13	12
4	8	96	99
4	9	22	22
4	10	76	78
5	1	96	99
5	2	99	100
5	3	11	10
5	4	168	165
5	5	16	12
5	6	37	37
5	7	93	93
5	8	95	96
5	9	36	35
6	1	138	140
6	2	167	167
6	3	16	17
6	4	62	64
6	5	144	140
6	6	28	28
6	7	108	107
6	8	22	22
6	9	19	19
7	1	143	145
7	2	61	59
7	3	13	7
7	4	58	58
7	5	77	77
7	7	84	85
7	8	59	59
7	9	22	21
8	2	27	26
8	4	135	133
8	5	74	74
8	6	18	17
8	8	54	52
9	1	99	99
9	2	96	95
9	3	12	5
9	4	125	124
9	5	37	39
9	6	17	14
9	7	89	91
10	1	83	82
10	2	55	53
10	3	42	43
10	4	25	20
10	5	50	50
11	1	103	103
11	2	15	10
11	4	24	20
11	5	73	72
12	1	20	18
12	2	18	19
12	3	16	15

H = 2			
K	L	Fo	Fc
0	0	14	14
0	1	29	29
0	2	18	20
0	3	234	227
0	4	73	72
0	5	120	118
0	7	50	48
0	9	39	39
0	10	49	49
1	0	26	24
1	1	71	70
1	2	77	76
1	3	207	203
1	4	48	48
1	5	102	100
1	6	57	57
1	7	49	49
1	9	19	19
1	10	16	11
2	0	191	189
2	1	58	56
2	2	247	240
2	3	235	229
2	4	34	34
2	5	162	164
2	6	231	230
2	7	69	68
2	8	82	82
2	9	96	97
2	10	15	12
3	0	17	13
3	1	89	89
3	2	62	61
3	3	118	118
3	5	47	47
3	6	49	47
3	8	20	18
3	9	16	13
3	10	18	11
4	1	51	52
4	2	47	45
4	3	175	177
4	4	48	49
4	5	83	85
4	6	33	33
4	7	21	23
4	9	38	39
4	10	35	36
5	0	66	66
5	1	45	46
5	2	137	138
5	3	228	225
5	4	67	67
5	5	120	117
5	6	122	121
5	7	62	63
5	8	18	11
5	9	29	26
6	0	174	175
6	1	73	74
6	2	160	160
6	3	137	139
6	4	21	20
6	5	100	99
6	6	160	161
6	7	25	25
6	8	75	75
6	9	84	85
7	0	60	62
7	1	53	51
7	2	88	88
7	3	40	40
7	4	18	19
7	5	15	10
7	6	83	83
7	8	35	35
8	0	12	3
8	1	60	58
8	2	70	70
8	3	61	61
8	4	16	15
8	5	26	26
8	6	56	58
8	7	20	14
9	0	102	99
9	1	55	52
9	2	101	102
9	3	175	175
9	4	54	54
9	5	93	93
9	6	105	108
9	7	41	43
10	0	115	114
10	1	56	55
10	2	67	67
10	3	38	36
10	4	14	5
10	5	35	34
10	6	83	81
11	0	84	82
11	1	15	8
11	2	52	50
11	3	20	19
11	4	18	17
12	0	18	16
12	1	31	30
12	2	62	64

H = 3			
K	L	Fo	Fc
0	1	246	247
0	2	156	158
0	3	29	30
0	4	97	96
0	5	234	231
0	6	36	34
0	7	254	252
0	8	25	1
0	9	43	42
0	10	31	31
1	1	52	53
1	2	76	80
1	4	58	61
1	6	62	62
1	7	48	48
1	8	66	66
1	9	14	12
1	10	40	42
2	1	200	197
2	2	71	70
2	3	23	24
2	4	92	93
2	5	33	33
2	6	51	52

2	7	73	74	10	4	25	25	5	0	162	161	0	7	68	68	7	5	45	46
2	8	17	15	10	5	20	21	5	1	126	128	0	8	14	13	7	6	46	46
2	9	67	67	10	6	23	21	5	2	12	9	0	9	27	27	7	7	28	28
2	10	24	21	11	1	23	19	5	3	137	137	0	10	63	61	7	8	27	28
3	1	74	75	11	2	135	135	5	4	14	13	1	1	93	92	8	1	17	16
3	2	175	174	11	3	16	15	5	5	97	94	1	2	73	74	8	2	57	56
3	3	77	76	11	4	132	131	5	7	17	18	1	3	45	46	8	3	79	79
3	4	143	141	12	1	40	37	5	8	58	58	1	4	69	70	8	4	16	14
3	5	63	63					5	9	89	89	1	5	100	99	8	6	24	23
3	6	21	21		H =	4		6	0	220	219	1	7	40	39	9	1	117	120
3	7	67	68	K	L	Fo	Fc	6	2	103	103	1	8	87	86	9	2	104	104
3	8	107	105	0	0	95	99	6	3	88	89	1	9	17	2	9	3	45	46
3	10	89	90	0	1	254	252	6	4	63	64	1	10	81	80	9	4	83	82
4	1	222	225	0	2	45	46	6	5	93	95	2	1	228	226	9	5	117	118
4	2	108	109	0	3	221	224	6	6	85	85	2	2	138	144	9	6	27	26
4	3	29	29	0	4	29	30	6	8	64	64	2	3	122	121	10	1	69	66
4	4	42	42	0	5	107	106	6	9	39	39	2	4	270	264	10	2	65	64
4	5	202	203	0	6	21	21	7	0	198	200	2	5	113	113	10	3	18	17
4	7	211	214	0	8	18	16	7	1	29	27	2	6	20	19	10	4	54	54
4	9	32	33	0	9	165	162	7	2	48	48	2	7	149	149	10	5	75	74
4	10	21	22	0	10	17	9	7	3	34	34	2	8	99	100	11	1	45	44
5	1	27	26	1	0	34	33	7	4	36	37	2	9	45	45	11	2	30	27
5	2	30	29	1	1	123	125	7	5	32	30	2	10	87	87	11	3	15	7
5	3	51	50	1	2	29	30	7	6	99	100	3	1	20	21	11	4	22	18
5	4	25	26	1	3	124	126	7	8	107	110	3	2	24	23				
5	5	53	51	1	5	92	92	8	0	104	101	3	3	23	23		H =	6	
5	6	78	77	1	6	36	39	8	1	67	65	3	4	52	54	K	L	Fo	Fc
5	7	25	24	1	7	20	21	8	2	27	26	3	6	40	40	0	0	233	232
5	8	20	21	1	9	76	75	8	3	131	129	3	8	56	56	0	1	24	24
5	9	16	10	1	10	20	17	8	4	24	25	3	9	21	19	0	2	269	270
6	1	107	108	2	0	280	286	8	5	50	49	3	10	42	40	0	3	18	17
6	2	89	87	2	1	97	101	8	7	29	30	4	1	35	36	0	4	86	84
6	3	23	23	2	2	133	136	9	0	132	130	4	2	95	97	0	5	48	48
6	4	16	16	2	3	129	130	9	1	87	87	4	3	89	89	0	6	257	252
6	7	22	25	2	4	91	91	9	2	29	29	4	4	74	76	0	7	41	41
6	9	47	46	2	5	139	138	9	3	112	113	4	5	14	11	0	8	92	91
7	1	50	50	2	6	112	112	9	4	20	19	4	7	41	43	0	9	50	51
7	2	185	185	2	7	16	16	9	5	75	76	4	8	16	9	0	10	19	16
7	3	62	63	2	8	98	97	9	6	43	43	4	9	21	19	1	0	93	95
7	4	161	161	2	9	100	101	10	0	115	114	5	1	128	128	1	1	59	60
7	5	57	56	2	10	16	9	10	1	52	53	5	2	129	128	1	2	38	39
7	7	54	55	3	0	171	172	10	2	61	61	5	3	76	76	1	3	82	84
7	8	108	109	3	1	69	70	10	3	30	30	5	4	78	77	1	4	64	65
8	1	124	124	3	2	27	27	10	4	36	35	5	5	149	150	1	5	55	57
8	2	35	34	3	3	80	82	10	5	40	40	5	6	34	34	1	6	61	62
8	3	21	21	3	4	26	27	10	6	50	49	5	7	66	67	1	9	18	19
8	4	27	26	3	5	64	64	11	0	129	126	5	8	94	96	2	0	91	93
8	5	130	131	3	6	83	80	11	1	20	18	5	9	18	13	2	1	51	50
8	6	26	26	3	7	15	15	11	2	63	62	6	1	153	153	2	2	71	72
8	7	124	126	3	8	94	93	11	3	14	12	6	2	115	117	2	3	107	107
9	1	27	25	3	9	40	41	11	4	34	33	6	3	58	57	2	4	68	67
9	2	52	52	3	10	45	44	12	0	82	84	6	4	162	165	2	5	93	92
9	3	20	21	4	0	105	103					6	5	103	104	2	6	96	96
9	4	58	57	4	1	195	198		H =	5		6	6	34	33	2	7	64	64
9	5	29	29	4	2	37	36	K	L	Fo	Fc	6	7	95	97	2	8	51	52
9	6	61	60	4	3	201	202	0	1	71	72	6	8	75	77	2	9	51	50
9	7	22	22	4	4	30	29	0	2	110	112	7	1	32	33	3	0	103	103
10	1	19	13	4	5	88	89	0	3	84	87	7	2	49	49	3	1	39	38
10	2	74	74	4	6	13	13	0	4	132	133	7	3	32	33	3	2	12	4
10	3	16	14	4	9	121	123	0	5	23	23	7	4	14	14	3	3	196	193

3	4	53	53
3	5	127	122
3	6	41	41
3	7	48	49
3	9	36	35
4	0	222	224
4	1	30	29
4	2	222	218
4	3	26	26
4	4	64	65
4	5	45	45
4	6	203	208
4	7	43	43
4	8	88	88
4	9	40	41
5	0	69	69
5	1	46	47
5	2	55	54
5	3	33	35
5	4	59	58
5	5	12	11
5	6	65	66
5	7	28	28
6	0	76	78
6	3	70	70
6	4	33	34
6	5	65	66
6	6	27	29
6	7	41	42
6	8	49	50
7	0	68	69
7	1	47	47
7	3	201	206
7	4	35	35
7	5	128	129
7	6	27	25
7	7	51	52
7	8	17	5
8	0	165	168
8	1	30	30
8	2	101	101
8	3	36	35
8	4	29	29
8	5	36	36
8	6	108	108
8	7	39	41
9	0	57	56
9	2	37	37
9	3	56	57
9	4	38	40
9	5	29	29
9	6	49	50
10	0	34	31
10	2	49	51
10	3	36	35
10	5	38	38
11	0	30	30
11	1	62	62
11	3	147	149

H = 7

K	L	Fo	Fc
0	1	109	110
0	2	242	247
0	3	87	88
0	4	214	212
0	5	87	86
0	6	71	72
0	8	106	105
0	9	36	36
1	1	72	73
1	2	89	88
1	4	42	43
1	5	34	36
1	6	37	38
1	7	27	27
1	8	58	56
2	1	91	91
2	2	61	61
2	3	12	9
2	4	134	131
2	5	77	77
2	6	21	21
2	7	139	140
2	8	37	37
3	1	144	147
3	3	16	14
3	4	69	68
3	5	92	90
3	6	78	79
3	7	86	85
3	8	28	30
3	9	27	27
4	1	71	71
4	2	215	213
4	3	48	48
4	4	173	177
4	5	57	57
4	6	57	59
4	7	16	14
4	8	87	87
4	9	28	29
5	1	14	12
5	2	125	123
5	3	18	18
5	4	25	25
5	5	17	16
5	7	28	27
5	8	67	67
6	1	44	44
6	2	20	21
6	3	31	30
6	4	69	70
6	5	88	90
6	6	15	11
6	7	87	89
6	8	16	16
7	1	158	158
7	2	20	20
7	3	20	19

7	4	45	44
7	5	101	102
7	6	71	72
7	7	101	105
8	1	15	13
8	2	127	128
8	3	13	6
8	4	97	97
8	6	35	34
9	1	42	42
9	2	87	88
9	3	20	17
9	4	38	40
9	5	34	32
10	2	18	18
10	3	42	43
10	4	17	8
11	1	121	122

H = 8

K	L	Fo	Fc
0	0	92	90
0	1	24	24
0	2	13	13
0	3	52	52
0	4	26	25
0	5	97	97
0	6	43	43
0	7	21	18
0	8	58	58
0	9	49	50
1	0	115	115
1	1	80	80
1	2	16	17
1	3	94	91
1	4	27	28
1	5	45	45
1	6	68	68
1	7	18	18
1	8	68	67
1	9	33	31
2	0	263	267
2	1	176	176
2	2	93	91
2	3	207	205
2	4	33	32
2	5	65	66
2	6	106	105
2	7	29	24
2	8	122	121
2	9	119	118
3	3	54	54
3	5	17	16
3	6	27	28
3	8	15	16
3	9	24	22
4	0	37	37
4	3	34	36
4	4	21	21
4	5	78	80

4	6	37	39
4	7	14	11
4	8	31	32
5	0	171	170
5	1	120	119
5	2	38	37
5	3	107	106
5	4	41	41
5	5	65	63
5	6	91	92
5	7	28	27
5	8	95	95
6	0	166	167
6	1	109	107
6	2	88	88
6	3	149	152
6	4	25	25
6	5	45	45
6	6	84	86
6	7	28	29
7	0	50	50
7	1	31	32
7	2	21	21
7	4	14	6
7	7	16	5
8	0	39	40
8	1	35	35
8	2	17	13
8	5	43	44
8	6	25	23
9	0	143	143
9	1	84	85
9	2	47	47
9	3	97	100
9	4	38	38
9	5	62	62
10	0	60	60
10	1	41	41
10	2	64	63
10	3	82	81

H = 9

K	L	Fo	Fc
0	1	201	198
0	2	21	22
0	3	15	11
0	4	84	84
0	5	174	173
0	6	39	38
0	7	116	116
0	8	19	16
0	9	59	58
1	1	83	84
1	2	19	20
1	3	29	28
1	4	30	29
1	5	59	58
1	7	65	65
1	8	42	42
2	1	115	115

2	2	143	140
2	3	111	111
2	4	72	73
2	5	88	88
2	6	41	40
2	7	97	97
2	8	49	48
3	1	48	47
3	2	71	68
3	3	61	61
3	4	74	71
3	5	80	81
3	6	16	10
3	7	35	35
3	8	63	63
4	1	167	168
4	2	38	38
4	3	25	24
4	4	57	59
4	5	134	135
4	6	21	21
4	7	99	100
4	8	18	18
5	1	95	94
5	2	28	28
5	4	97	99
5	5	34	34
5	6	15	8
5	7	75	76
6	0	12	0
6	1	69	70
6	2	84	86
6	3	63	63
6	4	81	83
6	5	32	33
6	7	65	67
7	1	25	24
7	2	90	91
7	3	49	50
7	4	104	105
7	5	64	65
7	6	16	14
8	1	98	97
8	2	54	55
8	3	38	38
8	4	23	22
8	5	60	61
9	1	70	71
9	2	50	50
9	4	90	93
10	1	22	17
10	2	39	38

H = 10

K	L	Fo	Fc
0	0	27	27
0	1	27	27
0	2	13	13
0	3	230	232
0	5	164	163

0	6	24	23
0	7	101	98
0	8	37	14
1	0	59	59
1	2	23	22
1	3	57	55
1	4	47	49
1	5	58	58
1	6	54	54
2	0	140	140
2	1	38	37
2	2	57	57
2	3	110	109
2	4	23	24
2	5	44	45
2	6	49	50
2	7	15	12
2	8	35	34
3	0	84	83
3	1	20	21
3	2	103	101
3	3	33	34
3	4	73	72
3	5	41	41
3	6	121	122
3	8	15	9
4	0	35	32
4	1	40	41
4	2	16	12
4	3	184	191
4	5	133	134
4	6	17	17
4	7	72	74
5	0	18	18
5	1	16	14
5	2	42	42
5	3	63	62
5	4	21	20
5	5	60	61
5	6	17	12
6	0	95	96
6	1	47	49
6	2	44	45
6	3	42	44
6	4	18	18
6	6	33	35
7	0	101	103
7	1	23	22
7	2	110	112
7	3	17	13
7	4	70	71
7	5	25	23
7	6	131	135
8	0	40	40
8	1	49	50
8	2	15	11
8	3	98	100
8	5	72	74
9	0	29	27
9	1	16	14
9	2	41	42
9	3	53	54

H = 11

K	L	Fo	Fc
0	1	125	126
0	2	75	74
0	3	12	5
0	4	23	25
0	5	34	34
0	6	32	32
0	7	48	46
1	1	116	116
1	2	18	19
1	3	23	24
1	4	33	30
1	5	47	46
1	6	28	27
1	7	54	52
2	1	70	70
2	2	159	160
2	3	56	55
2	4	138	139
2	5	113	112
2	6	65	66
2	7	96	96
3	1	47	49
3	2	14	13
3	4	28	26
3	5	44	46
3	6	31	31
4	1	102	104
4	2	41	41
4	3	14	3
4	4	18	15
4	5	21	20
4	6	15	14
4	7	37	36
5	1	145	145
5	2	44	43
5	3	37	37
5	4	71	70
5	5	46	45
5	6	20	17
6	1	45	45
6	2	94	97
6	3	31	31
6	4	121	124
6	5	74	74
6	6	32	30
7	1	15	4
7	2	34	33
7	4	50	50
7	5	26	24
8	1	59	59
8	3	15	13
9	1	120	121

H = 12

K	L	Fo	Fc
0	0	178	183
0	1	25	25
0	2	92	93
0	3	38	36
0	4	17	14
0	5	24	23
0	6	108	106
0	7	31	29
1	0	80	81
1	1	14	13
1	2	19	16
1	3	20	20
1	4	36	37
1	6	50	49
1	7	16	10
2	0	149	150
2	1	111	112
2	2	30	30
2	3	82	82
2	4	62	62
2	5	26	23
2	6	71	70
3	0	32	31
3	1	68	68
3	2	28	27
3	3	69	67
3	4	36	36
3	5	28	27
3	6	45	46
4	0	140	141
4	1	37	37
4	2	83	85
4	3	29	30
4	5	22	20
4	6	92	93
5	0	105	103
5	1	32	32
5	2	14	9
5	3	28	26
5	4	32	32
5	5	30	28
6	0	76	77
6	1	67	68
6	2	25	25
6	3	71	73
6	4	44	44
6	5	19	19
7	0	14	8
7	1	76	76
7	2	19	20
7	3	86	88
7	4	28	28
8	0	56	56
8	1	50	51
8	2	60	61

H = 13

K	L	Fo	Fc
0	1	19	13
0	2	171	176
0	3	70	72
0	4	174	172
0	5	54	53
0	6	20	18
1	0	14	0
1	1	48	49
1	3	19	17
1	4	17	11
1	5	23	23
2	1	17	15
2	2	16	12
2	3	14	13
2	4	61	61
2	5	39	39
2	6	26	25
3	1	96	95
3	2	15	12
3	3	34	34
3	4	50	51
3	5	67	67
4	1	16	15
4	2	152	154
4	3	50	51
4	4	143	143
4	5	33	33
5	1	13	1
5	3	15	1
5	4	23	21
6	1	19	16
6	2	14	3
6	3	31	31
7	1	106	108

H = 14

K	L	Fo	Fc
0	0	28	26
0	1	23	22
0	2	73	69
0	3	26	23
0	4	24	21
0	5	21	20
1	0	40	38
1	2	42	39
1	3	14	8
1	4	32	32
1	5	34	33
2	0	95	93
2	1	44	45
2	2	81	81
2	3	121	122
2	4	34	33
2	5	73	73
3	2	17	15
3	3	44	43
3	4	23	21
4	0	29	30
4	1	18	17
4	2	45	46
4	3	15	12
4	4	18	16
5	0	65	64
5	1	15	11
5	2	53	53
5	3	50	49
6	0	85	85
6	1	34	33

H = 15

K	L	Fo	Fc
0	1	77	76
0	2	17	11
0	3	16	8
0	4	18	17
1	1	69	69
1	2	47	46
1	3	14	6
2	1	116	118
2	2	47	47
3	1	56	57
4	1	56	56

H = 16

K	L	Fo	Fc
0	0	31	30
0	1	90	89
1	0	43	44

APPENDIX F: CALCULATED AND OBSERVED STRUCTURE FACTOR AMPLITUDES FOR Ca_5Bi_3F

H = 0

K	L	Fo	Fc
0	2	702	697
0	4	558	554
0	6	868	854
0	8	689	668
0	10	158	175
1	1	146	146
1	3	442	440
1	5	255	256
1	9	169	186
2	0	318	316
2	2	204	206
2	6	369	372
2	8	293	289
3	1	571	589
3	3	730	734
3	5	445	443
3	9	434	439
4	0	1729	1752
4	2	621	626
4	4	459	461
4	6	709	736
4	8	516	518
4	10	134	124
5	1	185	187
5	3	65	53
6	0	87	91
6	2	163	166
6	8	99	102
7	1	571	556
7	3	805	781
7	7	78	72
7	9	504	486
8	0	865	838
8	2	435	425
8	4	288	279
8	8	244	244
9	1	153	145
9	3	156	152
9	4	64	0
9	5	78	90
9	6	68	0
10	0	317	305
11	3	673	627
12	0	326	300
12	2	206	191

H = 1

K	L	Fo	Fc
0	2	672	699
0	3	323	327
0	4	845	881
0	6	220	221
0	8	390	392
0	9	87	71
0	10	351	348
0	11	102	105
1	2	467	457
1	4	387	394
1	7	73	85
1	8	306	304
1	10	238	231
1	11	74	60
2	1	748	760
2	2	934	958
2	3	109	113
2	4	449	449
2	6	186	181
2	7	471	479
2	8	215	223
2	9	95	77
2	10	324	326
3	1	400	405
3	2	353	362
3	5	217	223
3	7	178	182
3	10	153	161
4	2	485	495
4	3	172	180
4	4	719	722
4	5	79	88
4	6	152	156
4	8	311	316
4	9	81	58
4	10	336	278
5	1	342	341
5	2	434	438
5	4	566	564
5	5	97	110
5	6	77	65
5	7	281	283
5	8	305	309
5	9	103	93
5	10	252	258
6	1	555	547
6	2	517	515
6	3	57	36
6	4	303	298
6	6	73	83
6	7	393	391
6	8	118	123
6	9	77	52
7	1	502	495
7	2	157	159
7	4	77	81
7	7	299	296
7	8	149	145
7	9	75	65
8	2	184	184
8	4	416	402
8	6	69	51
8	8	161	163
9	1	367	359
9	2	412	393
9	4	451	430
9	7	299	293
10	2	161	154
10	3	86	88
10	4	99	95
11	2	66	26
11	4	68	24
12	1	104	108
12	2	75	18

H = 2

K	L	Fo	Fc
0	1	203	209
0	3	814	843
0	4	126	139
0	5	387	397
0	7	136	146
0	9	204	211
0	10	116	123
1	0	152	145
1	1	270	263
1	2	203	207
1	4	132	136
1	5	279	286
1	6	181	176
1	7	163	179
1	9	138	147
2	0	884	900
2	1	307	312
2	2	831	848
2	3	900	908
2	4	229	231
2	7	205	213
2	8	278	294
2	9	349	360
3	0	92	94
3	1	249	252
3	2	161	166
3	3	351	355
3	5	124	125
3	6	119	138
3	7	72	89
3	8	63	66
3	9	86	87
4	1	223	225
4	2	76	86
4	3	592	597
4	4	79	81
4	5	282	294
4	6	66	64
4	7	84	82
4	9	219	187
4	10	93	96
5	0	346	351
5	1	226	232
5	2	397	400
5	3	762	771
5	4	208	214
5	7	203	210
5	8	93	97
5	9	187	189
6	0	686	687
6	1	274	280
6	2	483	488
6	3	522	512
6	4	153	154
6	7	87	101
6	8	245	246
6	9	284	283
7	0	283	283
7	1	112	117
7	2	259	259
7	3	93	106
7	4	85	85
7	7	65	42
7	8	139	135
8	1	168	173
8	2	158	166
8	3	214	209
8	5	99	111
8	6	124	146
8	8	75	21
9	0	457	431
9	1	228	232
9	2	326	313
9	3	607	590
9	4	186	183
9	7	149	152
10	0	421	395
10	1	158	159
10	2	219	214
10	3	161	161
10	4	79	75
10	5	123	115
11	0	329	312
11	2	171	169
11	3	74	39
11	4	88	74
12	0	94	110
12	1	76	59
12	2	158	163

H = 3

K	L	Fo	Fc
0	1	1251	1221
0	2	396	399
0	3	83	85
0	4	178	180
0	5	912	908
0	7	891	903
0	9	132	142
1	1	182	174
1	2	292	294
1	4	254	241
1	5	60	62
1	6	113	130
1	7	120	140
1	8	198	200
1	10	117	127
2	1	646	660
2	2	236	244
2	3	83	90
2	4	272	272
2	5	207	172
2	6	89	94
2	7	313	272
2	9	165	168
2	10	102	80
3	1	198	201
3	2	652	661
3	3	158	160
3	4	540	547
3	5	88	97
3	7	207	174
3	9	72	19
4	1	951	975
4	2	251	259
4	3	76	79
4	4	77	59
4	5	716	764
4	7	743	745
4	8	114	19
4	9	158	116
5	1	114	119
5	2	71	75
5	3	103	106
5	4	79	75
5	5	133	154
5	6	156	179
5	7	86	95
6	1	295	306
6	2	249	256
6	3	71	74
6	4	69	87
6	5	65	60
6	7	106	109
6	8	74	40
6	9	119	116
7	1	120	125
7	2	683	696
7	3	118	126
7	4	637	624
7	5	83	87
7	7	121	127
7	8	362	379
8	1	511	509
8	2	96	97
8	3	65	54
8	4	81	80
8	6	66	65
8	7	432	426
9	1	112	108
9	2	175	178
9	4	200	197
9	5	88	92
9	6	125	147
9	7	91	91
10	2	194	196
11	1	78	48
11	2	531	515
11	4	526	500

H = 4

K	L	Fo	Fc
0	0	255	245

0	1	951	904	8	1	217	220	5	2	476	482	2	9	208	184	0	3	184	181
0	3	931	961	8	2	81	77	5	3	163	164	2	10	159	54	0	4	920	846
0	4	74	77	8	3	471	467	5	4	353	354	3	0	311	320	0	5	204	193
0	5	432	444	8	4	91	81	5	5	436	482	3	1	200	200	0	6	198	194
0	7	74	92	8	6	75	52	5	6	68	95	3	3	692	672	0	8	407	418
0	9	500	537	8	7	112	112	5	7	253	268	3	4	150	156	0	10	404	431
0	10	87	18	8	8	76	43	5	8	294	301	3	5	395	358	1	1	225	231
1	1	390	369	9	0	408	398	6	1	559	564	3	6	186	156	1	2	333	306
1	2	66	80	9	1	261	267	6	2	462	469	3	7	197	173	1	4	202	194
1	5	288	263	9	2	146	148	6	3	97	94	4	0	941	950	1	5	158	143
1	6	117	108	9	3	417	411	6	4	554	554	4	2	715	716	1	7	113	112
1	9	230	251	9	4	76	82	6	6	89	93	4	3	95	104	1	8	182	176
1	10	70	52	9	6	174	189	6	7	350	364	4	4	276	280	2	1	394	385
2	0	1116	1126	9	7	77	52	6	8	244	278	4	5	86	93	2	2	292	272
2	1	338	344	10	0	383	369	7	1	145	142	4	7	143	120	2	8	153	139
2	2	465	459	10	1	91	99	7	2	97	100	4	9	147	112	3	1	527	529
2	3	536	518	10	2	187	185	7	5	119	132	5	0	274	278	3	4	203	206
2	4	345	318	10	3	101	86	7	6	93	102	5	1	68	74	3	6	191	168
2	8	324	286	10	4	125	124	7	7	123	114	5	2	175	185	3	8	122	92
2	9	314	310	10	5	96	97	7	8	78	65	5	3	114	121	4	1	128	130
2	10	153	84	11	0	501	473	8	2	153	150	5	4	174	181	4	2	807	818
3	0	602	612	11	2	261	251	8	3	168	174	5	5	94	67	4	3	96	91
3	1	202	200	11	4	154	150	9	1	445	456	5	6	218	232	4	4	709	694
3	2	151	155	12	0	252	245	9	2	409	403	5	7	108	48	4	5	135	132
3	3	263	265	12	2	101	82	9	3	86	97	6	0	288	285	4	6	168	158
3	4	130	129					9	4	364	356	6	1	73	60	4	7	74	46
3	5	163	171		H =	5		9	7	296	294	6	3	266	273	5	1	82	73
3	6	313	306	K	L	Fo	Fc	10	0	73	0	6	4	95	97	5	2	386	399
3	8	309	257	0	1	249	235	10	1	251	258	6	5	166	195	5	4	170	178
3	9	204	147	0	2	410	396	10	2	237	233	6	6	117	137	5	5	93	51
3	10	169	121	0	3	197	200	10	4	200	205	6	7	109	118	5	6	112	9
4	0	262	262	0	4	417	436	11	0	83	0	6	8	164	161	5	7	94	87
4	1	615	619	0	7	174	183	11	1	160	169	7	0	195	199	5	8	222	213
4	2	74	82	0	9	91	91	11	2	85	72	7	1	250	249	6	1	225	231
4	3	801	805	0	10	196	197	11	4	81	76	7	3	735	732	6	2	98	117
4	4	79	79	1	1	331	328	12	1	128	118	7	4	99	106	6	3	74	68
4	5	346	366	1	2	345	320					7	6	104	98	6	4	231	233
4	7	112	109	1	3	81	94		H =	6		7	7	169	185	6	5	268	307
5	0	442	447	1	4	328	286	K	L	Fo	Fc	8	0	618	609	6	6	98	59
5	1	376	377	1	5	343	315	0	0	1181	1080	8	2	330	330	6	7	256	270
5	3	492	491	1	7	141	153	0	4	364	354	8	3	120	124	6	8	91	59
5	5	269	284	1	8	240	257	0	5	104	98	8	4	146	143	7	1	580	591
5	6	87	93	1	10	203	228	0	6	898	923	8	7	116	108	7	4	113	112
5	8	150	158	2	1	890	888	0	7	111	120	9	0	235	231	7	6	137	148
5	9	298	294	2	2	664	643	0	8	348	360	9	1	74	61	7	7	374	399
6	0	724	729	2	3	234	227	0	9	121	133	9	2	132	134	8	2	457	464
6	2	324	331	2	7	743	542	1	0	340	334	9	3	218	214	8	4	372	384
6	3	319	325	2	9	128	128	1	1	184	174	9	4	118	126	8	6	100	86
6	4	222	225	2	10	346	324	1	2	153	148	9	5	120	129	8	7	110	113
6	5	249	272	3	4	153	161	1	3	299	265	9	6	164	184	9	1	175	179
6	8	177	195	3	6	72	84	1	4	222	197	10	0	79	65	9	2	287	298
6	9	152	137	3	8	179	151	1	5	132	141	10	2	101	106	9	4	193	199
7	0	710	704	3	9	81	55	1	6	252	220	10	3	135	151	9	5	127	121
7	1	76	79	3	10	156	105	2	0	427	424	10	5	109	114	10	3	99	91
7	2	234	238	4	1	122	126	2	2	270	268	11	0	106	87	11	0	83	0
7	3	101	104	4	2	320	320	2	3	436	401	11	3	542	537	11	2	74	10
7	4	172	171	4	3	198	203	2	4	221	205								
7	5	74	74	4	4	267	267	2	5	301	265		H =	7			H =	8	
7	8	301	316	4	7	124	112	2	7	214	169	K	L	Fo	Fc	K	L	Fo	Fc
8	0	270	277	5	1	481	483	2	8	238	205	0	1	251	226	0	0	361	328

0	3	218	212
0	5	284	264
0	6	211	199
0	7	124	35
0	8	202	193
0	9	155	143
1	0	424	411
1	1	219	226
1	2	120	120
1	3	331	300
1	4	120	127
1	5	154	151
1	6	299	263
1	8	210	186
1	9	153	133
2	0	1013	993
2	1	590	573
2	2	388	363
2	4	197	178
2	5	305	301
2	7	188	156
3	3	127	126
3	6	95	96
3	8	123	38
3	9	82	31
4	0	162	172
4	2	71	76
4	3	125	145
4	5	206	211
4	6	156	162
4	8	135	124
4	9	98	87
5	0	606	610
5	1	349	348
5	2	197	202
5	3	398	399
5	4	168	183
5	5	220	230
5	6	356	367
6	0	586	596
6	1	355	353
6	2	299	311
6	3	566	572
6	4	131	137
6	5	193	212
6	6	315	334
6	7	139	140
6	8	228	223
7	0	127	139
7	1	102	94
7	3	77	37
7	4	80	20
7	7	102	14
8	0	92	68
8	1	91	80
8	5	113	99
9	0	529	525
9	1	248	260
9	2	220	220
9	3	382	389
9	4	166	171
9	5	202	226
10	0	233	239
10	1	139	151
10	2	188	194
10	3	277	289
10	4	92	75
11	0	132	122

H = 9

K	L	Fo	Fc
0	1	890	795
0	4	226	221
0	5	682	637
0	6	122	106
0	7	521	486
0	8	128	89
0	9	180	167
1	1	334	319
1	2	109	72
1	5	253	230
1	7	238	221
1	8	108	110
2	1	458	448
2	2	507	483
2	3	279	262
2	4	387	346
2	5	355	319
2	6	119	103
2	8	243	201
2	9	109	92
3	1	186	198
3	2	275	286
3	3	117	117
3	4	324	298
3	5	294	256
3	7	153	130
3	8	238	204
4	1	655	657
4	2	132	128
4	4	173	166
4	8	129	92
5	1	345	350
5	2	129	132
5	4	279	278
5	5	177	185
5	7	270	256
6	1	256	264
6	2	310	318
6	3	130	147
6	4	311	327
6	5	141	141
6	7	234	218
7	1	104	108
7	2	364	383
7	3	106	88
7	4	400	415
7	5	160	188
8	1	353	366
8	2	158	168
8	4	104	91
8	5	206	244
9	1	256	273
9	2	207	212
9	3	92	22
9	4	290	292
10	2	162	166

H = 10

K	L	Fo	Fc
0	1	306	277
0	5	599	565
0	6	122	58
0	7	339	310
1	0	232	240
1	2	125	96
1	3	181	172
1	4	183	162
1	5	165	144
1	6	216	190
2	0	424	416
2	1	145	145
2	2	178	182
2	3	403	376
2	4	130	90
2	5	214	192
2	6	217	197
2	8	126	96
3	0	423	419
3	2	358	340
3	3	116	99
3	4	275	257
3	5	109	92
3	8	159	9?
4	1	271	276
4	3	793	770
4	7	260	243
5	0	90	24
5	2	113	111
5	3	213	204
5	5	142	160
6	0	275	279
6	1	144	140
6	2	133	143
6	3	151	155
6	5	107	84
6	6	141	138
6	7	108	78
7	0	497	510
7	2	363	383
7	4	259	260
8	0	107	95
8	1	203	223
8	2	98	37
8	3	402	418
8	5	213	263
9	0	138	138
9	1	105	73
9	2	116	131
9	3	188	183
10	0	134	138
10	1	89	77

H = 11

K	L	Fo	Fc
0	1	481	447
0	2	199	187
0	5	198	181
0	7	236	214
1	1	413	397
1	4	135	119
1	5	226	215
1	6	110	54
1	7	226	213
1	8	145	87
2	1	378	372
2	2	639	635
2	3	154	142
2	4	590	546
2	5	428	391
2	6	176	156
2	7	395	375
2	8	358	341
3	1	159	163
3	2	105	50
3	4	108	82
3	5	183	157
3	7	121	38
4	1	357	364
4	5	134	129
4	7	171	168
5	1	504	511
5	2	200	211
5	4	273	266
5	5	265	249
6	1	241	248
6	2	402	412
6	4	444	452
6	5	239	261
7	2	140	143
7	4	189	181
8	1	185	191
9	1	401	439
9	2	215	231

H = 12

K	L	Fo	Fc
0	0	748	704
0	2	362	354
0	3	124	117
0	4	135	130
1	0	334	318
1	2	123	105
1	4	149	133
1	6	232	217
2	0	550	559
2	1	354	361
2	2	192	191
2	3	393	389
2	4	227	218
2	5	175	162
2	6	344	329
2	7	108	62
3	0	159	156
3	1	193	197
3	2	135	106
3	3	254	238
3	5	137	110
3	6	191	174
4	0	526	545
4	2	302	310
4	3	122	105
4	4	138	102
5	0	381	390
5	1	129	124
5	2	136	101
5	3	182	168
5	4	154	122
5	5	124	115
5	6	214	226
6	0	303	306
6	1	216	229
6	2	162	137
6	3	317	328
6	4	150	148
7	0	103	66
7	1	224	240
7	2	119	62
7	3	336	340
7	4	126	9?
8	0	237	243
8	1	150	145
8	2	182	198

H = 13

K	L	Fo	Fc
0	2	717	717
0	3	169	160
0	4	689	710
0	5	140	144
1	1	194	194
1	5	151	126
2	0	118	0
2	2	134	124
2	4	245	234
2	5	129	116
3	1	379	393
3	2	125	12
3	3	124	86
3	4	130	115
3	5	294	294
3	6	129	41
4	2	591	617
4	3	134	110
4	4	592	590
6	0	129	0
6	3	124	82
7	1	434	458

H = 14

K	L	Fo	Fc
0	0	288	278
0	2	242	268
0	3	111	72
0	4	119	126
1	0	233	234
1	2	150	149
2	0	378	383
2	1	205	220
2	2	287	291
2	3	487	506
2	4	141	116
2	5	264	276
3	3	178	174
3	4	116	88
4	0	239	254
4	2	180	194
4	4	109	99
5	0	314	333
5	2	198	199
5	3	187	185
6	0	286	309
6	1	169	160
6	2	170	158

H = 15

K	L	Fo	Fc
0	1	303	326
1	1	252	264
1	2	143	137
1	4	126	40
2	1	463	470
2	2	255	279
2	4	367	401
3	0	115	0
3	1	201	198
3	2	132	65
4	1	239	247

H = 16

K	L	Fo	Fc
0	0	125	103
0	1	328	362
1	0	159	162
1	1	109	19
1	2	104	35
2	1	131	124

APPENDIX G: CALCULATED AND OBSERVED STRUCTURE FACTOR AMPLITUDES FOR $Ba_4Sb_{2.5}I_{0.5}$

H = -12

K	L	Fo	Fc
2	2	49	65
3	1	84	75

H = -11

K	L	Fo	Fc
2	1	27	36
3	2	40	50
4	1	70	62
4	3	20	22
5	2	38	49

H = -10

K	L	Fo	Fc
1	1	117	109
3	1	20	23
3	3	61	56
4	2	82	99
5	1	46	53
5	3	85	77
5	5	47	53
6	4	40	47
7	1	30	30

H = -9

K	L	Fo	Fc
2	1	155	147
3	2	23	26
4	1	28	32
4	3	69	78
5	2	34	34
5	4	73	66
6	3	40	48
6	5	27	24
7	2	15	13
7	4	38	38
8	1	22	21

H = -8

K	L	Fo	Fc
2	2	126	119
3	1	41	40
4	2	86	80
4	4	67	76
5	1	111	129
5	3	31	32
6	2	45	41
6	6	113	107
7	1	27	29
7	5	19	15
8	4	21	23

H = -7

K	L	Fo	Fc
2	1	129	119
3	2	63	57
4	1	39	40
4	3	106	120
5	2	112	108
5	4	76	74
6	1	35	34
6	5	54	51
7	2	61	60
7	6	55	50

H = -6

K	L	Fo	Fc
1	1	184	205
3	1	82	68
3	3	110	105
4	2	101	83
5	1	79	75
5	3	76	75
5	5	128	126
6	4	34	34

H = -5

K	L	Fo	Fc
2	1	44	44
3	2	138	148
4	1	159	149
4	3	51	32

H = -4

K	L	Fo	Fc
2	2	170	182
3	1	148	155
4	4	247	228

H = -3

K	L	Fo	Fc
2	1	182	202
3	2	123	135

H = -2

K	L	Fo	Fc
1	1	45	41

H = 2

K	L	Fo	Fc
1	1	48	46
2	0	62	60

H = 3

K	L	Fo	Fc
1	0	229	293
2	1	184	201
3	2	134	137

H = 4

K	L	Fo	Fc
2	0	139	146
2	2	172	184
3	1	146	151
4	0	50	45
4	4	242	218

H = 5

K	L	Fo	Fc
1	0	45	47
2	1	44	41
3	0	57	58
3	2	143	151
4	1	153	146
4	3	49	32
5	2	135	113

H = 6

K	L	Fo	Fc
1	1	184	204
2	0	183	195
3	1	83	64
3	3	119	108
4	0	105	107
4	2	105	86
4	4	16	0
5	1	81	73
5	3	77	78
5	5	122	128
6	0	105	104
6	4	32	36

H = 7

K	L	Fo	Fc
1	0	41	30
2	1	139	119
3	0	30	9
3	2	68	53
4	1	41	40
4	3	118	118
5	0	138	130
5	2	100	107
5	4	74	72
6	1	33	33
6	3	95	94
6	5	50	50
7	2	61	60
7	6	51	50

H = 8

K	L	Fo	Fc
0	0	32	20
3	1	40	42
4	0	76	73
4	2	85	80
4	4	76	77
5	1	138	130
5	3	29	32
6	0	14	3
6	2	41	42
6	4	65	64
6	6	106	107
7	1	27	29
7	3	99	103
7	5	19	17
8	0	194	185
8	4	20	24

H = 9

K	L	Fo	Fc
1	0	35	39
2	1	154	146
3	2	24	28
4	1	33	32
4	3	65	79
5	0	125	118
5	2	37	34
5	4	68	68
6	3	49	48
6	5	23	24
7	0	40	42
7	2	14	11
7	4	32	38
8	1	20	21
8	3	76	71

H = 10

K	L	Fo	Fc
2	0	64	58
3	1	19	24
4	0	73	66
4	2	79	98
5	1	59	53
5	3	59	76
5	5	55	51
6	4	51	46
7	1	32	29

H = 11

K	L	Fo	Fc
2	1	42	38
3	0	26	28
3	2	57	50
4	1	49	63
4	3	20	22
5	0	41	36
5	2	55	48

H = 12

K	L	Fo	Fc
2	0	37	50
3	1	84	76

APPENDIX H: CALCULATED AND OBSERVED STRUCTURE FACTOR AMPLITUDES FOR $Ca_{16}Sb_{11}$

Values of 10^Fobs and 10^Fcalc for Cal6Sb11

H	K	L	Fobs	Fcalc	SigF	H	K	L	Fobs	Fcalc	SigF	H	K	L	Fobs	Fcalc	SigF	H	K	L	Fobs	Fcalc	SigF
0	0	3	1323	1235	64	0	6	10	2357	2280	72	1	2	12	1168	1201	121	1	9	2	963	971	86
0	0	4	7329	7286	116	0	6	11	2053	2145	63	1	2	13	1319	1386	65	1	9	5	1196	1292	65
0	0	5	1085	983	39	0	7	3	1321	1362	47	1	3	0	4493	4612	89	1	9	6	861	798	84
0	0	6	2489	2479	56	0	7	4	750	748	94	1	3	1	676	720	81	1	9	7	1094	1033	81
0	0	8	3503	3506	71	0	7	5	766	732	87	1	3	2	1165	1166	44	1	9	9	1166	1109	80
0	0	11	2335	2497	54	0	7	7	1867	1847	73	1	3	3	3254	3289	56	1	9	10	1227	1150	77
0	0	12	1181	1414	98	0	7	11	1166	1171	80	1	3	4	1878	1854	76	1	10	0	1782	1762	76
0	0	13	1529	1388	98	0	8	0	1340	1346	41	1	3	5	1191	1195	37	1	10	3	1208	1252	58
0	1	3	474	461	67	0	8	2	3702	3695	63	1	3	6	642	605	66	1	10	4	1952	1941	85
0	1	5	1603	1610	36	0	8	3	3299	3309	69	1	3	7	920	1006	55	1	10	5	1054	1031	62
0	1	7	1145	1105	79	0	8	5	1043	968	86	1	3	8	1622	1696	44	1	10	7	1415	1286	85
0	1	9	742	812	77	0	8	6	2733	2657	96	1	3	9	1020	1085	60	1	10	8	1712	1681	63
0	1	11	948	1034	92	0	8	9	1995	1981	54	1	3	10	1333	1261	56	1	11	0	1440	1452	109
0	2	2	1335	1320	32	0	9	8	1136	1096	113	1	3	11	1365	1581	54	1	11	2	1735	1721	43
0	2	3	2940	2934	80	0	10	0	1027	1096	61	1	4	0	2711	2797	47	1	11	3	969	971	86
0	2	4	3031	3093	72	0	10	3	1050	1083	65	1	4	1	1595	1611	60	1	11	6	1867	1835	74
0	2	5	971	898	39	0	10	4	1015	1004	67	1	4	2	4775	4801	44	1	12	0	1444	1436	50
0	2	6	2217	2229	49	0	10	6	1097	1118	76	1	4	3	1566	1576	40	1	12	4	922	847	75
0	2	7	1229	1202	53	0	10	7	1501	1405	72	1	4	4	1612	1567	42	1	13	3	1201	1234	69
0	2	8	754	731	74	0	11	3	1330	1374	54	1	4	5	985	1067	71	2	2	0	2625	2705	34
0	2	9	1004	1142	71	0	11	7	1279	1255	74	1	4	6	2124	2118	53	2	2	1	1023	973	26
0	3	3	1648	1664	43	0	12	0	1734	1662	68	1	4	7	1540	1544	49	2	2	2	618	569	72
0	3	4	798	854	54	0	12	1	1164	1198	82	1	4	9	1019	1019	61	2	2	3	4247	4259	41
0	3	5	746	756	54	0	12	2	2155	2170	54	1	4	10	937	827	89	2	2	4	522	674	61
0	3	7	1656	1641	41	0	12	3	728	707	89	1	4	11	1435	1456	88	2	2	5	1653	1643	40
0	3	9	1416	1437	80	0	12	5	1111	1088	70	1	5	0	2773	2896	47	2	2	6	769	776	55
0	3	13	935	984	81	0	12	6	1020	1025	82	1	5	1	920	977	38	2	2	7	1817	1771	43
0	4	0	1734	1659	45	0	13	1	816	772	106	1	5	2	1903	1988	53	2	2	8	947	1115	61
0	4	1	1025	995	52	0	14	0	1777	1831	53	1	5	3	1276	1327	52	2	2	9	1537	1554	45
0	4	2	2504	2495	64	0	14	2	957	1050	78	1	5	5	1848	1808	67	2	2	10	1702	1683	43
0	4	3	1059	1120	55	1	1	0	390	356	37	1	5	6	2692	2739	74	2	2	11	1248	1377	57
0	4	4	4381	4361	80	1	1	1	445	503	38	1	5	7	1478	1434	71	2	2	13	1201	1199	65
0	4	7	2570	2505	57	1	1	2	627	716	34	1	5	9	1497	1575	48	2	3	0	1048	1060	47
0	4	8	1556	1525	44	1	1	3	806	757	68	1	6	0	1572	1587	37	2	3	1	1087	1028	32
0	4	10	793	712	78	1	1	4	2273	2323	48	1	6	2	505	528	76	2	3	2	2659	2698	112
0	4	11	1301	1172	57	1	1	5	1255	1237	32	1	6	4	1176	1195	52	2	3	4	1500	1473	40
0	4	12	842	673	96	1	1	6	1221	1139	35	1	6	5	819	730	100	2	3	5	1447	1448	44
0	5	3	840	859	57	1	1	7	2224	2306	55	1	6	7	760	756	93	2	3	6	977	955	47
0	5	6	1004	981	60	1	1	8	1041	1002	53	1	7	0	1951	1889	47	2	3	8	1229	1290	50
0	5	10	1018	1003	87	1	1	9	692	803	80	1	7	3	2030	1994	50	2	4	0	4899	4968	87
0	5	11	992	981	127	1	1	11	1254	1187	55	1	7	4	2651	2626	66	2	4	1	1066	998	33
0	6	0	5098	5040	130	1	2	2	3523	3556	123	1	7	10	1216	1162	66	2	4	3	1576	1593	41
0	6	1	1118	1095	39	1	2	3	1050	1043	40	1	8	1	884	866	56	2	4	4	690	766	76
0	6	2	1370	1370	42	1	2	4	857	910	40	1	8	2	2218	2256	144	2	4	6	1360	1311	42
0	6	3	3029	3065	115	1	2	5	1582	1649	45	1	8	3	975	1063	68	2	4	7	1232	1209	50
0	6	4	1540	1600	134	1	2	6	2458	2417	55	1	8	6	1307	1327	67	2	5	2	3561	3532	104
0	6	5	1219	1207	57	1	2	7	752	770	102	1	8	7	1161	1097	91	2	5	3	1118	1125	42
0	6	6	832	805	78	1	2	8	1578	1629	41	1	8	11	816	796	115	2	5	5	717	659	93
0	6	7	1059	1195	66	1	2	9	1793	1804	44	1	9	0	2166	2190	54	2	5	6	2322	2288	58
0	6	8	1770	1839	50	1	2	10	858	1004	97	1	9	1	1359	1380	70	2	5	8	835	881	74

H	K	L	Fobs	Fcalc	SigF	H	K	L	Fobs	Fcalc	SigF	H	K	L	Fobs	Fcalc	SigF	H	K	L	Fobs	Fcalc	SigF
2	5	9	1184	1130	56	3	3	5	803	745	87	3	10	3	1044	1052	71	4	8	5	1165	1195	56
2	5	10	743	744	83	3	3	6	1936	1953	48	3	10	4	829	769	71	4	8	7	1084	1124	75
2	6	0	1914	2015	108	3	3	7	2717	2610	72	3	10	7	1203	1241	74	4	8	9	992	860	87
2	6	1	1000	970	40	3	3	8	2042	1981	50	3	11	2	2055	2103	62	4	8	10	1317	1301	70
2	6	2	843	866	72	3	3	9	1064	1143	59	3	11	3	1219	1211	69	4	9	0	1337	1318	96
2	6	3	887	859	52	3	3	11	2105	1928	47	3	11	4	669	629	91	4	9	2	1029	1070	55
2	6	4	1504	1500	45	3	3	12	777	786	88	3	11	6	1062	1104	72	4	9	5	660	719	88
2	6	5	2029	2048	86	3	4	1	605	610	58	4	4	0	5441	5518	42	4	10	0	2630	2601	60
2	6	6	2536	2472	168	3	4	3	1135	1106	51	4	4	1	630	654	52	4	10	1	989	982	64
2	6	7	1867	1924	79	3	4	4	687	724	67	4	4	2	2067	2140	46	4	10	3	1174	1123	51
2	6	9	1506	1552	60	3	4	5	1110	1107	71	4	4	3	3536	3533	59	4	10	6	897	806	78
2	6	11	972	946	76	3	4	7	1579	1585	53	4	4	4	1614	1607	41	4	11	0	701	709	79
2	7	0	2434	2383	54	3	4	9	740	667	103	4	4	5	1121	1057	63	4	11	2	783	828	73
2	7	2	765	913	66	3	4	11	1013	1038	69	4	4	6	2200	2148	126	4	12	0	2147	2108	55
2	7	3	1440	1379	43	3	5	0	3102	3142	48	4	4	7	968	943	58	4	12	1	934	968	92
2	7	4	2409	2323	57	3	5	1	939	890	40	4	4	8	1615	1718	44	4	12	2	1209	1130	63
2	7	5	818	796	81	3	5	2	2427	2427	54	4	4	9	1194	1240	116	4	12	3	1310	1346	55
2	7	7	1253	1192	66	3	5	5	1053	1064	65	4	4	11	1684	1835	51	4	12	5	1195	1143	70
2	7	8	1712	1707	57	3	5	6	615	574	91	4	5	0	667	637	54	4	12	6	1856	1883	52
2	8	0	2958	2998	62	3	5	7	1117	1031	60	4	5	2	1469	1497	61	4	13	3	782	752	82
2	8	1	900	915	56	3	5	9	1156	982	56	4	5	3	1239	1202	49	4	13	4	1083	1071	67
2	8	2	1407	1442	42	3	5	10	1317	1203	56	4	5	4	1241	1197	65	5	5	0	2158	2098	48
2	8	3	1752	1746	52	3	6	0	1432	1518	66	4	5	5	1266	1310	50	5	5	1	978	986	43
2	8	5	1291	1306	62	3	6	1	897	954	44	4	5	6	1390	1411	75	5	5	2	865	790	94
2	8	6	769	788	100	3	6	3	772	768	57	4	5	7	1046	1135	146	5	5	3	1875	1905	48
2	8	9	908	825	87	3	6	4	853	864	62	4	5	8	1568	1561	88	5	5	4	2973	2938	63
2	8	10	965	902	85	3	6	5	1415	1475	50	4	5	9	1170	1234	119	5	5	5	1579	1597	42
2	9	0	1823	1818	47	3	6	8	1124	1060	60	4	5	10	728	790	88	5	5	6	905	881	83
2	9	2	1047	1039	56	3	6	9	897	948	74	4	5	11	691	759	100	5	5	9	1488	1536	63
2	9	4	1448	1415	64	3	7	0	4765	4757	57	4	6	3	2597	2466	58	5	5	10	1301	1264	57
2	10	0	2376	2335	58	3	7	2	1437	1413	41	4	6	4	2297	2297	61	5	6	0	1322	1298	38
2	10	3	1108	1121	65	3	7	3	959	918	54	4	6	5	953	908	66	5	6	1	787	768	78
2	10	5	770	662	85	3	7	4	1935	1897	46	4	6	6	1247	1304	110	5	6	2	1655	1600	39
2	11	0	1138	1102	53	3	7	6	1682	1657	53	4	6	7	835	738	122	5	6	3	792	815	75
2	11	1	1224	1270	52	3	7	8	1169	1103	67	4	6	9	763	845	86	5	6	4	1323	1273	54
2	11	2	1464	1487	47	3	8	0	751	663	64	4	6	10	698	726	96	5	6	5	819	795	67
2	11	5	864	913	83	3	8	1	670	629	71	4	7	0	2124	2140	62	5	6	8	807	753	81
2	12	1	734	761	81	3	8	2	860	932	68	4	7	2	1910	1871	49	5	7	0	1597	1597	40
2	12	3	1615	1615	48	3	8	3	1177	1194	49	4	7	3	1192	1232	54	5	7	2	1510	1532	45
2	12	4	1437	1434	118	3	8	5	870	874	75	4	7	4	1683	1742	41	5	7	3	1660	1643	55
2	12	5	1067	1028	123	3	8	7	940	941	88	4	7	5	901	873	73	5	7	6	1510	1504	48
2	12	6	1141	1151	95	3	9	1	1083	1080	52	4	7	6	1230	1140	60	5	7	9	933	951	88
2	13	0	1577	1607	57	3	9	2	1827	1807	45	4	7	7	1404	1367	90	5	8	1	1029	1041	52
2	13	4	1286	1309	62	3	9	3	1235	1221	51	4	7	8	1362	1311	62	5	8	2	1993	2024	57
2	14	0	1240	1247	79	3	9	4	1712	1733	46	4	7	9	1507	1418	58	5	8	3	783	735	108
2	14	3	1265	1332	64	3	9	5	1750	1697	49	4	7	11	1255	1256	67	5	8	6	1016	998	67
3	3	0	4036	4096	54	3	9	6	2361	2368	60	4	8	1	1321	1335	43	5	9	0	1678	1772	44
3	3	2	1404	1432	35	3	9	7	1178	1135	72	4	8	2	1946	2025	50	5	9	3	2136	2083	52
3	3	3	1118	1199	101	3	9	9	1575	1582	68	4	8	3	976	915	67	5	9	5	1362	1351	51
3	3	4	4758	4856	150	3	10	0	615	556	82	4	8	4	1555	1613	44	5	9	8	1175	1186	95

Values of 10*Fobs and 10*Fcalc for Cal6Sb11

H	K	L	Fobs	Fcalc	SigF	H	K	L	Fobs	Fcalc	SigF	H	K	L	Fobs	Fcalc	SigF	H	K	L	Fobs	Fcalc	SigF
5	9	9	1127	1042	95	7	7	4	1220	1226	51												
5	10	0	1883	1908	75	7	7	6	690	647	85												
5	10	2	682	689	76	7	7	7	2069	2064	46												
5	10	4	1570	1616	49	7	8	0	746	803	69												
5	10	6	791	771	86	7	8	2	1390	1396	44												
5	10	8	880	899	94	7	8	5	899	891	67												
5	11	1	839	876	67	7	8	6	1105	1078	91												
5	11	4	968	1034	76	7	9	0	1048	1021	61												
5	11	5	714	797	90	7	9	1	856	904	61												
5	11	6	1103	1123	69	7	9	3	771	857	79												
5	11	7	1499	1481	61	7	10	0	689	749	80												
5	12	0	806	884	74	7	10	2	1473	1516	69												
5	12	4	657	701	95	7	10	4	942	966	65												
5	13	0	1057	1049	73	7	10	5	783	816	80												
6	6	0	4620	4517	54	7	10	6	1317	1324	80												
6	6	1	971	965	53	7	10	7	782	729	104												
6	6	2	1530	1542	66	7	11	0	1541	1487	44												
6	6	3	2147	2068	52	7	11	2	1158	1161	55												
6	6	4	1775	1689	52	7	11	3	962	978	71												
6	6	5	739	825	77	7	11	5	748	681	85												
6	6	7	1100	1139	72	8	8	0	3992	4013	63												
6	6	8	1594	1608	61	8	8	1	715	765	93												
6	6	9	768	718	91	8	8	3	1617	1599	47												
6	6	10	1557	1463	55	8	8	4	1302	1306	50												
6	7	1	972	986	53	8	8	5	1143	1129	64												
6	7	3	1076	1063	52	8	8	6	1393	1438	54												
6	7	4	633	605	84	8	8	8	1137	1123	72												
6	7	5	782	833	73	8	9	0	589	650	89												
6	7	7	1172	1163	106	8	9	1	721	720	73												
6	8	0	1359	1412	43	8	9	4	684	588	81												
6	8	2	1419	1399	45	8	9	5	769	708	77												
6	8	3	662	684	79	8	10	3	1628	1588	46												
6	8	4	1053	1034	55	8	10	4	943	942	66												
6	8	5	759	719	81	8	11	1	714	680	77												
6	8	6	2113	2099	68	8	12	1	877	894	68												
6	8	7	1349	1266	57	9	9	0	788	828	74												
6	8	9	1009	981	98	9	9	2	1001	1062	61												
6	9	0	788	830	63	9	9	4	1731	1705	46												
6	9	1	706	633	84	9	9	6	1164	1193	107												
6	9	2	1687	1714	47	9	10	5	794	802	96												
6	10	3	2083	2049	51	9	11	0	1536	1593	49												
6	10	4	1312	1400	100	10	10	0	2056	2160	51												
6	10	7	848	919	88	10	10	1	967	1023	121												
6	11	3	1181	1209	73																		
6	12	0	2494	2541	59																		
6	12	2	1220	1220	72																		
6	12	3	941	907	88																		
6	13	2	878	874	73																		
7	7	0	584	509	85																		
7	7	2	1450	1490	48																		